Feasibility and Constraints of Bragg Peak FLASH Proton Therapy Beam Delivery and Treatment Planning



Nathalie Lövgren

St Cross College

University of Oxford

A thesis submitted for the degree of

Doctor of Philosophy in Oncology

January, 2026

Acknowledgements

There are many who need to be thanked and acknowledged for their contributions to this thesis and for shaping me into the researcher I am today. To Kristoffer Petersson, for your help and guidance, for your unwavering trust in my academic abilities, and for your constant support and encouragement throughout the years. To Rasmus Nilsson, Erik Traneus, Ingrid Fagerström Kristensen, Rudi Labarbe, Lucian Hotoiu, Salomé Paillas, Jia-Ling Ruan, Sovan Sarkar, and many others, for your support, guidance, and collaborations throughout the years. To Iain Tullis, for the infinite cups of tea, and for always challenging my thinking whether it be related to my work, your work, no work, or radar. To Boris Vojnovic, for improving my understanding of accelerators and radiation physics, one lunchtime discussion at a time. To Mamma, for your unconditional love and support. All my achievements are as much yours as they are mine, for without your hard work and selflessness, this would not have been possible. To Izzo, whose determination and kindness inspire me everyday, I would not be who I am today without you. I cannot express enough gratitude to you and Simon for all your help, and for bringing laughter to even the most difficult times. To Tessa and Rupert, for your unending support and encouragement throughout the years. To all my family and friends, for all the laughter and adventures we have shared, making the stressful times easier and the wonderful times even better. For all those who have asked 'How long is left of the PhD?', this is it. Finally, to Ben, whose inquisitiveness, encouragement, and unconditional support makes me a better researcher everyday. You have made the past four years an adventure full of joy and laughter, and I am so excited for the many adventures still to come.

Publications

This thesis is based on my first-author publications, together with a manuscript under review, which form the basis of Chapters 2-5. The specific chapters and sections to which each publication applies are also indicated in the footnotes of the relevant sections.

> **Lövgren, N.**, Nilsson, R., Traneus, E., Petersson, K. The Impact of Dose Rate Optimisation and Robust Optimisation on FLASH Proton Therapy Treatment Plan Quality and Dose Rates. *Frontiers in Oncology.* 2025.
>
> **Lövgren, N.**, Fagerström Kristensen, I, Petersson, K. Feasibility and Constraints of Bragg Peak FLASH Proton Therapy Treatment Planning. *Frontiers in Oncology.* 2024.
>
> **Lövgren, N.**, Nilsson, R., Traneus, E., Petersson, K. Initial Beam Energy and Target Volume Dependency of Spread-Out Bragg Peak FLASH Proton Therapy on Treatment Plan Quality and Achievable Dose Rates for Brain Targets *(under review).*

I have also contributed to research conducted during my DPhil that does not form part of this thesis, but which resulted in a co-authored publication and a manuscript currently under review. The former is cited in this thesis in Chapters 4 and 5.

> Paillas, S., Taylor, ERJF., **Lövgren, N.**, et al. Quantifying the FLASH Effect and its Dependence on Average Dose Rate In Vivo for 6 MeV Electron and 6 MV Photon Beams. *Clinical and Translational Radiation Oncology.* 2026.

Ruan, JL., Lee, C., Sharma, O., **Lövgren, N.**, et al. FLASH Radiotherapy Enables Dose Escalation and Improves Survival in an Orthotopic Muscle-Invasive Bladder Cancer Mouse Model. *British Journal of Radiology*. 2026.

To Mamma, Izzo, and Ben,

for being part of me and

therefore part of this work.

Abbreviations and Symbols

ADR	Average dose rate
CEM	Conformal energy modulator
CT	Computed tomography
CTV	Clinical target volume
D_{AV}	Average dose
$D_{prescribed}$	Prescribed dose
D_{thr}	Threshold dose
$D_{x\%}$	Dose to $x\%$ of volume
DADR	Dose-averaged dose rate
DMF	Dose modifying factor
DRO	Dose rate optimised
DR_{prct}	Percentile dose rate
DR_{thr}	Threshold dose rate
DVH	Dose volume histogram
FLASH-PT	Spread-out Bragg peak FLASH proton therapy
GTV	Gross tumour volume
Gy	Gray (joule per kilogram)
HI	Homogeneity index
IMPT	Intensity modulated proton therapy
LET	Linear energy transfer
MFO	Multi-field optimisation
MU	Monitor unit

OAR	Organ at risk
PBS	Pencil-beam scanning
PTV	Planning target volume
RBE	Relative biological effectiveness
RCI	Radiation conformity index
SBRT	Stereotactic body radiotherapy
SFRT	Spatially fractionated radiotherapy
SFO	Single-field optimisation
TPS	Treatment planning system

Contents

1 Introduction **1**

1.1 Proton Therapy 1

1.1.1 Biological Effects 2

1.1.2 Accelerators 3

1.1.3 Energy Selection System 5

1.1.4 Beam Delivery 5

1.1.5 Treatment Planning and Optimisation 7

1.1.6 Emerging Technologies 9

1.2 FLASH Proton Therapy 10

1.2.1 Biological Effects and Mechanisms 11

1.2.2 Pre-Clinical Studies 13

1.2.3 Clinical Studies 15

1.2.4 Beam Delivery 17

1.2.5 Treatment Planning 18

1.2.6 Dose Modifying Factor 19

1.2.7 Dose Rate Definitions 20

1.3 Core Thesis Aims 21

2 Materials and Methods **23**

2.1 Beam Delivery 23

2.2 Patient Data 24

2.2.1 Feasibility Studies: Multiple Target Types 25

2.2.2 Data Informed Study: Brain Targets 26
2.3 Treatment Planning 27
2.3.1 Intensity Modulated Proton Therapy 27
2.3.2 Spread-Out Bragg Peak FLASH Proton Therapy 28
2.3.3 MIROpt and ConformalFLASH 29
2.3.3.1 Dose Rate Optimisation and Calculation 30
2.3.4 RayStation 11B FLASH 33
2.3.4.1 Robust Optimisation 34
2.3.4.2 Dose Rate Calculation 35
2.3.5 Dose Optimisation and Fractionation Schemes 35
2.4 Plan Evaluations and Comparisons 37
2.4.1 Dose 37
2.4.2 Dose Rates 38

3 Feasibility and Constraints of Spread-Out Bragg Peak FLASH Proton Therapy Treatment Planning 39

3.1 Introduction 39
3.2 Materials and Methods 41
3.3 Results 44
3.4 Discussion 60

4 The Impact of Dose Rate Optimisation and Robust Optimisation on FLASH Proton Therapy Treatment Plan Quality and Dose Rates 64

4.1 Introduction 64
4.2 Materials and Methods 66
4.3 Results 69
4.4 Discussion 85

5 Non-Maximal Energy Spread-Out Bragg Peak FLASH Proton Therapy 91

5.1 Introduction 91

5.1.1 Scenario 1: High Energy Beam Delivery 94
5.1.2 Scenario 2: Reducing Momentum Spread with a Compact Gantry 95
5.1.3 Scenario 3: Variable Energy Cyclotron 96
5.2 Materials and Methods 97
5.3 Results 101
5.4 Discussion 116

6 Conclusion **122**

Bibliography **130**

A Treatment Plan Information and Data for MIROpt and RayStation Plans **155**

B Treatment Plan Data for Non-Maximal Energy SOBP FLASH Proton Therapy **177**

Abstract

Spread-out Bragg peak FLASH proton therapy (FLASH-PT) aims to use ultra-high dose rates to elicit a normal tissue sparing effect whilst maintaining the anti-tumour effectiveness of conventional proton therapy. Conventional energy-modulation techniques used in intensity modulated proton therapy (IMPT) are not fast enough to achieve ultra-high dose rates ($\geq$ 40 Gy/s); instead, FLASH-PT utilises monoenergetic protons (230 MeV) combined with static energy degraders. This thesis investigates the feasibility and constraints of FLASH-modified beam delivery and treatment planning in achieving dose distributions comparable to IMPT, forming an essential part of the clinical implementation of FLASH-PT.

Chapter 3 investigates the feasibility of FLASH-PT treatment planning compared to IMPT using a research treatment planning system incorporating dose rate optimisation. Margin-based FLASH-PT plans achieve sufficient ultra-high dose rate coverage. However, they demonstrate inferior target coverage and increased doses to organs at risk (OARs) compared to IMPT. Chapter 4 assesses the impact of dose rate optimisation on the quality of FLASH-PT treatment plans by utilising two treatment planning systems, one with and one without dose rate optimisation. Non-dose rate optimised planning and robust optimisation improves plan quality without compromising dose rates or increasing OAR doses; however, target coverage remains inferior to IMPT in worst-case scenarios. Finally, Chapter 5 explores whether reducing the initial beam energy from 228 MeV to that used in IMPT plans, thereby decreasing the required range shifter thickness, can improve plan quality by reducing scattering and range straggling.

Non-maximal energy FLASH-PT plans can achieve IMPT-equivalent target coverage, whilst reducing the gap between FLASH-PT and IMPT doses to OARs, at the expense of lower dose rates.

This work advances the understanding of relevant treatment planning optimisation techniques and beam delivery modifications, collectively improving the feasibility of spread-out Bragg peak FLASH proton therapy.

Chapter 1

Introduction

1.1 Proton Therapy

Protons interact with matter in three ways, they slow down, scatter, and create secondary particles through head-on collisions with a nucleus [1]. Together, these interactions form the characteristic behaviour discovered by William H. Bragg in 1903 when observing a sharp peak in energy loss of alpha particles from radium, later named the "Bragg peak" [1, 2]. Robert R. Wilson recognised the potential of this discovery for clinical application and in 1946 proposed the use of protons for treatments of cancer [3]. Cancer is one of the leading causes of death globally, accounting for almost one in six deaths according to estimates by the World Health Organization in 2020 [4]. Standard cancer treatments include surgery, chemotherapy, and radiotherapy. Estimates suggest that approximately 50% - 70% of cancer patients worldwide require radiotherapy, which is delivered using high energy photon (x-ray or gamma-ray) or particle (proton and electron) beams to induce tumour damage [5, 6]. Just over a decade after Wilson proposed the use of protons for treatments of cancer, the Lawrence Berkeley Laboratory performed the first clinical proton irradiations on patients with advanced breast cancer [7]. Nearly seventy years later, there are over a hundred facilities delivering proton therapy worldwide; however, further improvements and optimisation of treatment techniques are essential to enhance clinical outcomes [8].

As protons traverse through an absorbing medium, they lose energy along their path, with a sharp increase in energy deposited before coming to rest. The sharp peak in energy deposition is the Bragg peak. The range of protons can be approximated by:

$$R_0 = \alpha E_0^p, \tag{1.1}$$

where R_0 (cm) is the range, E_0 (MeV) is the initial energy, $p \approx 1.8$ for energies in the range of 10 MeV to 250 MeV, and $\alpha \approx \sqrt{A_{eff}}$, where A_{eff} is the atomic mass of the absorbing medium [1, 9]. A statistical error is assigned to the energy loss due to the large amounts of individual interactions, known as range straggling [1, 3]. In other words, protons of equal initial energies may not reach equal depths in the same absorbing material [3]. Additionally, multiple Coulomb scattering causes the proton beam to broaden laterally as it traverses the medium[1, 3]. This lateral spread becomes increasingly important with depth and contributes to the widening of the beam profile and loss of conformality near the distal region.

1.1.1 Biological Effects

Particle irradiation cause deoxyribonucleic acid (DNA) damage, and thus cell death, through direct and indirect effects. Direct effects involve energy deposition directly in the DNA, whereas indirect effects arise from ionisations of nearby water molecules, leading to the production of highly reactive radicals, most notably hydroxyl (OH) radicals, which can subsequently damage the DNA [1]. Compared to photon radiation, protons require a lower dose to induce equivalent biological damage. This discrepancy in biological effect is known as the relative biological effectiveness (RBE), with protons commonly assumed to be 10% more effective than photons at causing equivalent damage, corresponding to an RBE of 1.1 in clinical treatment planning [1]. It should be noted, however, that the actual RBE is not constant and can vary with factors such as depth, dose, and tissue type.[1] In addition to the RBE, an important parameter

[1]The relative biological effectiveness (RBE) is the ratio of a reference radiation dose (photons) to the dose of the radiation of interest (protons in this work) required to produce the same biological

to consider in radiotherapy is the linear energy transfer (LET), which is the energy transfer to the absorbing material per unit distance [1]. The amount and type of DNA damage induced, such as single- and double-strand breaks, as well as its clustered DNA damage, is dependent on LET. Here, clustered DNA lesions is defined as two or more lesions (e.g. base damage and/or strand breaks) occurring within one or two helical turns of the DNA. The probability and complexity of clustered damage typically increases with increasing LET, making it more difficult for the cell to repair [10, 48].

For protons, both dose and LET vary with depth: the dose remains relatively low in the entrance region before rising sharply to a maximum at the Bragg peak, whereas the LET increases gradually along the beam path and reaches its highest values near and just beyond the distal edge of the Bragg peak. Consequently, the highest LET, and therefore the highest RBE, is expected to occur at or beyond the distal fall-off, potentially extending into normal tissue distal to the target [1]. As a result, the biological dose delivered by a proton beam is not solely determined by the physical dose distribution but is also influenced by variations in LET and the corresponding changes in RBE. Regions of elevated LET, such as near the distal edge of the Bragg peak, may lead to an increased biological effect compared to that predicted by the physical dose alone. In general, for charged particles, as the LET increases the RBE increases to a maximum, beyond which saturation effects lead to a subsequent decrease the position of this peak is particle dependent. However, the peak in RBE is difficult to observe experimentally for protons due to their very short range at high LET [11].

1.1.2 Accelerators

Proton accelerators include isochronous cyclotrons, synchrocyclotrons, and synchrotrons. There are four main components of a cyclotron: a radio frequency (RF) system which accelerates the protons, a strong magnet which keeps the particles in a spiral orbit to be accelerated by the RF voltage, a proton source (protons extracted from ionised

effect.

hydrogen gas), and a beam extraction system [1]. Although isochronous cyclotrons are fixed-energy accelerators, with energy adjustment achieved downstream of the accelerators, they are advantageous due to their high intensity continuous wave (CW) characteristic (quasi-continuous pulse structure on a nanosecond scale) [1, 12, 13]. However, as the energy of the protons increase, the relativistic increase of mass of the particles becomes significant [14]. To compensate for this, one approach is to modulate the RF voltage synchronously with the increase in mass using a synchrocyclotron [14]. The frequency modulation requires the synchrocyclotron to operate periodically, and despite fast energy switching ($\sim$ 50 ms), the low pulse repetition rate in addition to the periodic operation reduces the associated intensity when compared to a CW isochronous cyclotron (pulse structure operates on a microsecond scale) [13–15]. To circumvent the drop in intensity, another (more modern) approach is for isochronous cyclotrons to account for relativistic effects, whilst allowing for the beam to remain CW, by increasing the magnetic field with respect to the radius, r, of orbit as:

$$B(r) = \gamma(r)B_0, \tag{1.2}$$

where B_0 is the non-relativistic magnetic field strength, and

$$\gamma(r) = \frac{1}{\sqrt{1 - \frac{v(r)^2}{c^2}}}, \tag{1.3}$$

where v is the velocity of the protons and c the speed of light [1]. Instead of a spiral orbit, synchrotron accelerators implements a fixed radius orbit, with a magnetic field which maintains orbit stability by increasing as the proton energy increases [14]. The synchrotron does not operate in a continuous mode, rather in "spills", where the desired energy of the protons can be selected, and bunches of protons are extracted into the beamline [1].

1.1.3 Energy Selection System

For synchrotrons, a variable beam energy can be extracted using varying magnetic field strengths. With cyclotrons being fixed energy accelerators, the particles need to pass through degraders in order to reach appropriate energies for therapeutic use. This energy degradation is performed by an energy selection system (ESS), which includes a degrader, collimators, magnetic spectrometers, energy slits, and beam stops [1, 16]. The degrader reduces the proton energy through energy loss in the material, the collimators reduce the angular spread (emittance) caused by the degrader, whilst the magnetic spectrometers and slits select protons with the relevant energy spread. The transmission efficiency of the beam is reduced with degraded beam energy; to compensate for this, higher intensities are utilised for lower energy beams such that the dose rate remains constant as the energies are lowered [1].

1.1.4 Beam Delivery

Proton therapy can be delivered using the plateau region of the beam, known as a transmission beam, or using the Bragg peak, as illustrated in Figure 1.1. Transmission beam proton therapy places the Bragg peak outside of the patient. For use of the Bragg peak, beams of varying energies can be superimposed to create a 'Spread-Out Bragg Peak' (SOBP), which extends the Bragg peak such that it covers the target volume, highlighted in Figure 1.1 [17]. Clinical proton beams typically have energies in the range of approximately 70 MeV - 230 MeV, corresponding to penetration depths in tissue of a few centimetres up to around 30 cm [1]. This technique is more advantageous as it utilises the finite range of protons and is not associated with an exit dose, thereby reducing the dose delivered to tissues beyond the target compared to transmission beam proton therapy. Proton beams can be delivered using passively scattered or actively scanned protons. Passive scattering involves mono-energetic protons passing through energy degraders to produce protons of varying energies, and hence depths, whilst conforming to the shape of the target [18]. Active scanning, also known as pencil beam scanning (PBS) or spot scanning, involves magnetically scanned proton beams;

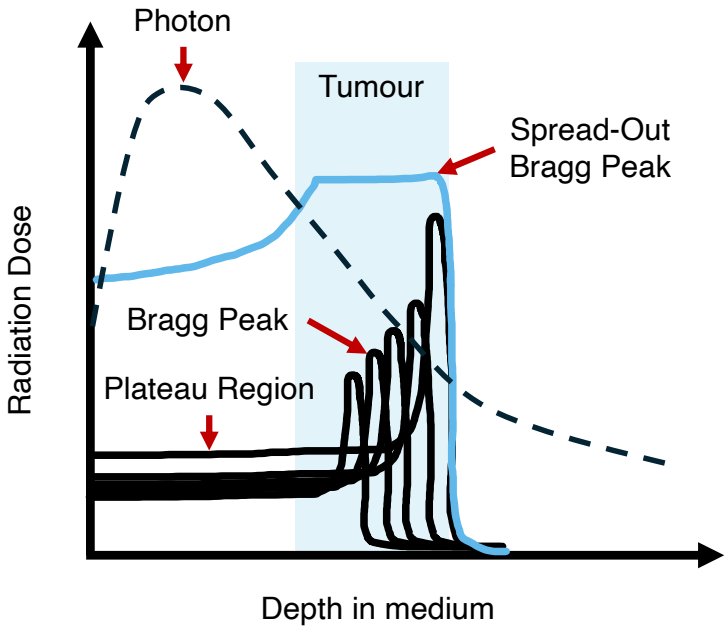


Figure 1.1: Illustration of depth-dose curves for photon (dashed line) and proton (solid line) radiation. Photons exhibit a gradual dose fall-off with depth, whereas protons show a low-dose plateau followed by a sharp Bragg peak. A spread-out Bragg peak (SOBP) is used to deliver a uniform dose across the tumour.

here, energy and intensity modulation occurs through an energy selection system (Section 1.1.3) before the protons are delivered to the treatment gantry [18]. To achieve a dose which covers the target volume in depth, the protons are delivered in energy layers through variations in beam energy [1]. Active scanning is therefore associated with improved dose conformity, whilst also reducing the production of secondary neutrons, when compared to passively scattered beams [19]. Intensity modulated proton therapy (IMPT) delivers protons using active scanning and optimises spot-intensities to achieve optimal dose coverage, and conformity, whilst reducing doses to organs at risk (OARs) [19, 20].

In IMPT, the proton beam is delivered as a series of narrow "pencil beams" (or spots) that are magnetically steered across the tumour in a raster-like pattern. The tumour is irradiated layer-by-layer in depth by varying the proton energy, such that each energy deposits dose at a different depth. By adjusting both the position and intensity of each spot, a highly conformal three-dimensional dose distribution can be constructed.

In clinical practice, IMPT typically employs multiple proton beams delivered from different angles around the patient. By combining contributions from several beam directions, the high-dose region can be conformed more precisely to the target volume, while minimising dose to surrounding healthy tissues. This multi-field optimisation is analogous to techniques used in photon radiotherapy (e.g. intensity-modulated radiation therapy and volumetric modulated arc therapy), but benefits additionally from the finite range of protons, further reducing exit dose [1]. With regards to beam monitoring, a beam monitor chamber (typically a parallel plate ionisation chamber) is used to quantify the machine output in terms of monitor units (MU), where 100 MU is the amount of radiation required to deliver 1 Gy of absorbed dose at a reference point and depth in a phantom [1, 21].

1.1.5 Treatment Planning and Optimisation

Particle simulations rely on accurate modelling of the energy deposition in the absorbing medium. Due to the probabilistic nature of particles, Monte Carlo simulations provide high accuracy of such modelling, with an associated error of $1/\sqrt{N}$, where N is the number of particles considered [1]. Compared to the use of analytical models, Monte Carlo simulations incorporate interaction physics based on theoretical models and experimental data [1]. With the use of Monte Carlo, along with computed tomography (CT) scans, target and OAR contours, beam delivery parameters (e.g., beam angles) and clinical information (e.g., dose prescription), a treatment plan can be simulated for a patient using a treatment planning system (TPS) [1, 22]. Treatment planning for IMPT is an optimisation problem, with the quality of the plan represented by an objective function f with the aim of minimising the function according to:

$$\underset{x}{\text{minimise}}\, f(d), \tag{1.4}$$

where, for a voxel i and pencil beam j:

$$d_i = \sum_j D_{ij} x_j, \tag{1.5}$$

where $x_j \geq 0$ is the fluence, d_i is the dose, and D_{ij} is the dose contribution of the pencil beam to that voxel [23]. For a given treatment plan, there are constraints on the target dose (min and max), and maximum dose constraints to OARs. The constraints are implemented into the TPS as individual dose objective functions. During the treatment plan optimisation, if a dose does not adhere to an imposed constraint, a penalty is added to the dose objective function until the objective is reached.

When simulating a treatment plan, the target structure must first be defined. To account for potential microscopic spread of cancer around the gross tumour volume (GTV), clinicians delineate an expanded volume of the GTV, referred to as the clinical target volume (CTV) [24]. To account for setup uncertainties in the treatment plan, margins can be applied to the CTV, forming the planning target volume (PTV). Treatment planning utilising the PTV as the target structure is known as margin-based planning. Protons are associated with an increase in sensitivity to density changes and heterogeneities along the path of the beam when compared to other radiotherapy techniques [25]. Instead of using a static expansion of the CTV, the range uncertainties due to the beam setup can be directly incorporated into the dose calculation and optimisation process through robust optimisation. Range uncertainty can be evaluated through the assumption that the dose influence matrix, D_{ij} in Equation 1.5, may be different for different range error scenarios [23]. For robust optimisation, the dose influence matrix can therefore be written as D^s_{ij}, where s is the index of possible error scenarios [23]. Overshoot and undershoot scenarios can then be evaluated by modifying the radiodensity of the CT scan (Hounsfield numbers), to model D^s_{ij} for particles that have less or more penetration than the nominal (no range error) scenario [23]. Two main methods of incorporating error scenarios into robust optimisation is through the probabilistic approach and the worst-case approach. Finding a treatment plan which

yields a good dose distribution in every error scenario is done through the probabilistic approach which minimises the weighted sum of objective function for all scenarios [23]. In contrast, the worst-case approach finds the optimal treatment plan in the worst error scenario by minimising the maximum objective function for all scenarios [23].

With regards to field-related optimisation, IMPT plans can be optimised using either single-field optimisation (SFO) or multi-field optimisation (MFO). For SFO, a single beam is used to cover the entire target and each beam is optimised individually. MFO, however, allows for use of multiple beams to cover the entire target, and the dose contribution from all beams is considered simultaneously in the dose calculation and optimisation. This improves target coverage whilst minimising dose to surrounding structures, which is why MFO is most commonly used for IMPT [17].

1.1.6 Emerging Technologies

The technology of proton therapy is ever evolving, with many advancements made since Wilson first proposed the use of protons for cancer treatment. Current developments include structural improvements to proton facilities aimed at reducing facility costs, such as the use of compact gantry systems [26]. In terms of beam delivery, spatial fractionation using proton minibeams or microbeams are being investigated, with both technologies currently in the pre-clinical stage of research [27, 28]. Spatially fractionated beams consist of arrays of narrow, parallel beamlets that produce a pattern of high-dose regions ("peaks") separated by low-dose regions ("valleys"). Proton minibeams typically have widths on the order of hundreds of micrometres to a few millimetres, whereas microbeams are much narrower, with widths of tens of micrometres [27]. This difference in scale leads to distinct biological responses, with microbeams generally requiring highly collimated synchrotron sources, while minibeams are more compatible with clinical proton systems. The underlying rationale of both approaches is that normal tissues are better able to tolerate spatially heterogeneous dose distributions, while tumours experience a more uniform dose at depth due to beam broadening

and scattering, potentially improving the therapeutic ratio [28].

Another area of interest is the use of ultra-high dose rate radiation. In 1966, Hornsey & Alper observed an unexpected dose rate effect following mice irradiation: the half lethal dose of mice exposed at 50 000 rads/min ($\sim$ 8.3 Gy/s) was higher than those exposed at 10 000 rads/min ($\sim$ 1.7 Gy/s) for the same dose [29]. Although not high enough to be considered ultra-high dose rates, the results indicated some dependence of the biological response on dose rate. It is also worth noting that other early *in vitro* studies explored the effects of delivering radiation in very short pulses (x-rays and electrons), achieving instantaneous dose rates orders of magnitude higher than those reported by Hornsey & Alper, and also demonstrated differential biological responses [30, 31]. More than half a century later, ultra-high dose rate research resurged with the pre-clinical observation of a differential effect between tumours and normal tissues following irradiation at dose rates $\geq$ 40 Gy/s using electron beams [32]. This so-called "FLASH effect" has since been predominantly demonstrated with electrons, with increasing evidence for the effect in protons, while evidence for photons remains more limited. Despite many technological developments in radiotherapy, clinical electron beams lack the depth penetration required for the treatment of deep-seated targets, and the production of ultra-high dose rate photons remains largely confined to pre-clinical studies due to substantial power requirements and Bremsstrahlung target heating effects associated with high dose rates [33]. In contrast, protons offer both clinically relevant depth penetration and a feasible pathway to ultra-high dose-rate delivery using modified clinical systems and are therefore of particular interest for FLASH radiotherapy.

1.2 FLASH Proton Therapy

FLASH radiotherapy (FLASH-RT), with its name attributed to the ultra-high dose rate ($\geq$ 40 Gy/s) radiation delivery, has been shown to elicit equivalent tumour damage to

conventional dose rate ($\sim$ 0.1 Gy/s) radiotherapy but with less normal tissue toxicity.[2] This sparing effect is known as the "FLASH-effect" and has been observed *in vitro* for different cell lines and *in vivo* for various animal models, independent of radiation type used (electron, proton, carbon, and x-ray) [36–46]. In addition to the sparing effect, the increase in dose rate would also allow for a substantial reduction in overall treatment time. FLASH-RT may therefore help mitigate uncertainties associated with intra-fractional motion. Furthermore, the reduced delivery time could increase patient throughput; however, this does not necessarily translate to improved accessibility, as FLASH-capable systems may involve increased technical complexity and cost compared to conventional radiotherapy (CONV-RT). Treatment sites that would benefit from FLASH-RT include those where organ motion is an issue, and would normally require the use of large margins, gating, or tracking, such as the lungs, bowels, and liver [47]. Additionally, due to the FLASH sparing effect, the technique would benefit treatments of regions where critical structures are in close proximity to the targets, such as the brain and spinal cord.

1.2.1 Biological Effects and Mechanisms

The precise mechanisms required to elicit a normal tissue sparing effect are not fully understood, with different hypotheses attempting to provide an explanation for the experimental observations.

The oxygen depletion hypothesis theorises that a transient reduction in oxygen levels may induce radioresistance in normal tissues when irradiated at ultra-high dose rates. This concept is closely linked to the well-established oxygen enhancement ratio (OER), defined as the ratio of doses required under hypoxic and aerated conditions to achieve the same biological effect. For low LET radiation, the OER is typically around 2.5 - 3, with cellular radiosensitivity strongly dependent on oxygen concentration, par-

[2]Section 1.2 is based on the published work by Lövgren et al., Feasibility and Constraints of Bragg Peak FLASH Proton Therapy Treatment Planning, *Frontiers in Oncology*, 2024 [34] and Lövgren et al., The Impact of Dose Rate Optimisation and Robust Optimisation on FLASH Proton Therapy Treatment Plan Quality and Dose Rates, *Frontiers in Oncology*, 2025 [35].

ticularly at low partial pressures (of the order of 0.5% oxygen) [48]. For higher LET radiation, this dependence is reduced, with the OER approaching unity above $\sim$ 100 keV/μm.

Normal tissues are typically well oxygenated ($\sim$ 3% - 7% oxygen), tumours often exhibit significantly lower oxygen levels ($\sim$ 0.3% – 4% oxygen), and many *in vitro* experiments are performed under atmospheric conditions ($\sim$ 21% oxygen) [49]. As a result, a transient reduction in oxygen concentration during FLASH irradiation is expected to have a greater relative impact in normal tissues than in tumours, which are already hypoxic. The biological basis of this effect can be understood through the oxygen fixation hypothesis [48]. Following irradiation, indirect damage will be produced in DNA, ultimately producing a DNA radical (DNA$\bullet$). If oxygen is present, then this radical can react to produce a non-restorable organic peroxide (DNA-O_2), which subsequently reacts to produce DNA-OOH. This chemically 'fixes' the damage and repair now requires enzymatic processing via a biological DNA repair pathways. However, in the absence of oxygen, the DNA radical can be restored to its reduced form in the presence of a reducing species, such as thiols, with a sulfhydryl (SH) group enabling restoration of the original undamaged DNA structure [10, 48]. This reaction occurs on timescales of the order of milliseconds, comparable to FLASH delivery times, suggesting that rapid oxygen depletion during irradiation may reduce the probability of fixation and therefore increase the likelihood of damage repair [50]. Already hypoxic tissues, such as tumours, would be less affected by this transient reduction in oxygen, and would therefore experience less of a protective effect compared to normal tissues [51–53].

Ultra-high dose rate irradiation has also been shown to induce lipid peroxidation and ferroptosis (iron dependent cell death pathway) in tumours but not normal tissues [54]. Elevated iron levels in normal tissues were associated with reduced sparing, suggesting that intrinsic differences in iron content between normal tissues and tumours may

contribute to the FLASH sparing effect [54]. This mechanism may also be linked to the oxygen depletion hypothesis, as a transient reduction in oxygen levels would likely reduce lipid peroxidation and ferroptosis, as observed in normal tissues compared with tumours.

Immune modulation is another potential mechanism involved in the sparing effect, with FLASH-RT being associated with a different local immune response compared to CONV-RT [55, 56]. It is also hypothesised that the ultra-high dose rate delivery leads to less exposure of the circulating immune cells, thereby reducing the cell kill associated with conventional dose rate beam delivery [57, 58].

1.2.2 Pre-Clinical Studies

The FLASH effect is commonly defined as a significant reduction in normal tissue toxicity while maintaining comparable tumour control relative to conventional dose-rate radiotherapy. This effect has been observed for different cell lines, mice, rats, and a mini-pig [32, 37, 39, 40, 43, 52, 59–63]. A number of *in vitro* studies have reported differential responses between FLASH and CONV-RT, investigating endpoints such as clonogenic cell survival, DNA double-strand break (γH2AX foci) formation, transforming growth factor beta (TGFβ) expression, premature senescence, and cell cycle synchronisation [40, 64]. However, these effects are not always consistently observed across different cell types, and it remains challenging to determine which observed differences translate into a beneficial therapeutic outcome. The feasibility of delivering FLASH-RT safely, using a single-beam fraction, to larger superficial targets has also been demonstrated for canines, a mini-pig, and a human [59, 65, 66]. *In vivo* studies have shown that FLASH-RT can reduce skin toxicities, bone damage, muscle damage, lung fibrosis, acute gastrointestinal toxicity, and improve short and long-term cognitive function, memory preservation, and overall survival when compared to CONV-RT [32, 39, 43, 59, 67].

Pre-clinical studies have mainly focused on single-dose delivery, although fractionated, split beam, and multi-beam delivery have also been explored. In a gastrointestinal model, fractionated ultra-high dose rate electron beam delivery showed a reduced FLASH sparing effect with increasing number of fractions, comparing single-fraction (14 Gy - 20 Gy), two-fraction (8 Gy - 13 Gy per daily fraction), and ten-fraction (5 Gy - 7 Gy per daily fraction) regimens [68]. Average dose rates of 0.5 Gy/s and > 200 Gy/s were used for conventional and FLASH irradiations, respectively [68].

Comparable reductions in sparing have also been reported for split-beam delivery and multi-beam proton delivery, as well as for ultra-high dose rate photon delivery [69–71]. For split-beam delivery, 39.3 Gy was delivered in 2, 3, 4, or 6 fractions with inter-beam pauses of 2 min, using field dose rates of 0.37 Gy/s (conventional) and 80 Gy/s (FLASH). Multi-beam proton delivery used 2×15 Gy or 2×17.5 Gy for a single pause, and 3×10 Gy or 3×11.6 Gy for two pauses, with 2 min inter-beam pauses and field averaged dose rates of 1 Gy/s (conventional) and 100 Gy/s (FLASH). Similarly, ultra-high dose rate photon delivery using a Small Animal Radiation Research Platform delivered 18.1 Gy, 21.3 Gy, and 25.8 Gy as single or dual pulses. Instantaneous dose rates were 0.05 Gy/s (conventional) and 72 Gy/s - 81 Gy/s (FLASH), whilst average dose rates were 0.05 Gy/s (conventional), 1.9–2.8 Gy/s for split-dose FLASH, and 72 Gy/s - 81 Gy/s for single-dose FLASH irradiations [69–71]. These studies consistently indicate that the magnitude of the FLASH sparing effect decreases with increasing fraction number, beam number, or temporal separation between dose deliveries, and is most pronounced for single, high-dose exposures. Although some sparing remains with multiple beams, it may be less effective than single-dose delivery [68–71].

There are cases in which the sparing effect of FLASH-RT has not been observed [72–75]. This could be accredited to differences in beam delivery parameters as the magnitude of the FLASH effect has been found to vary with different factors such as the dose, dose

rate, type of cell lines irradiated, and the available oxygen concentration at the time of irradiation [40, 52, 76, 77]. More pre-clinical studies are required to better understand the parameters needed to elicit the sparing effect. Further to this, clinical trials are underway to determine the safety and feasibility of implementing the ultra-high dose rate technique.

1.2.3 Clinical Studies

Clinical ultra-high dose rate electron radiotherapy has been investigated in the Irradiation of Melanoma in a Pulse (IMPulse, NCT04986696) dose-escalation trial at the Centre Hospitalier Universitaire Vaudois (CHUV, Lausanne, Switzerland) [78, 79]. The IMPulse trial evaluated the maximum tolerated dose using a single-fraction delivery, escalating from 22 Gy to 28 Gy in 2 Gy increments [80]. Treatments were delivered using 9 MeV electrons at an average dose rate of 200 Gy/s (10 pulses over 90 ms) [80]. Building on this, the randomised Phase II FLASH Radiotherapy for Skin Cancer (LANCE) trial (NCT05724875), also at CHUV, aims to compare the toxicity and efficacy of FLASH-RT with conventional electron radiotherapy for cutaneous basal cell carcinoma (BCC) and squamous cell carcinoma (SCC) [81]. Patients receive either single-fraction (22 Gy) or fractionated (5 x 6 Gy in less than two weeks) treatments depending on lesion size [78]. FLASH-RT is delivered using 9 MeV electrons, with mean dose rates of approximately 220 Gy/s (10 pulses over 100 ms) for single-fraction delivery and 270 Gy/s (3 pulses over 22 ms) for fractionated delivery, whilst CONV-RT is delivered at 10 MeV [78]. A single-arm Phase I study at Henan Cancer Hospital (Zhengzhou, China; ChiCTR2400080935) is investigating the safety and acute toxicities of electron FLASH-RT for BCC and SCC [82]. Patients receive either 3 x 8 Gy or 5 x 8 Gy, with instantaneous dose rates of 82500 Gy/s and an average dose rate of 120 Gy/s (fractions and dose rates are assumed to be per day, although this was not specified by the authors) [82]. Additionally, an ongoing Phase I trial at the University of Zurich (FLASH-Skin I, NCT06549439) is evaluating the feasibility and safety of electron FLASH for melanoma [83, 84]. This study employs a mixed delivery scheme

of 3 x 9 Gy (2 fractions per week), combining FLASH-RT (2 fractions) and CONV-RT (1 fraction). Treatments are delivered using 9 MeV electrons, with average dose rates of 216 Gy/s and instantaneous dose rates of 2.4 x 10^5 Gy/s per fraction [83].

The single-arm Feasibility Study of FLASH Radiotherapy for the Treatment of Symptomatic Bone Metastases (FAST-01) (NCT04592887) trial was conducted at the Cincinnati Children's/UC Medical Center Proton Therapy Center (Ohio, USA) and used ultra-high dose rate transmission protons [85, 86]. FAST-01 showed the successful delivery of 8 Gy in a single fraction to palliative patients with bone metastases in the extremities, giving the same prescription as the standard of care CONV-RT treatment using megavoltage photons [85]. However, the use of transmission protons instead of megavoltage photons increased the skin dose, and so the patients in this trial did receive 8 Gy to the skin [85]. Despite this, FAST-01 was associated with a 67% pain relief response rate, which was comparable to that of the RTOG 9714 study of 65%, where the use of a single-fraction versus the conventional multifraction beam delivery (1 x 8 Gy versus 10 x 3 Gy) in a palliative setting was investigated [87]. Dose rates were planned as 60 Gy/s, with delivered dose rates in the range 51 Gy/s - 61 Gy/s, however, how these were defined and how they translate from pre-clinical dose rate definitions was not explicitly discussed [85]. Following on from FAST-01, the FLASH Radiotherapy for the Treatment of Symptomatic Bone Metastases in the Thorax (FAST-02) (NCT05524064), also conducted at the Cincinnati Children's/UC Medical Center Proton Therapy Center, is an active single-arm trial aiming to investigate toxicities and pain relief associated with the ultra-high dose rate technique [88, 89]. A dose of 8 Gy will be delivered in a single fraction. Similarly to FAST-01, dose rates were not explicitly defined and were only cited as a minimum of 40 Gy/s [89].

To better exploit the benefits of proton therapy, the natural progression is to utilise the Bragg peak instead of transmission beams as spread-out Bragg peak proton therapy allows for improved dose conformity with fewer beams and reduced doses to OARs com-

pared to transmission beam proton therapy [90, 91]. The use of fewer beams would also allow for an increase in dose rates delivered by each beam, making spread-out Bragg peak FLASH proton therapy more favourable than transmission beam FLASH proton therapy. The rapid progression of FLASH-RT, from pre-clinical studies to clinical trials, necessitates a full understanding of the capabilities, limitations, and safety of the treatment modality before it is fully implemented into clinical practice, with the FLASH sparing effect yet to be demonstrated for larger clinical trials. This is particularly important as there are no guidelines regarding the treatment planning process of this novel technique.

1.2.4 Beam Delivery

Different spread-out Bragg peak FLASH proton therapy (FLASH-PT) beam delivery methods, involving the use of passive scattering or active scanning, have been proposed and studied [17, 25, 59, 61, 92–97]. Transmission beam FLASH proton therapy is readily available for pre-clinical experiments and clinical use as few modifications to clinically used systems are required. However, to deliver FLASH-PT, conventional energy modulation cannot be adopted as the energy selection system is not fast enough to allow ultra-high dose rates to be achieved (energy layer switching is on the order of seconds) [98].

Previous studies have adopted the use of range shifters or ridge filters, with the inclusion of collimators, along the path of a mono-energetic proton beam [90, 99–101]. The most promising beam delivery technique for FLASH-PT is utilising a patient-specific 3D range modulator with mono-energetic protons to create a spread-out Bragg peak whilst minimising beam delivery time [98]. The mono-energetic protons traverse through the different thicknesses of the ridge filter, thereby spreading out and altering the range of the particles to produce a spread-out Bragg peak [98]. For conventional proton beam delivery systems, the use of energy degraders in the energy selection system (see Section 1.1.3) is associated with an increase in multiple Coulomb scattering

and decrease in beam intensity. This leads to significant beam loss and a decrease in dose rate [17, 95]. To be able to utilise conventional proton beamlines whilst also minimising the beam loss, thereby increasing the dose rate, minimal energy degradation is required. The mono-energetic protons should therefore be delivered at the maximum energy allowed by the treatment machine to allow for ultra-high dose rates to be achieved [95]. Further to this, a range shifter and an aperture are also inserted downstream of the modulator to set the distal range of the delivered dose to the target and to reduce dose contributions due to scattering [102].

The time scale of gantry rotation for standard proton therapy machines are drastically longer than the treatment delivery time required for FLASH-PT. Multi-beam fractions can therefore not be utilised for the ultra-high dose rate technique. To bypass this limitation, and to simplify the treatment setup due to the use of patient- and field-specific static energy degraders, it may be beneficial to deliver FLASH-PT using one-beam-per-fraction. In addition to using fewer beams to improve dose rates and normal tissue sparing, as discussed in Sections 1.2.2 and 1.2.3, the adoption of hypofractionated one-beam-per-fraction treatment schemes would also be favourable due to the implementation of patient-specific beamline components.

1.2.5 Treatment Planning

The treatment planning process forms a crucial part of the clinical implementation of a novel radiotherapy technique, as generated plans can be used to determine the feasibility of the modality. For FLASH-PT, planning studies have mainly focused on transmission beams for targets such as the brain and lungs, whereas spread-out Bragg peak plans have been produced for lung cases and arbitrary targets in water phantoms [17, 25, 95, 97, 103–105]. Without accounting for a normal tissue sparing FLASH effect, these studies show that FLASH-PT is associated with inferior plan quality compared with IMPT, likely related to both the beam delivery and treatment planning process; however, this has not been extensively explored [17, 90]. Furthermore, the incorpora-

tion of dose rates into the plan optimisation has not been needed prior to FLASH-RT, and so the software capabilities and limitations are not well understood.

FLASH-PT will likely be delivered using a single-field per fraction due to the use of patient-specific energy degraders in the beam setup. This is ideal for treatments of simple structures such as the vertebrae. However, for more advanced structures such as brain and lung targets, the use of a single-field is not an option. Few studies focusing on treatment plans for FLASH-PT delivered in one field per fraction have been conducted for spread-out Bragg peak proton beams, and no guidelines regarding the treatment planning process for FLASH-PT exists.

1.2.6 Dose Modifying Factor

Biological differences in normal tissue sparing effects can be quantified using the dose modifying factor (DMF), defined as the ratio of doses from two irradiations (eg., CONV-RT and FLASH-RT) required to produce an equivalent biological effect [106]. Pre-clinically, this ratio has been investigated for varying murine models, toxicity endpoints, doses, dose rates, and radiation types with DMFs ranging from 0.97-1.58 [43, 46, 60, 68, 71, 107]. This corresponds to up to a 58% increase in the dose required to achieve the same level of normal tissue damage under FLASH conditions compared to conventional radiotherapy, reflecting a substantial but highly variable sparing effect depending on the biological endpoint and experimental conditions. The sparing effect, and thus DMF, of FLASH-RT has also been observed to significantly differ depending on the cell type irradiated [40]. Further pre-clinical and clinical studies are required to properly quantify the DMF, and due to the variability of the factor, it might not be of interest to include it in patient dose evaluations and treatment plans yet as it may not accurately model the differential effect.

1.2.7 Dose Rate Definitions

Dose rates can be defined in a multitude of ways, and several definitions have been proposed in the literature including the percentile dose rate (DR_{prct}), the dose averaged dose rate (DADR), the average dose rate (ADR), and the instantaneous dose rate [108–110]. Although the majority of reported dose rates range between 40 and 1000 Gy/s, there is currently no standard definition of 'dose rate' in the literature, and it is still unclear which definition best describes the behaviour leading to the FLASH sparing effect [64, 73, 94, 95, 100, 103, 104, 109, 111–115]. This can become problematic if there are drastically different dose rates achieved for a patient case depending on the definition used. For most *in vivo* and *in vitro* experiments, a static beam is used and any time components due to beam scanning or radiation spot placements can be neglected [41, 45, 62]. However, for clinical proton therapy beam delivery, the use of pencil beam scanning and spot placements may impact the dose rate. Consequently, specific dose rate definitions may need to be used.

The DR_{prct} for a voxel i, is defined by Folkerts et al. [108] as:

$$DR_{prct} = \frac{D(i) - 2d_{thr}(i, t_0)}{t_1 - t_0}, \tag{1.6}$$

where $D(i)$ is the total prescribed dose (100%), $d_{thr}(i, t_0)$ (%) is a minimum dose threshold given as a percentage of the total dose, t_0 is the time at which the dose threshold at i is exceeded, and t_1 is the time at which the accumulated dose $d(i, t_1) = D(i) - d_{thr}(i, t_0)$ [108]. The DADR definition does not explicitly incorporate dose delivery time and is defined by van de Water et al. [109], for a voxel i, as:

$$DADR_i = \sum_{j=1}^{n} \frac{(d_{ij} w_j)(d_{ij} BI_j)}{\sum_{j=1}^{n} d_{ij} w_j}, \tag{1.7}$$

where j represents a spot, w is the associated spot weight, d is the dose-influence matrix, and BI is the beam intensity [109]. The ADR can be defined as the total dose delivered divided by the total irradiation time [110]. Further investigations into

the impact of dose rate definitions on the achievable dose rates and the associated biological sparing effects will need to be conducted in order to determine which is the most applicable for ultra-high dose rate proton therapy.

1.3 Core Thesis Aims

The rapid progression of FLASH-PT, from pre-clinical studies to clinical trials, necessitates a full understanding of the capabilities, limitations, and safety of the treatment modality before it is implemented into clinical practice. Few studies focusing on treatment plans for FLASH-PT delivered in one-beam-per-fraction have been conducted for spread-out Bragg peak proton beams, and no guidelines regarding the treatment planning process for this technique exists. The work in this thesis aims to determine whether spread-out Bragg peak FLASH-modified proton therapy beam delivery can achieve comparable treatment plans to that of intensity modulated proton therapy. This thesis will tackle these questions in three parts by:

1. Investigating the feasibility and potential constraints of spread-out Bragg peak FLASH proton therapy treatment planning to determine how the FLASH-modified proton therapy beam delivery may impact the treatment plans generated for clinically relevant target sites and sizes.

2. Evaluating the capabilities of the treatment planning software, and how these can be exploited to improve both the treatment plan quality of the ultra-high dose rate plans, and how this may impact the dose rate.

3. Exploring how the hardware may be modified to further improve plan quality by changing the initial energy of the FLASH proton therapy beams, determining what impact this has on plan quality, and evaluate the dose rates for three different beam delivery scenarios:

   (a) A realistic scenario representing an existing beamline.

   (b) An improved scenario, with increased momentum acceptance.

(c) A hypothetical, best-case, scenario of using a variable energy cyclotron which will allow for a constant beam current, independent of initial beam energy.

Chapter 2

Materials and Methods

2.1 Beam Delivery

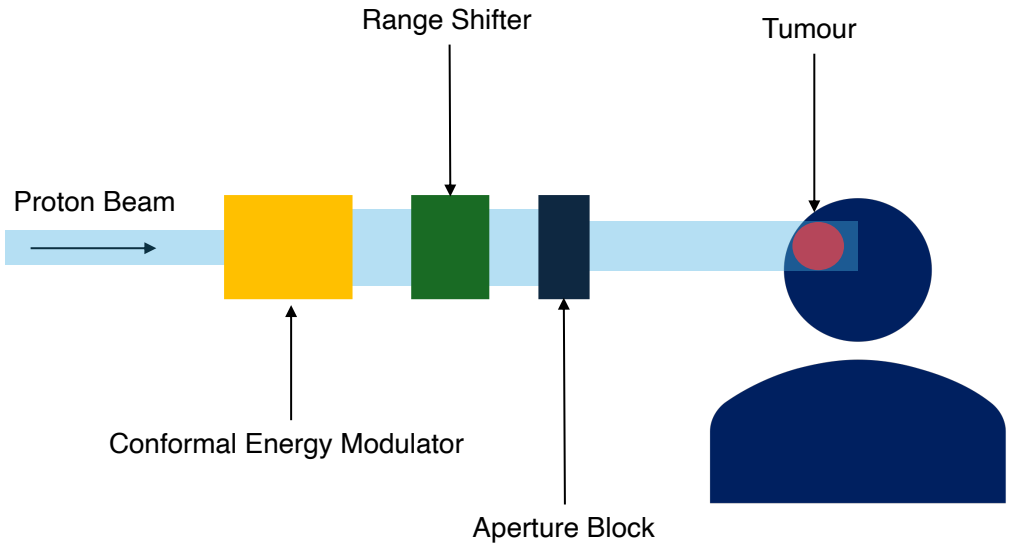


Figure 2.1: A schematic representation of the FLASH-PT beam setup used to deliver the ultra-high dose rate protons to the target. Mono-energetic spot scanned protons travel through a conformal energy modulator, a range shifter, and an aperture, before reaching the target.

All treatment plans were simulated for use on the IBA Proteus®Plus (Louvain-la-Neuve, Belgium) machine, with protons produced and accelerated using a quasi-continuous isochronous cyclotron with maximum beam energy of 230 MeV and beam currents of 300 nA and 500 nA for intensity modulated proton therapy (IMPT) and spread-out

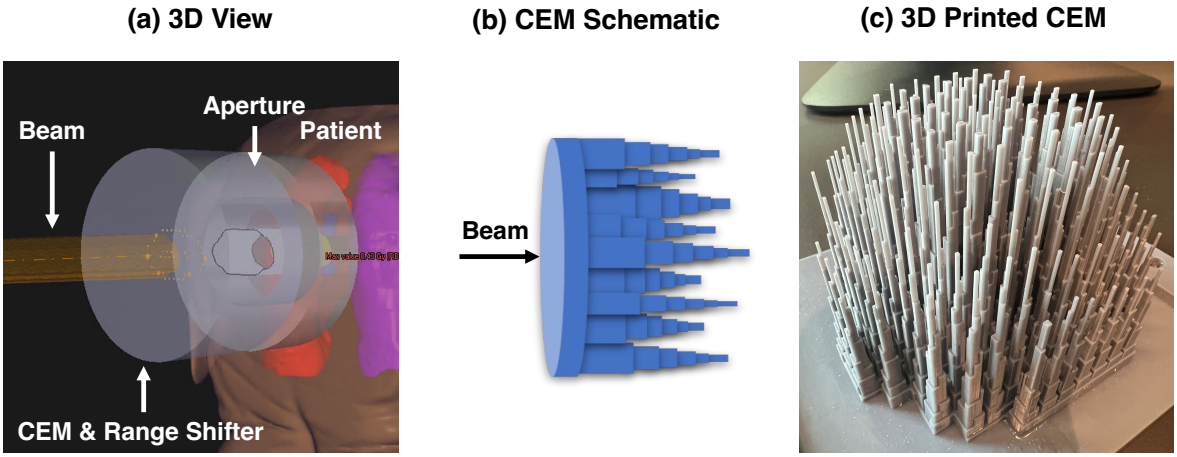


Figure 2.2: Visualisation of the spread-out Bragg peak FLASH proton therapy beam delivery and conformal energy modulator (CEM). (a) Beam delivery components in a 3 dimensional (3D) view, highlighting the incoming beam, CEM, range shifter, aperture, and patient. (b) Schematic of the CEM. (c) 3D printed CEM, photo courtesy of Rasmus Nilsson, RaySearch Laboratories AB, Stockholm, Sweden.

Bragg peak FLASH proton therapy (FLASH-PT), respectively.[1] Pencil-beam scanning (PBS) was adopted for both beam delivery techniques. To produce spread-out Bragg peak FLASH protons, mono-energetic spot scanned protons, at the maximum beam energy, travel through a conformal energy modulator (CEM), an aluminium range shifter, and a brass aperture block, before reaching the target, as illustrated in Figure 2.1. The CEM is a patient-specific ridge filter, also known as a 'hedgehog', which modulates the protons to the 3D shape of the target, as illustrated in Figure 2.2. The range shifter is used to set the distal range of the delivered dose to the target, and the aperture reduces the dose contributions from scattered particles, thereby sharpening the penumbra.

2.2 Patient Data

Different types of patient cases were considered in this work depending on the study conducted. For studies investigating the feasibility of FLASH-PT treatment planning using a research treatment planning system (TPS), a variety of target sites were con-

[1]Chapter 2 is based on the published work by Lövgren et al., Feasibility and Constraints of Bragg Peak FLASH Proton Therapy Treatment Planning, *Frontiers in Oncology*, 2024 [34] and Lövgren et al., The Impact of Dose Rate Optimisation and Robust Optimisation on FLASH Proton Therapy Treatment Plan Quality and Dose Rates, *Frontiers in Oncology*, 2025 [35].

sidered. This allowed for the evaluation of feasibility, as well as constraints, that may arise depending on different target locations and target sizes. From this, we found that targets located in the brain appeared to be of most benefit when using FLASH-PT, informing the targets considered in the final study in this thesis.

The treatment regimens considered in this work were selected to reflect clinical scenarios in which a FLASH effect is most likely to be observed. Hypofractionated treatments, with a small number of high-dose fractions, are expected to maximise the FLASH sparing effect, as higher doses per fraction and fewer beam deliveries are associated with increased dose rates and reduced temporal separation between dose deliveries. Therefore, single- and few-fraction treatment schemes were prioritised in this study. This choice is further supported by previous studies discussed in Section 1.2.2, which demonstrated that the magnitude of the FLASH sparing effect decreases with increasing number of fractions and beam deliveries. Therefore, single- and few-fraction treatment schemes were considered most appropriate for evaluating the potential benefits of FLASH-PT in this work.

The patient data was provided as Digital Image and Communications in Medicine (DICOM) files containing computed tomography (CT) scans with contours of organs at risk (OARs) and target structures delineated by clinicians at the Skåne University Hospital (Lund, Sweden).

2.2.1 Feasibility Studies: Multiple Target Types

The first two studies, making up Chapters 3 and 4, investigate the feasibility and constraints of FLASH-PT treatment planning, the impact of using dose rate optimisation as part of the treatment planning process, and the difference between margin-based planning versus robust optimisation on the FLASH-PT treatment plan quality and dose rates. The use of different target locations and target sizes were therefore of interest, motivating the use of ten patient cases consisting of bone (vertebrae) (n = 3), brain

(n = 4), and lung (n = 3) targets. The target size, total prescribed dose, and number of fractions for each patient case are outlined in Table 2.1. Target volumes ranged between 1.42 cm^3 - 324.09 cm^3, with a median volume of 16.18 cm^3. Beam angles used for these cases were chosen such that exposure to normal tissues, and overlap between beams, were minimised. For the conventional IMPT plans, the number of fields per fraction was defined to match the total number of treatment fractions. For example, for a three-fraction IMPT regimen, three fields were delivered within each fraction. Information on beam angles used can be found in Table A.1 in Appendix A.

Table 2.1: Table outlining the target type, target size (cm^3), prescribed dose (Gy [RBE]), number of fractions, and the setup and range uncertainties used in the treatment plans for each patient case for the feasibility studies in Chapters 3 and 4. The dose is defined in terms of relative biological effectiveness (RBE).

Patient	**Target Size (cm^3)**	**Prescribed Dose (Gy [RBE])**	**Number of Fractions**	**Setup Uncertainty (mm)**	**Range Uncertainty (%)**
Bone 1 (vertebrae)	62.20	8	1	7	3.5
Bone 2 (vertebrae)	324.09	8	1	8	3.5
Bone 3 (vertebrae)	207.07	8	1	9	3.5
Brain 1	19.71	20	2	3	3.5
Brain 2	1.42	30	3	3	3.5
Brain 3	2.26	30	3	4	3.5
Brain 4	12.65	34	2	3	3.5
Lung 1	11.98	45	3,4,5	3	4.5
Lung 2	10.66	45	3,4,5	3	4.5
Lung 3	21.61	45	3,4,5	3	4.5

2.2.2 Data Informed Study: Brain Targets

Following on from the studies in Chapters 3 and 4, targets located in the brain were associated with the least compromise in FLASH-PT plan quality compared to IMPT. Therefore, for the study discussed in Chapter 5, we decided to only investigate the use of FLASH-PT on 10 brain cases, all who had previously received conventional proton therapy. Patient information for Chapter 5 is outlined in Table 2.2. Tumour volumes ranged between 9.98 cm^3 - 92.97 cm^3, with a median tumour volume of 36.70 cm^3 (Table 2.2). The clinical proton therapy treatment plans were available; therefore, the exact same beam angles used for the patient treatments were utilised in the simulation

studies presented in Chapter 5. For the conventional IMPT plans, the number of fields per fraction was again defined to match the total number of treatment fractions. Information on beam angles used can be found in Table B.1 in Appendix B.

Table 2.2: Table outlining the tumour volume (cm^3), total prescribed dose (Gy [RBE]), the number of fractions, and the setup and range uncertainties used for robust optimisation for the study discussed in Chapter 5. The dose is defined in terms of relative biological effectiveness (RBE).

Patient	**Target Size (cm^3)**	**Prescribed Dose (Gy [RBE])**	**Number of Fractions**	**Setup Uncertainty (mm)**	**Range Uncertainty (%)**
1	92.97	30	3	4	3.5
2	87.95	30	3	3.5	3.5
3	31.59	30	3	4	3.5
4	75.38	30	3	4	3.5
5	28.04	30	3	4	3.5
6	9.98	30	3	3	3.5
7	29.41	30	3	3	3.5
8	41.80	30	3	3.5	3.5
9	15.21	30	3	3	3.5
10	42.56	30	3	4	3.5

2.3 Treatment Planning

All treatment plans utilised inverse planning, the spread-out Bragg peak, and pencil beam scanning.

2.3.1 Intensity Modulated Proton Therapy

The IMPT plans were generated using conventional beam delivery as described in Section 1.1.4, utilising PBS, multi-field optimisation, and multi-field fractions. The intensity modulation process uses an energy selection system, as described in Section 1.1.4. The IMPT plans were created such that, for each field, there were several spots scanned across different energy layers, corresponding to the different depths of the target, as highlighted in Equation 1.1 in Section 1.1. Dose objectives were implemented for target and OAR structures, with the optimisation utilising an objective function as outlined in Section 1.1.5. Spot sizes and spot spacings were either pre-defined, or

had a default value assigned which could change depending on the treatment plan optimisation in order to compromise between the OAR and target constraints with the aim of minimising the objective function.

2.3.2 Spread-Out Bragg Peak FLASH Proton Therapy

FLASH-PT treatment planning utilises the concept of a reference "mother" IMPT plan. This reference plan uses multiple energy layers, and forms the basis of which the single-energy layer FLASH-PT plan, and CEM, is based on. Consequently, FLASH-PT plans have a multitude of optimisation parameters which are dependent on each other, including the shape of the CEM, the spot scanning delivery pattern, and the weighting of the individual spots [116]. Here, we outline the main components of the FLASH-PT treatment plan generation and optimisation, going from the reference IMPT plan to the final single-energy layer FLASH-PT plan [116]:

1. A reference PBS IMPT plan with multiple energy layers is created using the same principles as conventional proton therapy treatment planning, with the addition of a range shifter and an aperture.

2. The reference plan is optimised with pencil beam spots of lateral spread σ_{FLASH}, where σ_{FLASH} is the standard deviation of the Gaussian obtained with the FLASH-modified beam setup (Figure 2.1).

3. The CEM is generated based on the reference IMPT energy layer fluence, where fluence is the total number of particles crossing a unit area .

4. The multi-energy layer reference plan is converted into a single-energy layer FLASH-PT plan, with the CEM creating spread-out Bragg peaks for the mono-energetic protons.

5. The objective function for the generation and optimisation of the CEM is defined as the difference between the reference IMPT fluence and the fluence achieved in the single-energy layer plan, which is dependent on the CEM. The shape of the

CEM is iteratively modified and optimised until the objective function reaches a minimum, and the corresponding single-energy layer FLASH-PT plan is the closest match in terms of reproducing the reference IMPT plan.

In order for the conversion of the multi-energy layer plan to the single-energy layer FLASH-PT plan to be feasible, all reference IMPT spots across the different energy layers must be aligned in the direction of the incoming protons. The reference IMPT plan requires spot properties to be defined for each energy layer; however, because FLASH-PT uses a single energy, the IMPT energy layers are treated as virtual, and the spot properties for all layers are set equal to those of the maximum-energy spots. The beam data library for the FLASH-PT plans therefore only contain spot properties for the maximum energy layers, regardless of the energy used to generate the reference plans [116]. Further to this, dose rates will need to be computed for the reference IMPT plan so that dose rate optimisation can be incorporated into the treatment planning process. To do so for the single-energy layer FLASH-PT plan, whilst maintaining multiple energy layers for the reference plan, it is assumed that all of the reference IMPT energy layers are delivered at the same time.

2.3.3 MIROpt and ConformalFLASH

A research treatment planning system, MIROpt (now open-source and known as OpenTPS), produced by UCLouvain and accessed through OpenREGGUI, was used to generate IMPT plans in Chapter 3 and 4 [117]. MIROpt is a MATLAB-based simulation software which utilises a Monte Carlo engine known as MCsquare (many-core Monte Carlo) [118, 119]. MIROpt, along with a ConformalFLASH library (`www.openFLASH.software`), developed by Ion Beam Applications SA (IBA), was used to simulate the FLASH-PT plans. This ConformalFLASH library implements the beam setup shown in Figure 2.1, and allows for dose rate calculation and optimisation. The FLASH-PT plan generation, and CEM production and optimisation, follow the steps outlined in Section 2.3.2. The CEM is made from a 3D printed plastic-like material called 'Tusk', with a density of 1.19 g/cm^3 [116]. The maximum field-size implemented in the Con-

formalFLASH library for this beam setup is 8 cm × 8 cm × 8 cm [116].

The generate FLASH-PT treatment plans with this library, manual input and optimisation of the spot spacing (mm), energy layer spacing (mm), target margin (mm), and aperture margin (mm) was required. The target margin dilates the target volume, allowing for spot placements arount the target structure, thereby reducing setup errors due to the use of the static energy modulator. Further to this, the aperture margin dilated the target volume to define the aperture hole [116]. Manual inputs of the spot and layer spacings was also required for the IMPT plans.

Robust optimisation was not available for the FLASH-PT plans generated using the MIROpt TPS. Therefore, to allow for fair comparisons between the FLASH-PT and IMPT treatment plans, all plans in Chapter 3 were simulated using margin-based planning. Furthermore, a couch angle of 0° was used for all MIROpt plans as the TPS did not allow for other couch angles when simulating the treatment plans.

The University of Oxford Advanced Research Computing (ARC) facility was used to simulate all MIROpt treatment plans due to the computationally expensive nature of Monte Carlo simulations and the ability to run simulations in parallel.

2.3.3.1 Dose Rate Optimisation and Calculation

The ConformalFLASH library allows for dose rate optimisation, an optimisation objective which has not been part of conventional treatment planning before. This meant that, in addition to the dose objectives in the treatment planning calculation and optimisation, dose rate objectives were also considered and optimised.

The dose rate objective function used in this work evaluates the minimum average of the 98^{th} percentile dose rate, as shown in Listing 2.1, and defined in Equation 1.6. For a given OAR, the objective function aims to increase the dose rate such that it

achieves the reference dose rate given, in the OAR voxels which receive a certain dose threshold. More specifically, the input parameters in the dose rate objective for a specific OAR are: a minimum (total) dose to each OAR voxel (D_{thr} (Gy)), a reference dose rate (DR_{thr} (Gy/s)), and an importance weight.

The objective function works for a given OAR structure, evaluates the dose and dose rate on a voxel-by-voxel basis, and averages the dose rate across all voxels receiving a dose $\geq D_{thr}$. If $DR_{Av} < DR_{thr}$, where DR_{AV} represents the average dose rate, then a penalty proportional to (DR_{AV} - DR_{thr})^2 is added to the objective function [116]. In this work, D_{thr} = 2 Gy and DR_{thr} = 40 Gy/s were set as the minimum dose and reference dose rate thresholds, respectively. Low importance weights ($\sim 10^{-8}$ on a scale of 0 - 1) were assigned to the dose rate objectives to ensure that the dose constraints were prioritised, and plan quality not significantly sacrificed, whilst still involving dose rate objectives in the optimisation process.

```
- name: minDR          # Type of objective function:  minDR
                         (minimum average of the  98th
                         percentile dose rate)
    ROIname: ct_OAR    # Name for the ROI to which the
                         objective function needs to be
                         applied
    Dref: 2            # Dose (Gy / FRACTION) in OAR above
                         which the dose rate condition must
                         be respected
    DRref: 40          # Reference dose rate in Gy/s
    impw: 0.00000001   # Importance weight for the current
                         objective function (impw > 0)
```

Listing 2.1: Simplified version of a dose rate objective function in the MIROpt YAML configuration file, outlining the type of objective, the organ at risk it should be evaluated for, the minimum dose threshold it should be applied to, the mimimum dose rate, and the importance weight of the objective function.

Dose rates were calculated using the ConformalFLASH library as part of the treatment planning process using Equations 1.6 and 1.7 using the dose influence matrices and the defined beam current. In this context, dose and dose rate correspond to local (voxel-level) quantities, rather than whole-organ or field-averaged values, unless otherwise stated.

In conventional spot-scanning proton therapy, the dose is delivered as a sequence of individual pencil beam spots, typically ranging from a few hundred up to 3 x 10^4 spots depending on the tumour size, with delivery times per spot ranging from approximately 0.5 ms to 100 ms [120]. While the instantaneous dose rate within an individual spot may be high, the effective dose rate at a given voxel is reduced due to the sequential delivery of spots across the field and the resulting temporal gaps between dose deposition events. This leads to relatively low effective dose rates compared to those

required for the FLASH effect. In contrast, the ConformalFLASH approach assumes that contributions from different energy layers at a given (x,y) position are delivered effectively simultaneously, leading to more continuous dose deposition at the voxel level and consequently higher effective dose rates [116].

The use of a CEM does not significantly alter the total number of protons delivered (i.e. the beam current); however, it modifies the energy distribution and spatial–temporal deposition of dose. By delivering contributions from multiple energy layers simultaneously at a given (x,y) position, the CEM reduces the temporal separation between dose deposition events at the voxel level. As a result, the effective dose rate experienced within a voxel can be increased compared to conventional spot-scanning delivery, despite a similar underlying proton flux.

More information on the FLASH-PT beam delivery, CEM generation, and dose rate optimisation can be found on the conformalFLASH github: `openFLASH/conformalFLASH/wiki/algorithms` [116].

2.3.4 RayStation 11B FLASH

A research version of RayStation® (RaySearch Laboratories AB, Stockholm, Sweden), RayStation 11B FLASH, was used to generate FLASH-PT and IMPT treatment plans for the studies discussed in Chapters 4 and 5. The workstation used for simulating data in RayStation was a A 13th Gen Single Intel Core i9-13900K 3.00 GHz processor with 64.0 GB of RAM and a Nvidia RTX A5000 (24 GB) graphics card.

The FLASH-PT plans were generated using the same principle as MIROpt, as outlined in Section 2.3.2. The maximum beam energy for these plans was implemented as 228 MeV, which represents the measured energy at the isocentre. The CEM is made from a 3D plastic called Accura® ClearVue with a density of 1.17 g/cm^3, and the maximum recommended field-size implemented in RayStation 11B FLASH, for which the

dose has been validated, is 10 cm × 10 cm × 8.4 cm [102]. FLASH-PT and IMPT treatment plans were simulated using the principles described in Sections 2.3.2 and 2.3.1, respectively. For the FLASH-PT plans, the default initial beam energy used was the maximum machine energy, with a beam current of 500 nA at the isocentre. RayStation allows for robust optimisation for the FLASH-PT treatment plans, as well as the use of a rotating couch.

2.3.4.1 Robust Optimisation

For the patient cases considered in the feasibility studies (Table 2.1), setup uncertainties were implemented as the difference between clinical target volume (or gross tumour volume if a clinical target volume was not available) and planning target volume, and were set as 3.5% for bone and brain targets and 4.5% for the lung targets, as shown in Tables 2.1 and 2.2. In the feasibility studies, we were interested to see if the use of robust optimisation could improve target coverage whilst also keeping OAR doses within the acceptable bounds of the OAR dose protocols. Therefore, we did not set a robustness pass rate (in the worst case scenario) requirement for the work in Chapter 4. The results in Chapter 4 found that robust optimisation did improve target dose coverage, but could not achieve 100% robustness pass rate whilst also achieving OAR doses which adhered to dose protocols. For the study in Chapter 5, we therefore decided to investigate how the OAR doses could be reduced, and implemented a requirement of 100% robustness pass rate in the worst-case scenario which was required for D95% $\geq$ 95% and D2% $\leq$ 105%. Plans were optimised and modified until this criteria was achieved, allowing for an improved plan comparison as each individual plan had to adhere to the same target dose criteria. The nominal (non-shifted) scenarios were considered in the plan evaluations, and the worst-case scenarios were considered when explicitly stated.

2.3.4.2 Dose Rate Calculation

Dose rate calculations were performed using scripts provided by RaySearch, which allowed for user-input and modifications if required. The scripts were set up to evaluate the percentile dose rate (Equation 1.6) and the dose averaged dose rate (Equation 1.7). The average dose rate (Section 1.2.7) was added later in an updated version of the RayStation 11B FLASH system. The scripts evaulated the dose rate, for the different definitions, with the assumption of the maximum beam energy being used, as discussed in Section 1.2.4, and therefore the maximum beam current of 500 nA at the nozzle. Chapter 5 considers non-maximal energy beam delivery and treatment planning. Lower initial beam energies are associated with reduced beam currents. The dose rate scripts were adapted such that the corresponding beam current to initial beam energy was implemented for the non-maximal energy dose rate calculations. More information regarding the beam currents for the beam energies in Table 5.1 can be found in Chapter 5.

2.3.5 Dose Optimisation and Fractionation Schemes

The IMPT spots were placed in a hexagonal pattern for optimal dose coverage, and a constant relative biological effectiveness (RBE) of 1.1 was assumed for both IMPT and FLASH-PT plans. As discussed in Section 1.2.6, pre-clinical studies have found varying values for the dose modifying factor. Therefore, for simplicity in this project, and since a radiobiological model describing the FLASH effect has not been developed, a dose modifying factor of 1 was assumed for all treatment plans.

Multi-field optimisation (MFO), where multiple beams are used to cover the entire target and the dose contribution of each beam is considered in the dose calculation and optimisation of the other beams, was adopted for the IMPT plans. The use of MFO improves target coverage whilst reducing the dose to surrounding OARs. This makes MFO the standard optimisation technique for proton therapy in the clinic [17]. However, the use of the patient-specific FLASH-PT beam setup necessitates the treat-

ments to be delivered using one-beam-per-fraction, with the intention of delivering the treatment using daily fractions. The FLASH-PT beams were therefore optimised independently of each other using single-field optimisation (SFO). Hence, the number of beams used were determined by the number of fractions required, and varied depending on the patient case. For more simplistic target sites such as bone (vertebrae) the use of a single-fraction single-field treatment was feasible; however, for treatments of more complex target sites such as the brain or lung, the use of a single-field is not an option. Multiple beams, delivered using one-beam-per-fraction, with different beam angles, were therefore used for the brain and lung targets in this thesis. The exact same beam angles and number of fractions used for the FLASH-PT plans were also used for the IMPT plans.

For plans requiring multiple beams, the total FLASH-PT dose was evaluated by summing the SFO plans across all fractions. Standard conventional plans are delivered using multiple beams within a fraction, and MFO. To allow for a fair comparison between standard IMPT and FLASH-PT, MFO IMPT plans were generated. SFO IMPT plans were also produced such that the impact of SFO versus MFO on treatment planning quality could be evaluated.

The number of fractions considered for each patient case are outlined in Tables 2.1 and 2.2. In line with standard fractionation schemes used for lung targets (Table 2.1), we adopted the use of 3 and 5 fraction treatments. However, as the number of fractions increase, the dose per fraction decreases, thereby reducing the dose rate. We therefore wanted to investigate whether the use of 4 fractions could offer a middle ground, with better dose conformity than 3 fractions, but with potentially higher dose rates than the 5-fraction plans, and therefore investigated the use of 3, 4, and 5 fractions for the lung patients.

2.4 Plan Evaluations and Comparisons

2.4.1 Dose

All plans were normalised such that $D_{50\%} = D_{prescribed}$, that is, the dose to 50% of the target volume (i.e., the median dose) is equal to the prescribed dose. Target dose optimisation constraints were set as $D_{95\%} \geq 95\%$, and $D_{2\%} \leq 105\%$ of the relative target volumes. With regard to doses to OARs, no established treatment protocols currently exist for FLASH-PT. Therefore, stereotactic body radiotherapy (SBRT) protocols were used for reference due to their use of hypofractionation, making them more applicable to the beam delivery method considered in this work, as discussed in Section 2.3.5. For the patient cases considered in Table 2.1, the following protocols were used: RTOG 0631 for the bone targets, Dose–Volume Constraints fOr oRganS At risk In Radiotherapy (CORSAIR) for both brain and lung targets, and the UK Consensus on Normal Tissue Dose Constraints for Stereotactic Radiotherapy for the lung cases [121–123]. For the patient cases presented in Table 2.2, additional reference SBRT protocols were provided by Skåne University Hospital (Lund, Sweden), courtesy of Ingrid Fagerström Kristensen, for the work conducted in Chapter 5. It should be noted, however, that SBRT targets are typically smaller than those considered in this work. All treatment plans were optimised such that the OAR doses adhered to the protocols where possible.

Dose distribution maps and dose volume histograms (DVHs) were used to qualitatively compare the dose distributions of MFO IMPT, SFO IMPT, and FLASH-PT plans. Quantitative comparisons were made using DVH parameters, allowing for evaluations of dose statistics, dose conformity, and target dose homogeneity. Statistical comparisons of dose and dose rate data were evaluated using the two-sided Wilcoxon Rank Sum test, using the *ranksum* function in MATLAB, with significance defined for $p < 0.05$ [119]. Given two independent samples, which can be of different lengths, the Wilcoxon Rank Sum test evaluates whether the samples originate from continuous distributions with the same median, against the alternative of a difference in medians

[119]. The Radiation Conformity Index (RCI) was defined as the ratio of the target volume (V_{target}) to the total volume receiving 95% of the prescribed dose ($V_{95\%}$) [124]:

$$RCI = \frac{V_{target}}{V_{95\%}}. \tag{2.1}$$

The homogeneity index (HI) was defined using the ICRU Report 83 as [125]:

$$HI = \frac{D_{2\%} - D_{98\%}}{D_{50\%}}, \tag{2.2}$$

The Spearman's Rank Correlation Coefficient (ρ_{SRC}), and the Pearson Correlation Coefficient (ρ_{PCC}) were used for further comparisons of the dose statistics. For the feasibility studies, and patients shown in Table 2.1, the dose distributions were evaluated on the clinical target volume (CTV), except for Brain 2, Brain 3, and Brain 4, where no CTV was available and the gross tumour volume was used instead. The CTV was used for all patient cases in Chapter 5, with patients outlined in Table 2.2.

2.4.2 Dose Rates

In this work, we defined dose rate coverage as the relative number of non-target voxels which receive a total dose $\geq x$ Gy at dose rates $\geq y$ Gy/s, where x and y are variable dose and dose rate thresholds, respectively.

Chapter 3

Feasibility and Constraints of Spread-Out Bragg Peak FLASH Proton Therapy Treatment Planning

3.1 Introduction

The rapid progression of FLASH proton therapy, from pre-clinical studies to the successful FAST-01 trial and ongoing FAST-02 trial, reinforces the need to understand the feasibility and potential constraints that may arise for the clinical implementation of the novel modality [86, 88].[1] Ultra-high dose rate transmission beam proton therapy, used in FAST-01 and FAST-02 (Section 1.2.3), has shown promising results, however, the technique does not leverage the associated benefits of the Bragg peak. The advantages include improved dose conformity whilst reducing the number of beam required, and the elimination of exit doses due to the finite range of protons, thereby reducing doses to organs at risk (OARs) when compared to transmission beams [90, 91].

With regards to ultra-high dose rate proton beam delivery, the use of fewer beams for Bragg peak proton therapy compared to transmission beams, will increase the dose delivered by each beam, subsequently increasing the dose rates for each beam. This makes the use of Bragg peak proton therapy more suitable for ultra-high dose rate

[1] Section 3.1 is based on the published work by Lövgren et al., Feasibility and Constraints of Bragg Peak FLASH Proton Therapy Treatment Planning, *Frontiers in Oncology*, 2024 [34].

beam delivery compared to the use of transmission beams. Previous studies, comparing the use of both Bragg peak and transmission beam FLASH proton therapy, found that the ultra-high dose rate techniques were associated with worse plan qualities compared to their conventional counterparts [17, 90]. The degraded plan quality could be attributed to the FLASH-modified beam delivery and the treatment planning process, however, as the use and evaluation of dose rates as part of the treatment planning process has not previously been explored, the capabilities and limitations to both the FLASH-modified hardware and software are not well understood.

Few studies focusing on spread-out Bragg peak FLASH proton therapy (FLASH-PT) treatment plans delivered in one-beam-per-fraction, when compared directly to intensity modulated proton therapy (IMPT) treatment plans, have been conducted. Due to the novelty of the treatment delivery technique, there are no guidelines for ultra-high dose rate proton therapy treatment planning using a one-beam-per-fraction delivery. The impact of the FLASH-modified beam setup, such as enlarged spot sizes and increased spot-to-spot distances, on the achievable treatment plan quality has not been well established either. Further to this, the ability of alternative beam setups and treatment planning optimisations to mitigate for the degraded plan quality has not been explored.

In this Chapter, we aim to investigate the feasibility and constraints of FLASH-PT treatment planning. Our aim is to determine whether clinically acceptable FLASH-PT treatment plans can be generated using a FLASH-modified beam setup. The FLASH-PT treatment plans will be compared to IMPT plans. Due to the variations in biological (FLASH) sparing effects observed following irradiations at ultra-high dose rates, along with the uncertainty of whether the FLASH effect will be elicited, we have opted to not consider any biological FLASH effect in this work. The purpose of this is to compare the delivered dose distributions, with the aim of delivering FLASH-PT beams and doses that match that of conventional proton therapy. This will ensure that

any additional sparing which may occur due to the use of ultra-high dose rates will be of benefit to the patient.

3.2 Materials and Methods

As a consequence of the rapid progression of FLASH-PT, there was limited availability of treatment planning systems (TPSs) that had implemented ultra-high dose rate spread-out Bragg peak protons. An exception to this was the ConformalFLASH library developed by Ion Beam Applications SA (Louvain-la-Neuve, Belgium) (IBA), and implemented into the MIROpt TPS (see Section 2.3.3). At the time, the ConformalFLASH library was not open-source, and any software issues had to be communicated directly to IBA, as they could not be resolved by the end user. The library became open-source around 2023. Both FLASH-PT and IMPT plans in this Chapter were simulated using the MIROpt TPS along with the ConformalFLASH library, outlined in Section 2.3.3; with plans generated using the IMPT and FLASH-PT planning methods described in Sections 1.1.4 and 2.3.2, respectively.

As this Chapter focuses on the feasibility of FLASH-PT treatment planning, ten patient cases with different target sites such as bone (n = 3), brain (n = 4), and lung (n = 3), were considered. More detailed information regarding the patient data can be found in Section 2.2.1. The optimisation objectives used for an example brain case can be found in Listing A.1 in Appendix A. Margin-based planning was adopted for all treatment plans, with plans optimised for the planning target volume and evaluated on the clinical target volume. For Brain 2, Brain 3, and Brain 4, the gross tumour volume was used instead. Any subsequent references to target dose refer to dose delivered to the clinical target volume, or to the gross tumour volume in the case of Brain 2, Brain 3, and Brain 4.

Ultra-high dose rate spread-out Bragg peak protons are delivered to the target using mono-energetic (230 MeV) spot scanning, with the scanned protons traversing through

a patient- and field-specific conformal energy modulator (CEM), a range shifter, and an aperture, with the beam delivery described in Section 2.1. Due to the use of the patient- and field-specific CEM, a one-beam-per-fraction delivery was adopted for the FLASH-PT plans, along with the use of single-field optimisation, as discussed in Section 2.3.5. In contrast, conventional IMPT plans were optimised using multi-field optimisation (MFO), as described in Section 1.1.5. The use of SFO, in combination with the FLASH-modified beam delivery, may influence FLASH-PT plan quality compared to IMPT plans optimised with MFO. To isolate the effect of SFO, IMPT plans using SFO were also generated alongside the MFO IMPT plans. This allowed for direct comparisons between IMPT and FLASH-PT plans, both optimised with SFO, to determine any differences which are not due to the one-beam-per-fraction optimisation. Individual fraction plans for FLASH-PT and IMPT were subsequently summed to allow comparison of total dose distributions with those from MFO IMPT plans.

Spot and layer spacings were manually selected and optimised for both IMPT and FLASH-PT plans. As discussed in Section 2.3.3, the generation of FLASH-PT plans requires the manual input of both a target margin and an aperture margin. The target margin essentially defines the margin of spot placement, whilst the aperture margin defines the aperture opening. Both margins were manually selected and optimised as part of the treatment planning process with spacings and margins outlined in Tables A.8 - A.10 in Appendix A.

Dose rate optimisation was incorporated into the treatment planning system through the ConformalFLASH library, as described in Section 2.3.3.1. Dose rates were optimised using the 98^{th} percentile dose rate definition described in Section 1.2.7. The dose rate objective specifies a minimum dose threshold (D_{thr}) for a defined OAR structure, together with a reference dose rate (DR_{thr}) to be optimised for regions of the OAR receiving at least D_{thr}. In this study, D_{thr} = 2 Gy and DR_{thr} = 40 Gy/s were applied. As with standard dose objectives, an importance weight was assigned to each

dose rate objective. However, it was observed that dose rate optimisation using standard importance weights dominated the overall treatment plan optimisation, resulting in degradation of plan quality. Consequently, relatively low importance weights were selected for the dose rate objectives to mitigate this effect and preserve overall plan quality, as highlighted in Section 2.3.3.1.

To generate files containing the dose rate information for an OAR for a given simulation, a dose rate objective had to be included in the optimisation for that particular OAR structure. However, if a dose rate objective was defined for an OAR that ultimately received no dose (and therefore no dose rate), the treatment planning system would crash and terminate. In principle, this issue could be addressed by first generating a treatment plan without dose rate objectives, identifying which OARs received dose, and excluding the remaining OARs when introducing dose rate objectives into the optimisation. In practice, however, the inclusion of dose rate objectives could alter the resulting dose distribution and, consequently, the doses delivered to OARs. Essentially, an OAR that previously did not receive any dose could potentially receive dose following the use of dose rate optimisation. This behaviour made it difficult to, in advance, determine which OARs should be assigned dose rate objectives to ensure that dose rate data could be generated and analysed. Consequently, a time-consuming iterative workflow was required, particularly because dose rates were calculated at the end of the optimisation process, meaning that software failures would only occur at the final stages of the simulation. Treatment plans were first optimised with all relevant OARs included, after which dose rate objectives were introduced sequentially, one OAR at a time. If the inclusion of a particular dose rate objective caused the software error, that objective was excluded and the next OAR was tested. Further to this, another common cause of the treatment planning system failure was due to the limited physical space between the CEM and the range shifter in the treatment head for certain beam angles. Certain beam angles had to be adjusted in response to this size constraint, details on the beam angles used can be found in Table A.1 in Appendix A.

Dose rate coverage was defined as the relative number of non-target voxels receiving total doses ≥ 2 Gy at dose rates ≥ 40 Gy/s, and were evaluated for each organ at risk within each individual fraction. Dose rate coverages below 1% were excluded as values below this limit were smaller than the associated uncertainty of the simulated data.

All treatment plans were evaluated and compared using the methods described in Section 2.4, and a relative biological effectiveness (discussed in Section 1.1.1) of 1.1 was assumed for all IMPT and FLASH-PT plans.

3.3 Results

The field size of 8 cm $\times$ 8 cm $\times$ 8 cm implemented by the ConformalFLASH library imposed a size constraint on the targets that could be included in this study.[2] This was due to the limitation in the physical space available between the CEM and the range shifter in the FLASH-PT adapted beam nozzle. Treatment plans could therefore not be simulated for targets with width (inline and crossline) above 70 mm. Patient cases Bone 1, Bone 2, Bone 3, and Brain 1 all exceeded the target size limit and therefore had to be excluded from the study.

A minimum angle criterion of $\geq 40°$ between each adjacent beam was chosen to reduce beam overlap and hotspots for all SFO plans. However, the combination of target size and margins for spot placements, and therefore the CEM size, sometimes exceeded the 70 mm depending on which beam angle was used. FLASH-PT plans for three cases could therefore not adhere to the minimum angle criterion: Lung 1 (5 fractions) and Lung 3 (3 and 5 fractions).

IMPT MFO achieved the imposed target dose constraints, with $D_{95\%} \geq 95\%$ and

[2]Section 3.3 is based on the published work by Lövgren et al., Feasibility and Constraints of Bragg Peak FLASH Proton Therapy Treatment Planning, *Frontiers in Oncology*, 2024 [34].

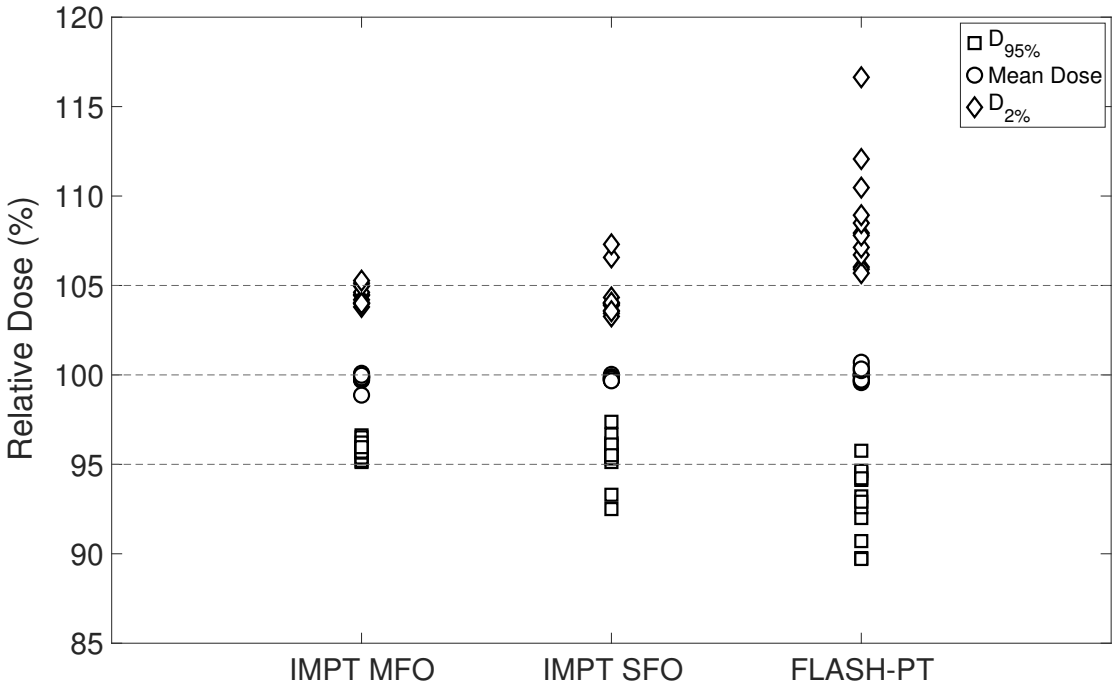


Figure 3.1: Plot summarising target dose metrics. $D_{95\%}$ (square), mean dose (circle), and $D_{2\%}$ (diamond) are normalised with respect to the prescribed dose for all patient cases and for each treatment technique. The dashed lines indicate 95%, 100%, and 105% of the prescribed dose

Table 3.1: Table of median values of: mean dose (%), $D_{95\%}$ (%), $D_{2\%}$ (%), radiation conformity index, and homogeneity index for intensity modulated proton therapy (IMPT) with multi-field optimisation (MFO), IMPT with single-field optimisation (SFO), and spread-out Bragg peak FLASH proton therapy (FLASH-PT). The Wilcoxon Rank Sum Test was performed using the dose parameters for each patient case and for each treatment technique, with the median value used as a representative metric. FLASH-PT plans are significantly inferior in the majority of dose metrics compared to both IMPT techniques. $^{***}p < 0.001$, $^{**}p < 0.01$, $^{*}p < 0.05$.

Dose Parameters	**IMPT MFO**	**IMPT SFO**	**FLASH-PT**
Mean Dose (%)	99.86	99.79	99.98
$D_{95\%}$ (%)	95.79	95.54	93.06 **
$D_{2\%}$ (%)	104.47	103.98	107.87 ***
$V_{95\%}$ (%)	96.87	96.76	87.26 **
Radiation Conformity Index	0.93	0.87	0.80
Homogeneity Index	0.10	0.09	0.16 ***

$D_{2\%} \leq 105\%$, as seen in Figure 3.1. IMPT SFO had two cases where the dose constraints were not adhered to: Brain 2 and Brain 3, which are the two smallest targets considered (Table 2.1). FLASH-PT, however, only achieved similar mean doses to IMPT MFO and IMPT SFO, with significantly different $D_{95\%}$ and $D_{2\%}$ compared to both IMPT techniques, as highlighted in Table 3.1. Since the IMPT MFO and IMPT SFO were comparable with regards to target dose coverage, the discrepancy observed for the FLASH-PT plans was not only due to the use of a single beam per fraction, but could also be attributed to limitations imposed by delivering protons at ultra-high dose rates.

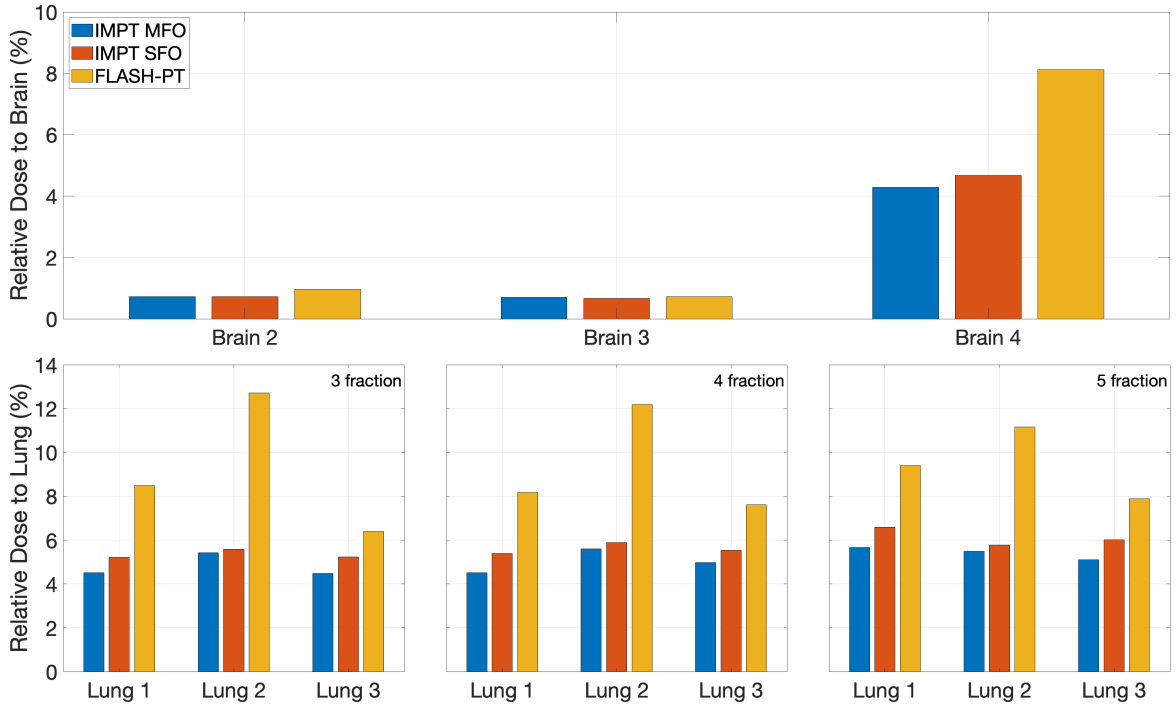


Figure 3.2: Bar charts representing the mean doses delivered to OARs for IMPT MFO, IMPT SFO and FLASH-PT, normalised with respect to the prescribed dose for each patient case. The considered OAR structures are the total brain (top) and the ipsilateral lung containing the target (bottom). For the lung cases, the doses to the lung are shown for the 3, 4, and 5 fraction plans.

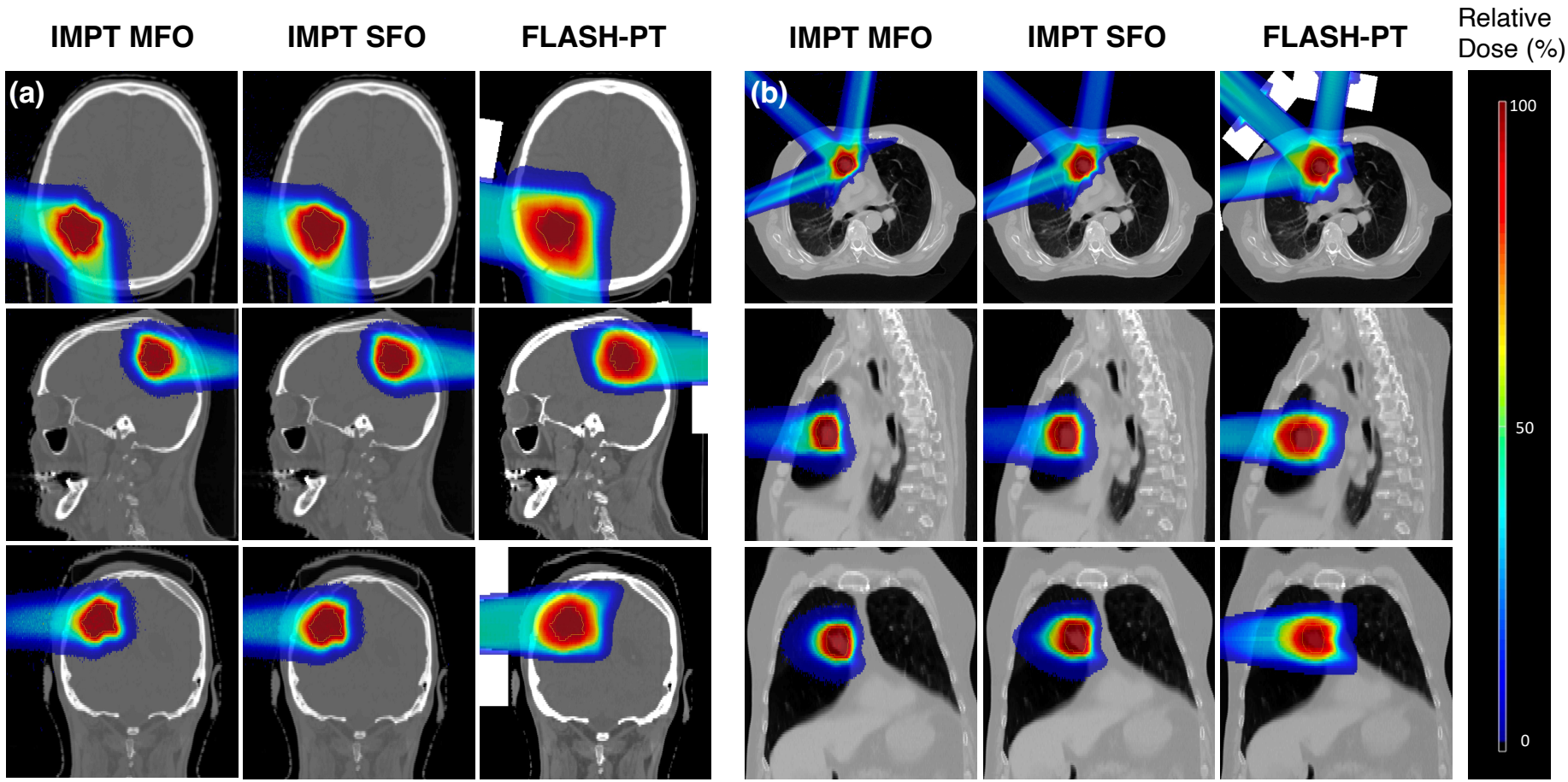


Figure 3.3: Dose maps for an example (a) brain case (Brain 4) and (b) lung case (Lung 3, 3 fractions). Comparisons of IMPT MFO, IMPT SFO, and FLASH-PT are made in the axial, sagittal, and coronal directions. Doses are normalised with respect to the prescribed dose.

Furthermore, FLASH-PT plans were also associated with significantly higher doses to OARs compared to IMPT, as seen in Figure 3.2, although the doses were still within the acceptable limits of the dose protocols as defined by RTOG 0631, CORSAIR, and the UK Consensus on Normal Tissue Dose Constraints for Stereotactic Radiotherapy, as can be seen in Tables A.2 - A.5 in Appendix A. An increase in the dose to the distal edge of the targets was also observed for the FLASH-PT plans compared to IMPT, with examples shown in relative doses in Figure 3.3, and absolute doses for the example Brain case and Lung case in Figures 3.4 and 3.5, respectively. This is likely attributed to range straggling of the high-energy protons following interactions with the energy degraders used in the FLASH-PT-modified beam setup, which may also contribute to the increased doses to OARs observed for the FLASH-PT plans. Dose volume histograms (DVHs) for the different patient cases, fractionation schemes, and treatment techniques are shown in Figures A.1 - A.4 in Appendix A.

Spearman's Correlation Coefficient showed a very strong ($p < 0.01$) negative correlation (ρ_{SRC} = -0.80) between the radiation conformity index and the target size in the IMPT SFO case; this was not the case for the FLASH-PT plans, likely due to the inclusion of the aperture in the beam setup. Pearson's Correlation Coefficient showed a significant ($p < 0.05$) positive correlation ($\rho_{PCC} = 0.63$) between the homogeneity index and the target sizes for the FLASH-PT treatment plans. An increase in target size was therefore correlated to a linear increase in homogeneity index, and thereby a worsened target homogeneity. The relationship between homogeneity index and target size was not found for IMPT MFO or IMPT SFO.

FLASH-PT plan quality also appeared to be dependent on the target shape, target position, smoothness of the distal edge of the target, and distance from the nozzle of the beam to the target. FLASH-PT treatment plans generated using the same treatment planning parameters (spot spacings, layer spacings, and margins for spot placements) as the IMPT plans varied greatly with respect to the dose distributions and

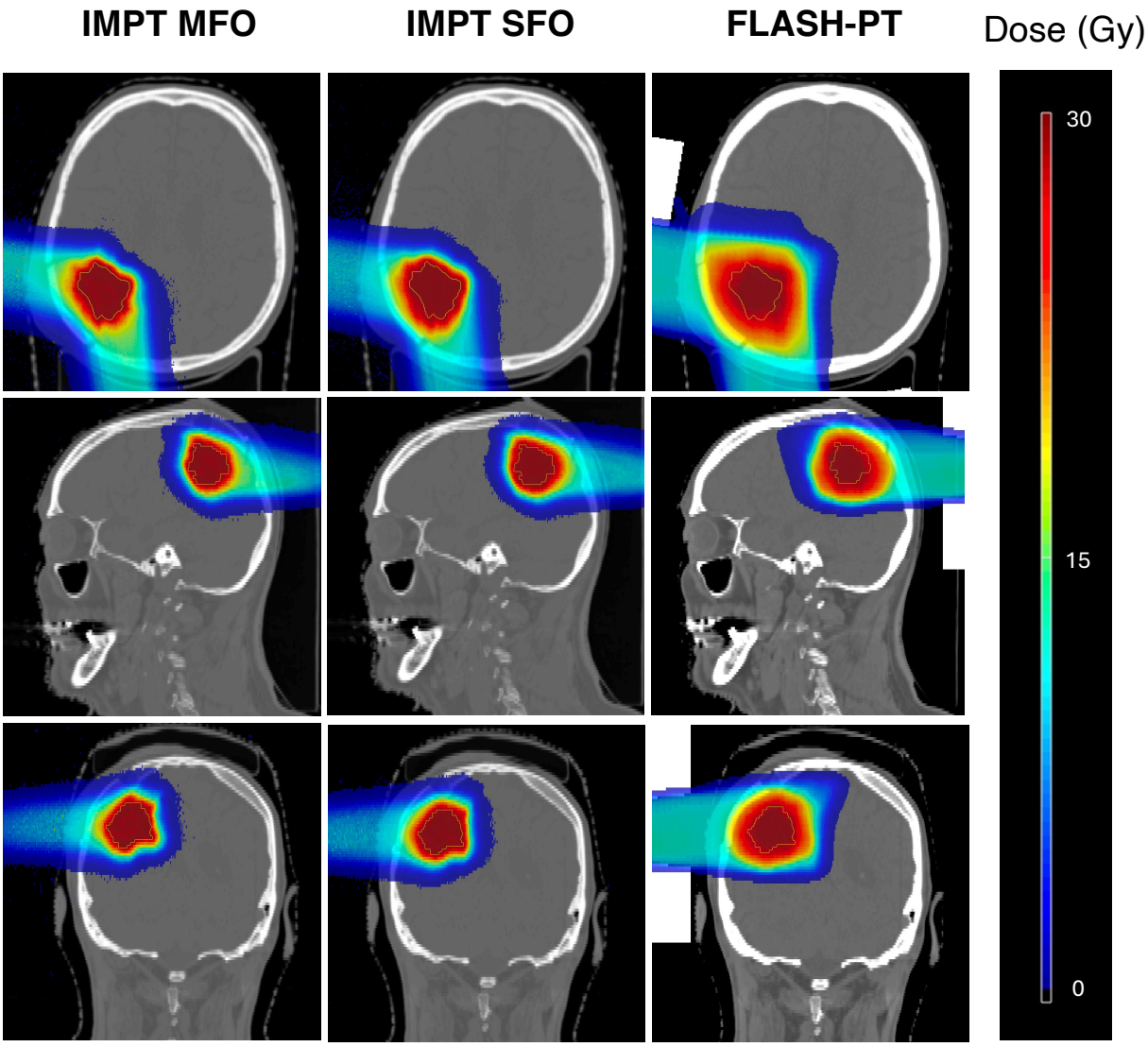


Figure 3.4: Dose maps for an example brain case (Brain 4). Comparisons of IMPT MFO, IMPT SFO, and FLASH-PT are made in the axial, sagittal, and coronal directions. Doses are shown as absolute dose (Gy).

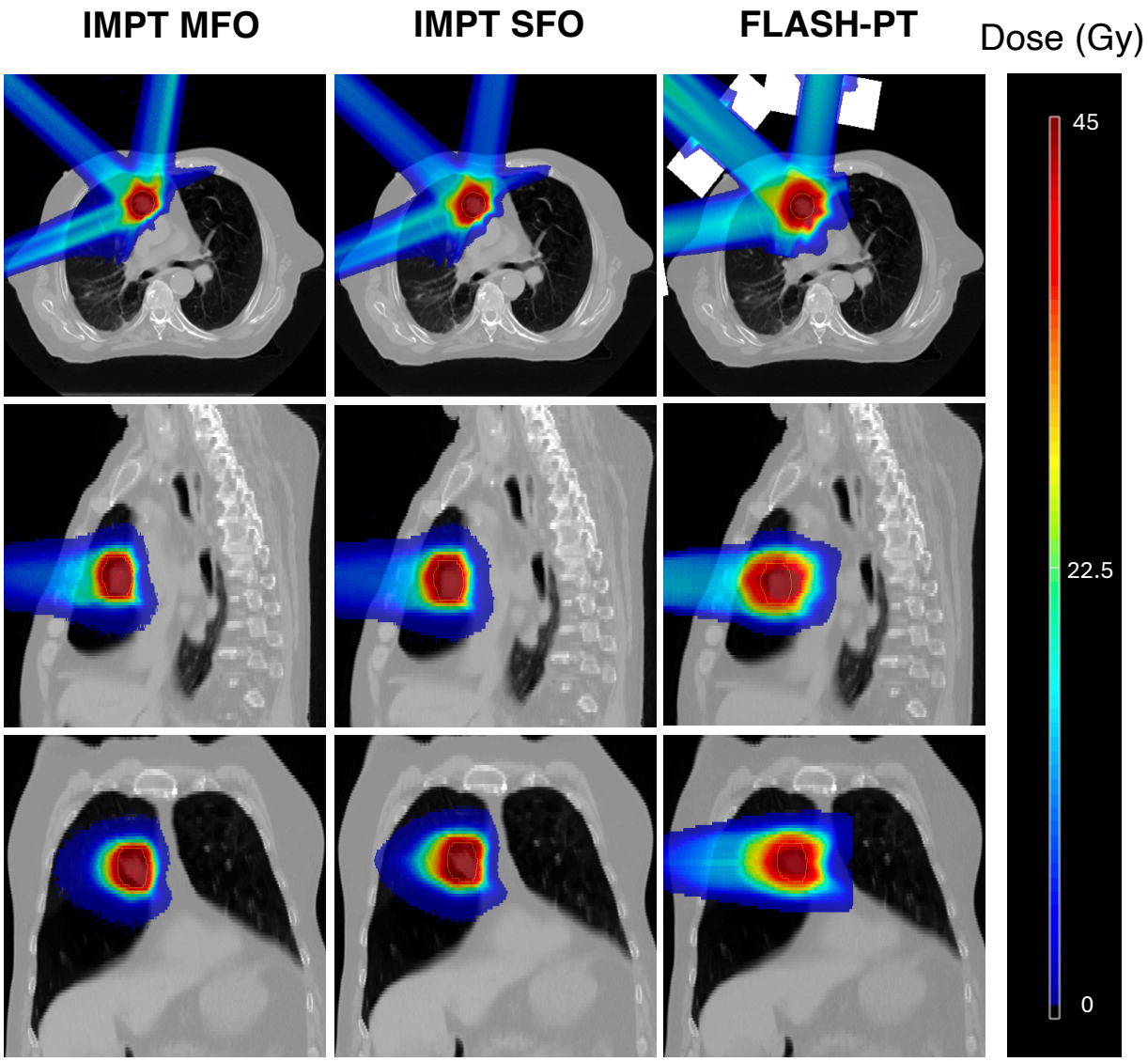


Figure 3.5: Dose maps for an example lung case (Lung 3, 3 fractions). Comparisons of IMPT MFO, IMPT SFO, and FLASH-PT are made in the axial, sagittal, and coronal directions. Doses are shown as absolute dose (Gy).

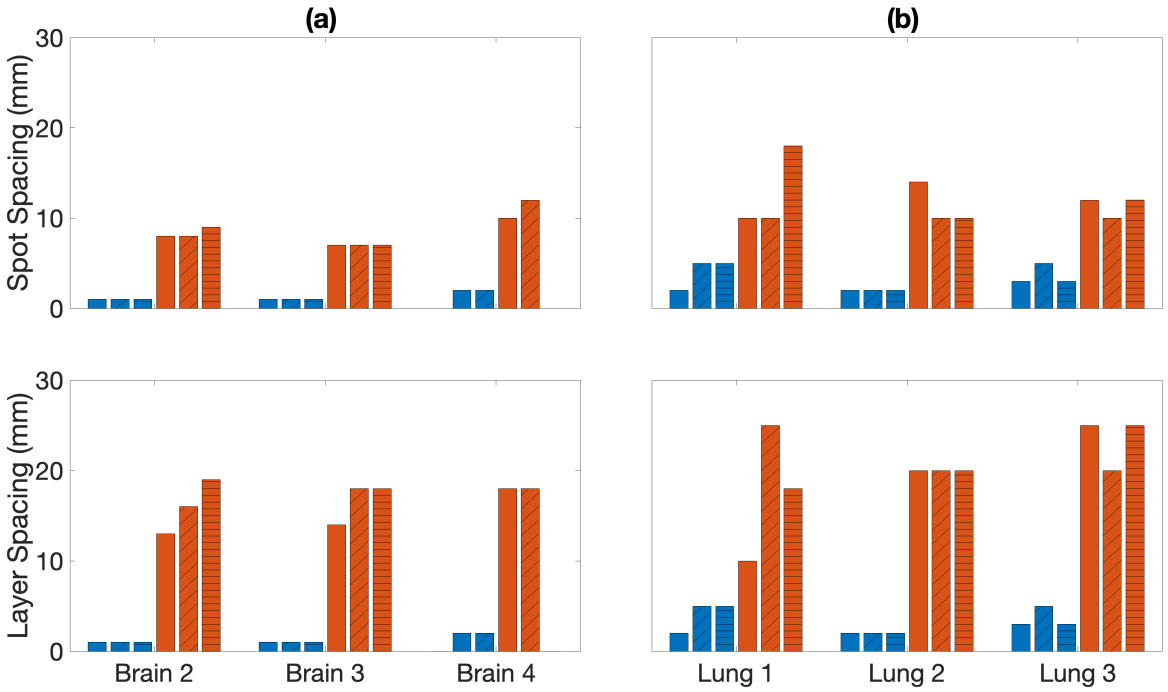


Figure 3.6: Bar charts of the spot spacings (mm) and layer spacings (mm) used to simulate the single-field optimised intensity modulated proton therapy (IMPT SFO) (blue) and spread-out Bragg peak FLASH proton therapy (FLASH-PT) (orange) treatment plans for the (a) brain and (b) lung patients. Spacings are shown for each individual beam, with beam 1, beam 2, and beam 3 indicated by no lines, diagonal lines, and horizontal lines, respectively.

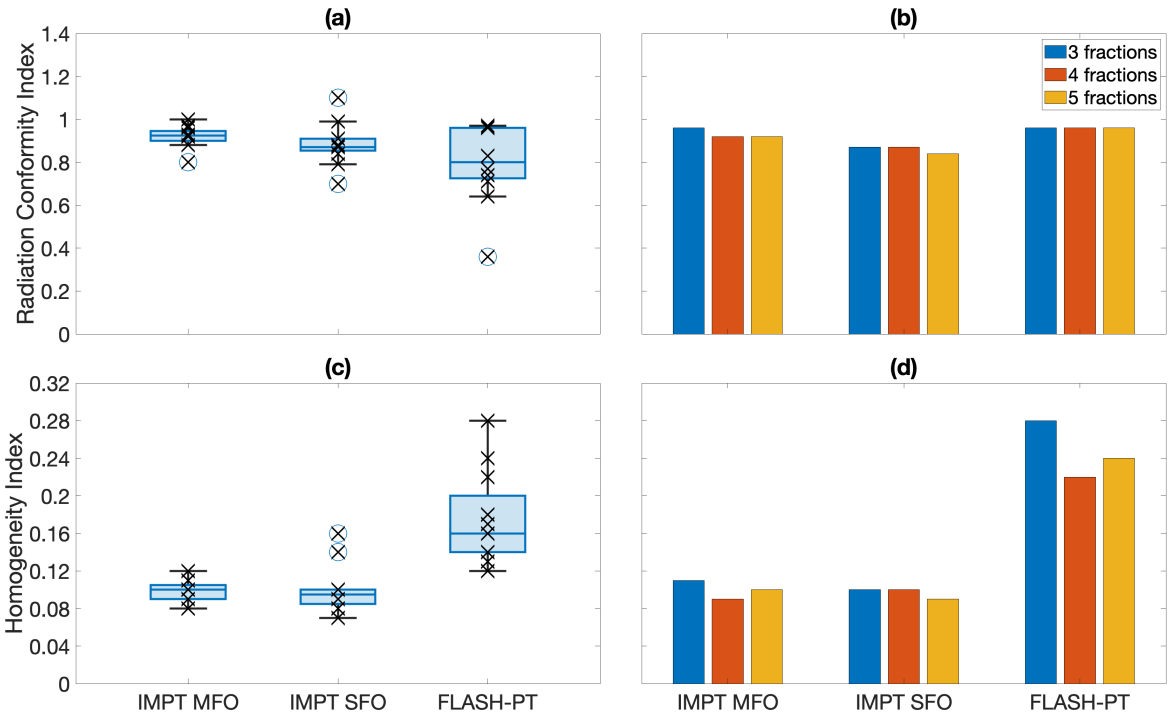


Figure 3.7: Boxplots of the (a) radiation conformity index (RCI) and (c) homogeneity index (HI) evaluated for each patient case and each treatment technique. Bar charts of the (b) RCI and (d) HI for 3,4, and 5 fractions shown for Lung 3. Each point (x) shows the exact RCI and HI for each patient case. The line within the box represents the median value, the bottom and top of the box represents the 25th and 75th percentiles, the whiskers show the range of the data points (excluding outliers), and outliers are shown using individual (o) markers.

subsequent plan quality achieved. To circumvent this, FLASH-PT treatment planning parameters suitable for each patient case and each treatment fraction were used and obtained through manual parameter optimisation. This required the use of patient- and fraction-specific treatment planning parameters, with significantly larger spot spacings and layer spacings needed to achieve mean doses similar to those of standard IMPT. Spot and layer spacings were at least twice as large for FLASH-PT plans compared to those used for IMPT, as can be seen in Figure 3.6. An increase in the spacings limited the number of spots that could be placed on the target, making it more difficult for the TPS to generate and optimise for both conformal and homogeneous FLASH-PT treatment plans (Figure 3.7 (a) and (c)). The use of relatively large margins for spot placements, however, improved the FLASH-PT target coverage, albeit at the expense of increasing the dose to nearby OARs. In addition, target margins and aperture margins had to be manually and iteratively optimised in conjunction with the spot and layer spacings. Further details on the spot spacings, layer spacings, margins for spot placements, and aperture margins for each patient case and treatment fraction are shown in Tables A.8 - A.10 in Appendix A.

FLASH-PT plans were associated with a reduced radiation conformity index compared to both IMPT MFO and IMPT SFO plans (Figures 3.3 and 3.7 (a)), although not significantly. Dose conformity for the FLASH-PT plans could be improved by increasing the resolution at which the CEM is calculated, however, this would be at the expense of drastically increasing the simulation time using this TPS. IMPT MFO and IMPT SFO plans produced comparable homogeneity indices, indicating that the inferior target homogeneity observed for the FLASH-PT plans (Table 3.1 and Figure 3.7(c)) is mainly attributed to the limitations imposed by the use of ultra-high dose rate protons, and not the SFO delivery approach. More specifically, the worsened target homogeneity is likely due to the increase in spot sizes and subsequent decrease in number of spots that can be placed, in addition to the impact of target size. Further to this, as there are multiple objectives in the TPS, the optimiser struggles to fulfil the

main dose objectives with fewer spots than what is conventionally used for IMPT.

Lung 3, which has the largest target volume and the greatest number of OARs among the patient cases considered in this study (Table 2.1), was selected as a representative example to demonstrate the capabilities of the treatment planning optimiser and the subsequent FLASH-PT treatment plan quality. The relatively large target size, and the number of OARs, for this case led to inferior FLASH-PT treatment plans and so it is shown as a "worst-case" scenario in comparison to the rest of the samples. As shown in Figure 3.7(b), the FLASH-PT radiation conformity index was comparable to both IMPT MFO and IMPT SFO, for all fractionation schemes. Figure 3.7(d), however, shows a drastic reduction in target homogeneity. The same result was also observed for the FLASH-PT plans generated for the other lung cases using 3 fractions. However, a comparison of the dose volume histograms shown in Figures A.2 - A.4 in Appendix A yielded no general difference in target dose coverage or reduction in OAR dose with increasing number of fractions.

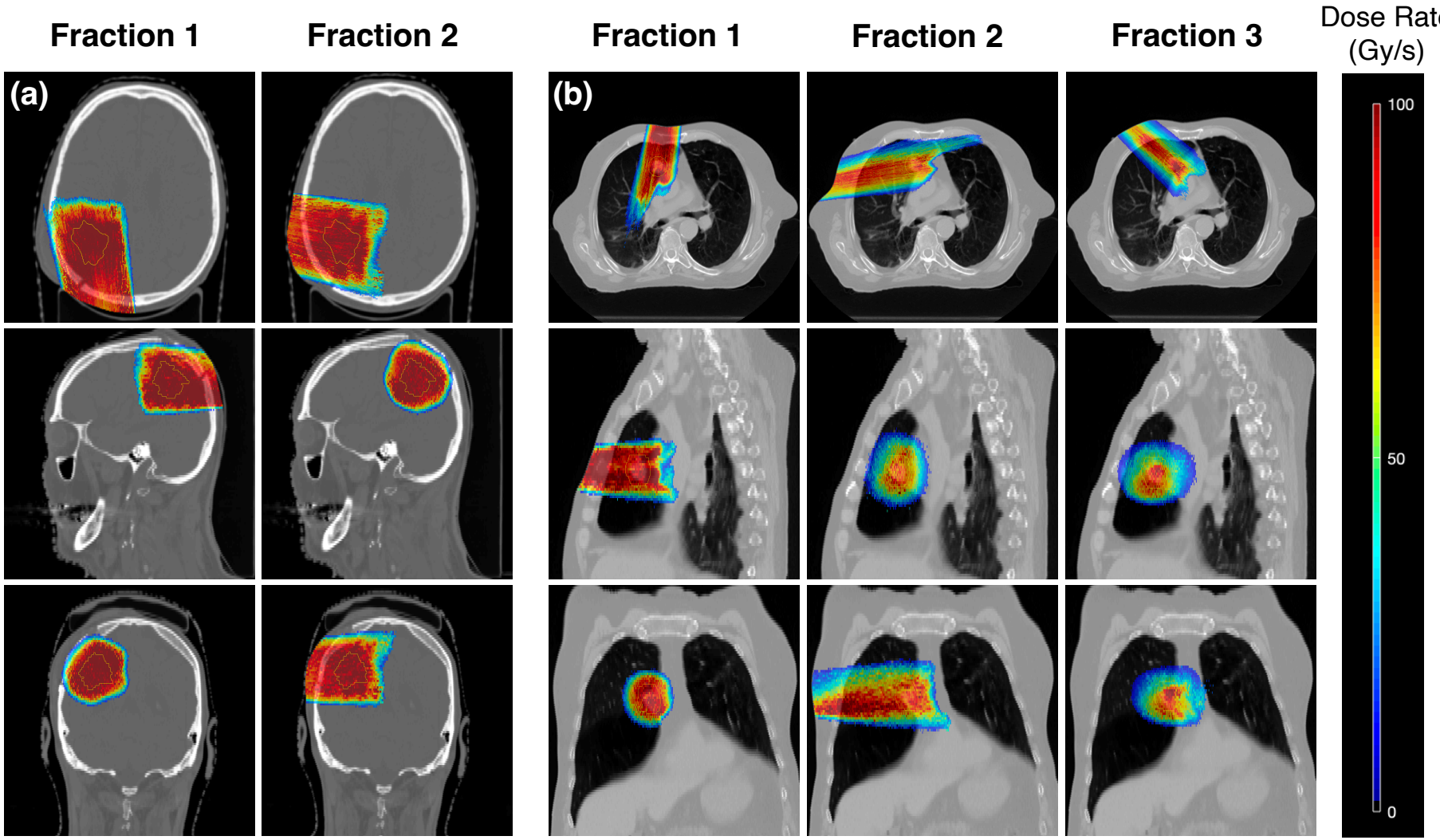


Figure 3.8: Dose rate maps for an example (a) brain case (Brain 4) and (b) lung case (Lung 3, 3 fractions), showing the 98^{th} percentile dose rate in Gy/s. Comparisons of the dose rates achieved in each fraction are made in the axial, sagittal, and coronal directions.

For the same example case, variations in dose rates appeared to be dependent on the target location as well as the number of fractions, and thus beams, used to deliver the treatment (Figures 3.8 and 3.9). Comparing the brain and lung case shown in Figure 3.8, the use of two fractions to treat a target with fewer density differences along the path of the beam (brain) led to higher dose rates to the surrounding normal tissues compared to the use of three fractions treating a target in a location where more density differences are present (lung).

Focusing on the dose rates for the "worst-case" scenario (Lung 3) using dose rate volume histograms as shown in Figure 3.9. Figure 3.9 does not represent a direct volume correspondance between the horizontal dose threshold lines and the dose rate volume histograms. Instead, it highlights which OAR volumes adhered to the minimum dose and dose rate constraints: OAR doses $\geq$ 2 Gy represented by histogram lines above the horizontal dashed lines, and dose rates $\geq$ 40 Gy/s represented by histogram lines to the right, and inclusive of, the vertical dashed line. The minimum dose rate constraint was not fully achieved for the Right Lung (for any fraction); this meant that there were volumes of the OAR which received doses $\geq$ 2 Gy (horizontal dashed lines) that did not receive dose rates $\geq$ 40 Gy/s (dose rate threshold indicated by the vertical dashed lines), as shown in Figure 3.9(a). This was likely due to low-dose, and consequently low dose rate, regions at the edges of the beam, as shown in Figure 3.8, which may arise from strict OAR dose constraints. Similarly, for the Thoracic Wall, only fraction 2 achieved the dose rate optimisation criterion, whilst fractions 1 and 3 did not (Figure 3.9(b)). In contrast, the criterion was achieved for fractions 2 and 3 for the Great Vessel and for all fractionation schemes for the Heart (Figures 3.9(c) and (d)). Larger OARs such as the Right Lung and Thoracic Wall, exhibited more low-dose regions due to the beam-path chosen (and the beam spread) compared to structures such as the Heart and Great Vessel, which due to their proximity to the target receive most of the dose at much higher dose rates.

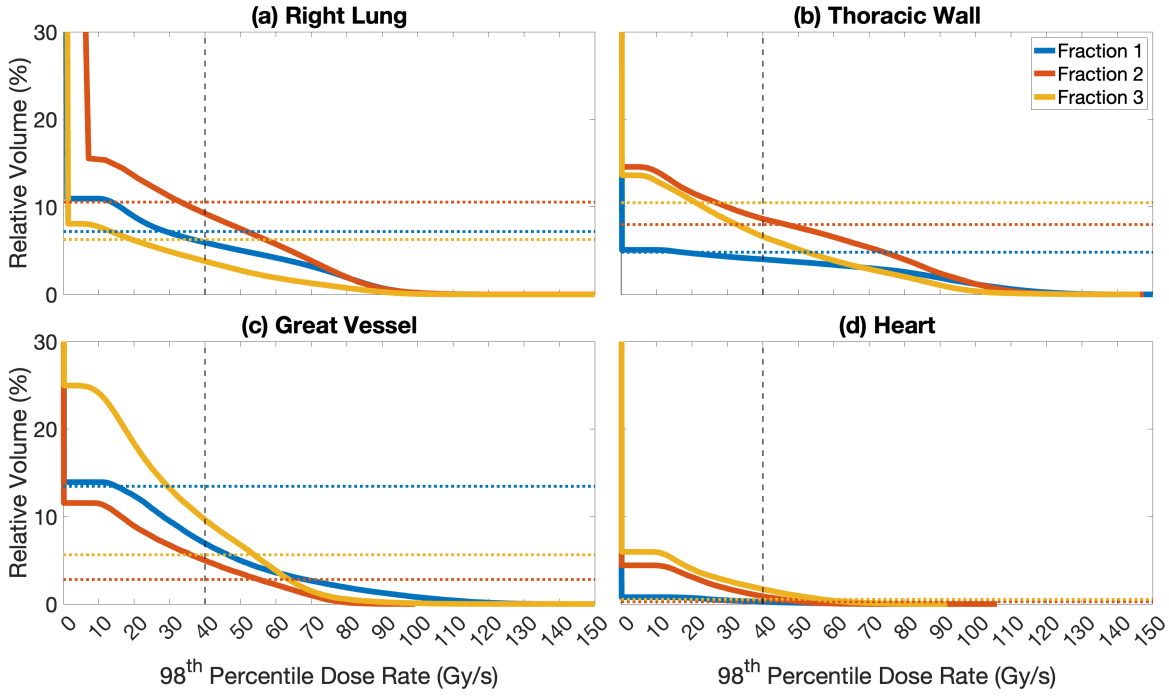


Figure 3.9: Dose rate volume histograms of the (a) Right Lung, (b) Thoracic Wall, (c) Great Vessel, and (d) Heart structures for Lung 3, separated for the 3 fractions planned. For simplicity, as no OAR receives FLASH dose rates to relative volumes $\geq 30\%$ in this study, only relative volumes in the range of 0-30% are included in these plots. Solid lines represent the dose rate, different colours indicate the different fractions planned, horizontal dashed lines represent the volume of the OAR which receives doses ≥ 2 Gy, and vertical dashed lines represent the 40 Gy/s dose rate threshold. In the case of the Right Lung, the optimisation criterion was not fully achieved, as there are volumes receiving doses ≥ 2 Gy (dashed lines) that do not receive the dose at dose rates ≥ 40 Gy/s (solid lines); fraction 2 nearly fulfils it. Similar, for the Thoracic Wall, only fraction 2 fully achieves the dose rate optimisation criterion, while fractions 1 and 3 do not. The criterion is fully achieved for fractions 2 and 3 for the Great Vessel, and for all fractions for the Heart

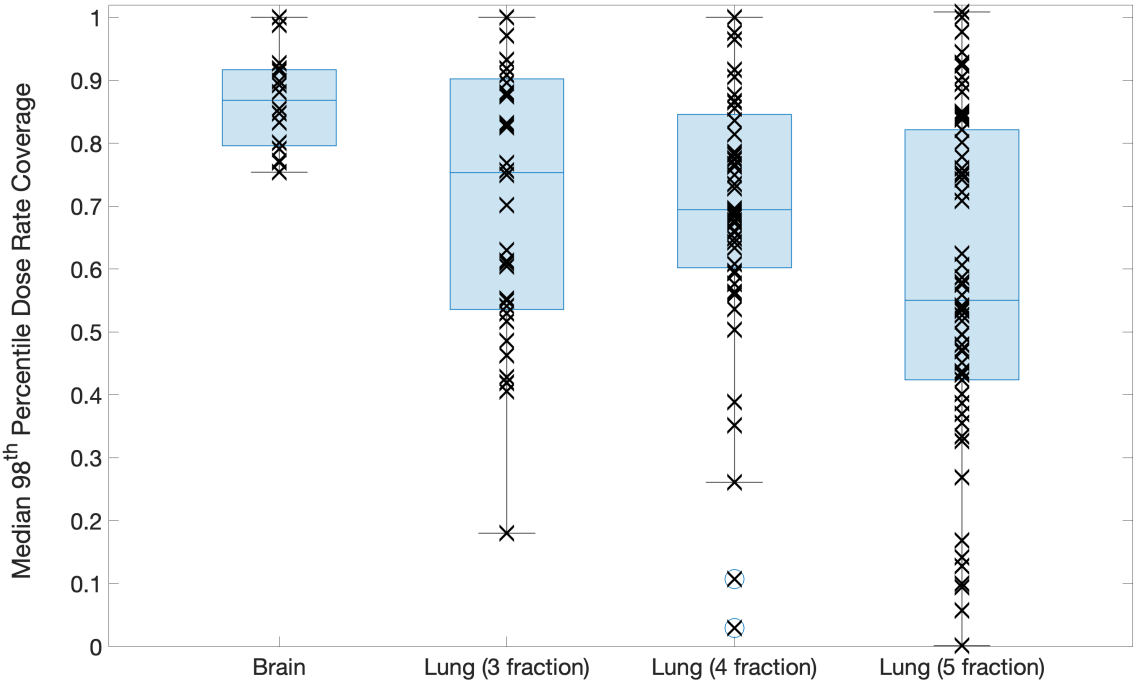


Figure 3.10: Boxplot showing the dose rate coverage of the OARs defined for the brain and lung cases for each fractionation scheme investigated. The dose and dose rate threshold considered were 2 Gy and 40 Gy/s, respectively. Each point shows the exact dose rate coverage for each OAR in each patient case, the line across the box represents the median value, the bottom and top of the box represent the 25^{th} and 75^{th} percentiles, the whiskers show the range of the data point (excluding outliers).

Median values of dose rate coverages, where dose rate coverage was defined as the relative number of non-target voxels which receive a total dose ≥ 2 Gy at dose rates $\geq$ 40 Gy/s, for the brain plans and 3-, 4-, and 5-fraction lung plans were 87%, 71%, 69%, and 56%, respectively. For the different fractionation schemes investigated for the lung patients, the 5-fraction plans had significantly ($p < 0.05$) lower dose rates than the 3- and 4-fraction plans. This is likely due to the reduced intra-fraction dose making it harder for the optimiser to fulfil the ultra-high dose rate objectives, as it paradoxically must increase the dose to OARs to achieve ultra-high dose rates whilst also adhering to OAR dose constraints. An increase in the number of fractions for the lung cases led to an increase in the spread of dose rate coverages achieved to OARs, as seen in Figure 3.10. This was expected as the dose per fraction decreased. Significantly higher dose rate coverages were achieved for the brain cases compared to the lung cases for all fractionation schemes investigated. This could be due to the increase in density differences along the path of the beam for the lung cases compared to the brain cases.

3.4 Discussion

Due to the novelty of ultra-high dose rate proton therapy utilising the spread-out Bragg peak, few studies focusing on the clinical implementation, and specifically the treatment planning process, had been conducted at the time of which the work in this Chapter was produced.[3] This Chapter aimed to determine the feasibility, and outline any potential constraints, of producing spread-out Bragg peak FLASH proton therapy treatment plans, using a one-beam-per-fraction delivery, and whether the generated plans were comparable to those generated for a clinically used technique such as IMPT.

To minimise the impact of the use of SFO on comparisons between FLASH-PT and IMPT, additional IMPT plans optimised using SFO were generated alongside the MFO IMPT plans. This allowed for direct comparisons between SFO FLASH-PT and SFO

[3]Section 3.4 is based on the published work by Lövgren et al., Feasibility and Constraints of Bragg Peak FLASH Proton Therapy Treatment Planning, *Frontiers in Oncology*, 2024 [34].

IMPT, thereby isolating the effect of the one-beam-per-fraction delivery on the plan quality. Comparisons between IMPT plans optimised using MFO and SFO revealed no significant differences, indicating that the use of a one-beam-per-fraction delivery does not significantly affect plan quality when evaluated using this TPS. In contrast, FLASH-PT plans were associated with significant differences across several dose parameters when compared to IMPT SFO plans. Consequently, without accounting for the normal tissue sparing effect attributed to the ultra-high dose rate technique, IMPT plans demonstrated improved target coverage, dose conformity, target dose homogeneity, and reduced doses to OARs compared to the FLASH-PT plans using the FLASH-modified beam setup and its implementation into the MIROpt TPS through the ConformalFLASH library.

An interplay between the FLASH-modified beam setup, target location, and treatment planning optimisation was evident, influencing overall FLASH-PT plan quality. The use of the FLASH-modified beam setup, or its implementation into the TPS, required patient- and fraction-specific treatment planning parameters to be used for the FLASH-PT plans. Standard IMPT parameters could not be applied, and achieving improved FLASH-PT plan quality therefore required extensive, time-consuming manual parameter optimisation. The significantly larger spot and layer spacings used for the FLASH-PT plans, in comparison to IMPT, made it more difficult for the TPS to generate conformal and homogeneous dose distributions. In addition, larger target volumes were associated with inferior FLASH-PT plan quality relative to IMPT, with increasing target size leading to reduced dose homogeneity and decreased target dose conformity. The inferior plan quality observed for FLASH-PT relative to IMPT may also, in part, be attributed to the inclusion of dose rate objectives, which were found to dominate the overall treatment plan optimisation. Further investigation of FLASH-PT plan quality and achievable dose rates without the inclusion of dose rate objectives in the treatment planning optimisation would be of interest.

Density differences along the path of the beam appeared to lead to variations in the dose distributions achieved; target sites with fewer density differences, such as the brain, showed less variations whilst also achieving better target dose coverages, reduced doses to OARs, and improved dose rate coverages compared to the lung cases. In this study, brain cases appeared to achieve better FLASH-PT plans compared to the lung targets, although the sample size was not large enough to ensure statistical significance. Density heterogeneities along the beam path affected the robustness of the achievable dose distributions and dose rate coverage. Target sites with fewer density variations, such as the brain, exhibited more homogeneous dose distributions, improved target dose coverage, reduced doses to OARs, and superior dose rate coverage compared with the lung cases. Consequently, brain cases generally achieved higher-quality FLASH-PT plans than lung targets in this study; however, the limited sample size for each specific target site precluded assessment of statistical significance.

The ultra-high dose rate coverages for the brain and lung (3 fractions) cases, with OAR volumes receiving doses $\geq$ 2 Gy at dose rates $\geq$ 40 Gy/s, was comparable to the coverages of approximately 80% reported in previous treatment planning studies [25, 90, 96, 99, 100, 104]. In terms of fractionated FLASH-PT treatment delivery, increasing the number of fractions for the lung cases did not result in any major difference in the target dose distributions or doses to OARs. However, a reduction in intra-fraction dose rate coverage was observed, which was expected given the decrease in intra-fraction dose with increasing fraction number. The use of hypo-fractionated beam delivery will be more favourable if the FLASH sparing effect is to be fully exploited, nonetheless, ensuring clinically acceptable target coverage is achieved is still a priority.

Limitations in this study include the implementation of the CEM from the ConformalFLASH library to the MIROpt research TPS, the sample size, and the imposed target size constraint. However, the MIROpt TPS provided valuable information re-

garding the FLASH-PT treatment planning process. This included the evaluation of fractionated beam delivery, dose comparisons between different target types, the effect of target size on the plan quality, and the capability of achieving ultra-high dose rates to the irradiated OAR volumes. Nevertheless, the implementation of the FLASH-modified beam setup into a clinically used and validated system, such as RayStation® (RaySearch Laboratories AB, Stockholm, Sweden), could allow for more efficient optimisation along with additional degrees of freedom, thereby improving the FLASH-PT plan quality.

The aim of this Chapter was to determine the feasibility and constraints of producing IMPT equivalent FLASH-PT treatment plans using a research TPS. Without accounting for the FLASH sparing effect attributed to the delivery of ultra-high dose rates, IMPT plans were superior in target coverage, dose conformity, target homogeneity, and OAR sparing compared to FLASH-PT using the FLASH-modified beam setup. Establishing whether the limitations found are software or hardware related will be key in further developing, improving, and demonstrating the feasibility of clinically implementing spread-out Bragg peak FLASH-PT.

Chapter 4

The Impact of Dose Rate Optimisation and Robust Optimisation on FLASH Proton Therapy Treatment Plan Quality and Dose Rates

4.1 Introduction

Building on the findings of Chapter 3, which found that spread-out Bragg peak FLASH proton therapy (FLASH-PT) treatment plans were associated with worse target coverage and target dose homogeneity, as well as increased doses to organs at risk (OARs) compared to intensity modulated proton therapy (IMPT); this Chapter aims to develop an improved understanding of the feasibility and limitations of the FLASH-PT hardware (i.e., the FLASH-modified beam delivery) and software (i.e., the treatment planning system and optimisation).[1]

An important question to address is whether there is a need to implement dose rate objectives into the optimisation and treatment planning process. Historically, dose rates have not been of interest when generating and optimising clinical treatment plans [126]. However, with the emergence of ultra-high dose rate radiotherapy, dose rate calculation

[1]Section 4.1 is based on the published work by Lövgren et al., The Impact of Dose Rate Optimisation and Robust Optimisation on FLASH Proton Therapy Treatment Plan Quality and Dose Rates, *Frontiers in Oncology*, 2025 [35].

and optimisation are becoming increasingly relevant, as surpassing a certain dose rate threshold could be essential for the efficacy of the treatment. Dose rate distributions should also be carefully characterised and controlled during treatment planning to determine whether sufficient ultra-high dose rate coverage to regions of interest can be achieved, and how it may impact treatment plans. It is therefore important to understand the impact this additional optimisation may have on the treatment plan quality.

Common dose rate definitions include the dose-averaged dose rate (DADR), percentile dose rate (DR_{prct}) (also known as pencil beam scanning dose rate), and the average dose rate, as described in Section 1.2.7 [108, 109]. However, as no standard definition is used in the literature, varying ultra-high dose rate coverages have been reported [34, 100, 103, 109, 112, 114, 115, 127]. This can become problematic if there are drastically different dose rates achieved for a patient case depending on the definition used.

With regards to treatment planning techniques, margin-based planning is the most common technique adopted for FLASH-PT, as shown in Chapter 3; however, it is suboptimal for proton therapy due to range errors associated with the particle beam delivery [128]. Instead, robust treatment planning should be implemented for FLASH-PT to make the treatment plans more robust to range uncertainties whilst also allowing for a just comparison between FLASH-PT and IMPT plans [23]. Furthermore, the use of robust optimisation may also improve FLASH-PT target coverage compared to margin-based planning. Robust FLASH-PT treatment planning and its potential impact on achievable dose rates, along with direct dose comparisons to robust IMPT, have not yet been explored.

The aim of this Chapter is to compare FLASH-PT plans generated using two different treatment planning systems (TPSs) to evaluate the impact of using dose rate objectives in the treatment planning optimisation on both the treatment plan quality and achievable dose rates. Further to this, margin-based versus robust FLASH-PT

treatment plans are compared to investigate the impact of robust optimisation on the FLASH-PT dose and dose rate coverage (for both DR_{prct} and DADR). FLASH-PT plans are also compared to IMPT plans, for each TPS and each optimisation technique (margin and robust), to determine the clinical applicability of spread-out Bragg peak FLASH proton therapy.

4.2 Materials and Methods

Treatment plans were simulated for use on the IBA Proteus®Plus (Louvain-la-Neuve, Belgium) machine with maximum beam currents of 300 nA and 500 nA for IMPT and FLASH-PT, respectively. The FLASH-modified beam setup considered in Chapter 3 was also implemented into RayStation, with a maximum beam energy of 228 MeV measured at the isocentre. The monoenergetic spot scanned protons traverse through a conformal energy modulator (CEM), a range shifter, and an aperture, before reaching the target. More information on the beam delivery can be found in Section 2.1.

The treatment plans generated in Chapter 3 using MIROpt and the conformalFLASH library will be compared to FLASH-PT and IMPT plans simulated using RayStation 11B FLASH, a research version of RayStation® (RaySearch Laboratories AB, Stockholm, Sweden). The comparison between a research TPS (MIROpt and conformalFLASH) to a research version of a clinically validated system (RayStation) was due to the limited availability of TPSs such as MIROpt which are able to generate dose rate optimised FLASH-PT treatment plans. RayStation increased the degrees of freedom of the FLASH-PT treatment planning process by providing capabilities to generate margin-based and robust treatment plans, as well as increasing the maximum field size compared to MIROpt. More detailed information on MIROpt, the conformalFLASH library, and the dose rate optimisation can be found in Section 2.3.3, with information about the treatment planning process in RayStation found in Section 2.3.4.

Treatment plans were generated for the same ten patient cases considered in Chap-

ter 3, including bone (n = 3), brain (n = 4), and lung (n = 3) cases, with patient data outlined in Table 2.1. IMPT plans were generated using a conventional beam setup and multi-field optimisation (MFO), as discussed in Sections 1.1.4 and 1.1.5. For each patient case, the number of fields and beam angles used were the same for both IMPT and FLASH-PT plans. Due to the patient-specific beam setup, all FLASH-PT plans were generated for a one-beam-per-fraction delivery along with single field optimisation (SFO). The optimisation objectives used for an example brain case, for FLASH-PT plans simulated using both MIROpt and RayStation (margin and robust), can be found in Appendix A (Listing A.1 for MIROpt and Figures A.8 and A.9 for RayStation).

To better understand the impact of dose rate optimisation on the plan quality and achievable dose rates, margin-based plans were generated using RayStation, and were directly compared to the MIROpt plans in Chapter 3. For FLASH-PT plans simulated using MIROpt, dose rates (98^{th} percentile) were optimised using a dose rate objective function. Input parameters in this objective function include: a minimum dose to the OAR (D_{thr} (Gy)) at which the dose rate is evaluated, a reference dose rate (DR_{thr} (Gy/s)), and an importance weight for the function. A minimum dose threshold of D_{thr} = 2 Gy (total dose) and reference dose rate of DR_{thr} = 40 Gy/s were used in the dose rate objective function (evaluated for the 98^{th} percentile) for all OARs receiving a non-zero dose in the MIROpt FLASH-PT plans. Low importance weights had to be used for the dose rate objectives as the dose rate optimisation would otherwise dominate the treatment plan optimisation, severely degrading the plan quality. More detailed information regarding the dose rate optimisation can be found in Section 2.3.3.1. Dose rate improvements in RayStation involved the removal of low-weighted spots (spots with monitor units (MU) less than 20 MU/fx), unless the plan quality was severely impacted.

In this Chapter, dose rate coverage was defined as the relative number of non-target voxels receiving total doses $\geq x$ Gy at dose rates $\geq y$ Gy/s, where $x = \{2, 4, 6, 8\}$ and y

$= \{40, 70, 100\}$. Dose rate coverages were evaluated using both the 98^{th} percentile dose rate (DR_{prct}) definition and the dose averaged dose rate (DADR) definitions (explicitly discussed in Section 1.2.7) for each organ at risk within each individual fraction. Dose rate coverages below 1% were excluded as values below this limit were smaller than the associated uncertainty of the simulated data.

Robust FLASH-PT and IMPT plans were generated using RayStation, and were compared to the margin-based plans generated in the same TPS. Set-up uncertainties and range uncertainties can be found in Table 2.1, with more information about the robust optimisation discussed in Section 2.3.4.1. Worst-case scenarios were evaluated for $D_{95\%}$ and $D_{2\%}$ for the robust treatment plans. Additionally, the same worst-case scenario evaluation used for robust optimisation was applied to the margin-based plans to determine how effects due to setup errors were handled by the planning technique for the FLASH-PT plans. Any subsequent reference to target dose, for any treatment plan, refers to dose to the CTV (and GTV for Brain 2, Brain 3, and Brain 4) in the nominal scenario unless the worst-case scenario is explicitly stated.

FLASH-modified dose distributions have shown large variations in the potential OAR sparing depending on the tumour location, with some FLASH radiotherapy scenarios even leading to no net sparing [129]. Therefore, if the FLASH-PT plans can be as similar to IMPT plans as possible, any sparing effect that may be elicited due to the FLASH effect will be an additional benefit to the patient. Consequently, this study investigates FLASH-PT plan quality without accounting for a sparing effect.

FLASH-PT plans generated using MIROpt and RayStation will be referred to as dose rate optimised (DRO) and non-dose rate optimised (non-DRO) plans, respectively. A relative biological effectiveness of 1.1 was assumed for all IMPT and FLASH-PT plans, and treatment plan evaluations and comparisons were performed using the methods described in Section 2.4.

4.3 Results

For the inter-system comparisons, Bone 1, Bone 2, Bone 3, and Brain 1 were excluded due to target size constraints using the MIROpt TPS; this was imposed by the field size which limited the space available for the CEM in the nozzle, as discussed in Chapter 3 Section 3.3.[2]

With regards to IMPT plans, both TPSs achieved $D_{95\%} \geq 95\%$ and $D_{2\%} \leq 105\%$, as shown in Table 4.1, except for the MIROpt plan for Brain 2 which reached $D_{2\%} = 105.13$. Furthermore, target dose homogeneity and doses to organs at risk were similar across the TPSs (Table 4.1 and Figure 4.1). The similarity of the IMPT plans generated by both TPSs therefore provides a useful baseline, demonstrating that treatment plans meeting the prescribed target dose objectives can be produced using either software. Consequently, any discrepancies observed in the FLASH-PT plans are unlikely to arise from differences in conventional treatment planning capability, and can instead be attributed to differences in FLASH-specific plan optimisation between the systems, or even the FLASH-modified beam delivery.

[2]Section 4.3 is based on the published work by Lövgren et al., The Impact of Dose Rate Optimisation and Robust Optimisation on FLASH Proton Therapy Treatment Plan Quality and Dose Rates, *Frontiers in Oncology*, 2025 [35].

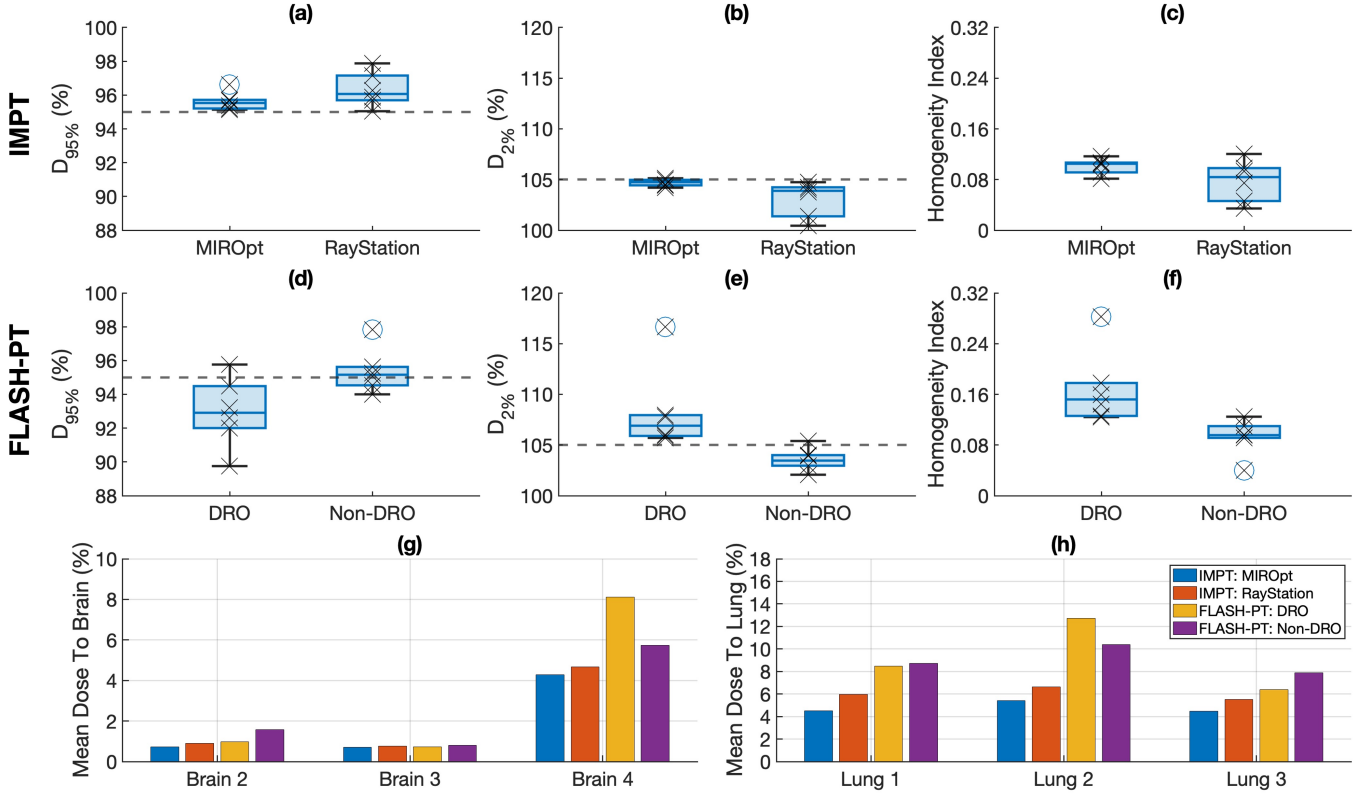


Figure 4.1: Target and organ at risk dose comparisons for margin-based plans for the different treatment planning systems (TPSs) (MIROpt vs. RayStation) and optimisation techniques (dose rate optimised (DRO) and non-dose rate optimised (non-DRO)). Boxplots comparing (a) $D_{95\%}$ (%), (b) $D_{2\%}$ (%), and (c) the homogeneity index (HI) (($D_{2\%}$ (%) - $D_{98\%}$ (%))/$D_{50\%}$ (%)) for IMPT plans generated using MIROpt and RayStation are shown in the top panel. The middle panel shows boxplots comparing (d) $D_{95\%}$ (%), (e) $D_{2\%}$ (%), and (f) the HI for DRO and non-DRO FLASH-PT plans. Each point (x) shows the exact $D_{95\%}$ (%), $D_{2\%}$ (%), and HI for each patient case. The line within the box represents the median value, the bottom and top of the box represent the 25th and 75th percentiles, the whiskers show the range of the data points (excluding outliers), and outliers are shown using individual (o) markers. Grey dashed lines indicate target dose limits of (a) $D_{95\%} = 95\%$ and (b) $D_{2\%} = 105\%$. Mean doses to the (g) brain structure and (h) (irradiated) lung structure for the different TPSs and treatment techniques are represented using bar charts. All doses are normalised with respect to the prescribed dose.

Table 4.1: Table of median values of: mean dose (%), $D_{95\%}$, $D_{2\%}$ (%), and homogeneity index for IMPT simulated using MIROpt, IMPT simulated using RayStation, dose rate optimised (DRO) FLASH-PT, and non-dose rate optimised (Non-DRO) FLASH-PT.

	IMPT		**FLASH-PT**	
Dose Parameter	**MIROpt**	**RayStation**	**DRO**	**Non-DRO**
Mean Dose (%)	99.86	99.76	99.86	99.67
$D_{95\%}$ (%)	95.52	96.07	92.90	95.16
$D_{2\%}$ (%)	104.74	103.90	106.92	103.45
Homogeneity Index	0.10	0.06	0.15	0.10

The minimum target dose limit of $D_{95\%} \geq 95\%$ was not achieved for all margin-based FLASH-PT plans, irrespective of TPS. No significant differences in $D_{95\%}$ were found between the DRO and non-DRO FLASH-PT plans, or between IMPT and FLASH-PT plans within each TPS (Figure 4.1 (a) and (d)). The non-DRO FLASH-PT plans were associated with significantly lower target $D_{2\%}$ compared to the DRO plans (Table 4.1 and Figure 4.1 (e)), with RayStation improving $D_{2\%}$ for the IMPT plans compared to MIROpt (Figure 4.1 (b)). FLASH-PT target homogeneity was also significantly improved for non-DRO plans (Figure 4.1 (f)). IMPT target homogeneity was similar across the TPSs (Figure 4.1 (c))

All margin-based FLASH-PT plans (both DRO and non-DRO), except for the DRO FLASH-PT plan for Lung 3, adhered to the mandatory OAR dose constraints, with more information found in Tables A.2 - A.7 in Appendix A. No significant differences in mean dose to the brain were found between the TPSs for IMPT, and dose rate optimisation techniques (DRO versus non-DRO), despite there being a difference of approximately 2 Gy for Brain 4 between the DRO and non-DRO FLASH-PT plans (Figure 4.1 (g)). A trend of increased mean dose to the lung was observed for the FLASH-PT plans compared to that of IMPT, however, no significant differences was found between the TPSs or dose rate optimisation techniques used (Figure 4.1 (h)). Compared to IMPT, FLASH-PT plans were associated with non-significant increases in OAR doses and reduced dose conformity for plans simulated using both TPSs, as seen in Figures 4.1 (g) and (h).

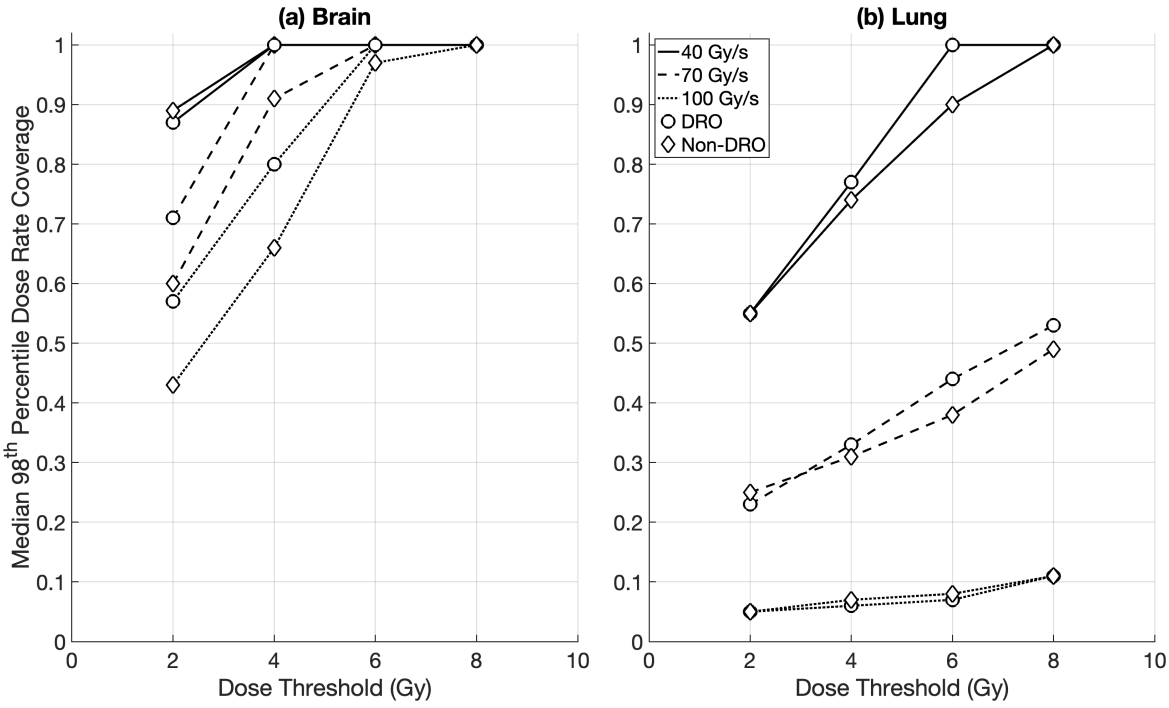


Figure 4.2: Median percentile dose rate (98^{th} DR_{prct}) coverage for margin-based plans for (a) brain and (b) lung cases for the different optimisation techniques: dose rate optimised (DRO) (circle), and non- dose rate optimised (non-DRO) (diamond). Dose rate coverages were evaluated for all organs at risk using dose thresholds of 2 Gy, 4 Gy, 6 Gy, and 8 Gy, and dose rate thresholds of 40 Gy/s, 70 Gy/s, and 100 Gy/s.

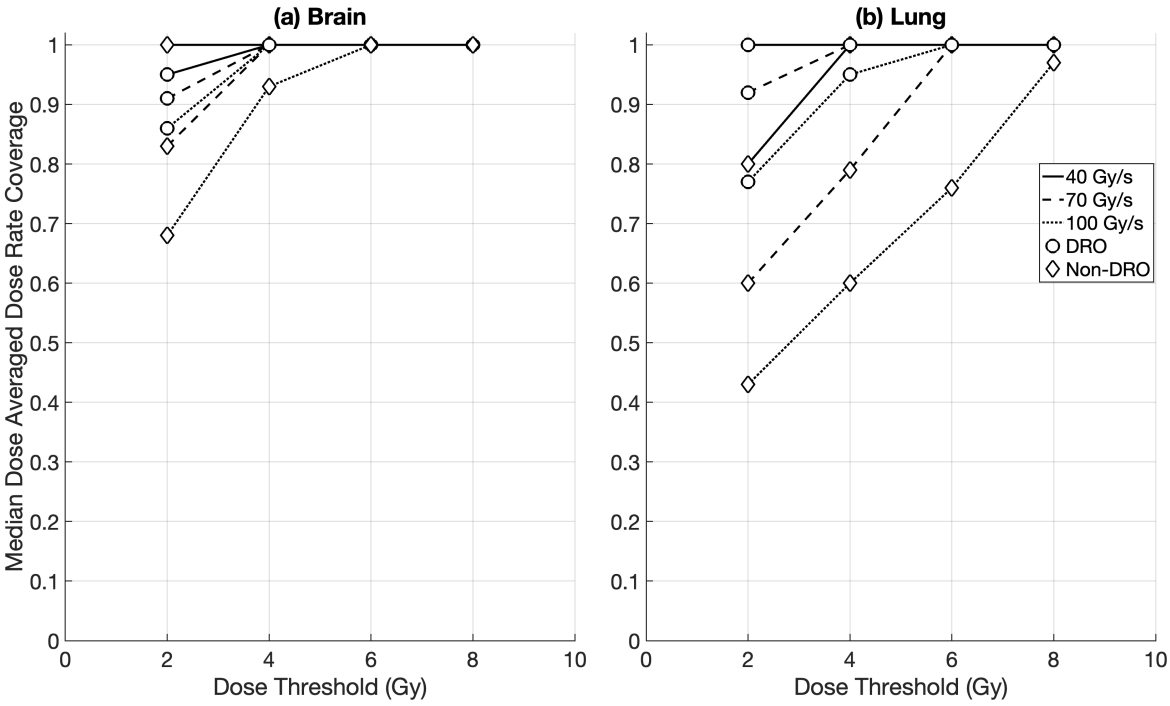


Figure 4.3: Median dose averaged dose rate (DADR) coverage for margin-based plans for (a) brain and (b) lung cases for the different optimisation techniques: dose rate optimised (DRO) (circle), and non- dose rate optimised (non-DRO) (diamond). Dose rate coverages were evaluated for all organs at risk using dose thresholds of 2 Gy, 4 Gy, 6 Gy, and 8 Gy, and dose rate thresholds of 40 Gy/s, 70 Gy/s, and 100 Gy/s.

Intra-fraction DR_{prct} coverages for the brain OARs were similar between the DRO and non-DRO plans, except for DR_{thr} = 70 Gy/s, where the use of dose rate optimisation achieved significantly higher coverage (median $\geq$ 71%) compared to plans with no dose rate optimisation (median $\geq$ 60%) (Figure 4.2 (a)). Non-DRO FLASH-PT plans achieved significantly lower DR_{prct} coverages for the lung cases for DR_{thr} = 40 Gy/s compared to DRO plans (although both had median coverages of $\geq$ 55%); although not visibly clear in Figure 4.2 (b), the difference was highlighted by evaluating the coverages across each individual fraction and dose threshold, yielding median coverages of 87% and 76% for the DRO and non-DRO plans, respectively. No significant differences were found for the lung cases at the two higher dose rate thresholds (Figure 4.2 (b)). For the DADR coverages, DRO plans outperformed the non-DRO plans for all dose and dose rate thresholds, and for both brain and lung targets, except for DR_{thr} = 40 Gy/s for the brain cases where DRO plans and non-DRO plans achieved median coverages of $\geq$ 95% and 100%, respectively (Figure 4.3).

As discussed in Chapter 3, large margins for spot placement had to be used for the dose rate optimised FLASH-PT lung plans to achieve a reasonably high $D_{95\%}$ ($\geq$ 85%); this drastically reduced the DRO FLASH-PT dose conformality in comparison to that achieved for the corresponding non-DRO plans, as seen in Figure 4.4. FLASH-PT plans were associated with reduced dose conformity compared to IMPT, irrespective of treatment planning technique used (margin-based versus robust) (relative doses in Figure 4.4 and absolute doses in Figure 4.5). The reduction in conformity, however, was not as prominent for targets located in areas with fewer density differences (e.g., bone and brain) compared to the lung targets (Figure 4.4).

The increased field size allowed by RayStation reduced the target size constraint previously imposed by the MIROpt TPS, as discussed in Chapter 3 Section 3.3. All patient cases were therefore included in the evaluations and comparisons between margin-based

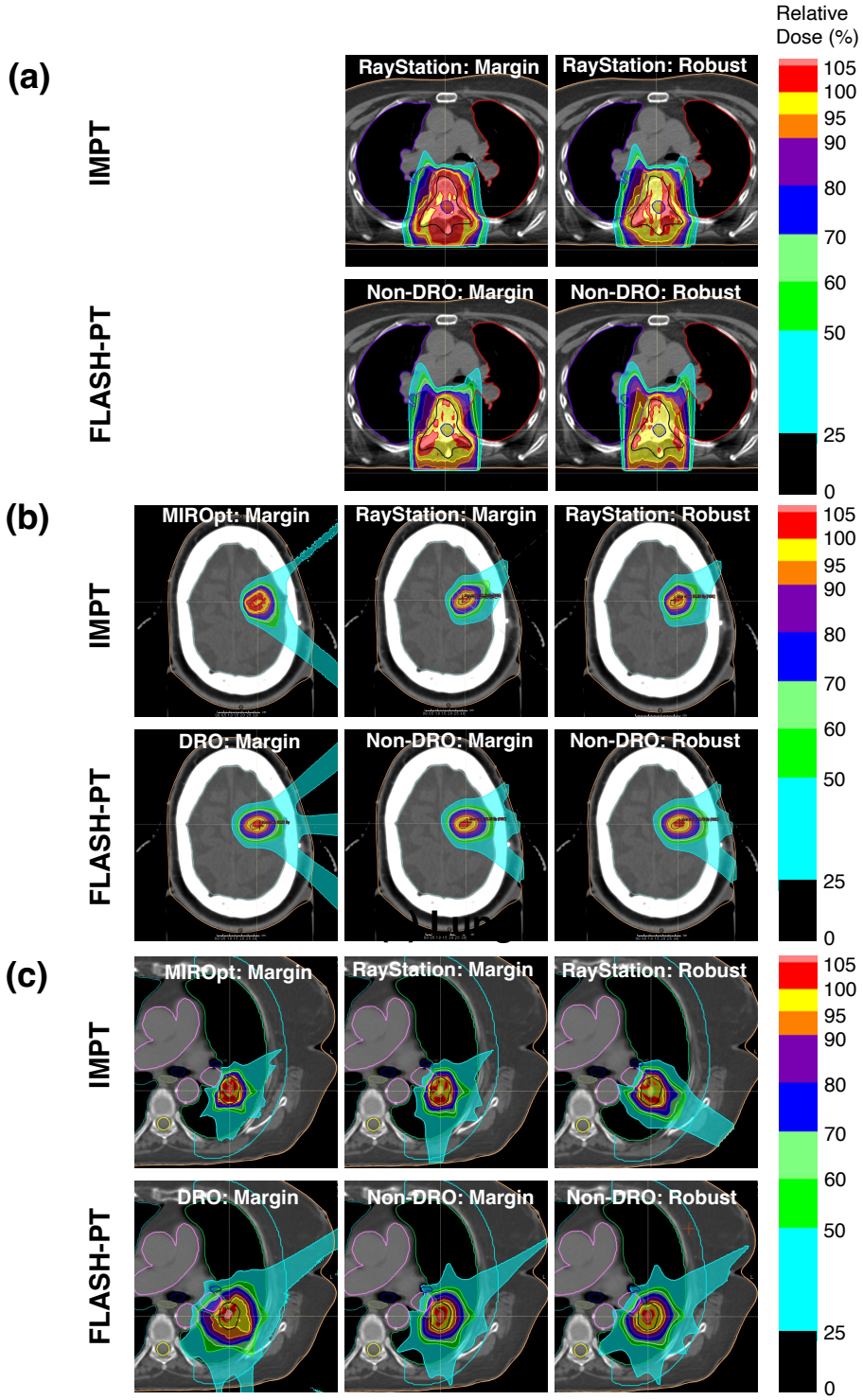


Figure 4.4: Dose map comparisons of example patient cases for the (a) bone, (b) brain, and (c) lung targets using the different treatment planning systems (MIROpt and RayStation) for the IMPT plans, optimisation techniques (dose rate optimised (DRO) and non-dose rate optimised (non-DRO)) for the FLASH-PT plans, and treatment planning techniques (margin-based and robust optimisation) for both FLASH-PT and IMPT plans. Doses are normalised with respect to the prescribed dose. Plans could not be generated for the bone cases in MIROpt due to target size constraints. The specific cases considered are Bone 1, Brain 2, and Lung 2.

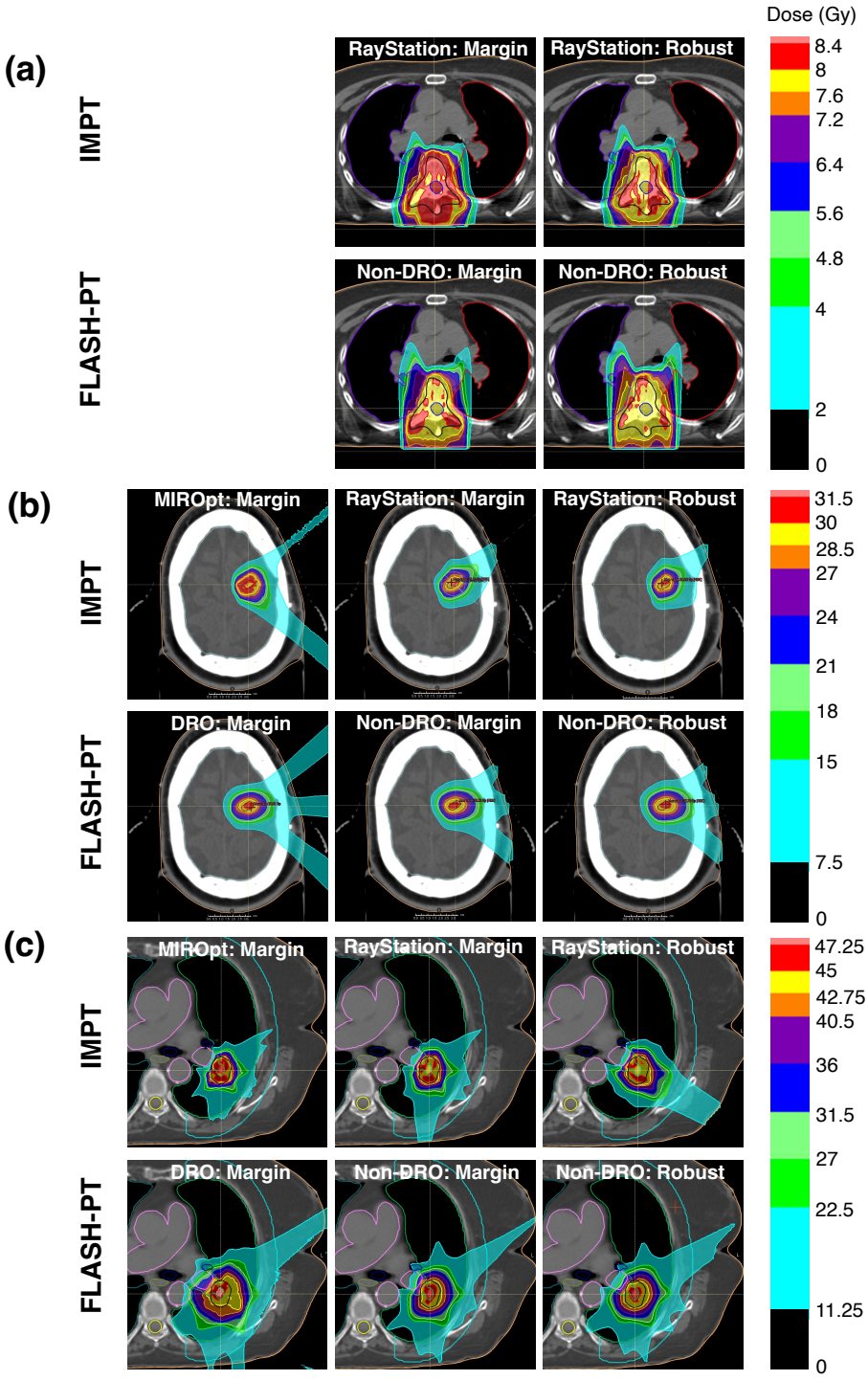


Figure 4.5: Dose map comparisons of example patient cases for the (a) bone, (b) brain, and (c) lung targets using the different treatment planning systems (MIROpt and RayStation) for the IMPT plans, optimisation techniques (dose rate optimised (DRO) and non-dose rate optimised (non-DRO)) for the FLASH-PT plans, and treatment planning techniques (margin-based and robust optimisation) for both FLASH-PT and IMPT plans. Doses are shown as absolute dose (Gy). Plans could not be generated for the bone cases in MIROpt due to target size constraints. The specific cases considered are Bone 1, Brain 2, and Lung 2.

plans and plans generated using robust optimisation; this led to margin-based FLASH-PT plans generated in RayStation to generally achieve $D_{95\%} \geq 95\%$ (Table 4.2). Still, on an individual-case basis, several margin-based FLASH-PT plans (Bone 2, Lung 1, and Lung 3) did not fulfil the target dose constraints.

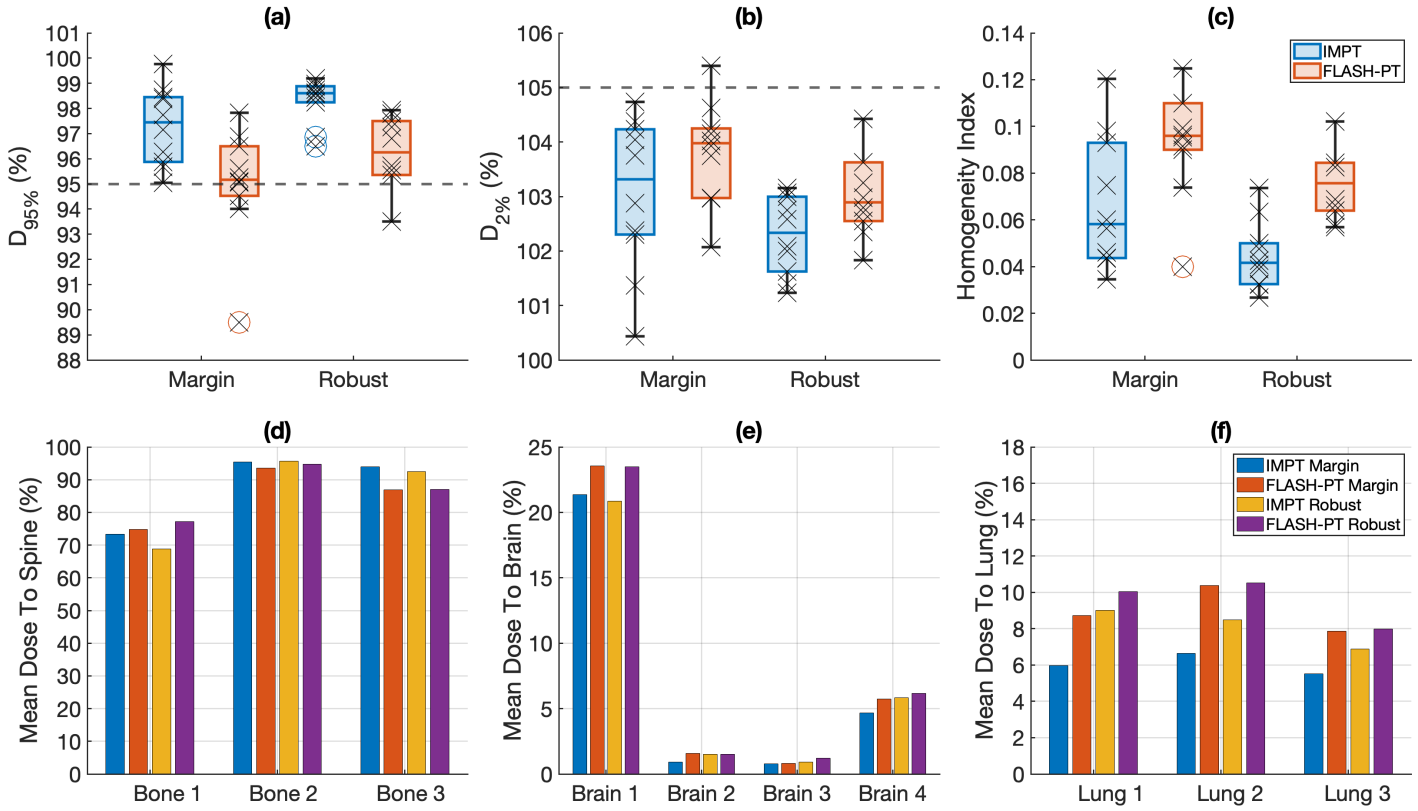


Figure 4.6: Target and organ at risk dose comparisons for the different treatment planning techniques (margin-based vs. robust optimisation). Boxplots comparing (a) $D_{95\%}$ (%), (b) $D_{2\%}$ (%), and (c) the homogeneity index (HI) (($D_{2\%}$ (%) – $D_{98\%}$ (%))/$D_{50\%}$ (%)) for each treatment planning technique and each treatment technique (IMPT (blue) and FLASH-PT (red)). Each point (x) shows the exact $D_{95\%}$ (%), $D_{2\%}$ (%), and HI for each patient case. The line within the box represents the median value, the bottom and top of the box represents the 25th and 75th percentiles, the whiskers show the range of the data points (excluding outliers), and outliers are shown using individual (o) markers. Grey dashed lines indicate target dose limits of (a) $D_{95\%} = 95\%$ and (b) $D_{2\%} = 105\%$. Mean doses to the (d) spine, (e) brain structure and (f) (irradiated) lung structure for the different planning techniques and treatment techniques are represented using bar charts. All doses are normalised with respect to the prescribed dose.

Table 4.2: Table of median values from the nominal scenario of the: mean dose (%), $D_{95\%}$, $D_{2\%}$ (%), and homogeneity index for margin-based IMPT, robust IMPT, margin-based FLASH-PT, and robust FLASH-PT simulated using RayStation.

	IMPT		**FLASH-PT**	
Dose Parameter	**Margin**	**Robust**	**Margin**	**Robust**
Mean Dose (%)	99.99	99.98	99.75	99.71
$D_{95\%}$ (%)	97.45	98.60	95.17	96.26
$D_{2\%}$ (%)	103.32	102.33	103.98	102.89
Homogeneity Index	0.06	0.04	0.10	0.08

The use of robust optimisation improved $D_{95\%}$ for both FLASH-PT and IMPT plans compared to the margin-based plans in both the nominal and worst-case scenario (Table 4.2 and Figure 4.6 (a)). All robust FLASH-PT plans, except for Bone 2, adhered to the target dose limits ($D_{95\%} \geq 95\%$ and $D_{2\%} \leq 105\%$); the width (inline and crossline) of the Bone 2 target was greater than the maximum field size used for the FLASH-PT modified beam setup in RayStation. Robust optimisation produced FLASH-PT and IMPT plans with reduced $D_{2\%}$ (nominal and worst-case) and improved target homogeneity compared to their margin-based counterparts (Tables 4.2 and 4.3, and Figures 4.6 (b) and (c)). There were non-significant differences in the nominal scenarios between margin-based and robust plans for both FLASH-PT and IMPT, except for the IMPT homogeneity index which was significantly improved when using robust optimisation. Comparisons between robust IMPT and FLASH-PT yielded significant differences in $D_{95\%}$ and the homogeneity index (Figures 4.6 (a) and (c)). Robust optimisation significantly improved the worst-case scenarios for both $D_{95\%}$ and $D_{2\%}$ compared to the margin-based worst-case scenarios, as seen in Table 4.3 (more detail

Table 4.3: Median worst-case (WC) $D_{95\%}$ and $D_{2\%}$ for intensity modulated proton therapy (IMPT) spread-out Bragg peak FLASH proton therapy plans (FLASH-PT), comparing margin-based planning and robust optimisation. Median values were evaluated across all treatment plans.

	Worst Case $D_{95\%}$		**Worst Case $D_{2\%}$**	
Optimisation Method	**IMPT**	**FLASH-PT**	**IMPT**	**FLASH-PT**
Margin	84.76	86.50	106.25	106.89
Robust	95.33	90.64	103.60	105.00

in Figure A.10 in Appendix A). However, unlike IMPT, FLASH-PT plans could not adhere to both target dose constraints for the worst-case scenarios when aiming to minimise doses to OARs such that they adhered to the OAR dose protocols. FLASH-PT achieved significantly lower worst-case $D_{95\%}$ compared to IMPT, as highlighted in Table 4.3. However, the majority of worst-case FLASH-PT plans still adhered to $D_{2\%} \leq 105\%$.

Similar to the margin-based FLASH-PT plans, robust FLASH-PT plans were also associated with non-significant increases in OAR doses compared to IMPT, with the lung cases showing the largest increase. The same trend was seen when comparing margin-based planning to robust optimisation for both IMPT and FLASH-PT (Figures 4.6 (d-f)). All margin, and robust, IMPT and FLASH-PT plans generated using RayStation adhered to the imposed OAR constraints, and are outlined in Tables A.6 - A.7 in Appendix A.

DR_{prct} coverage was not achieved for the margin-based bone plans for any dose or dose rate threshold. In contrast, minimal coverage was found for the robust bone plans for $DR_{thr} = 40$ Gy/s as seen in (Figure 4.7 (a)). The dose rate coverage observed for the bone cases in Figure 4.7(a) applies only to the Bone 1 patient, as Bone 2 and Bone 3 exhibited no ultra-high dose rate coverage. A key factor differentiating these cases is the target size (see Table 2.1 in Section 2.2), with Bone 1, Bone 2, and Bone 3 having target volumes of 62.20 cm^3, 324.09 cm^3, and 207.07 cm^3, respectively. Target size could therefore be an important factor when evaluating patient suitability for ultra-high dose rate proton therapy treatments in the future. For Bone 1, dose rate coverages were acheived to the BODY and Spine structures. The discrepancy in dose rate coverage between the margin-based and robust plans does not appear to be due to differences in mean OAR dose or number of spots, as OAR doses were comparable and the plans used 38 and 41 spots, respectively. However, differences were observed in the monitor units (MU), with the highest MU/spot in the margin-based plan reaching

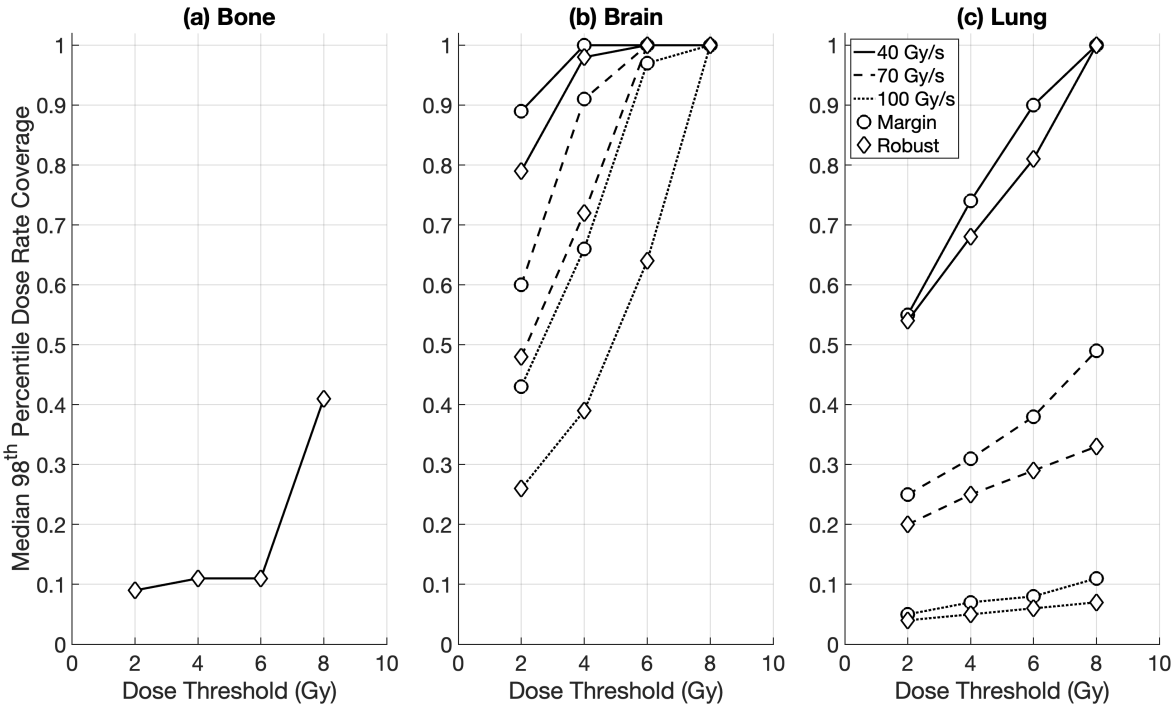
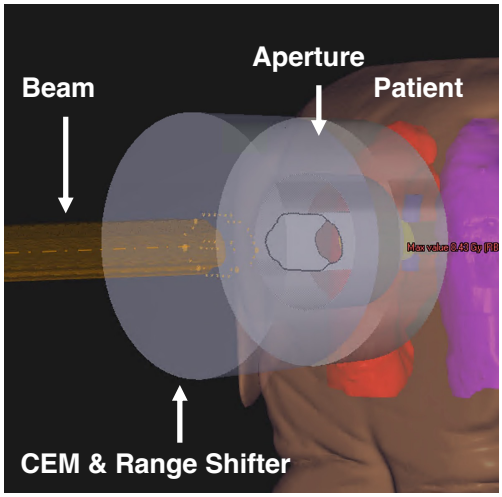
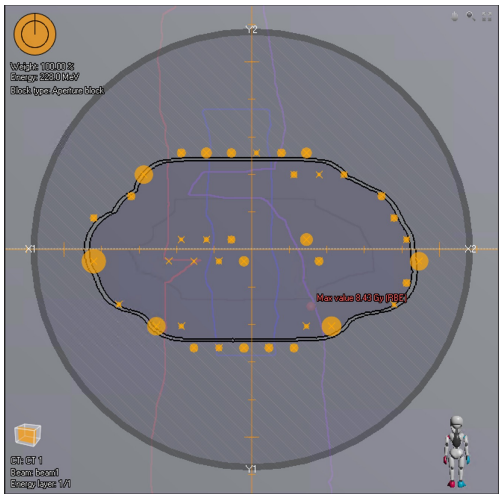


Figure 4.7: Median percentile dose rate (98^{th}th DR_{prct}) coverage for RayStation plans for (a) bone, (b) brain, and (c) lung cases for the different treatment planning optimisation techniques: margin-based (circle), and robust (diamond). Dose rate coverages were evaluated for all organs at risk using dose thresholds of 2 Gy, 4 Gy, 6 Gy, and 8 Gy, and dose rate thresholds of 40 Gy/s, 70 Gy/s, and 100 Gy/s. No dose rate coverage was achieved for margin-based bone plans for any dose or dose rate threshold, or for the robust bone plans at dose rate thresholds of 70 Gy/s and 100 Gy/s.

(a) 3D View



(b) Margin



(c) Robust

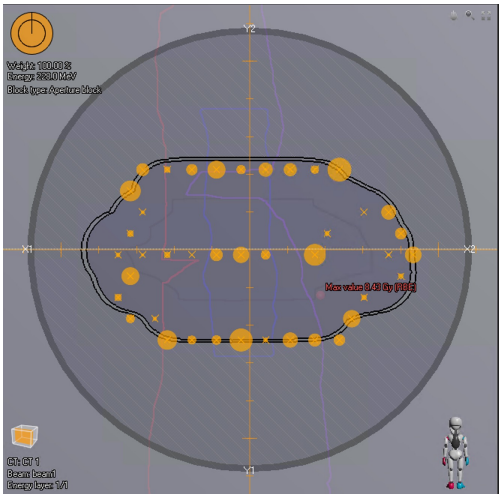


Figure 4.8: Beam eye view of the spots placed for the Bone 1 patient for margin-based and robust FLASH proton therapy plans. A 3 dimensional view is shown in (a) highlighting the incoming beam, the conformal energy modulator (CEM), the range shifter, the aperture, and the patient. Beam eye view of spot placement through the aperture hole are shown for the (b) margin-based and (c) robust FLASH proton therapy treatment plan for the Bone 1 patient. The size of the spots is proportional to the associated monitor unit of the spot.

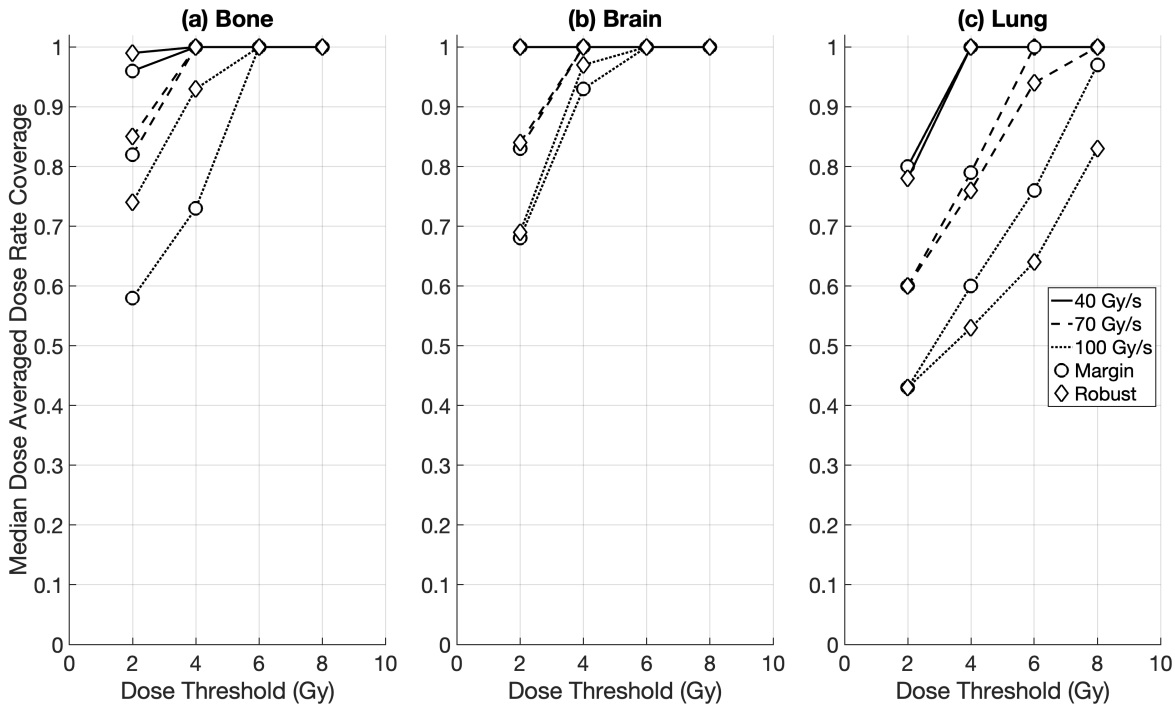


Figure 4.9: Median dose averaged dose rate (DADR) coverage for RayStation plans for (a) bone, (b) brain, and (c) lung cases for the different treatment planning optimisation techniques: margin-based (circle), and robust (diamond). Dose rate coverages were evaluated for all organs at risk using dose thresholds of 2 Gy, 4 Gy, 6 Gy, and 8 Gy, and dose rate thresholds of 40 Gy/s, 70 Gy/s, and 100 Gy/s.

169, compared to 113 for the robust plan. The spot placement in the beam eye view can be seen in Figure 4.8, where the size of each spot is proportional to its associated MU (see Section 2.1). The margin-based plan (4.8(b)) contains a few 'high' MU spots, appearing to have focused on high dose delivery through a limited number of spots. In contrast, the robust plan (4.8(c)) appears to have prioritised increasing the MU across several spots, as indicated by the lower maximum MU value compared to the margin based plan. For this relatively large target volume, the broader distribution of moderately increased MU per spot appears to improve the dose rate coverage of the plan. As per the DR_{prct} definition (see Section 1.2.7), a threshold dose must be reached within a certain time interval for an ultra-high dose rate to be achieved for that specific voxel. Distributing MU across a larger number of spots could increase the number of voxels receiving sufficient dose within short time intervals, thereby improving the DR_{prct}, even if the dose rate per spot is reduced. The reliance on dose rate definition then becomes apparent, as Figure 4.9 shows that the DADR achieves drastically higher dose rate coverage than the DR_{prct} definition for the same spot placements and MU/spot shown in Figure 4.8.

Due to margin-based bone plans not achieving any dose rate coverages, no statistical DR_{prct} comparisons could be made between the margin-based and robust treatment plans for the bone targets. For the remaining cases, the differences between margin-based and robust DR_{prct} were non-significant, except for DR_{prct} = 100 Gy/s and DR_{prct} = 70 Gy/s for the brain and lung cases, respectively (Figure 4.7 (b) and (c)). No major difference was found between the 95^{th} and the 98^{th} DR_{prct} definitions across all patient cases and optimisation techniques (margin versus robust). DADR coverages were significantly higher than the DR_{prct} coverages for all cases and optimisation techniques. Similar DADR coverages were achieved for margin-based and robust FLASH-PT plans for each dose rate threshold and target type, as seen in Figure 4.9.

Dose volume histograms for the different TPSs, treatment techniques, and treatment

planning techniques for the example patient cases shown in Figure 4.4 are shown in Figures A.5 - A.7 in Appendix A.

4.4 Discussion

Potential FLASH-related normal tissue sparing effects were not accounted for in the FLASH-PT treatment planning process. The results in this Chapter therefore only represent the feasibility and limitations of the dose distributions achieved using the FLASH-PT modified beam setup when compared to IMPT.[3]

Non-DRO FLASH-PT plans were associated with significant improvements in target dose coverage ($D_{2\%}$ and homogeneity) compared to DRO plans. There were non-significant differences in OAR doses between the optimisation techniques, despite the non-DRO FLASH-PT plans showing a trend of reduced doses to OARs. DRO FLASH-PT plans consistently achieved higher dose rate coverages than non-DRO plans across dose thresholds, dose rate thresholds, target types, and dose rate definitions. This was particularly exemplified for the brain cases, where the DRO plans maintained higher DR_{prct} coverages at the higher dose rate thresholds ($\geq$ 70 Gy/s) across more dose levels, indicating a greater ability to sustain high-dose rate conditions compared to the non-DRO plans. For the lung cases, a clear discrepancy was observed: margin-based non-DRO plans produced significantly lower DR_{prct} at 40 Gy/s, whereas DRO plans were able to maintain higher coverages despite the challenges of tissue heterogeneity. The higher dose rate coverages associated with the DRO plans were also seen for the DADR definition.

Regions of greater density differences (such as lungs), where it is inherently more difficult to achieve high dose rate coverages, may require dose rate optimisation compared to regions with fewer density differences (such as the brain). However, the large

[3]Section 4.4 is based on the published work by Lövgren et al., The Impact of Dose Rate Optimisation and Robust Optimisation on FLASH Proton Therapy Treatment Plan Quality and Dose Rates, *Frontiers in Oncology*, 2025 [35].

variation in dose rate coverages along with the difficulty in controlling the dose rates for the lung cases (for the different TPSs, treatment planning techniques, and dose rate definitions) serve as an indication of the lungs being a poor FLASH-PT site candidate.

A clinical observation by Daartz et al. (2024) found that areas of elevated (sub-FLASH) instantaneous dose rates correlated to regions of necrosis in a brain patient who had received proton therapy [126]. Areas of elevated dose rates also receive more dose, and as the area of necrosis was distal to the target, it is not implausible that it could also be correlated to an increase in linear energy transfer and relative biological effectiveness [130]. However, if sub-FLASH instantaneous dose rates do cause normal tissue damage, the use of a TPS which utilises a dose rate optimiser may be of greater interest to minimise the prevalence of sub-FLASH dose rate hotspots in normal tissues. Conversely, *in vivo* studies by Paillas et al. (2025) and Singers Sørensen et al. (2024) found reduced normal tissue toxicities at dose rates as low as 1 Gy/s and 2 Gy/s for single dose deliveries, respectively [70, 107]. Both studies also showed an increase in the normal tissue sparing effect with increasing dose rate. So, if the FLASH effect can be elicited for a range of dose rates (given increased fraction doses), with an effect proportional to the dose rate, a dose rate optimising TPS may not be essential, and a TPS resulting in plans with improved target and OAR doses may be of more benefit. While the studies by Daartz et al., Paillas et al., and Singers Sørensen et al. differ in many aspects, they still highlight the need for further investigations into the impact of dose rates below the 40 Gy/s threshold, and the corresponding fraction doses, on normal tissue toxicity.

With respect to dose rate coverages achieved, dose rate optimised FLASH-PT plans outperformed the non-dose rate optimised plans, which is not unexpected. Nevertheless, target and OAR doses remain the top priority, and DRO plans were also associated with worsened plan quality compared to non-DRO plans.

Given the low importance weight required for the MIROpt dose rate objective function to not dominate over the treatment plan optimisation, the inclusion of the dose rate objective could the one of the reasons for the reduction in plan quality. Once a similar dose rate optimisation function has been implemented in RayStation, a future comparison between the two systems may offer more insight; until then, dose rate optimisation which directly impact the dose optimisation should be used with caution, as it may significantly degrade treatment plan quality. However, different strategies have been shown to increase the dose rate without explicitly being part of the dose calculation and optimisation, with examples including: a sequential scan-pattern optimisation proposed by José Santo et al. (2023), a fast spot order demonstrated by Wase et al. (2025), a spot delivery sequence optimisation demonstrated by Zhao et al. (2024), and a spot-position and spot-weight optimisation proposed by Lansonneur et al. (2024) [131–134].

Robust FLASH proton therapy has only been investigated in the context of comparing spread-out Bragg peak to transmission beam treatment plans, with other studies comparing robust IMPT to margin-based FLASH-PT [100, 112, 113, 135]. The results in this Chapter therefore provide important insights into the feasibility and limitations of robust and margin-based FLASH-PT by directly comparing the FLASH-PT plans to their conventional IMPT counterparts. Robust FLASH-PT plans yielded significantly better target dose coverage in the worst-case scenarios than the corresponding margin-based plans. Despite robust FLASH-PT plans trending towards improved target dose coverage in the nominal scenarios, the differences when compared to margin-based plans were non-significant. The improvement may become statistically significant if each target type is investigated individually with larger sample sizes.

DR_{prct} and DADR coverages were generally unaffected by the treatment planning technique used, except for the DR_{prct} coverages at $DR_{thr} = 100$ Gy/s and $DR_{thr} = 70$ Gy/s for the brain and lung cases, respectively. These thresholds may indicate a limit at which margin-based and robust planning begin to diverge, with brain cases having a

higher threshold than lungs. However, as the DR_{prct} coverage for the lung cases at $DR_{thr} = 100$ Gy/s (for the two techniques) converged again, the behaviour may not be so straightforward. Nevertheless, the benefits of improved target dose coverage associated with robust FLASH-PT planning can be exploited without sacrificing ultra-high dose rate coverage, potentially up to a certain limit depending on the target location.

In terms of clinical applicability, however, robust FLASH-PT plans still do not match target dose coverage, doses to OARs, and dose conformality when compared to their IMPT counterparts. This could partly be due to the use of SFO for the FLASH-PT plans compared to the use of MFO for IMPT. However, as shown in Chapter 3 Section 3.3, for the exact same patient cases considered in this Chapter, no significant differences in target dose coverage was found when comparing MFO to SFO for margin-based IMPT plans generated using MIROpt [34]. As the discrepancy between the FLASH-PT and IMPT plans extend across TPSs and treatment planning techniques, the difference in treatment plan quality is more likely due to the FLASH-modified beam setup which impose scattering effects and range straggling. The scattering effects lead to increased spot sizes, making it more difficult to achieve an equivalent dose distribution between the two techniques.

The choice of dose rate definition used in studies is critical given the variations in dose rate coverages reported in the literature, and as shown in this Chapter [34, 100, 103, 109, 112–115]. The use of the DADR definition significantly increased the dose rate coverages compared to the DR_{prct} definition, regardless of TPS, treatment planning technique (margin vs. robust), or target type (bone, brain, lung). The impact of this substantial increase is particularly exemplified by the difference in dose rate coverage for the bone cases. The use of the DR_{prct} definition warranted exclusion of the bone cases from the study as the dose rate coverage was too low for the FLASH sparing effect to be of benefit to the patient. However, the DADR definition would favour FLASH-PT for the patient cases due to its potential dose rate coverage of $\geq$

80% for dose rates of 40 Gy/s and 70 Gy/s. The same trend was observed for the lung cases. The significant increase in dose rate coverage is likely a by-product of the DADR formulation (Equation 1.7 in Section 1.2.7), where the cumulative effect of all the low-dose voxels amounts to a higher DADR without explicitly incorporating the irradiation time. In contrast, the DR_{prct} definition, which depends on the irradiation time (Equation 1.6 in Section 1.2.7), leads to more variations in dose rate coverages; these variations appear dependent on the dose threshold, dose rate threshold, distribution of spot placement, MU/spot, and target location. Multiple dose rate definitions should therefore be incorporated in treatment planning studies to ensure that the data is fairly represented. A recent meta-analysis study by Colizzi et al. (2025) showed that, for pencil beam scanned proton beams, the percentile dose rate (see Section 1.2.7) was the only definition consistent with the FLASH sparing effect observed pre-clinically [136]. It may therefore be of interest to include this in future dose rate analyses to determine if ultra-high percentile dose rates are achievable to clinically relevant target volumes, as has been shown to vary depending on target location in this work.

Robust optimisation enhanced target dose coverage and improved FLASH-PT and IMPT treatment plans irrespective of target location, significantly improving the worst-case scenarios for both treatment techniques compared to margin-based planning. The reduction in scattering effects and range straggling, due to the FLASH-PT modified beam delivery, will be key in generating IMPT-equivalent FLASH-PT treatment plans. It would be of interest to investigate how these scattering effects can be reduced whilst maintaining ultra-high dose rates. A potential avenue to explore is reducing the initial energy of the FLASH-PT beam; this would reduce the amount of material needed in the range shifter, thereby reducing scattering and range straggling. Further to this, if the energy selection process can occur more rapidly through the use of a superconducting gantry, as proposed by Zeng et al., the static energy modulators will become redundant, and the scattering effects reduced [113]. If either solution can be realised, spread-out Bragg peak FLASH proton therapy will be one step closer to clinical im-

plementation.

In this Chapter, we aimed to investigate the impact of dose rate optimisation and robust optimisation on FLASH-PT treatment plan quality and dose rates. Comparisons between FLASH-PT and IMPT plans were also made to determine the clinical applicability of FLASH-PT, without accounting for a FLASH sparing effect. The use of dose rate optimisation as part of the FLASH-PT treatment planning process led to higher dose rate coverages for both dose rate definitions considered. FLASH-PT plans generated without a dose rate optimiser significantly improved $D_{2\%}$ and target dose homogeneity but were associated with reduced dose rate coverages. Although dose rate optimisation might be useful for increasing dose rate coverage, it should be used with caution as it could significantly degrade the plan quality. Robust FLASH-PT treatment planning can enhance target dose coverage without compromising doses to OARs or ultra-high dose rates, compared to margin-based planning. However, FLASH-PT plans still do not match target dose coverage, doses to OARs, and dose conformality when compared to their IMPT counterparts. For both nominal and worst-case scenarios, the FLASH-PT plans struggle to achieve IMPT-equivalent $D_{95\%}$. Furthermore, robust FLASH-PT plans could only adhere to $D_{2\%} \leq 105\%$, and not $D_{95\%} \geq 95\%$, in the worst-case scenarios when attempting to reduce doses to OARs in line with IMPT. The dose rate definition is critical when evaluating FLASH-PT plans. The DADR definition led to significantly higher coverages compared to the DR_{prct} definition for both TPSs and optimisation techniques (margin vs. robust) used.

Chapter 5

Non-Maximal Energy Spread-Out Bragg Peak FLASH Proton Therapy

5.1 Introduction

We have so far in Chapters 3 and 4 investigated the feasibility and constraints of spread-out Bragg peak FLASH proton therapy (FLASH-PT) treatment planning using different treatment planning systems (TPSs) and optimisation techniques (robust versus margin-based planning and dose rate versus non-dose rate optimisation).[1] A commonality between these comparisons is the increase in doses to organs at risk (OAR) associated with the FLASH-PT plans when compared to their intensity modulated proton therapy (IMPT) counterparts. Further to this, robust optimisation was found to improve $D_{95\%}$ for the FLASH-PT plans in the nominal scenario, however, still with significant differences between FLASH-PT and IMPT in the worst-case scenarios when attempting to reduce doses to OARs in line with IMPT [35].

As the increase in OAR doses extended across TPSs and treatment planning techniques, we are interested in investigating whether the inferior FLASH-PT plan quality is due to the use of the maximum beam energy, which leads to increased scattering and range straggling (see Section 1.1) [34, 112]. It is therefore of interest to evaluate

[1] Chapter 5 is based on the work by Lövgren et al., Initial Beam Energy and Target Volume Dependency of Spread-Out Bragg Peak FLASH Proton Therapy on Treatment Plan Quality and Achievable Dose Rates for Brain Targets (*under review*).

whether further modifications to the FLASH-PT beam delivery may offer improvements to the FLASH-PT dose distributions. To mitigate for the scattering effects and range straggling, one way would be to reduce the amount of material needed to degrade the energy of the incoming particles.

In this Chapter, we will explore the idea of using non-maximal beam energies ($<$ 230 MeV), instead of the maximum, in combination with the FLASH-PT beam setup discussed in Chapter 2 Section 2.1. By lowering the initial energy of the proton beam, the amount of range shifter material is decreased, thereby reducing scattering and range straggling. This should reduce spot sizes, allowing for more conformal dose delivery, whilst also reducing doses to OARs. Chapters 3 and 4 implemented the maximum beam energy as it maximises the transmission efficiency, and thus dose rate, of the protons. Lower energies, however, are associated with increased beam losses and therefore reduced transmission efficiencies, with the transmission efficiency being directly proportional to the beam current [105, 137]. Beam currents can therefore be evaluated if the transmission efficiency of a beamline and the beam current at the cyclotron exit are known. To account for the beam losses, beam currents corresponding to the non-maximal energies will be implemented into the dose rate calculations. The impact of the changing beam current on the achievable dose rates will therefore be investigated for three different scenarios:

1. A realistic scenario where the beam current is equivalent to that of an existing high energy proton therapy beamline (detailed description in Section 5.1.1).

2. An improved scenario, where the momentum spread of the protons is reduced (also known as momentum cooling), which increases the transmission efficiency (detailed description in Section 5.1.2).

3. An ideal, albeit not currently available, scenario of using a variable energy cyclotron where the beam current at the isocentre can remain constant for varying energies (detailed description in Section 5.1.3).

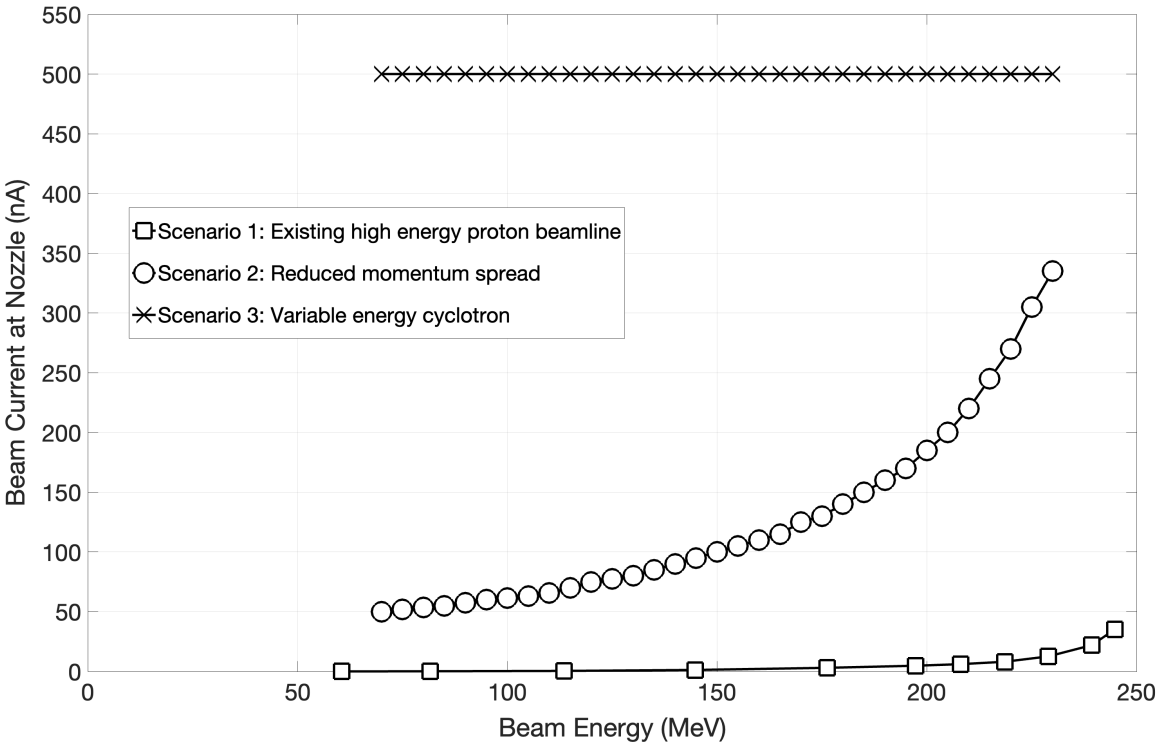


Figure 5.1: Beam current at nozzle (nA) with respect to the degraded beam energy (MeV) of the proton beam shown for different beam delivery scenarios. Scenario 1: existing high energy proton beamline (square) by Aylward et al. (2023) [138]. Scenario 2: reduced momentum spread for a compact gantry (o) demonstrated by Maradia et al. (2023) [139]. Scenario 3: the use of a light and compact variable energy cyclotron (x) as proposed by Winklehner et al. (2025) [140].

Several studies investigating improvements to proton beamlines and energy selection systems report on the transmission efficiencies for a range of degraded beam energies. However, it is common for these studies to only report the total transmission from the cyclotron exit to the degrader in the energy selection system (see Section 1.1.3) and not to the nozzle due to the dependency of the transmission on the particular proton therapy facility and beamline considered [141–144]. As this work aims to evaluate dose rates at the patient level, knowledge of the beam current at the nozzle is essential, as it is representative of the current delivered at the isocentre. In this context, the impact of the FLASH-modified beam delivery must also be considered. The inclusion of a range shifter and conformal energy modulator (described in Section 2.1) should not lead to any reduction in beam current as they do not remove any protons from the beam. The aperture, however, may reduce the transmission efficiency of the pencil beam spots that are placed on the edge of the block due to absorption. The potential reduction in transmission efficiency due to the inclusion of the aperture is currently unknown and so, for simplicity, it is assumed that it does not lead to any significant changes in current. Further to this, it is worth noting that the beam delivery scenarios considered in this study only serve as indications on the magnitude of dose rates that can be achieved and does not account for all the intricacies of the different beam delivery methods considered.

5.1.1 Scenario 1: High Energy Beam Delivery

For Scenario 1, we are considering the use of an operational high energy proton therapy research beamline presented and characterised by Aylward et al. (2023) to determine its ultra-high dose rate capabilities [138]. This beamline is utilised at The Christie (NHS Foundation Trust, Manchester, United Kingdom) and, in its clinical configuration, allows for beam energies of 70 MeV to 245 MeV when utilising the maximum cyclotron current supplied by an isochronous cyclotron at 800 nA[138].

A double-carbon wedge energy selection system is used to produce varying beam ener-

gies, with a maximum achievable transmission (at 245 MeV) of 7.05% ± 0.10%, with a beam current of 56.4 nA ± 0.8 nA [138]. Interestingly, when investigating the achieved ultra-high dose rates for individual spots, Aylward et al. (2023) found that at the maximum beam energy, the highest dose rate occurred in the plateau region of the proton beam, not at the Bragg peak [138]. This behaviour arises from the use of narrow pencil beams, where lateral equilibrium is not established. As protons undergo multiple Coulomb scattering with increasing depth, particles are scattered away from the central axis without being replenished from surrounding regions. This leads to a reduction in on-axis fluence and hence a lower instantaneous dose rate at the Bragg peak. Therefore, the observed reduction in dose rate at depth is not solely due to geometric spot broadening, but rather to the combined effect of lateral scattering and the absence of lateral particle equilibrium. At lower beam energies, where the proton range is shorter and lateral scattering is reduced, this loss of on-axis fluence is less pronounced. As a result, the relative dose rate at the Bragg peak should increase compared to high-energy beams, allowing for potential sparing of normal tissues which already receive high doses. The beam current at the nozzle with respect to degraded beam energy for this scenario can be found in Figure 5.1 [138].

5.1.2 Scenario 2: Reducing Momentum Spread with a Compact Gantry

For Scenario 2, we are considering the use of momentum cooling (reduced momentum spread) for a compact proton therapy gantry, as demonstrated by Maradia et al. (2023) [139]. The authors experimentally show that the use of a single wedge, instead of a momentum selection slit which absorbs the high- and low-energy protons, can improve transmission. The wedge is designed such that the higher energy protons have to traverse through the thicker part of the wedge, whilst the lower energy protons traverse through the thinner part of the wedge; this leads to a more uniform momentum spread without the associated beam losses of standard momentum selection slits [139].

The compact proton therapy gantry was based on a commercial 250 MeV cyclotron with a beryllium energy degrader, and a maximum extraction current of 800 nA [139]. The wedge is made of polyethylene, with a density of 0.94 g cm^{-3}, and its thickness is dependent on the beam energy (and thus momentum) [139]. The design of the beamline following the wedge is based on that of the Paul Scherrer Institute's Gantry 2; with the Monte Carlo based Beam Delivery Simulation (BDSIM) code which was used to evaluate the transmission efficiency having previously been experimentally validated for this beamline [139, 145, 146].

Of course, transmission efficiency is dependent on the specific beamline used, however, for the sake of investigating the potential dose rates which could be achieved, we are only interested in the achievable beam current at the nozzle. The beam current at the nozzle for this particular compact proton therapy system with a momentum cooling wedge for a range of clinical beam energies can be found in Figure 5.1 [139].

5.1.3 Scenario 3: Variable Energy Cyclotron

For Scenario 3, we are considering the use of a variable energy cyclotron. As discussed in Section 1.1.2, protons can be accelerated using a cyclotron, which has a fixed extraction energy. Lower energies can be obtained through the use of an energy selection system (see Section 1.1.3) or with the use of static energy degraders. A variable energy cyclotron, however, would, as its name suggests, allow for extractions of protons at variable energies.

Now, there are no clinically used variable energy cyclotrons, with the only one operating at clinically relevant energies (70 MeV - 230 MeV) being the 520 MeV cyclotron at TRIUMF (Vancouver, Canada) [147]. TRIUMF, in addition to being a research facility, is also one of the largest normal conducting cyclotrons in the world. More compact, variable energy cyclotrons have been suggested for implementation into clinical facilities. Baumgarten et al. (2013) and Hori et al. (2019) both tackled this problem

through different approaches, focusing solely on the mechanics of the cyclotron systems, although neither outlined information regarding the extracted beam current achieved for the suggested acceleration systems [137, 148]. Winklehner et al. (2025), however, recently proposed a compact, lightweight, variable energy (synchro)cyclotron with the requirement of achieving a 500 nA after extraction for any given beam energy [140]. The proposed cyclotron eliminates the need for an iron yoke, that is, the heavy structure which facilitates the creation of the magnetic field and instead adopts the use of superconducting coils [140, 149]. This significantly reduces the weight of the system, and also allows for a linear relationship in beam current and magnetic field, leading to smoother variation in beam energy than with a conventional cyclotron [140]. The feasibility of the proposed variable energy cyclotron was demonstrated through simulations studies, and due to it being an idealised particle accelerator system, evaluations did not include emittance or energy spread. The beam current at the nozzle for this scenario can be found in Figure 5.1 [140].

5.2 Materials and Methods

Given the improved target dose coverage and organ at risk (OAR) dose rate coverage for the brain targets in Chapter 4, this Chapter focuses solely on brain targets. Ten brain patients were considered, with target volumes ranging between 9.98 cm^3 - 92.97 cm^3, with a median volume of 36.70 cm^3. A prescribed dose of 30 Gy in 3 fractions was used for all treatment plans. Detailed patient information can be found in Table 2.2 in Section 2.2.2.

Chapter 4 also showed that FLASH-PT plans generated with robust optimisation were associated with improved target doses, compared to margin-based plans, without sacrificing dose rates. Robust optimisation was therefore adopted for all FLASH-PT and IMPT plans in this study, with setup and range uncertainties outlined in Table 2.2 in Section 2.2.2. Worst-case scenarios were evaluated for $D_{95\%}$ and $D_{2\%}$. In this Chapter, all treatment plans were required to pass $D_{95\%} \geq 95\%$ and $D_{2\%} \leq 105\%$ in the worst-

case scenarios; creating a baseline for all plans for which the reduction in OAR doses could then be investigated. Any subsequent reference to target dose, for any treatment plan, refers to the dose to the clinical target volume in the nominal scenario, unless the worst-case scenario is explicitly stated.

Robust FLASH-PT and IMPT treatment plans were generated using RayStation as described in more detail in Section 2.3.4. IMPT plans were generated using the principles described in Section 2.3.1, and the maximum energy layer used for each beam was noted down. For the non-maximal energy FLASH-PT plans, the maximum energy layer of the corresponding IMPT beam was used as the initial beam energy, as this should, in theory, ensure that the protons reach the required depth for each beam. If the FLASH-PT plans do not achieve 100% robustness pass rate for the IMPT-based initial energy, the beam energy was increased in increments of 10 MeV until robustness was achieved. Robustness was evaluated for each of the individual FLASH-PT fractions. The treatment planning process is outlined in a flowchart shown in Figure 5.2, and the beam energies used for the variable energy plans are outlined in Table 5.1. Lateral margin sizes remained the same between the maximum and non-maximal energy plans; the results presented in this Chapter are therefore only dependent on the actual energy change.

FLASH-PT plans were again, due to the patient- and field-specific beam setup, simulated for a one-beam-per-fraction delivery along with single field optimisation. Dose rate optimisation was not considered in this Chapter, but dose rate improvements were performed through the removal of low-weighted spots (spots with monitor units (MU) less than 20 MU/fraction), unless the plan quality was severely impacted and lower MU/fraction thresholds (5 Mu/fraction - 10 MU/fraction) were instead adopted. Low-weight spot removal was performed for both maximum energy and non-maximal energy FLASH-PT plans.

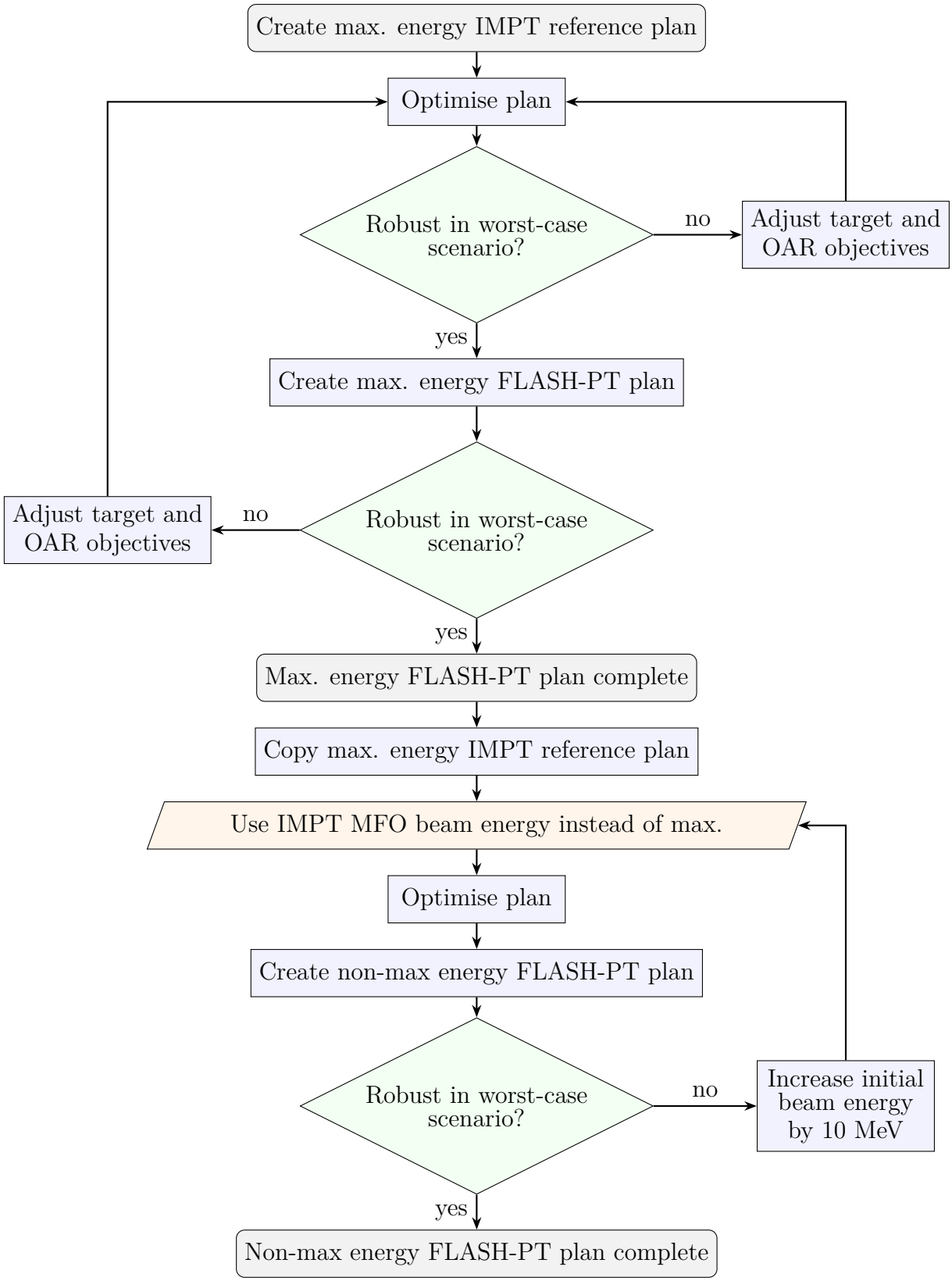


Figure 5.2: Flowchart outlining the non-maximal energy FLASH-PT treatment planning process. Rounded boxes denote the start/end, sharp corner boxes denote processes, diamonds denote decisions, and parallelograms denote inputs. The box 'Max. energy FLASH-PT plan complete' is the end of the maximum beam energy FLASH-PT treatment planning process, and also forms the foundation and start for the non-maximal (non-max) energy FLASH-PT planning process.

Dose rate coverage was defined as the relative number of non-target voxels receiving total doses $\geq x$ Gy at dose rates $\geq y$ Gy/s, and were evaluated using the 95^{th} percentile dose rate (DR_{prct}), the dose averaged dose rate (DADR), and the average dose rate (ADR) definitions, as outlined in Section 1.2.7. Colizzi et al. (2025) recently demonstrated that, for pencil beam-scanned proton beams, the DR_{prct} was a dose rate definition that consistently described the FLASH sparing effect, based on a meta-analysis of murine skin data [136]. Further to this, Grilj et al. (2025) also recently showed that the ADR may be one of the main beam parameters related to the FLASH effect, although for electron beams [110]. It would therefore be interesting to investigate the behaviour of the ADR in comparison to the DR_{prct} and DADR for proton beams in the context of clinical targets, and so the ADR was also included in the dose rate evaluations. Furthermore, in this Chapter, we decided to increase the amount of dose and dose rate thresholds included to reflect findings in the literature by Paillas et al. (2025) and Singers Sørensen et al. (2024) which found a normal tissue sparing FLASH effect (for single dose deliveries) at dose rates as low as 1 Gy/s and 2 Gy/s, respectively [70, 107]. Both studies reported increasing normal tissue sparing for increasing dose rates. The dose and dose rate thresholds were therefore set as x = {2, 4, 6, 8, 10} Gy and y = {1, 2, 5, 10, 20, 30, 40, 50, 60, 70, 80, 90, 100} Gy/s. Dose rate coverages were calculated for each OAR within each individual fraction, and dose rate coverages below 1% were excluded from the evaluations as values below this limit were smaller than the associated uncertainty of the simulated data.

FLASH-PT plans generated using the maximum and non-maximal beam energy will be referred to as FLASH Max and FLASH Non-max, respectively. Similarly to Chapters 3 and 4, a biological FLASH sparing effect is not accounted for in order to evaluate the physical dose distributions achieved with the FLASH-PT modified beam delivery. A relative biological effectiveness of 1.1 was assumed for all IMPT and FLASH-PT plans, and treatment plan evaluations and comparisons are described in Section 2.4.

5.3 Results

Table 5.1 shows the beam energies used for the FLASH Non-max plans; beam energies denoted with an asterisk (*) indicate the plans for which the IMPT energy did not achieve 100% robustness pass rate, and the energy had to be increased. For Patient 3 (Beam 3), the maximum beam energy of 228 MeV had to be utilised as a robust FLASH-PT plan could not be achieved for any lower beam energy.

All treatment plans adhered to the target dose constraints of $D_{95\%} \geq 95\%$ and $D_{2\%} \leq 105\%$ in both the nominal and worst-case scenarios. FLASH-PT plans with the maximum beam energy were still associated with significantly lower $D_{95\%}$ than IMPT, with IMPT and FLASH Non-max being similar to each other, as seen in Figure 5.3 (a). No significant differences were found for the $D_{2\%}$ or homogeneity index between the techniques, as shown in Figures 5.3 (b) and (c).

FLASH Non-max was associated with a reduction in the dose distal to the target structure compared to FLASH Max, as shown in relative doses in Figure 5.4 and absolute doses in Figure 5.5. Evaluations of the radiation conformity index using Equation 2.1 (see Section 2.4), revealed no differences between the modalities; further illustrated by the dose maps for Patients 1, 6, and 10, shown as representative cases in Figure 5.4. Only the IMPT plans showed a significant (Pearson) correlation between target size and dose homogeneity, with an increased target size being associated with more homogeneous target dose ($\rho_{PCC} = 0.71$, $p = 0.023$). The reduction in initial beam energy led to a significant increase in the number of spots placed with median number of spots of 38 and 71 for FLASH Max and FLASH Non-max, respectively.

Dose volume histograms of the median dose to OARs, evaluated across all patient cases and for the different treatment modalities, further highlighted the reduction in dose to surrounding normal tissues, as shown in Figure 5.6. The dose constraints and planning doses for each OAR and each patient case can be found in Tables B.2 - B.10

in Appendix B. OAR structures located in the beam path, such as the Chiasm (Figure 5.6 (c) and Table 5.2), were expected to have similar doses when comparing FLASH Max and FLASH Non-max. However, for structures which were further away from the target, such as the Optic Nerves, Eyes, and Lenses, where FLASH Max was typically associated with increased doses compared to IMPT, FLASH Non-max achieved lower doses across all the OARs (Figure 5.6 (g-l)). Dose volume histograms for the example cases in Figures 5.4 and 5.7 are shown in Figures B.1 - B.4 in Appendix B.

This discrepancy in OAR doses was also highlighted in Table 5.2, where the ratio between mean OAR doses for FLASH Max and FLASH Non-max were evaluated with respect to IMPT. That is, for each OAR, the ratio of mean dose delivered using FLASH Max versus IMPT and FLASH Non-max versus IMPT was calculated, with Table 5.2 showing the median ratio across all patient cases. Ideally, the ratio between the FLASH-PT techniques to IMPT with regards to OAR doses should be as close to 1 as possible, however, as seen in Table 5.2, that was not the case. FLASH Max led to mean OAR doses that were between a factor of 1.03 - 3.04 higher than that of conventional IMPT depending on the OAR considered. FLASH Non-max, however, led to doses ranging between 0.96 - 2.22 to that of IMPT, depending on the OAR. Generally, FLASH Non-max was associated with lower mean doses to OARs compared to FLASH Max, with a difference in mean dose ratio between -0.01 to 1.51, depending on the OAR considered. The largest reductions in ratios occurred for the OARs located further away from the target, also demonstrated in Figure 5.6. One can appreciate that for clinical evaluations, relative doses are not as important as absolute doses; nevertheless, it is still important to quantify differences between dose distributions as done in Table 5.2 whilst also considering absolute doses, as demonstrated in Figure 5.6. With respect to planning dose constraints, stereotactic body radiation therapy-based protocols were used for guidance, as they are the closest available for the fractionation scheme considered. However, these protocols are designed for smaller lesions and are not directly transferable. Therefore, the results should be interpreted as indicative

rather than demonstrating agreement with established clinical constraints, highlighting the need for FLASH-specific or hypofractionated proton dose guidelines.

The difference in OAR doses can also be seen in relative doses in Figure 5.7 and absolute doses in Figure 5.8, for the same patient cases considered in Figure 5.4. Figure 5.7 shows that both FLASH Max and FLASH Non-max achieves equivalent target dose distributions, also demonstrated in Figure 5.3, with a clear difference in doses surrounding the target. FLASH Max is associated with approximately a 5% - 25% increase in doses to surrounding structures, relative to the prescribed dose. However, both of these techniques are associated with increased doses to surrounding OARs compared to IMPT, as highlighted in Figure 5.6 and Table 5.2.

Comparisons between the IMPT, FLASH Max, and FLASH Non-max plans with respect to stereotactic body radiotherapy (SBRT) dose protocols, as well as the clinical proton plans delivered to the patients (as discussed in Section 2.4) are presented in Tables B.2 - B.10 in Appendix B. SBRT protocols were used due to the lack of guidelines for FLASH-PT treatment planning, in addition to the hypofractionated regimen adopted for SBRT beam delivery. However, SBRT is typically used for target volumes smaller than those considered in this Chapter.

Figure 5.9 shows the DR_{prct} coverage for the Brain, Brain Stem, Right Hippocampus, and the Left Optic Nerve for different dose thresholds. Coverages are also shown for the different beam delivery scenarios: maximum beam energy (Max), high energy proton therapy beam delivery (Scenario 1), momentum cooling for a compact gantry (Scenario 2), and for the use of a variable energy cyclotron (Scenario 3). As expected, the dose rate coverage increases with increasing dose threshold, and decreases with increasing dose rate threshold.

Across OARs and dose thresholds, DR_{prct} coverages did not differ significantly between

Max and Scenario 3, except for the Right Hippocampus at 10 Gy, where Scenario 3 showed a reduced coverage at 60 Gy/s whereas Max remained at full coverage. This is likely due to the FLASH Max plans being associated with increased doses to OARs. Scenario 2 was significantly different from Max and Scenario 3, except for the Left Hippocampus and Right Hippocampus, both at a threshold dose of 10 Gy. Unsurprisingly, Scenario 1 was significantly different from Max, Scenario 2, and Scenario 3. Considering the 40 Gy/s "FLASH" threshold with regards to the achieved dose rate coverages at the 2 Gy dose threshold, the Max plans were associated with median coverages of 30% - 60%, depending on the OAR. Scenario 1 could not achieve this for any OAR or dose threshold (Figure 5.9 (e - h)). Scenario 2 had median coverages of 5% - 45% for the OARs considered in Figure 5.9 (i - l). Finally, Scenario 3 achieved median coverages in the range of 40% - 60%, increasing the minimum median coverage at the 2 Gy dose threshold by almost 10% compared to the Max energy plans, depending on the OAR (Figure 5.9 (m-p)). This could potentially be attributed to a reduction in scattering occurring off-axis of the proton beam, consequently reducing low-dose off-axis contributions and therefore increasing the associated dose rate.

Similar trends were found for the ADR, as shown in Figure 5.10, with no significant differences in coverages between the Max and Scenario 3 plans, except for the Left Hippocampus at 2 Gy and 4 Gy threshold dose, and the Right Hippocampus and Left Optic Nerve, both at 10 Gy. Scenario 1 led to significantly lower coverages compared to the other scenarios. Scenario 2 was also significantly lower in the achieved coverages compared to Max and Scenario 3, with the exception of the Left Hippocampus (at all threshold doses evaluated) and the Right Hippocampus and Left Optic Nerve (both at 10 Gy) when compared to Scenario 3. With regards to dose rate coverages at the 40 Gy/s threshold, FLASH Max plans had minimum median ADR coverages of 15% - 35% (Figure 5.10 (a-d)). Scenario 1, similarly to the DR_{prct} definition, could not achieve any ultra-high dose rate coverage (Figure 5.10 (e-h)), which was also the case for Scenario 2 (Figure 5.10 (i-l)). Scenario 3 was associated with a minimum (2 Gy

Table 5.1: Table of the maximum (Max) and non-maximal (Non-max) beam energies (MeV) used for each beam for each patient case. The asterisk (*) notes the beams where the lower beam energy could not match that of the IMPT energy and had to be increased in order for the FLASH-PT plans to be robust in the worst-case scenario.

Patient	**Beam 1 Energy (MeV)**		**Beam 2 Energy (MeV)**		**Beam 3 Energy (MeV)**	
	Max	**Non-max**	**Max**	**Non-max**	**Max**	**Non-max**
1	228	144	228	152	228	160
2	228	180*	228	170	228	173
3	228	190*	228	170*	228	228*
4	228	159	228	152	228	170*
5	228	138	228	135	228	135
6	228	170*	228	152	228	139
7	228	152	228	160*	228	170*
8	228	169	228	149	228	143
9	228	134	228	136	228	142
10	228	155	228	168	228	167

threshold) median ADR coverage of 30% - 40%, depending on the OAR (Figure 5.10 (m-p)), again, achieving higher coverages than Max, potentially due to less low-dose distributions, thereby increasing the dose rate.

The DADR definition led to significantly higher dose rates compared to the DR_{prct} and ADR definitions, achieving almost full coverage for the different OARs and dose thresholds considered, as shown in Figure 5.11. Unlike the DR_{prct} and ADR definitions, the Max and Scenario 3 coverages had more differences between them, with the maximum energy DADR coverages starting to drop below a median of 100% at 40 Gy/s for the 2 Gy threshold, across the different OARs (Figure 5.11 (a-d)). For Scenario 3, however, DADR coverages remained at a median of 100% for dose rates up to 80 Gy/s for the 2 Gy dose threshold. All other dose thresholds, for both Max and Scenario 3 remained at a median coverage of 100% across the different OARs. Scenario 1, again, did not reach any ultra-high dose rate coverages (Figure 5.11 (e-h)), with Scenario 2 reaching minimum median coverages of 70% - 80 % depending on the OAR considered. FLASH Max and Scenario 3 reached full coverage of 100% for dose rates of 40 Gy/s for all OARs considered in Figure 5.11 (a-d) and (m-p).

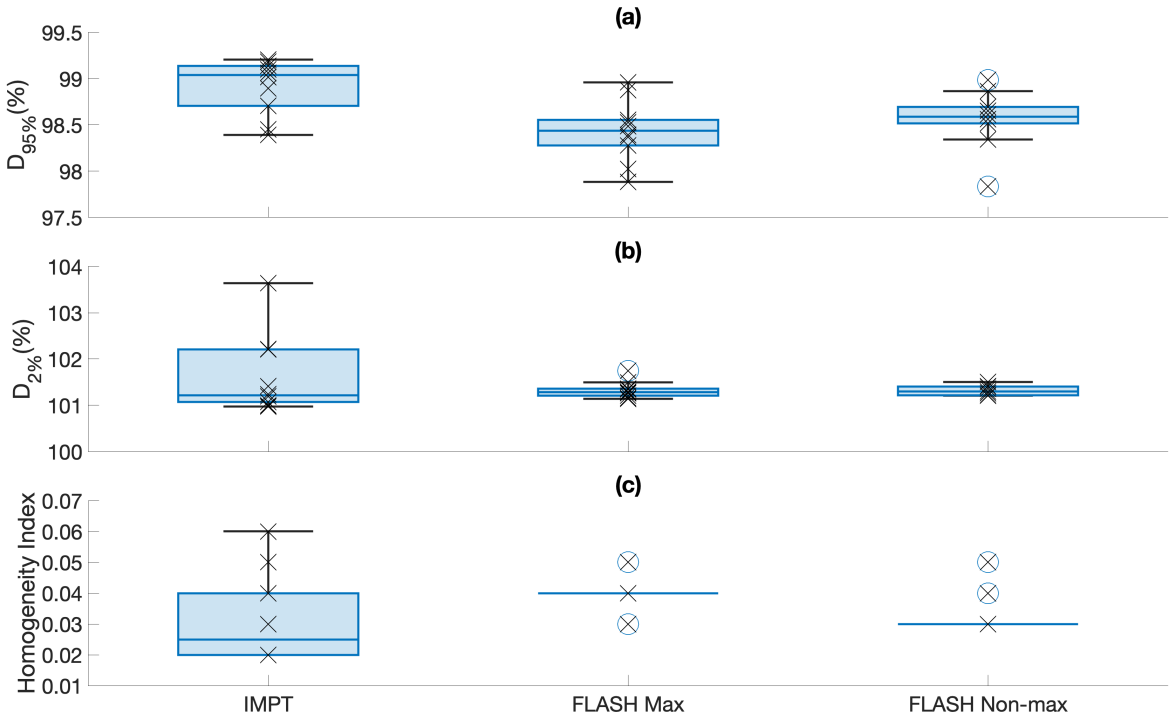


Figure 5.3: Target dose comparisons for intensity modulated proton therapy (IMPT) plans, FLASH-PT plans generated with the maximum beam energy (FLASH Max), and FLASH-PT plans generated with non-maximal energy beams (FLASH Non-max). Boxplots comparing (a) $D_{95\%}$ (%), (b) $D_{2\%}$ (%), and (c) the homogeneity index (HI) (($D_{2\%}$ (%) - $D_{98\%}$ (%))/$D_{50\%}$ (%)). Each point (x) shows the exact $D_{95\%}$ (%), $D_{2\%}$ (%), and HI for each patient case. The line within the box represents the median value, the bottom and top of the box represent the 25th and 75th percentiles, the whiskers show the range of the data points (excluding outliers), and outliers are shown using individual (o) markers. All doses are normalised with respect to the prescribed dose.

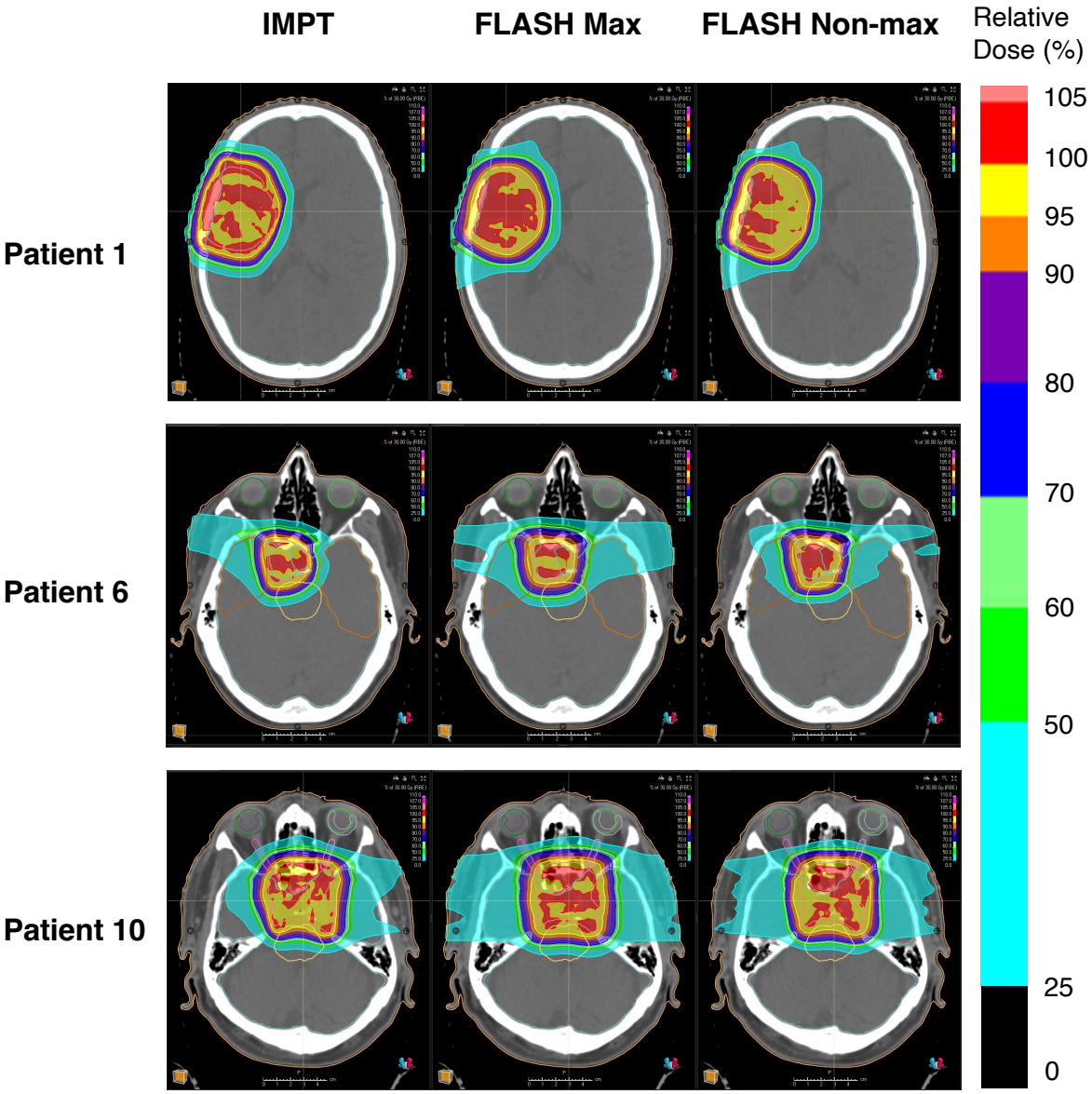


Figure 5.4: Dose map comparisons of Patient 1, Patient 6, and Patient 10, for intensity modulated proton therapy (IMPT) plans, FLASH proton therapy plans using the maximum beam energy (FLASH Max), and FLASH-PT plans generated using non-maximal beam energies (FLASH Non-max). Doses are normalised with respect to the prescribed dose.

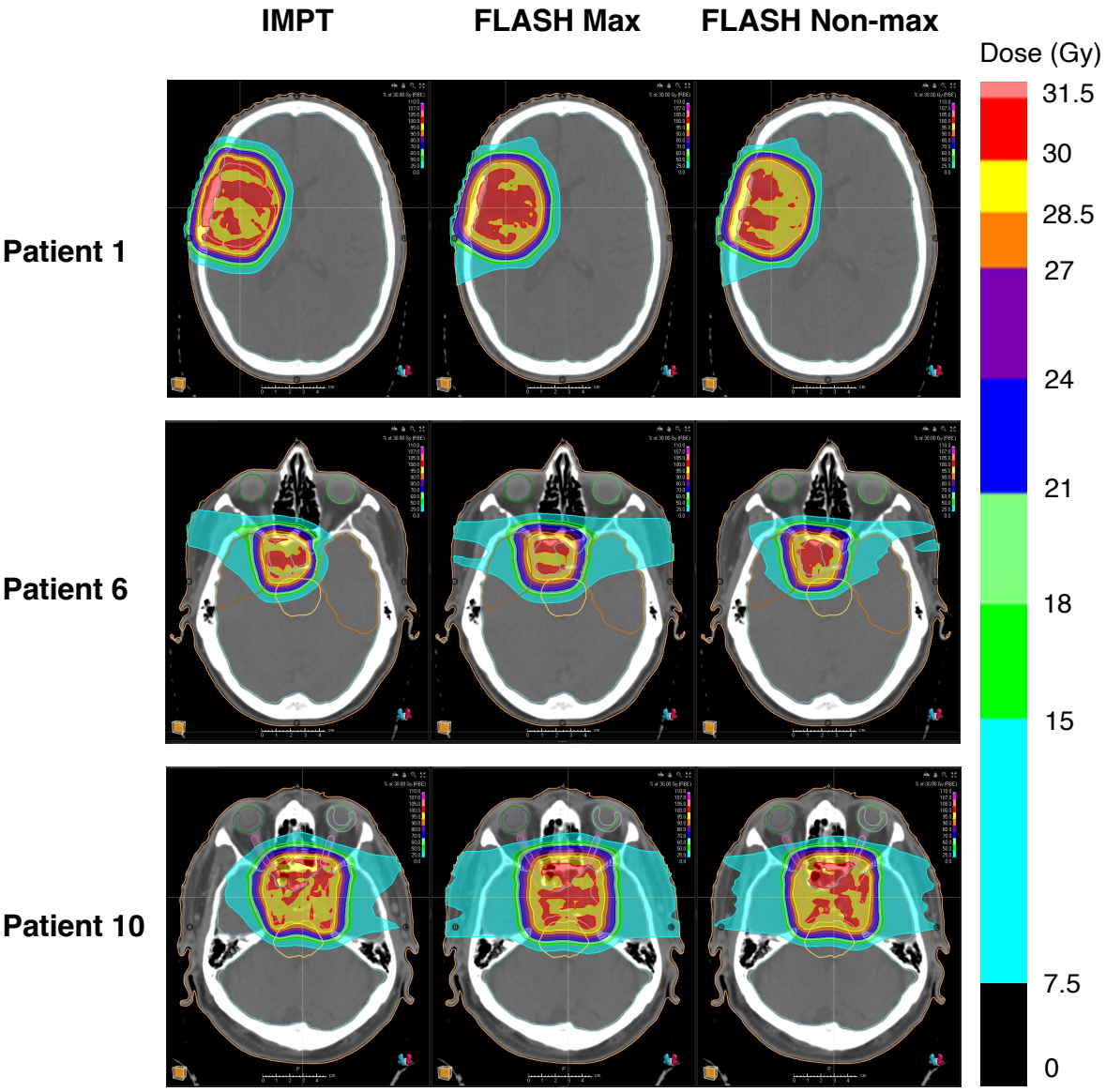


Figure 5.5: Dose map comparisons of Patient 1, Patient 6, and Patient 10, for intensity modulated proton therapy (IMPT) plans, FLASH proton therapy plans using the maximum beam energy (FLASH Max), and FLASH-PT plans generated using non-maximal beam energies (FLASH Non-max). Doses are given as absolute dose (Gy).

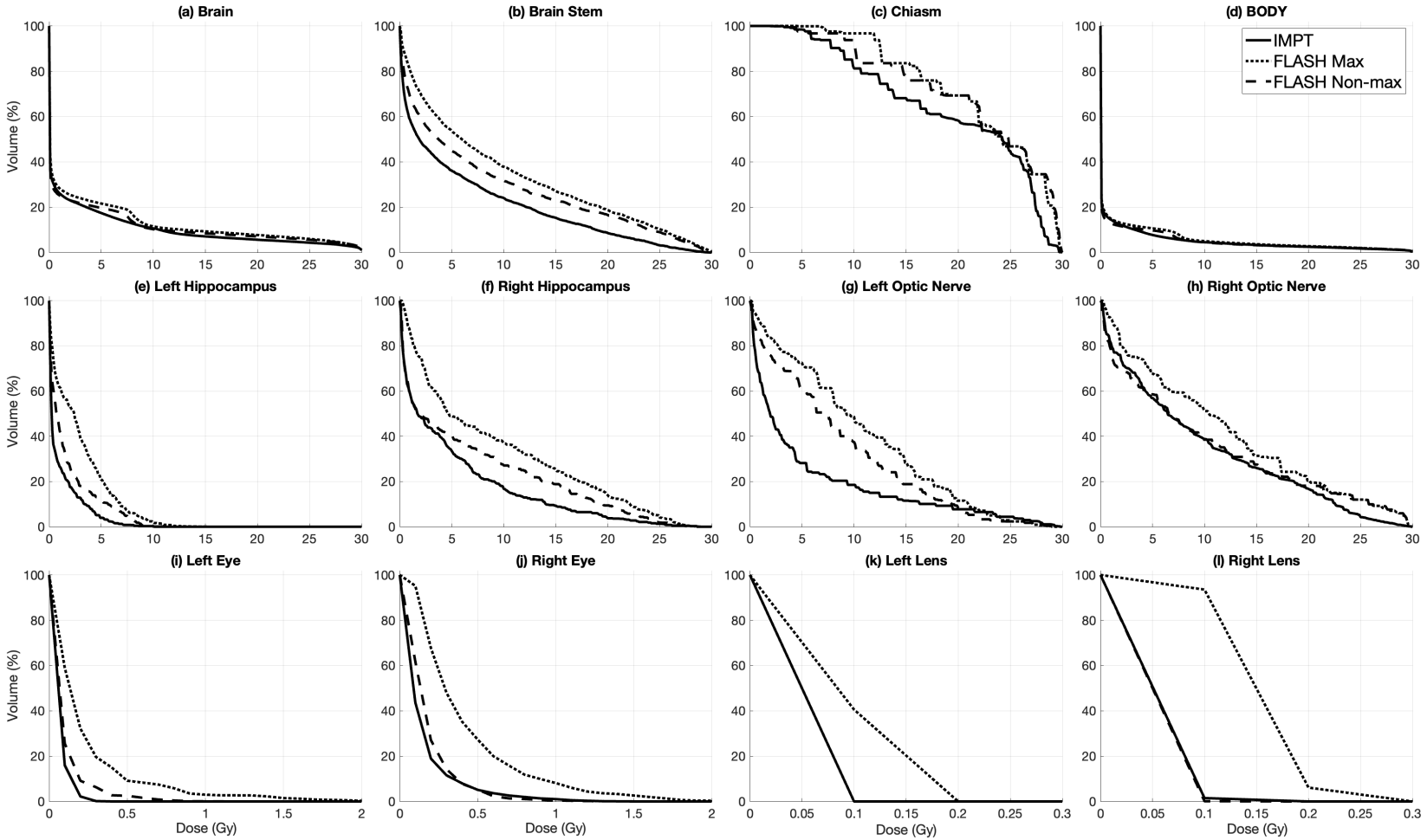


Figure 5.6: Dose volume histograms (DVHs) representing the median dose to a specific organ at risk (a-l) evaluated across all patient cases for treatment plans generated for intensity-modulated proton therapy (IMPT), FLASH-PT with maximum beam energy (FLASH Max), and FLASH-PT with non-maximal energy (FLASH Non-max). DVHs are computed on a voxel-by-voxel basis and represent the distribution of dose within each organ; the plotted curves therefore reflect the median volume-dose relationship across patients.

Table 5.2: The median ratio of mean dose to an organ at risk (OAR) for FLASH-PT with the maximum beam energy (FLASH Max) versus intensity modulated proton therapy (IMPT) and FLASH-PT with non-maximal beam energy (FLASH Non-max) versus IMPT, evaluated for each OAR across all patient cases.

OAR	**FLASH Max/IMPT**	**FLASH Non-max/IMPT**
Brain	1.13	0.99
Brain Stem	1.75	1.59
Chiasm	1.03	1.04
BODY	1.11	0.96
Left Hippocampus	1.62	1.27
Right Hippocampus	2.21	1.58
Left Optic Nerve	1.43	1.34
Right Optic Nerve	1.43	1.20
Left Lens	2.56	1.05
Right Lens	2.82	1.34
Left Eye	3.04	2.22
Right Eye	2.73	1.45

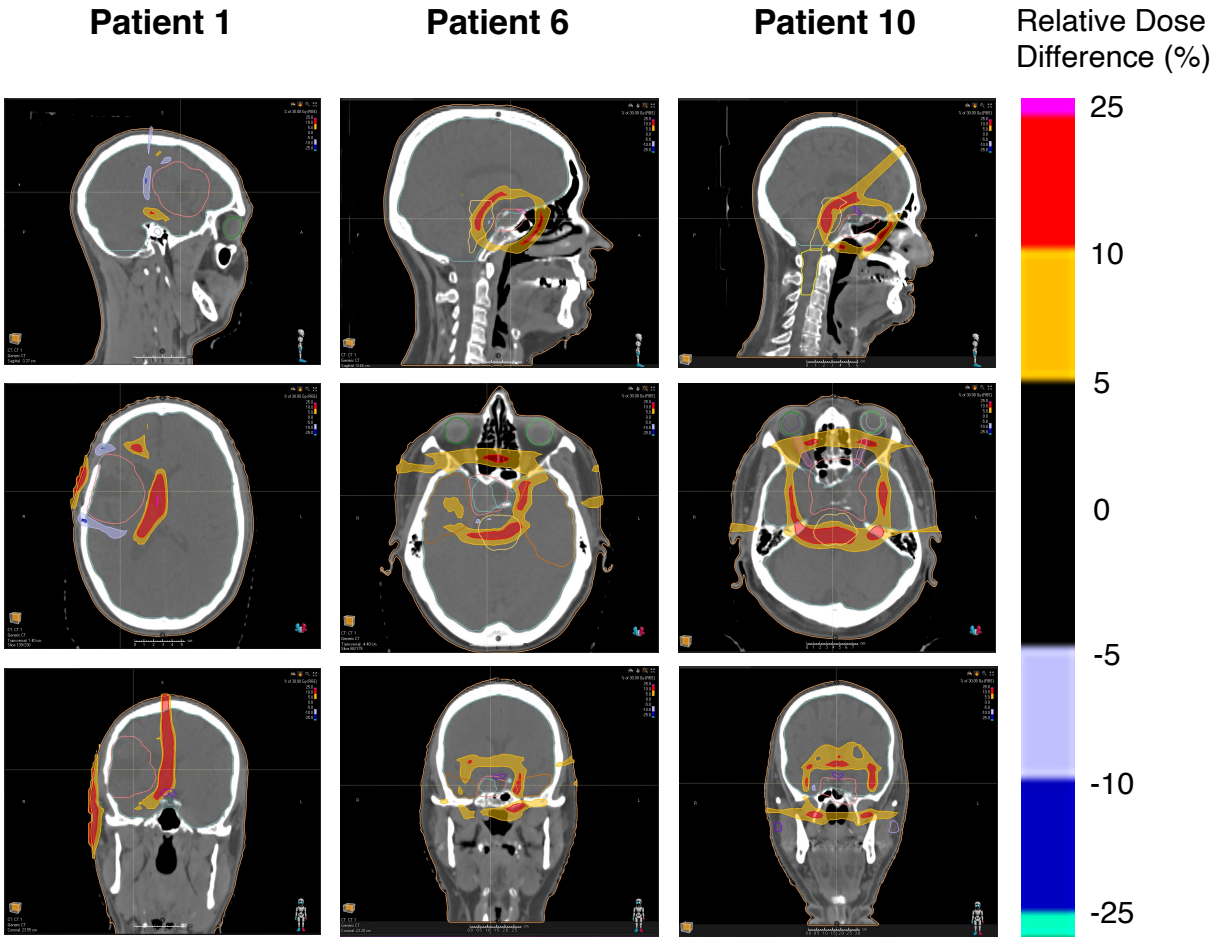


Figure 5.7: Dose map differences for Patient 1, Patient 6, and Patient 10, demonstrating the difference in dose between the FLASH-PT plans generated with the maximum energy versus FLASH-PT plans generated with non-maximal beam energy. Doses are normalised with respect to the prescribed dose, and the relative dose difference is scaled according to the colour bar on the right.

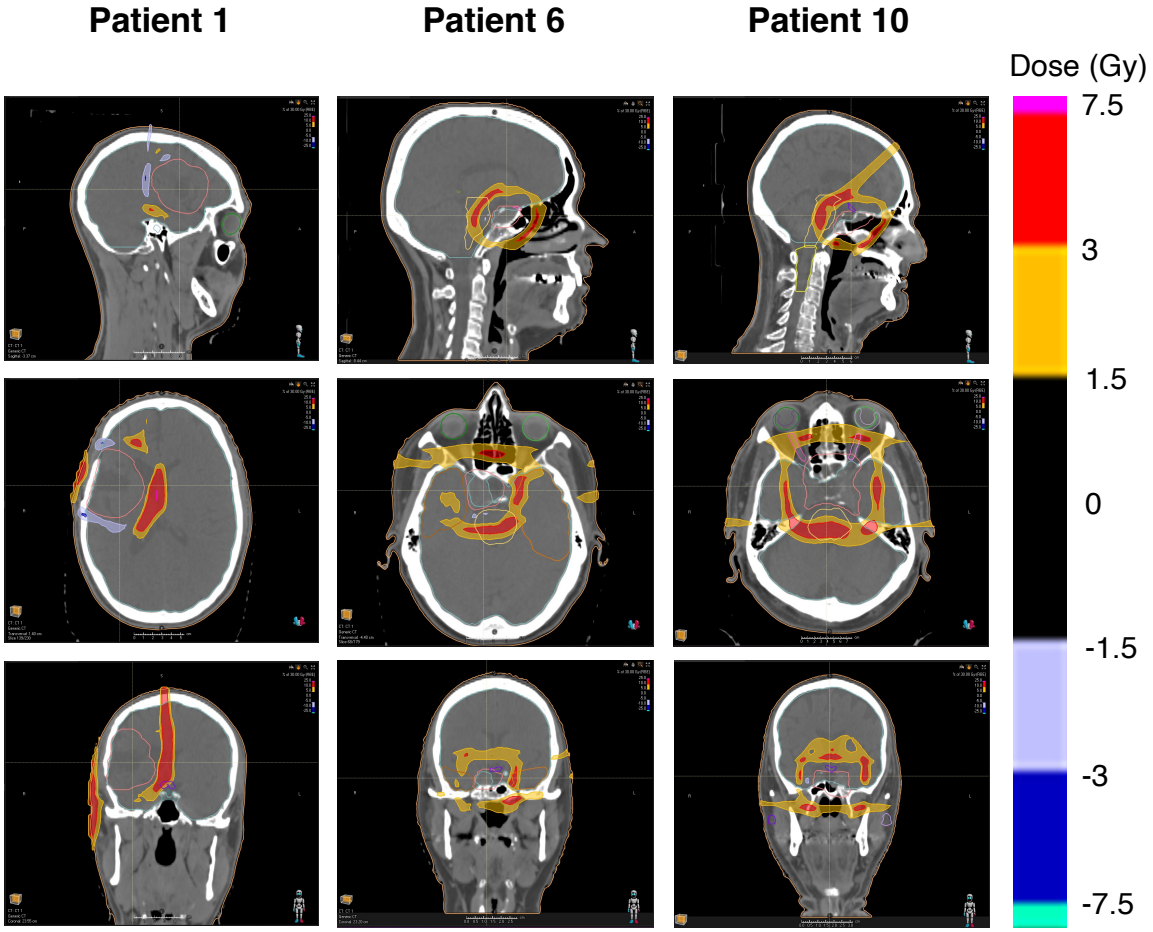


Figure 5.8: Dose map differences for Patient 1, Patient 6, and Patient 10, demonstrating the difference in dose between the FLASH-PT plans generated with the maximum energy versus FLASH-PT plans generated with non-maximal beam energy. Doses are given as absolute dose, and the dose difference is scaled according to the colour bar on the right.

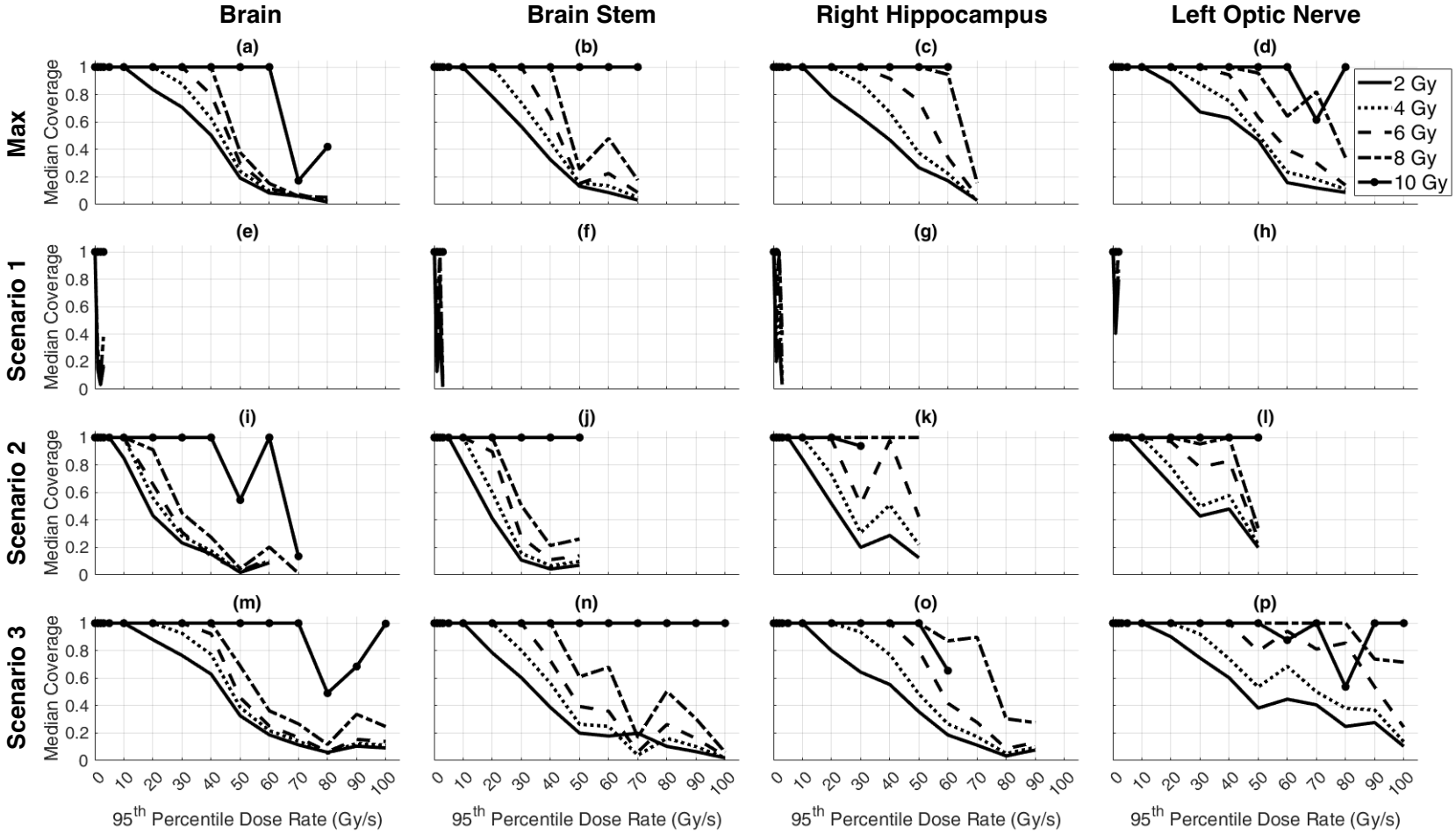


Figure 5.9: Median 95^{th} percentile dose rate (DR_{prct}) coverage for the different beam energy scenarios: Max beam energy, Scenario 1 - adopting a conventional beam delivery, Scenario 2- implementing a momentum wedge to increase the momentum acceptance, and Scenario 3 - representing the output of a variable energy cyclotron. The dose rate coverages are shown for the Brain structure, the Brain Stem, the Right Hippocampus, and the Left Optic Nerve. Each line type represents the dose threshold at which the dose rate coverage was evaluated for: 2 Gy, 4 Gy, 6 Gy, 8 Gy, and 10 Gy.

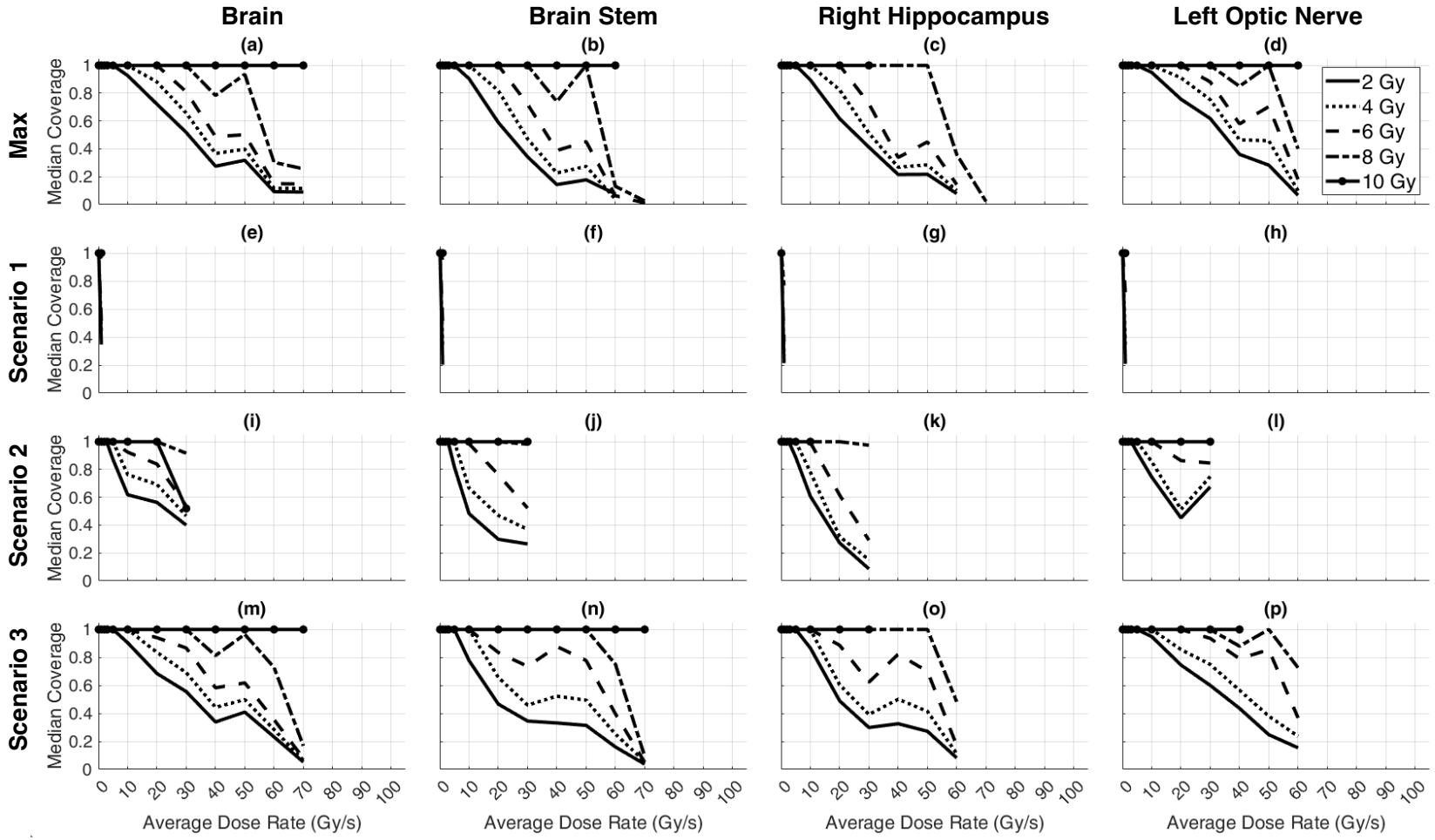


Figure 5.10: Median average dose rate (ADR) coverage for the different beam energy scenarios: Max beam energy, Scenario 1 - adopting a conventional beam delivery, Scenario 2 - implementing a momentum wedge to increase the momentum acceptance, and Scenario 3 - representing the output of a variable energy cyclotron. The dose rate coverages are shown for the Brain structure, the Brain Stem, the Right Hippocampus, and the Left Optic Nerve. Each line type represents the dose threshold at which the dose rate coverage was evaluated for: 2 Gy, 4 Gy, 6 Gy, 8 Gy, and 10 Gy.

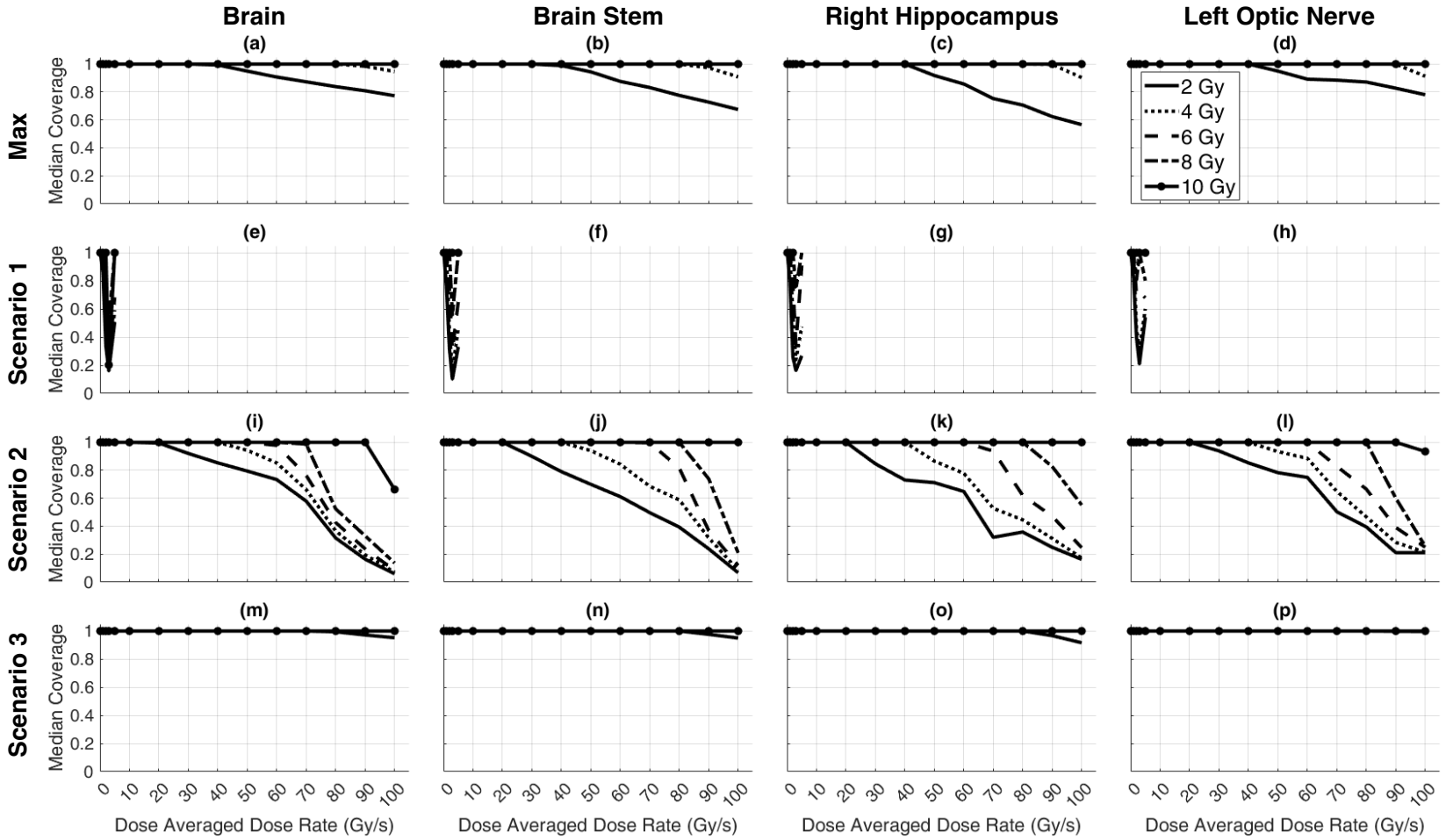


Figure 5.11: Median dose averaged dose rate (DADR) coverage for the different beam energy scenarios: Max beam energy, Scenario 1 - adopting a conventional beam delivery, Scenario 2 - implementing a momentum wedge to increase the momentum acceptance, and Scenario 3 - representing the output of a variable energy cyclotron. The dose rate coverages are shown for the Brain structure, the Brain Stem, the Right Hippocampus, and the Left Optic Nerve. Each line type represents the dose threshold at which the dose rate coverage was evaluated for: 2 Gy, 4 Gy, 6 Gy, 8 Gy, and 10 Gy.

5.4 Discussion

This chapter explored whether reducing the initial FLASH-PT beam energy could improve target dose coverage, while reducing doses to OARs. Further to this, we also investigated the achievable dose rate coverages for different beam delivery scenarios, as lowering the initial beam energy impacts the transmission efficiency of a proton beamline, and therefore the dose rate. Dose rate coverages were evaluated for the maximum beam energy (Max), and for three different scenarios when a non-maximal beam energy (< 230 MeV) was used: Scenario 1 considered the use of high energy beams (not maximum) for an operational proton therapy facility, Scenario 2 represented beam delivery with reduced momentum spread using a compact gantry, and Scenario 3 investigated the use of a variable energy cyclotron. The DR_{prct}, ADR, and DADR definitions were included in the analysis, and different dose and dose rate thresholds were also considered. IMPT, maximum energy FLASH-PT, and non-maximal energy FLASH-PT plans were compared to determine the impact of initial beam energy reduction and the quality of both FLASH-PT techniques relative to conventional beam delivery.

To generate the non-maximal energy FLASH-PT plans, the beam energy used for the multi-field optimised (MFO) IMPT plans were applied as a starting point. However, IMPT beam energies sometimes failed to produce robust non-maximal energy FLASH-PT plans, and the beam energy had to be increased until robustness was achieved. This could be attributed to a higher energy requirement as a consequence of using a conformal energy modulator which has a minimum thickness associated to it due to its base. However, these energy increases only applied to 8 out of 30 beams (Table 5.1), suggesting that another factor may play a role in the plans failing to achieve the imposed target dose constraints in the worst-case scenarios. The robustness of the MFO IMPT plans was assessed for the use of multiple beams within a fraction. In contrast, the FLASH-PT plans were optimised for a one-beam-per-fraction delivery and using single-field-optimisation. Robustness for the FLASH-PT plans was therefore evaluated for each individual beam, instead of considering the contributions of each individual

beam to the total dose. Perhaps, if SFO IMPT energies had been used instead of the MFO energies, similarly to the investigation in Chapter 3, there would be fewer differences in beam energies between IMPT and non-maximal FLASH-PT plans. However, for simplicity, the energies considered in this Chapter were only increased in steps of 10 MeV; future work could involve an improved fine-tuning of the energy increases in order to balance OAR sparing with target coverage.

All treatment plans adhered to the target coverage criteria of $D_{95\%} \geq 95\%$ and $D_{2\%} \leq 105\%$ in both the nominal and worst case scenarios. Unlike FLASH Max, FLASH Non-max improved $D_{95\%}$, achieving comparable coverage to that of IMPT, with no significant differences in $D_{2\%}$ or homogeneity index between the techniques. As expected, the use of non-maximal energy FLASH-PT reduced doses to OARs compared to the maximum energy counterparts. The reduction in dose varied across the different patient cases and target locations. However, FLASH-PT was still associated with higher doses to OARs compared to IMPT, for both maximum and non-maximal energy plans.

The increase in doses to OARs observed for FLASH-PT could partially be attributed to the reduction in number of spots compared to that of IMPT. With IMPT delivering multiple spots per energy-layer, it may be easier to control the spot placements such that OAR doses are reduced whilst maintaining good target coverage. FLASH-PT, however, utilises a single energy-layer which reduces the degrees of freedom with respect to spot placement with depth, thereby reducing the control of spots which may lead to increased doses to OARs. The use of a lower beam energy increased the number of spots placed on the target compared to the maximum beam energy plans. This increase in number of spots is associated with a decrease in spot size, thereby improving control of the dose delivery and target dose coverage, whilst also lowering the doses to OARs. However, the increase in number of spots needs to be balanced with the resolution of the conformal energy modulator. As the spot sizes are reduced, the level of detail required in order for the conformal energy modulator to achieve a uniform

target dose increases, potentially making it more difficult to achieve the prescribed dose distributions [102]. Nevertheless, the potential benefit of the FLASH effect that might be achieved at higher dose rates must first offset the increased dose to OARs before the technique can, in theory, be associated with any beneficial patient outcome when compared to conventional proton therapy.

No FLASH sparing effect was accounted for in the evaluations of the FLASH-PT plans. However, comparisons of the OAR dose ratios between maximum energy FLASH-PT with respect to IMPT, and non-maximal energy FLASH-PT with respect to IMPT, highlighted differences in mean doses between the techniques. For the Brain Stem, the median ratio of the mean dose (evaluated across all patient cases and within each individual fraction) was a factor of 1.75 higher for FLASH Max compared to a factor of 1.59 for the non-maximal energy counterpart. In terms of absolute dose (for the total treatment plan), median values of the mean dose to the Brain Stem were 5.95 Gy, 9.32 Gy, and 8.05 Gy for IMPT, FLASH Max, and FLASH Non-max, respectively. Similarly, FLASH Max plans were associated with an increase in dose by a factor of 2.21, compared to the non-maximal energy case of 1.58, to the Right Hippocampus when compared to IMPT. The median mean dose to the Right Hippocampus was 4.24 Gy, 7.83 Gy, and 6.36 Gy, for IMPT, FLASH Max, and FLASH Non-max, respectively. Albeit small differences in absolute dose, it is worth noting the implications of hypofractionation. For example, an additional dose of 1 Gy per fraction delivered over 3 fractions, corresponds to a biologically equivalent dose of approximately 4.5 Gy to the Brain Stem, assuming an α/β ratio of 2 [1, 150]. To compensate for the additional dose associated with the FLASH-PT beam delivery, a dose modifying factor (DMF) would have to be at least equivalent to the increased dose ratios, whether it be for the maximum or non-maximal energy treatment plans (see Section 1.2.6 for more details on the DMF). That is, any further sparing for the non-maximal energy plans would require a DMF > 1.59 or DMF > 1.58 for the Brain Stem and Right Hippocampus, respectively. A higher DMF would be required for FLASH Max plans due to their

increased dose to OARs.

Given the increase in OAR doses for FLASH-PT when compared to the IMPT counterpart, it is clear that the DMF should not be used in isolation. The additional dose associated with the FLASH-PT beam delivery will need to be accounted for, and will also vary depending on the OAR in consideration. Furthermore, varying values for the DMF has been reported in the literature, as discussed in Section 1.2.6, and has only been shown for pre-clinical studies [40, 43, 46, 60, 68, 71, 107]. Understanding how the DMF may vary depending on the target site, and how it may scale from pre-clinical studies to clinical application will be crucial in the implementation and efficacy of FLASH-PT.

FLASH Non-max plans were expected to achieve lower dose rate coverages than the FLASH Max counterparts due to the reduction in OAR doses and significant increase in number of spots. However, considering both the DR_{prct} and ADR definitions, for the Max scenario and Scenario 3 (i.e., similar beam currents), no major differences in the achieved dose rate coverages were found, with the exception of a few OARs at the 10 Gy dose threshold. This finding is consistent with observations by Aylward et al. (2023), discussed in Section 5.1.1, where the use of a lower beam energy (for targets with relatively short beam path lengths) is associated with a reduction in lateral scattering off-axis of the proton beam, leading to an increase in dose rate [138]. This indicates that, despite there being an increase in spots delivered, similar dose rate coverages could in theory be achieved, provided that the beam current remains constant. Thus, reduced scattering and increased dose rates for short beam path distances may indicate target locations most likely to benefit from FLASH-PT.

The results in this chapter highlight differences in the resulting dose distributions and dose rate coverages for the different beam delivery methodologies. Due to the differences in beamlines for Max and Scenarios 1-3, and the use of estimated transmission

efficiencies for dose rate calculations, the results in this Chapter are for guidance only. Nonetheless, the disadvantages of the different beam delivery methodologies should be considered. Unsurprisingly, the realistic scenario using beam currents of an operational high energy beamline in Scenario 1 did not achieve any ultra-high dose rates coverage. The implementation of the wedge system in Scenario 2 requires a technological beamline development to allow for variations in wedge thicknesses for every 10 MeV energy increase [139]. The variable energy cyclotron considered in Scenario 3 is purely theoretical at this moment in time, and is also an idealised beam which does not account for any initial emittance or energy spread [140]. How the results in Scenario 3 may change for a less idealised implementation of the beam delivery will be of great interest with respect to the achievable dose rates. Further to these constraints, experimental measurements need to be obtained to verify the true dose rates achieved for the different beam delivery methods considered.

The presence of energy degraders increase scattering events and secondary neutron production, particularly when placed in the treatment head near the patient, subsequently increasing the neutron dose at the isocentre [141]. Secondary neutron production, in the context of the FLASH-PT modified beam delivery methods, has not been investigated extensively. A recent study by Chen et al. (2024) investigated the contributions due to a single ultra-high dose rate pencil beam spot, and found an increase in the production of secondary neutrons compared to a conventional dose rate spot [151]. The magnitude of the increase for larger, more clinically relevant, target volumes has yet to be determined. Furthermore, the increased scattering may attribute an increase in dose delivered to the skin. It would therefore be of interest to evaluate skin doses for the different FLASH-PT techniques, as well as for IMPT, to evaluate any potential differences arising from the beam delivery techniques.

Chapter 4 showed that FLASH-PT treatment plan quality could be improved through robust optimisation and the use of a TPS which does not incorporate dose rate op-

timisation. However, FLASH-PT plans were still significantly inferior to IMPT with respect to target dose coverage (in the worst-case scenario) and doses to OARs. In this Chapter, we investigated whether the discrepancy in plan quality was due to the FLASH-modified beam delivery, and more specifically, due to the use of the maximum beam energy. Lowering the initial beam energy improved the FLASH-PT plan quality, with comparable target doses to IMPT and reduced doses to OARs compared to the maximum energy FLASH-PT plans. Technological developments and implementations are, however, needed to utilise non-maximal beam energies in the context of FLASH-PT whilst also achieving the ultra-high dose rates required for a FLASH effect.

Chapter 6

Conclusion

FLASH radiotherapy research is quickly evolving, with numerous pre-clinical studies and several clinical trials ongoing across research centres and hospitals around the world. The rapid progression of the field necessitates an in-depth understanding of the technique before it is implemented into clinical practice. Treatment planning studies can be used to determine the feasibility, safety, and constraints of the clinical implementation, with few studies having investigated the use of spread-out Bragg peak FLASH proton therapy (FLASH-PT).

Chapter 3 evaluated the feasibility and constraints of FLASH-PT treatment planning, and whether the plans simulated using a research treatment planning system were comparable to conventional intensity modulated proton therapy (IMPT) plans. Due to the FLASH-modified beam delivery utilising patient-specific components, the ultra-high dose rate plans were generated for a one-beam-per-fraction delivery for a variety of patient cases (bone, brain, and lung) and using margin-based planning. The results did not account for any biological sparing effect, and purely focused on the dose distributions achieved when comparing FLASH-PT to IMPT. Across the different target types considered, IMPT achieved superior target coverage and organ at risk (OAR) sparing compared to the ultra-high dose rate treatment plans.

Chapter 4 aimed to establish whether the degraded FLASH-PT quality was due to the

research TPS and its direct incorporation of dose rate optimisation (Section 2.3.3.1), or the FLASH-PT modified beam setup. The impact of dose rate optimisation and robust optimisation on FLASH-PT treatment plan quality, and dose rates, was therefore investigated using the same patient cases and beam delivery used in Chapter 3. Dose rate optimised treatment plans were associated with reduced plan quality and non-significant differences in OAR doses compared to their non-dose rate optimised counterparts. Regions of increased tissue heterogeneity were associated with increased variability in dose rates, along with difficulty in controlling the dose rates when using the dose rate optimised TPS, suggesting that targets such as the lungs may be poor candidates for ultra-high dose rate proton therapy. Although the use of dose rate optimisation (implemented directly into the treatment plan optimisation) may be beneficial for increasing dose rates to OARs, it should be used with caution as it may significantly degrade treatment plan quality. Compared to margin-based planning, robust optimisation significantly improved target coverage in the worst-case scenarios, with non-significant differences in the nominal scenario, and no major compromise in OAR doses or dose rates. Nevertheless, FLASH-PT plan quality was still not comparable to that of IMPT, despite the use of different TPSs and treatment planning optimisation techniques. The worsened plan quality observed for FLASH-PT was therefore likely due to the FLASH modified beam delivery.

In an attempt to improve the FLASH-PT plan quality, Chapter 5 explored the idea of further modifying the FLASH-PT beam delivery to reduce scattering and range straggling. The modification included the reduction in range shifter material by using a lower (non-maximal) initial beam energy, compared to the maximum energy used in Chapters 3 and 4. Lower beam energies are associated with reduced transmission efficiency, and therefore dose rate, of the protons (measured from the cyclotron exit to the isocentre). To investigate the impact on the achievable dose rates, three different scenarios of beam delivery were considered in addition to the maximum beam energy scenario used in Chapters 3 and 4: conventional high energy proton therapy (Scenario

1), reduced momentum spread with a compact gantry (Scenario 2), and a variable energy cyclotron (Scenario 3). Other than the reduction in beam energy, the same beam setup considered in Chapter 3 and 4 was used. To reduce variability in the achieved dose rates due to tissue heterogeneities, Chapter 5 focused solely on brain targets. Target dose distributions were similar when comparing FLASH-PT (max and non-maximal energy) to IMPT in both the worst-case and nominal scenario. OAR doses were reduced when using a lower initial beam energy compared to the maximum, however, the FLASH-PT plans were still associated with an increased dose to OARs when compared to IMPT. Chapter 5 therefore showed that FLASH-PT plan quality can be improved through further modifying the FLASH-PT beam delivery. Nevertheless, depending on which dose rate definition and beam delivery scenario used, the improvement in plan quality was associated with a reduction in dose rate (percentile and average dose rate, and Scenario 1 and 2), except for the dose averaged dose rate and scenario 3 which achieved dose rates similar to that of the maximum energy FLASH-PT beam delivery for the majority of OARs considered.

The treatment planning studies in this work assume idealised CEM geometries as generated by the treatment planning system. However, recent experimental work has demonstrated that physically manufactured CEMs can reproduce these idealised dose distributions with clinically acceptable accuracy. Hotoiu et al. (2025) performed Monte Carlo simulations, 3D printing, and in-beam dosimetric measurements of CEM-based irradiation, showing that the resulting dose distributions agree with treatment planning calculations within $< 2.5\%$ [102]. These results indicate that CEMs are robust to typical manufacturing uncertainties, with geometric deviations on the order of 0.2 mm - 0.4 mm having minimal dosimetric impact [102]. Therefore, while the present work assumes idealised CEMs, available experimental evidence suggests that such assumptions are reasonable and that physically realised CEMs can achieve clinically relevant dose accuracy. Nevertheless, uncertainties related to manufacturing tolerances, range straggling, and material properties may introduce small deviations from the idealised

dose distribution and should be considered in future work. These deviations may be further exacerbated for more complex geometries, where increased modulation complexity places greater demands on manufacturing accuracy and dose modelling.

From a treatment planning perspective, FLASH-PT introduces competing requirements: achieving sufficiently high dose and dose rates within the planning target volume to potentially elicit the FLASH effect, whilst maintaining minimal dose to surrounding OARs. In practice, this suggests that dose outside the planning target volume should remain as low as achievable, as in conventional planning, while selectively maximising dose-rate coverage within the target. Balancing these competing objectives remains a key challenge for clinical implementation. In pencil-beam scanning, dose-rate coverage is inherently heterogeneous and tends to decrease with increasing field size and depth due to beam broadening. However, the biologically relevant spatial scale remains unclear, with no consensus as to whether the FLASH effect is governed by voxel-level, sub-volume, or whole-organ responses. Consequently, OAR assessment in FLASH-PT should consider both local dose-rate distributions and volumetric dose metrics, rather than relying on a single averaged quantity.

The FLASH sparing effect could potentially compensate for the increased dose to OARs observed throughout Chapters 3 - 5. However, variations in dose rate coverages have been observed, both in this thesis and in the literature, depending on the definition and target location considered [100, 103, 109, 112–115]. Further to this, there is still a lack of understanding of the underlying biological mechanism. The FLASH effect should therefore not be relied upon in a clinical setting, yet, as it could lead to patients receiving doses to OARs that are higher than what would be allowed in a conventional treatment. Although, Mascia et al. (2024) points out that there could potentially be an "optimal dose per beam" for which the FLASH effect could compensate for the increased physical dose, whilst still being safe for the patient [69]. What this optimal dose may be, and for which treatments it would apply to, remains to be determined.

The normal tissue sparing effect has been observed in pre-clinical studies, but has not yet been reproduced in clinical trials. It is therefore unclear whether the pre-clinical results will scale to clinical trials, that is, whether the results observed for small-field studies would apply to larger, and more clinically relevant, target volumes. The results of the FAST-02 trial, as discussed in Section 1.2.3, will hopefully provide more insight into the translational potential of the sparing effect for clinical use. Further to this, researchers at the University of Pennsylvania (Philadelphia, USA), in collaboration with Ion Beam Applications SA (Louvain-la-Neuve, Belgium) and RaySearch Laboratories AB (Stockholm, Sweden), have recently demonstrated, through treatment planning studies and dosimetric verifications, the feasibility of delivering FLASH-PT treatment plans for head and neck patients requiring re-irradiation [152]. Their work forms part of the feasibility studies required for clinically implementing FLASH-PT, and it might not be long until a clinical trial utilising ultra-high dose rate spread-out Bragg peak protons is enrolling patients.

Any potential variations in relative biological effectiveness (RBE) and linear energy transfer (LET) (Section 1.1.1) were beyond the scope of this thesis and were therefore not considered. However, it should be noted that the higher LETs associated with protons may have an impact on ultra-high dose rate dosimetry. Accurate dosimetry is crucial for both experimental research and clinical implementation, and a range of detectors are used depending on the application. Ionisation chambers remain the standard for absolute dosimetry under conventional conditions, but their use at ultra-high dose rates is complicated by ion recombination and saturation effects, which require *in situ* corrections [153]. Solid-state detectors such as diamond detectors offer improved temporal resolution, though their behaviour at ultra-high dose rates have mainly been demonstrated for small-field irradiations [154]. Calorimeters provide a direct and dose-rate independent measurement of absorbed dose and are often considered the gold standard for absolute dosimetry. However, their complexity and limited availability re-

strict their routine use in ultra-high dose rate experiments [1]. For the inter-comparison and validation of detector performance under ultra-high dose rate conditions, traceability to primary standards is essential. In this context, measurements performed at national standards laboratories (e.g. National Physical Laboratory) provide a reference for absolute dose and will be valuable for benchmarking detector response.

Radiochromic films are widely used for high-resolution two-dimensional relative dosimetry, with the optical density of the irradiated film being proportional to absorbed dose. However, their suitability for absolute dose measurements in ultra-high dose rate proton beams is limited by several factors. The raised LET of protons leads to an effect referred to as "quenching", resulting in an under-response of the film [155]. Quenching occurs when the secondary electrons produced from lower energy protons (higher LET) deposit energy near the primary proton track [156]. Unlike higher energy protons (lower LET) which are more likely to generate a detectable signal through the induction of a chemical process with the film, the deposited energy due to the higher LET protons is likely lost due to the proximity to the primary track and may not lead to a signal [156]. Radiochromic films have previously been shown to be dose rate independent for clinical dose rates, however, dose rate dependent behaviour has also been reported for proton doses exceeding 10 Gy at mean dose rates of approximately 7500 Gy/s, resulting in overestimation of the absolute dose [157, 158]. The opposing effects of LET-induced under-response and ultra-high dose rate-induced over-response mean that the net film response is not straightforward and may depend on the specific beam conditions. Therefore, whilst radiochromic film remains a valuable tool for relative dose verification, it must be used with caution when interpreting absolute dose measurements for ultra-high dose rate proton dose delivery.

A limited number of studies have investigated the production of secondary neutrons from ultra-high dose rate protons. Using the same FLASH-modified beam delivery considered in this thesis (see Section 2.1), Chen et al. (2024) evaluated the secondary

neutron production of a single ultra-high dose rate pencil beam spot [151]. These evaluations included a range shifter, but not a ridge filter due to the single spot evaluation. Monte Carlo simulations and experimental validation showed an increase in secondary neutron fluence for the aluminium range shifter compared to a conventional plastic range shifter [151]. However, the total increase in secondary neutron production remains to be quantified for larger field sizes; nevertheless, the use of lower (non-maximal) beam energies would aid in reducing the associated production of secondary neutrons from the ultra-high dose rate particles.

Due to the degraded FLASH-PT plan quality associated with homogeneous target dose delivery, a potential avenue for ultra-high dose rate protons is its combination with spatially fractionated radiotherapy (SFRT). Wei et al. (2025) demonstrated proof-of-concept treatment planning and experimental validation of ultra-high dose rate pencil beam scanned proton lattice radiotherapy using a similar beam configuration considered in this thesis (see Section 2.1) [159]. Their study showed that it is feasible to deliver such a treatment whilst achieving dose rates $\geq$ 40 Gy/s (using the percentile dose rate definition) to the skin for doses greater than 5 Gy [159]. As SFRT techniques do not require the total dose distribution to cover the entire target volume, the use of a patient-specific three-dimensional energy modulator may become redundant. Instead, dose can be delivered as larger "spots" or circular distributions within the delineated target structure, requiring modulation only in depth. Consequently, the field size per beam is reduced, which may allow for higher dose rates.

There is much left to uncover in the field of FLASH radiotherapy including the underlying biological mechanisms, the relevant beam parameters, how the sparing effect scales from pre-clinical studies to clinical trials, and how the beam delivery may be modified further to ensure safe delivery whilst also achieving ultra-high dose rates. Future developments in treatment planning may incorporate biological modelling of the FLASH effect, alongside established concepts such as variable relative biological effectiveness

and linear energy transfer-based optimisation. The integration of such models into optimisation frameworks could enable biologically guided FLASH-PT planning, although this will require a more complete understanding of the underlying mechanisms and their dependence on dose, dose rate, and tissue type. This thesis has shown that the modified FLASH-PT beam delivery does not yet lead to comparable treatment plans to IMPT with respect to doses to OARs. However, the results also indicate that doses to OARs could theoretically be reduced with further modifications to the FLASH-PT beam delivery. This work advances the understanding of relevant treatment planning optimisation techniques and beam delivery modifications, collectively improving the feasibility of FLASH-PT. Given the technological advancements in radiotherapy to date, spread-out Bragg peak FLASH proton therapy should be able to achieve treatment planning quality and beam delivery comparable to that of intensity modulated proton therapy in the near future.

Bibliography

[1] Paganetti, H, ed. *Proton Therapy Physics*. CRC Press, Apr. 2012. ISBN: 9780367803551. DOI: 10.1201/9780367803551.

[2] Bragg, W. "LXXIII. On the absorption of alpha rays, and on the classification of the alpha rays from radium". *The London, Edinburgh, and Dublin Philosophical Magazine and Journal of Science* 8, 48 Dec. 1904, pp. 719–725. DOI: 10.1080/14786440409463245.

[3] Wilson, R. R. "Radiological Use of Fast Protons". *Radiology* 47, 5 Nov. 1946, pp. 487–491. DOI: 10.1148/47.5.487.

[4] Ferlay, J, Ervik, M, Lam, F, Laversanne, M, Colombet, M, Mery, L, Piñeros, M, Znaor, A, Soerjomataram, I, and Bray, F. *Global Cancer Observatory: Cancer Today*. 2024. URL: https://gco.iarc.who.int/today.

[5] Atun, R., Jaffray, D. A., Barton, M. B., Bray, F., Baumann, M., Vikram, B., Hanna, T. P., Knaul, F. M., Lievens, Y., Lui, T. Y. M., Milosevic, M., O'Sullivan, B., Rodin, D. L., Rosenblatt, E., Dyk, J. V., Yap, M. L., Zubizarreta, E., and Gospodarowicz, M. "Expanding global access to radiotherapy". *The Lancet Oncology* 16, 10 Sept. 2015, pp. 1153–1186. DOI: 10.1016/S1470-2045(15)00222-3.

[6] Abdel-Wahab, M., Giammarile, F., Carrara, M., et al. "Radiotherapy and theranostics: a Lancet Oncology Commission". *The Lancet Oncology* 25, 11 Nov. 2024, e545–e580. DOI: 10.1016/S1470-2045(24)00407-8.

[7] Lawrence, J. H. "Proton irradiation of the pituitary". *Cancer* 10, 4 July 1957, pp. 795–798. DOI: 10.1002/1097-0142(195707/08)10:4<795::AID-CNCR2820100426>3.0.CO;2-B.

[8] Yan, S., Ngoma, T. A., Ngwa, W., and Bortfeld, T. R. "Global democratisation of proton radiotherapy". *The Lancet Oncology* 24, 6 June 2023, e245–e254. DOI: 10.1016/S1470-2045(23)00184-5.

[9] Bortfeld, T. "An analytical approximation of the Bragg curve for therapeutic proton beams". *Medical Physics* 24, 12 Dec. 1997, pp. 2024–2033. DOI: 10.1118/1.598116.

[10] Hill, M. "Radiation Track Structure: How the Spatial Distribution of Energy Deposition Drives Biological Response". *Clinical Oncology* 32, 2 Feb. 2020, pp. 75–83. DOI: 10.1016/j.clon.2019.08.006.

[11] Goodhead, D. T. "Radiation effects in living cells". *Canadian Journal of Physics* 68, 9 Sept. 1990, pp. 872–886. DOI: 10.1139/p90-125.

[12] Baumgarten, C. "Cyclotron beam extraction by acceleration". *Journal of Instrumentation* 18, 03 Mar. 2023, P03029. DOI: 10.1088/1748-0221/18/03/P03029.

[13] Darafsheh, A., Hao, Y., Zwart, T., Wagner, M., Catanzano, D., Williamson, J. F., Knutson, N., Sun, B., Mutic, S., and Zhao, T. "Feasibility of proton FLASH irradiation using a synchrocyclotron for preclinical studies". *Medical Physics* 47, 9 Sept. 2020, pp. 4348–4355. DOI: 10.1002/mp.14253.

[14] Wieszczycka, W. and Scharf, W. *Proton Radiotherapy Accelerators*. 1st ed. World Scientific, 2001.

[15] Ma, Y., Zhang, T., Selvaraj, B., Shen, J., Wei, S., Cheng, C., Gao, H., Poulsen, P. R., Li, H., Diffenderfer, E., Schuemann, J., Lin, L., Morris, Z., Durkee, B., Hesser, J., Lin, H., Simone, C. B., Kang, M., and Wu, H. "Advancing Proton FLASH Radiation Therapy: Innovations, Techniques, and Clinical Potentials". *International Journal of Radiation Oncology*Biology*Physics* 123, 3 Nov. 2025, pp. 876–890. DOI: 10.1016/j.ijrobp.2025.05.076.

[16] Schippers, J. M. and Lomax, A. J. "Emerging technologies in proton therapy". *Acta Oncologica* 50, 6 Aug. 2011, pp. 838–850. DOI: 10.3109/0284186X.2011.582513.

[17] Kang, M., Wei, S., Choi, J. I., Lin, H., and II, C. B. S. "A Universal Range Shifter and Range Compensator Can Enable Proton Pencil Beam Scanning Single-Energy Bragg Peak FLASH-RT Treatment Using Current Commercially Available Proton Systems". *International Journal of Radiation Oncology, Biology, Physics* 113, 1 2022, pp. 203–213. DOI: doi:10.1016/j.ijrobp.2022.01.009..

[18] James, S. S., Grassberger, C., and Lu, H.-M. "Considerations when Treating Lung Cancer with Passive Scatter or Active Scanning Proton Therapy". *Translational lung cancer research* 7, 2 2018, pp. 210–215. DOI: 10.21037/tlcr.2018.04.01.

[19] Hirayama, S, Matsuura, T, Yasuda, K, Takao, S, Fujii, T, Miyamoto, N, Umegaki, K, and Shimizu, S. "Difference in LET-Based Biological Doses Between IMPT Optimization Techniques: Robust and PTV-Based Optimizations". *Journal of Applied Clinical Medical Physics* 21, 4 2020, pp. 42–50. DOI: 10.1002/acm2.12844.

[20] Butkus, M. P., Brovold, N., Diwanji, T., Xu, Y., Ornelas, M. D., Pra, A. D., Abramowitz, M., Pollack, A., and Dogan, N. "Assessment of IMPT Versus VMAT Plans Using Different Uncertainty Scenarios for Prostate Cancer". *Radiation Oncology* 17, 162 2022. DOI: https://doi.org/10.1186/s13014-022-02126-y.

[21] Gomà, C, Lorentini, S, Meer, D, and Safai, S. "Proton beam monitor chamber calibration". *Physics in Medicine and Biology* 59, 17 Sept. 2014, pp. 4961–4971. DOI: 10.1088/0031-9155/59/17/4961.

[22] Nystrom, H., Jensen, M. F., and Nystrom, P. W. "Treatment planning for proton therapy: what is needed in the next 10 years?" *The British Journal of Radiology* 93, 1107 Mar. 2020. DOI: 10.1259/bjr.20190304.

[23] Unkelbach, J. and Paganetti, H. "Robust Proton Treatment Planning: Physical and Biological Optimization". *Seminars in Radiation Oncology* 28, 2 Apr. 2018, pp. 88–96. DOI: 10.1016/j.semradonc.2017.11.005.

[24] Fredriksson, A., Forsgren, A., and Hårdemark, B. "Minimax Optimization for Handling Range and Setup Uncertainties in Proton Therapy". *Medical Physics* 38, 3 2011, pp. 1672–1684.

[25] Wei, S., Lin, H., Choi, J. I., II, C. B. S., and Kang, M. "A Novel Proton Pencil Beam Scanning FLASH RT Delivery Method Enables Optimal OAR Sparing and Ultra-High Dose Rate Delivery: A Comprehensive Dosimetry Study for Lung Tumors". *Cancers* 13, 22 2021. DOI: 10.3390/cancers13225790.

[26] Vidal, M., Moignier, C., Patriarca, A., Sotiropoulos, M., Schneider, T., and Marzi, L. D. "Future technological developments in proton therapy – A predicted technological breakthrough". *Cancer/Radiothérapie* 25, 6-7 Oct. 2021, pp. 554–564. DOI: 10.1016/j.canrad.2021.06.017.

[27] Mazal, A., Prezado, Y., Ares, C., Marzi, L. de, Patriarca, A., Miralbell, R., and Favaudon, V. "FLASH and minibeams in radiation therapy: the effect of microstructures on time and space and their potential application to proton-therapy". *The British Journal of Radiology* 93, 1107 Mar. 2020. DOI: 10.1259/bjr.20190807.

[28] Prezado, Y., Grams, M., Jouglar, E., Martínez-Rovira, I., Ortiz, R., Seco, J., and Chang, S. "Spatially fractionated radiation therapy: a critical review on current status of clinical and preclinical studies and knowledge gaps". *Physics in Medicine & Biology* 69, 10 May 2024, 10TR02. DOI: 10.1088/1361-6560/ad4192.

[29] Hornsey, S. and Alper, T. "Unexpected Dose-rate Effect in the Killing of Mice by Radiation". *Nature* 210, 5032 Apr. 1966, pp. 212–213. DOI: 10.1038/210212a0.

[30] Phillips, T. L. and Worsnop, B. R. "Ultra-high Dose-rate Effects in Radiosensitive Bacteria". *International Journal of Radiation Biology and Related Stud-*

ies in Physics, Chemistry and Medicine 14, 6 Jan. 1969, pp. 573–575. DOI: 10.1080/09553006914551761.

[31] Berry, R. J., Hall, E. J., Forster, D. W., Storr, T. H., and Goodman, M. J. "Survival of mammalian cells exposed to X rays at ultra-high dose-rates". *The British Journal of Radiology* 42, 494 Feb. 1969, pp. 102–107. DOI: 10.1259/0007-1285-42-494-102.

[32] Favaudon, V., Caplier, L., Monceau, V., Pouzoulet, F., Sayarath, M., Fouillade, C., Poupon, M.-F., Isabel, B., Philippe, H., Bourhis, J., Janet, H., Fontaine, J.-J., and Vozenin, M.-C. "Ultrahigh Dose-Rate FLASH Irradiation Increases the Differential Response Between Normal and Tumour Tissue in Mice". *Science translational medicine* 6, 245 2014. DOI: 10.1126/scitranslmed.3008973.

[33] Taylor, E. R. J. F., Tullis, I. D. C., Vojnovic, B., and Petersson, K. "Megavoltage photon FLASH for preclinical experiments". *Medical Physics*, May 2025. DOI: 10.1002/mp.17891.

[34] Lövgren, N., Kristensen, I. F., and Petersson, K. "Feasibility and constraints of Bragg peak FLASH proton therapy treatment planning". *Frontiers in Oncology* 14, Apr. 2024. DOI: 10.3389/fonc.2024.1369065.

[35] Lövgren, N., Nilsson, R., Traneus, E., and Petersson, K. "The impact of dose rate optimisation and robust optimisation on FLASH proton therapy treatment plan quality and dose rates". *Frontiers in Oncology* 15, Dec. 2025. DOI: 10.3389/fonc.2025.1638319.

[36] Cunningham, S., McCauley, S., Vairamani, K., Speth, J., Girdhani, S., Abel, E., Sharma, R. A., Perentesis, J. P., Wells, S. I., Mascia, A., and Sertorio, M. "FLASH Proton Pencil Beam Scanning Irradiation Minimizes Radiation-Induced Leg Contracture and Skin Toxicity in Mice". *Cancers* 13, 5 Mar. 2021, p. 1012. DOI: 10.3390/cancers13051012.

[37] Alaghband, Y., Cheeks, S. N., Allen, B. D., Montay-Gruel, P., Doan, N.-L., Petit, B., Jorge, P. G., Giedzinski, E., Acharya, M. M., Vozenin, M.-C., and Limoli,

C. L. “Neuroprotection of Radiosensitive Juvenile Mice by Ultra-High Dose Rate FLASH Irradiation”. *Cancers* 12, 6 2020. DOI: 10.3390/cancers12061671.

[38] Evans, T., Cooley, J., Wagner, M., Yu, T., and Zwart, T. “Demonstration of the FLASH Effect Within the Spread-out Bragg Peak After Abdominal Irradiation of Mice”. *International Journal of Particle Therapy* 8, 4 2021, pp. 68–75. DOI: 10.14338/IJPT-20-00095.

[39] Levy, K, Natarajan, S, Wang, J, Chow, S, Eggold, J. T., Loo, P. E., Manjappa, R, Melemenidis, S, Lartey, F. M., Schüler, E, Skinner, L, Rafat, M, Ko, R, Kim, A, Al-Rawi, D. H., Eyben, R von, Dorigo, O, Casey, K. M., Graves, E. E., Bush, K, Yu, A. S., Koong, A. C., Maxim, P. G., Jr, B. W. L., and Rankin, E. B. “Abdominal FLASH Irradiation Reduces Radiation-Induced Gastrointestinal Toxicity for the Treatment of Ovarian Cancer in Mice”. *Scientific Reports* 10, 1 2020. DOI: 10.1038/s41598-020-78017-7.

[40] Adrian, G, Konradsson, E, Beyer, S, Wittrup, A, Butterworth, K. T., McMahon, S. J., Ghita, M, Petersson, K, and Ceberg, C. “Cancer Cells Can Exhibit a Sparing FLASH Effect at Low Doses Under Normoxic In Vitro-Conditions”. *Frontiers in Oncology* 11, 2021. DOI: 10.3389/fonc.2021.686142.

[41] Horst, F., Bodenstein, E., Brand, M., Hans, S., Karsch, L., Lessmann, E., Löck, S., Schürer, M., Pawelke, J., and Beyreuther, E. “Dose and dose rate dependence of the tissue sparing effect at ultra-high dose rate studied for proton and electron beams using the zebrafish embryo model”. *Radiotherapy and Oncology* 194, May 2024, p. 110197. DOI: 10.1016/j.radonc.2024.110197.

[42] Tinganelli, W., Puspitasari-Kokko, A., Sokol, O., Helm, A., Simoniello, P., Schuy, C., Lerchl, S., Eckert, D., Oppermann, J., Rehm, A., Janssen, S., Engel, D., Moeller, R., Romano, R., Horst, F., Boscolo, D., Fournier, C., Durante, M., and Weber, U. “FLASH Bragg-Peak Irradiation With a Therapeutic Carbon Ion Beam: First In Vivo Results”. *International Journal of Radiation Oncology*Biology*Physics*, Nov. 2024. DOI: 10.1016/j.ijrobp.2024.11.089.

[43] Ruan, J. L., Lee, C, Wouters, S, Tullis, I, Verslegers, M, Mysara, M, Then, C. K., Smart, S. C., Hill, M. A., Muschel, R. J., Giaccia, A. J., Vojnovic, B, Kiltie, A. E., and Petersson, K. "Irradiation at Ultra-High (FLASH) Dose Rates Reduces Acute Normal Tissue Toxicity in the Mouse Gastrointestinal System". *International Journal of Radiation Oncology, Biology, Physics* 111, 5 2021, pp. 1250–1261. DOI: 10.1016/j.ijrobp.2021.08.004.

[44] Montay-Gruel, P, Bouchet, A, Jaccard, M, Patin, D, Serduc, R, Aim, W, Petersson, K, Petit, B, Bailat, C, Bourhis, J, Bräuer-Krisch, E, and Vozenin, M. C. "X-rays can Trigger the FLASH Effect: Ultra-High Dose-Rate Synchrotron Light Source Prevents Normal Brain Injury after Whole Brain Irradiation in Mice". *Radiotherapy and oncology : journal of the European Society for Therapeutic Radiology and Oncology* 129, 3 2018, pp. 582–588. DOI: 10.1016/j.radonc.2018.08.016.

[45] Kristensen, L., Poulsen, P. R., Kanouta, E., Rohrer, S., Ankjærgaard, C., Andersen, C. E., Johansen, J. G., Simeonov, Y., Weber, U., Grau, C., and Sørensen, B. S. "Spread-out Bragg peak FLASH: quantifying normal tissue toxicity in a murine model". *Frontiers in Oncology* 14, July 2024. DOI: 10.3389/fonc.2024.1427667.

[46] Sørensen, B. S., Sitarz, M. K., Ankjærgaard, C., Johansen, J. G., Andersen, C. E., Kanouta, E., Grau, C., and Poulsen, P. "Pencil Beam Scanning Proton FLASH Maintains Tumor Control While Normal Tissue Damage is Reduced in a Mouse Model". *Radiotherapy and oncology : journal of the European Society for Therapeutic Radiology and Oncology* 175, 2022, pp. 178–184. DOI: 10.1016/j.radonc.2022.05.014.

[47] Wei, S., Lin, H., Shi, C., Xiong, W., Chen, C.-C., Huang, S., Press, R. H., Hasan, S., Chhabra, A. M., Choi, J. I., II, C. B. S., and Kang, M. "Use of Single-Energy Proton Pencil Beam Scanning Bragg Peak for Intensity-Modulated Proton Therapy FLASH Treatment Planning in Liver-Hypofractionated Radiation

Therapy". *Medical Physics* 49, 10 Oct. 2022, pp. 6560–6574. DOI: https://doi.org/10.1002/mp.15894. URL: https://doi.org/10.1002/mp.15894.

[48] Hall, E. and Giaccia, A. *Radiobiology for the Radiologist*. 7th. Lippincott Williams & Wilkins, 2012.

[49] McKeown, S. R. "Defining normoxia, physoxia and hypoxia in tumours—implications for treatment response". *The British Journal of Radiology* 87, 1035 Mar. 2014, p. 20130676. DOI: 10.1259/bjr.20130676.

[50] Wardman, P. "Time as a Variable in Radiation Biology: The Oxygen Effect". *Radiation Research* 185, 1 Jan. 2016, pp. 1–3. DOI: 10.1667/RR14323.1.

[51] Petersson, K., Adrian, G., Butterworth, K., and McMahon, S. J. "A Quantitative Analysis of the Role of Oxygen Tension in FLASH Radiation Therapy". *International Journal of Radiation Oncology*Biology*Physics* 107, 3 July 2020, pp. 539–547. DOI: 10.1016/j.ijrobp.2020.02.634.

[52] Cao, X., Zhang, R., Esipova, T. V., Allu, S. R., Ashraf, R., Rahman, M., Gunn, J. R., Bruza, P., Gladstone, D. J., Williams, B. B., Swartz, H. M., Hoopes, P. J., Vinogradov, S. A., and Pogue, B. W. "Quantification of Oxygen Depletion During FLASH Irradiation In Vitro and In Vivo". *International Journal of Radiation Oncology*Biology*Physics* 111, 1 Sept. 2021, pp. 240–248. DOI: 10.1016/j.ijrobp.2021.03.056.

[53] Adrian, G., Konradsson, E., Lempart, M., Bäck, S., Ceberg, C., and Petersson, K. "The FLASH effect depends on oxygen concentration". *The British Journal of Radiology* 93, 1106 Feb. 2020. DOI: 10.1259/bjr.20190702.

[54] Vilaplana-Lopera, N., Kim, J., Nam, G., Tullis, I. D. C., Paillas, S., Ruan, J.-L., Lee, P. J., Jiang, Y., Park, S., Hou, T., Nasir, A., Charlesworth, E., Walker, E., Abu-Halawa, A., Hill, M. A., Choi, C., Lee, I. J., Jeong, Y., Lakhal-Littleton, S., Then, C. K., Shen, S.-C., Giaccia, A. J., Petersson, K., and Moon, E. J. "Tissue-specific iron levels modulate lipid peroxidation and the FLASH radiotherapy

effect". *Cell Death & Disease* 16, 1 Sept. 2025, p. 668. DOI: 10.1038/s41419-025-07988-0.

[55] Durante, M., Brauer-Krisch, E., and Hill, M. "Faster and safer? FLASH ultra-high dose rate in radiotherapy". *The British Journal of Radiology*, Nov. 2017, p. 20170628. DOI: 10.1259/bjr.20170628.

[56] Zhu, H., Xie, D., Wang, Y., Huang, R., Chen, X., Yang, Y., Wang, B., Peng, Y., Wang, J., Xiao, D., Wu, D., Qian, C.-N., and Deng, X. "Comparison of intra-tumor and local immune response between MV X-ray FLASH and conventional radiotherapies". *Clinical and Translational Radiation Oncology* 38, Jan. 2023, pp. 138–146. DOI: 10.1016/j.ctro.2022.11.005.

[57] Jin, J.-Y., Gu, A., Wang, W., Oleinick, N. L., Machtay, M., and Kong, F.-M. S. "Ultra-high dose rate effect on circulating immune cells: A potential mechanism for FLASH effect?" *Radiotherapy and Oncology* 149, Aug. 2020, pp. 55–62. DOI: 10.1016/j.radonc.2020.04.054.

[58] Galts, A. and Hammi, A. "FLASH radiotherapy sparing effect on the circulating lymphocytes in pencil beam scanning proton therapy: impact of hypofractionation and dose rate". *Physics in Medicine & Biology*, Jan. 2023. DOI: 10.1088/1361-6560/ad144e.

[59] Velalopoulou, A., Karagounis, I. V., Cramer, G. M., Kim, M. M., Skoufos, G., Goia, D., Hagan, S., Verginadis, I. I., Shoniyozov, K., Chiango, J., Cerullo, M., Varner, K., Yao, L., Qin, L., Hatzigeorgiou, A. G., Minn, A. J., Putt, M., Lanza, M., Assenmacher, C.-A., Radaelli, E., Huck, J., Diffenderfer, E., Dong, L., Metz, J., Koumenis, C., Cengel, K. A., Maity, A., and Busch, T. M. "FLASH Proton Radiotherapy Spares Normal Epithelial and Mesenchymal Tissues while Preserving Sarcoma Response". *Cancer Research* 81, 18 2021, pp. 4808–4821. DOI: 10.1158/0008-5472.CAN-21-1500.

[60] Sørensen, B. S., Sitarz, M. K., Ankjærgaard, C., Johansen, J., Andersen, C. E., Kanouta, E., Overgaard, C., Grau, C., and Poulsen, P. "In Vivo Validation

and Tissue Sparing Factor for Acute Damage of Pencil Beam Scanning Proton FLASH". *Radiotherapy and oncology : journal of the European Society for Therapeutic Radiology and Oncology* 167, 2022, pp. 109–115. DOI: 10.1016/j.radonc.2021.12.022.

[61] Kim, M. M., Verginadis, I. I., Goia, D., Haertter, A., Shoniyozov, K., Zou, W., Maity, A., Busch, T. M., Metz, J. M., Cengel, K. A., Dong, L., Koumenis, C., and Diffenderfer, E. S. "Comparison of FLASH Proton Entrance and the Spread-Out Bragg Peak Dose Regions in the Sparing of Mouse Intestinal Crypts and in a Pancreatic Tumor Model". *Cancers* 13, 16 2021. DOI: 10.3390/cancers13164244.

[62] Diffenderfer, E. S., Verginadis, I. I., Kim, M. M., Shoniyozov, K., Velalopoulou, A., Goia, D., Putt, M., Hagan, S., Avery, S., Teo, K., Zou, W., Lin, A., Swisher-McClure, S., Koch, C., Kennedy, A. R., Minn, A., Maity, A., Busch, T. M., Dong, L., Koumenis, C., Metz, J., and Cengel, K. A. "Design, Implementation, and in Vivo Validation of a Novel Proton FLASH Radiation Therapy System". *International Journal of Radiation Oncology, Biology, Physics* 106, 2 2020, pp. 440–448. DOI: 10.1016/j.ijrobp.2019.10.049.

[63] Vozenin, M.-C., Burki, M., Ferrand, G., Patin, D., Bouchaab, H., Ozsahin, M., Bochud, F., Bailat, C., Devauchelle, P., and Bourhis, J. "The Advantage of FLASH Radiotherapy Confirmed in Mini-pig and Cat-cancer Patients". *Clinical cancer research : an official journal of the American Association for Cancer Research* 25, 1 2018, pp. 35–42. DOI: 10.1158/1078-0432.CCR-17-3375.

[64] Buonanno, M., Grilj, V., and Brenner, D. J. "Biological Effects in Normal Cells Exposed to FLASH Dose Rate Protons". *Radiotherapy and Oncology* 139, 2019, pp. 51–55. DOI: 10.1016/j.radonc.2019.02.009.

[65] Bourhis, J., Sozzi, W. J., Jorge, P. G., Gaide, O., Bailat, C., Duclos, F., Patin, D., Ozsahin, M., Bochud, F., Germond, J.-F., Moeckli, R., and Vozenin, M.-C.

"Treatment of a First Patient with FLASH-Radiotherapy". *Radiotherapy and Oncology* 139, 2019, pp. 18–22. DOI: 10.1016/j.radonc.2019.06.019.

[66] Konradsson, E, Arendt, M. L., Jensen, K. B., Børresen, B, Hansen, A. E., Bäck, S, Kristensen, A. T., Rosenschöld, P. M. A., Ceberg, C, and Petersson, K. "Establishment and Initial Experience of Clinical FLASH Radiotherapy in Canine Cancer Patients". *Frontiers in Oncology* 11, 2021. DOI: 10.3389/fonc.2021.658004.

[67] Soto, L. A., Casey, K. M., Wang, J., Blaney, A., Manjappa, R., Breitkreutz, D., Skinner, L., Dutt, S., Ko, R. B., Bush, K., Yu, A. S., Melemenidis, S., Strober, S., Englemann, E., Maxim, P. G., Graves, E. E., and Loo, B. W. "Flash irradiation results in reduced severe skin toxicity compared to conventional-dose-rate irradiation". *Radiation Research* 194, 6 Dec. 2020, pp. 618–624. DOI: 10.1667/RADE-20-00090.

[68] Sesink, A., Geyer, R., Devanand, P., Böhlen, T., Soutter, L., Moeckli, R., Bailat, C., Herrera, F., and Grilj, V. "Decrease in dose per fraction impairs the FLASH sparing effect in murine intestine model". *Radiotherapy and Oncology* 214, Jan. 2026, p. 111262. DOI: 10.1016/j.radonc.2025.111262.

[69] Mascia, A., McCauley, S., Speth, J., Nunez, S. A., Boivin, G., Vilalta, M., Sharma, R. A., Perentesis, J. P., and Sertorio, M. "Impact of Multiple Beams on the FLASH Effect in Soft Tissue and Skin in Mice". *International Journal of Radiation Oncology*Biology*Physics* 118, 1 Jan. 2024, pp. 253–261. DOI: 10.1016/j.ijrobp.2023.07.024.

[70] Sørensen, B. S., Kanouta, E., Ankjærgaard, C., Kristensen, L., Johansen, J. G., Sitarz, M. K., Andersen, C. E., Grau, C., and Poulsen, P. "Proton FLASH: Impact of Dose Rate and Split Dose on Acute Skin Toxicity in a Murine Model". *International Journal of Radiation Oncology*Biology*Physics* 120, 1 Sept. 2024, pp. 265–275. DOI: 10.1016/j.ijrobp.2024.04.071.

[71] Brown, K. H., Ghita-Pettigrew, M., McIvor, M. P., McDowell, M. P., McLaughlin, O., Prise, K. M., Sforza, D., Wong, J. W., Rezaee, M., McMahon, S. J., and Butterworth, K. T. "Dose, dose rate and split dose impacts murine skin responses following photon FLASH irradiation". *Radiotherapy and Oncology* 212, Nov. 2025, p. 111125. DOI: 10.1016/j.radonc.2025.111125.

[72] Venkatesulu, B. P., Sharma, A., Pollard-Larkin, J. M., Sadagopan, R., Symons, J., Neri, S., Singh, P. K., Tailor, R., Lin, S. H., and Krishnan, S. "Ultra High Dose Rate (35Gy/sec) Radiation Does Not Spare the Normal Tissue in Cardiac and Splenic Models of Lymphopenia and Gastrointestinal Syndrome". *Scientific Reports* 9, 2019. DOI: 10.1038/s41598-020-67913-7.

[73] Beyreuther, E., Brand, M., Hans, S., Hideghéty, K., Karsch, L., Leßmann, E., Schürer, M., Szabó, E. R., and Pawelke, J. "Feasibility of Proton FLASH Effect Tested by Zebrafish Embryo Irradiation". *Radiotherapy and oncology : journal of the European Society for Therapeutic Radiology and Oncology* 139, 2019, pp. 46–50. DOI: 10.1016/j.radonc.2019.06.024.

[74] Doyen, J, Sunyach, M. P., Almairac, F, Bourg, V, Naghavi, A. O., Bénazé, G. D. de, Claren, A, Padovani, L, Benezery, K, Noël, G, Hannoun-Lévi, J. M., Guedea, F, Giralt, J, Vidal, M, Baudin, G, Opitz, L, Claude, L, and Bondiau, P. Y. "Early Toxicities After High Dose Rate Proton Therapy in Cancer Treatments". *Frontiers in Oncology* 10, 2021. DOI: 10.3389/fonc.2020.613089.

[75] Williams, M. T., Regan, S. L., Fritz, A. L., Gollaway, B. M., Mascia, A. E., Vatner, R. E., Perentesis, J. P., and Vorhees, C. V. "Effects of whole brain proton irradiation at conventional or ultra-high dose rate (FLASH), in adult male Sprague Dawley rats". *Scientific Reports* 15, 1 Mar. 2025, p. 10602. DOI: 10.1038/s41598-025-94534-9.

[76] Montay-Gruel, P., Petersson, K., Jaccard, M., Boivin, G., Germond, J.-F., Petit, B., Doenlen, R., Favaudon, V., Bochud, F., Bailat, C., Bourhis, J., and Vozenin, M.-C. "Irradiation in a Flash: Unique Sparing of Memory in Mice after Whole

Brain Irradiation with Dose Rates Above 100Gy/s". *Radiotherapy and Oncology* 124, 3 2017, pp. 365–369. DOI: 10.1016/j.radonc.2017.05.003.

[77] Montay-Gruel, P, Acharya, M. M., Jorge, P. G., Petit, B, Petridis, I. G., Fuchs, P, Leavitt, R, Petersson, K, Gondré, M, Ollivier, J, Moeckli, R, Bochud, F, Bailat, C, Bourhis, J, Germond, J. F., Limoli, C. L., and Vozenin, M. C. "Hypofractionated FLASH-RT as an Effective Treatment against Glioblastoma that Reduces Neurocognitive Side Effects in Mice". *Clinical cancer research : an official journal of the American Association for Cancer Research* 27, 3 2021, pp. 775–784. DOI: 10.1158/1078-0432.CCR-20-0894.

[78] Kinj, R., Gaide, O., Jeanneret-Sozzi, W., Dafni, U., Viguet-Carrin, S., Sagittario, E., Kypriotou, M., Chenal, J., Duclos, F., Hebeisen, M., Falco, T., Geyer, R., Jorge, P. G., Moeckli, R., and Bourhis, J. "Randomized phase II selection trial of FLASH and conventional radiotherapy for patients with localized cutaneous squamous cell carcinoma or basal cell carcinoma: A study protocol". *Clinical and Translational Radiation Oncology* 45, Mar. 2024, p. 100743. DOI: 10.1016/j.ctro.2024.100743.

[79] NCT04986696, C. I. *Irradiation of Melanoma in a Pulse (IMPulse)*. 2021.

[80] Kinj, R., Schiappacasse, L., Grilj, V., Tsourti, Z., Duclos, F., Hebeisen, M., Jeanneret-Sozzi, W., Viguet-Carrin, S., Chenal, J., Jorge, P. G., Geyer, W. R., Guyer, G., Bailat, C., Bochud, F., Herrera, F. G., Moeckli, R., Dafni, U., Gaide, O., and Bourhis, J. "A phase I dose escalation of FLASH radiotherapy in patients with cutaneous metastases from melanoma: The IMPulse trial". *Radiotherapy and Oncology*, Jan. 2026, p. 111414. DOI: 10.1016/j.radonc.2026.111414.

[81] NCT05724875, C. I. *FLASH Radiotherapy for Skin Cancer (LANCE)*. 2023.

[82] Yang, C., Luo, H., Leijie, M., Mao, R., Lei, H., Zhang, Y., Xu, M., Wang, Y., Wu, M., Liu, H., Chen, P., and Ge, H. "A safety study of ultra-high dose rate FLASH radiotherapy in the treatment of superficial skin tumors: study protocol

of a phase I trial (ChiCTR2400080935)". *Precision Radiation Oncology* 9, 2 June 2025, pp. 72–76. DOI: 10.1002/pro6.70010.

[83] Grün, J. von der, Bello, R. D., Psoroulas, S., Krayenbuehl, J., Fesslmeier, D., Ramelyte, E., Mangana, J., Smith, W., Vilalta, M., Tirpak, L., Sharma, R. A., Guckenberger, M., Tanadini-Lang, S., and Balermpas, P. "First-in-human e-Flash radiotherapy using a modified conventional C-arm linear accelerator". *Clinical and Translational Radiation Oncology* 56, Jan. 2025, p. 101047. DOI: 10.1016/j.ctro.2025.101047.

[84] NCT06549439, C. I. *eFLASH for Skin Lesions of Malignant Melanomas (Flash-Skin I)*. 2024.

[85] Mascia, A. E., Daugherty, E. C., Zhang, Y., Lee, E., Xiao, Z., Sertorio, M., Woo, J., Backus, L. R., McDonald, J. M., McCann, C., Russell, K., Levine, L., Sharma, R. A., Khuntia, D., Bradley, J. D., II, C. B. S., Perentesis, J. P., and Breneman, J. C. "Proton FLASH Radiotherapy for the Treatment of Symptomatic Bone Metastases: The FAST-01 Nonrandomized Trial". *JAMA Oncology* 9, 1 2023, pp. 62–69. DOI: doi:10.1001/jamaoncol.2022.5843.

[86] NCT04592887, C. I. *Feasibility Study of FLASH Radiotherapy for the Treatment of Symptomatic Bone Metastases (FAST-01)*. 2020. URL: clinicaltrials.gov.

[87] Howell, D. D., James, J. L., Hartsell, W. F., Suntharalingam, M., Machtay, M., Suh, J. H., Demas, W. F., Sandler, H. M., Kachnic, L. A., and Berk, L. B. "Single-fraction radiotherapy versus multifraction radiotherapy for palliation of painful vertebral bone metastases—Equivalent efficacy, less toxicity, more convenient". *Cancer* 119, 4 Feb. 2013, pp. 888–896. DOI: 10.1002/cncr.27616.

[88] NCT05524064, C. I. *FLASH Radiotherapy for the Treatment of Symptomatic Bone Metastases in the Thorax (FAST-02)*. 2022. URL: ClinicalTrials.gov.

[89] Daugherty, E., Zhang, Y, Xiao, Z, Mascia, A., Sertorio, M, Woo, J, McCann, C, Russell, K., Sharma, R., Khuntia, D, Bradley, J., Simone, C., Breneman, J., and Perentesis, J. "FLASH radiotherapy for the treatment of symptomatic

bone metastases in the thorax (FAST-02): protocol for a prospective study of a novel radiotherapy approach". *Radiation Oncology* 19, 1 Mar. 2024, p. 34. DOI: 10.1186/s13014-024-02419-4.

[90] Wei, S., Lin, H., Shi, C., Xiong, W., Chen, C., Huang, S., Press, R. H., Hasan, S., Chhabra, A. M., Choi, J. I., Simone, C. B., and Kang, M. "Use of single-energy proton pencil beam scanning Bragg peak for intensity-modulated proton therapy FLASH treatment planning in liver-hypofractionated radiation therapy". *Medical Physics* 49, 10 Oct. 2022, pp. 6560–6574. DOI: 10.1002/mp.15894.

[91] Krieger, M., Water, S. van de, Folkerts, M. M., Mazal, A., Fabiano, S., Bizzocchi, N., Weber, D. C., Safai, S., and Lomax, A. J. "A quantitative FLASH effectiveness model to reveal potentials and pitfalls of high dose rate proton therapy". *Medical Physics* 49, 3 Mar. 2022, pp. 2026–2038. DOI: 10.1002/mp.15459.

[92] Liu, R., Charyyev, S., Wahl, N., Liu, W., Kang, M., Zhou, J., Yang, X., Baltazar, F., Palkowitsch, M., Higgins, K., Dynan, W., Bradley, J., and Lin, L. "An Integrated Biological Optimization Framework for Proton SBRT FLASH Treatment Planning allows Dose, Dose Rate, and LET Optimization Using Patient-Specific Ridge Filters". *arXiv* 2207, 08016 2022. DOI: 10.1016/j.ijrobp.2023.01.048.

[93] Zhang, X. "A Review of the Robust Optimization Process and Advances with Monte Carlo in the Proton Therapy Management of Head and Neck Tumors". *International Journal of Particle Therapy* 8, 1 2021, pp. 14–24. DOI: 10.14338/IJPT-20-00078.1.

[94] Patriarca, A., Fouillade, C., Auger, M., Martin, F., Pouzoulet, F., Nauraye, C., Heinrich, S., Favaudon, V., Meyroneinc, S., Dendale, R., Mazal, A., Poortmans, P., Verrelle, P., and Marzi, L. D. "Experimental Set-up for FLASH Proton Irradiation of Small Animals Using a Clinical System". *International Journal of Radiation Oncology, Biology, Physics* 102, 3 2018, pp. 619–626. DOI: 10.1016/j.ijrobp.2018.06.403.

[95] Marlen, P. van, Dahele, M., Folkerts, M., Abel, E., Slotman, B. J., and Verbakel, W. F. A. R. "Bringing FLASH to the Clinic: Treatment Planning Considerations for Ultrahigh Dose-Rate Proton Beams". *International Journal of Radiation Oncology, Biology, Physics* 106, 3 2020, pp. 621–629. DOI: DOI:10.1016/j.ijrobp.2019.11.011.

[96] Kang, M., Wei, S., Choi, J. I., II, C. B. S., and Lin, H. "Quantitative Assessment of 3D Dose Rate for Proton Pencil Beam Scanning FLASH Radiotherapy and Its Application for Lung Hypofractionation Treatment Planning". *Cancers* 13, 14 2021. DOI: 10.3390/cancers13143549.

[97] Verhaegen, F., Wanders, R.-G., Wolfs, C., and Eekers, D. "Considerations for Shoot-Through FLASH Proton Therapy". *Physics in Medicine and Biology* 66, 6 2021. DOI: 10.1088/1361-6560/abe55a.

[98] Simeonov, Y., Weber, U., Penchev, P., Ringbæk, T. P., Schuy, C., Brons, S., Engenhart-Cabillic, R., Bliedtner, J., and Zink, K. "3D range-modulator for scanned particle therapy: development, Monte Carlo simulations and experimental evaluation". *Physics in Medicine & Biology* 62, 17 Aug. 2017, pp. 7075–7096. DOI: 10.1088/1361-6560/aa81f4.

[99] Zhang, G., Gao, W., and Peng, H. "Design of Static and Dynamic Ridge Filters for FLASH–IMPT: A Simulation Study". *Medical Physics* 49, 8 Aug. 2022, pp. 5387–5399. DOI: 10.1002/mp.15717.

[100] Ma, C., Yang, X., Chang, C., Liu, R., Bohannon, D., Lin, L., Liu, T., Tian, S., and Zhou, J. "Feasibility Study of Hybrid Inverse Planning with Transmission Beams and Single-Energy Spread-Out Bragg Peaks for Proton FLASH Radiotherapy". *Medical Physics*, Mar. 2023. DOI: 10.1002/mp.16370.

[101] Ramesh, P., Gu, W., Ruan, D., and Sheng, K. "Dose and dose rate objectives in Bragg peak and shoot-through beam orientation optimization for FLASH proton therapy". *Medical Physics* 49, 12 Dec. 2022, pp. 7826–7837. DOI: 10.1002/mp.16009.

[102] Hotoiu, L., Stappen, F. V., Pin, A., Nilsson, R., Ivoc, J., Kim, M., Diffenderfer, E., Teo, B. K., and Labarbe, R. "Experimental validation of coarse ridge filters for FLASH proton therapy". *Medical Physics* 52, 9 Sept. 2025. DOI: 10.1002/mp.18044.

[103] Schwarz, M., Traneus, E., Safai, S., Kolano, A., and Water, S. van de. "Treatment planning for Flash radiotherapy: General aspects and applications to proton beams". *Medical Physics* 49, 4 Apr. 2022, pp. 2861–2874. DOI: 10.1002/mp.15579.

[104] Wei, S, Lin, H, Huang, S, Shi, C, Xiong, W, Zhai, H, Hu, L, Yu, G, Press, R. H., Hasan, S, Chhabra, A. M., Choi, J. I., II, C. B. S., and Kang, M. "Dose Rate and Dose Robustness for Proton Transmission FLASH-RT Treatment in Lung Cancer". *Frontiers in Oncology* 12, 2022. DOI: 10.3389/fonc.2022.970602.

[105] Zou, W., Diffenderfer, E. S., Cengel, K. A., Kim, M. M., Avery, S., Konzer, J., Cai, Y., Boisseu, P., Ota, K., Yin, L., Wiersma, R., Carlson, D. J., Fan, Y., Busch, T. M., Koumenis, C., Lin, A., Metz, J. M., Teo, B. K., and Dong, L. "Current Delivery Limitations of Proton PBS for FLASH". *Radiotherapy and oncology : journal of the European Society for Therapeutic Radiology and Oncology* 155, 2021, pp. 212–218. DOI: 10.1016/j.radonc.2020.11.002.

[106] Thames, H. D. and Rasmussen, S. L. "A Test for Dose-Modifying Factors". *Radiation Research* 76, 2 Nov. 1978, p. 308. DOI: 10.2307/3574781.

[107] Paillas, S., Taylor, E. R., Lövgren, N., Tullis, I. D., and Petersson, K. "Quantifying the flash effect and its dependence on average dose rate in vivo for 6 MeV electron and 6 MV photon beams". *Clinical and Translational Radiation Oncology* 56, Jan. 2025, p. 101052. DOI: 10.1016/j.ctro.2025.101052.

[108] Folkerts, M. M., Abel, E., Busold, S., Perez, J. R., Krishnamurthi, V., and Ling, C. C. "A framework for defining FLASH dose rate for pencil beam scanning". *Medical Physics* 47, 12 Dec. 2020, pp. 6396–6404. DOI: 10.1002/mp.14456.

[109] Water, S. van de, Safai, S., Schippers, J. M., Weber, D. C., and Lomax, A. J. "Towards FLASH Proton Therapy: The Impact of Treatment Planning and Machine Characteristics on Achievable Dose Rates". *Acta Oncologica* 58, 10 2019, pp. 1463–1469. DOI: 10.1080/0284186X.2019.1627416.

[110] Grilj, V., Zayas, A. V., Sesink, A., Devanand, P., Repáraz, D., Paisley, R., Sprengers, K., Passelli, K., Pernot, J., Böhlen, T. T., Geyer, R. W., Moeckli, R., Bailat, C., Germond, J.-F., Dagher, J., Bochud, F., Bourhis, J., and Herrera, F. G. "Average Dose Rate is the Major Temporal Beam Structure Parameter for Preserving Murine Intestines With Pulsed Electron FLASH Radiation Therapy". *International Journal of Radiation Oncology*Biology*Physics* 123, 2 Oct. 2025, pp. 593–601. DOI: 10.1016/j.ijrobp.2025.04.021.

[111] Dokic, I., Meister, S., Bojcevski, J., Tessonnier, T., Walsh, D., Knoll, M., Mein, S., Tang, Z., Vogelbacher, L., Rittmueller, C., Moustafa, M., Krunic, D., Brons, S., Haberer, T., Debus, J., Mairani, A., and Abdollahi, A. "Neuroprotective Effects of Ultra-High Dose Rate FLASH Bragg Peak Proton Irradiation". *International Journal of Radiation Oncology, Biology, Physics* 113, 3 2022, pp. 614–623. DOI: 10.1016/j.ijrobp.2022.02.020.

[112] Pennock, M., Wei, S., Cheng, C., Lin, H., Hasan, S., Chhabra, A. M., Choi, J. I., Bakst, R. L., Kabarriti, R., Simone, C. B., Lee, N. Y., Kang, M., and Press, R. H. "Proton Bragg Peak FLASH Enables Organ Sparing and Ultra-High Dose-Rate Delivery: Proof of Principle in Recurrent Head and Neck Cancer". *Cancers* 15, 15 Aug. 2023. DOI: 10.3390/cancers15153828.

[113] Zeng, Y., Li, H., Wang, W., Liu, X., Qin, B., Dai, S., Pang, B., Liu, M., Quan, H., Yang, K., Chang, Y., and Yang, Z. "Feasibility study of multiple-energy Bragg peak proton FLASH on a superconducting gantry with large momentum acceptance". *Medical Physics*, 2024. DOI: 10.1002/mp.16932.

[114] Marlen, P. van, Water, S. van de, Slotman, B. J., Dahele, M., and Verbakel, W. "Technical note: Dosimetry and FLASH potential of UHDR proton PBS for

small lung tumors: Bragg-peak-based delivery versus transmission beam and IMPT". *Medical Physics* 51, 10 Oct. 2024, pp. 7580–7588. DOI: 10.1002/mp.17185.

[115] Deffet, S., Hamaide, V., and Sterpin, E. "Definition of dose rate for FLASH pencil-beam scanning proton therapy: A comparative study". *Medical Physics* 50, 9 Sept. 2023, pp. 5784–5792. DOI: 10.1002/mp.16607.

[116] *ConformalFLASH, Ion Beam Applications SA*. 2022. URL: http://www.openflash.software.

[117] *OpenREGGUI*. 2022. URL: https://openreggui.org/.

[118] Souris, K. *MCsquare*. 2022. URL: http://www.openmcsquare.org/..

[119] *MATLAB, The MathWorks Inc., version: 9.7.0 (R2019b)*. 2019.

[120] Pedroni, E, Scheib, S, Böhringer, T, Coray, A, Grossmann, M, Lin, S, and Lomax, A. "Experimental characterization and physical modelling of the dose distribution of scanned proton pencil beams". *Physics in Medicine and Biology* 50, 3 Feb. 2005, pp. 541–561. DOI: 10.1088/0031-9155/50/3/011.

[121] Ryu, S., Pugh, S. L., Gerszten, P. C., Yin, F.-F., Timmerman, R. D., Hitchcock, Y. J., Movsas, B., Kanner, A. A., Berk, L. B., Followill, D. S., and Kachnic, L. A. "RTOG 0631 phase 2/3 study of image guided stereotactic radiosurgery for localized (1-3) spine metastases: Phase 2 results". *Practical Radiation Oncology* 4, 2 Mar. 2014, pp. 76–81. DOI: 10.1016/j.prro.2013.05.001.

[122] Bisello, S., Cilla, S., Benini, A., Cardano, R., Nguyen, N. P., Deodato, F., Macchia, G., Buwenge, M., Cammelli, S., Wondemagegnehu, T., Uddin, A. F. M. K., Rizzo, S., Bazzocchi, A., Strigari, L., and Morganti, A. G. "Dose–Volume Constraints fOr oRganS At risk In Radiotherapy (CORSAIR): An "All-in-One" Multicenter–Multidisciplinary Practical Summary". *Current Oncology* 29, 10 Sept. 2022, pp. 7021–7050. DOI: 10.3390/curroncol29100552.

[123] Hanna, G., Murray, L., Patel, R., Jain, S., Aitken, K., Franks, K., As, N. van, Tree, A., Hatfield, P., Harrow, S., McDonald, F., Ahmed, M., Saran, F., Webster, G., Khoo, V., Landau, D., Eaton, D., and Hawkins, M. "UK Consensus on Normal Tissue Dose Constraints for Stereotactic Radiotherapy". *Clinical Oncology* 30, 1 Jan. 2018, pp. 5–14. DOI: 10.1016/j.clon.2017.09.007.

[124] Knöös, T., Kristensen, I., and Nilsson, P. "Volumetric and dosimetric evaluation of radiation treatment plans: radiation conformity index". *International Journal of Radiation Oncology*Biology*Physics* 42, 5 Dec. 1998, pp. 1169–1176. DOI: 10.1016/S0360-3016(98)00239-9.

[125] "The International Commission on Radiation Units and Measurements". *Journal of the ICRU* 10, 1 Apr. 2010. DOI: 10.1093/jicru/ndq001.

[126] Daartz, J., Madden, T. M., Lalonde, A., Cascio, E., Verburg, J., Shih, H., MacDonald, S., Hachadorian, R., and Schuemann, J. "Voxel-wise dose rate calculation in clinical pencil beam scanning proton therapy". *Physics in Medicine & Biology* 69, 6 Mar. 2024, p. 065003. DOI: 10.1088/1361-6560/ad2713.

[127] Zeng, Y., Li, H., Zhang, Q., Wang, W., Liu, X., Qin, B., Pang, B., Liu, M., Yang, K., Quan, H., Chang, Y., and Yang, Z. "Biological-equivalent-dose-based integrated optimization framework for fast-energy-switching Bragg peak FLASH-RT using single-beam-per-fraction". *Medical Physics* 51, 9 Sept. 2024, pp. 6292–6304. DOI: 10.1002/mp.17264.

[128] Janson, M., Glimelius, L., Fredriksson, A., Traneus, E., and Engwall, E. "Treatment planning of scanned proton beams in RayStation". *Medical Dosimetry*, 2023. DOI: 10.1016/j.meddos.2023.10.009.

[129] Hörberger, F., Petersson, K., Ceberg, S., Bäck, S., Adrian, G., and Ceberg, C. "Investigating the therapeutic potential of FLASH radiotherapy – a treatment planning study". *Radiotherapy and Oncology*, 2025. DOI: 10.1016/j.radonc.2025.110947. URL: https://www.thegreenjournal.com/article/S0167-8140(25)04451-2/fulltext.

[130] Paganetti, H. “Proton Relative Biological Effectiveness – Uncertainties and Opportunities”. *International Journal of Particle Therapy* 5, 1 June 2018, pp. 2–14. DOI: 10.14338/IJPT-18-00011.1.

[131] Santo, R. J., Habraken, S. J., Breedveld, S., and Hoogeman, M. S. “Pencil-beam Delivery Pattern Optimization Increases Dose Rate for Stereotactic FLASH Proton Therapy”. *International Journal of Radiation Oncology, Biology, Physics* 115, 3 Mar. 2023, pp. 759–767. DOI: 10.1016/j.ijrobp.2022.08.053.

[132] Wase, V., Widenfalk, O., Nilsson, R., Fälth, C., and Fredriksson, A. “Fast spot order optimization to increase dose rates in scanned particle therapy FLASH treatments”. *Physics in Medicine & Biology* 70, 2 Jan. 2025, p. 025017. DOI: 10.1088/1361-6560/ada715.

[133] Zhao, X., Huang, S., Lin, H., Choi, J. I., Zhu, K., Simone, C. B., Yan, X., and Kang, M. “A Novel Dose Rate Optimization Method to Maximize Ultrahigh-Dose-Rate Coverage of Critical Organs at Risk Without Compromising Dosimetry Metrics in Proton Pencil Beam Scanning FLASH Radiation Therapy”. *International Journal of Radiation Oncology*Biology*Physics* 120, 4 Nov. 2024, pp. 1181–1191. DOI: 10.1016/j.ijrobp.2024.06.002.

[134] Lansonneur, P, Magliari, A, Rosa, L, Perez, J, Niemelä, P, and Folkerts, M. “Combined optimization of spot positions and weights for better FLASH proton therapy”. *Physics in Medicine & Biology* 69, 12 June 2024, p. 125010. DOI: 10.1088/1361-6560/ad4c53.

[135] Ma, C., Zhou, J., Chang, C. W., Wang, Y., Patel, P. R., Yu, D. S., Tian, S., and Yang, X. “Streamlined pin-ridge-filter design for single-energy proton FLASH planning”. *Medical Physics*, 2024. DOI: 10.1002/mp.16939.

[136] Colizzi, I., Poulsen, P. R., Sørensen, B., Meer, D., Lomax, A. J., and Psoroulas, S. “Which ‘dose rate’ definition describes the FLASH sparing effect for scanned proton beams? A meta-analysis of skin murine data”. *Radiotherapy and Oncology* 213, Dec. 2025, p. 111206. DOI: 10.1016/j.radonc.2025.111206.

[137] Hori, C., Aoki, T., and Seki, T. "Variable-energy isochronous accelerator with cotangential orbits for proton beam therapy". *Nuclear Instruments and Methods in Physics Research Section A: Accelerators, Spectrometers, Detectors and Associated Equipment* 922, Apr. 2019, pp. 352–356. DOI: 10.1016/j.nima.2019.01.005.

[138] Aylward, J. D., Henthorn, N, Manger, S, Warmenhoven, J. W., Merchant, M. J., Taylor, M. J., Mackay, R. I., and Kirkby, K. J. "Characterisation of the UK high energy proton research beamline for high and ultra-high dose rate (FLASH) irradiation". *Biomedical Physics & Engineering Express* 9, 5 Sept. 2023, p. 055032. DOI: 10.1088/2057-1976/acef25.

[139] Maradia, V., Meer, D., Dölling, R., Weber, D. C., Lomax, A. J., and Psoroulas, S. "Demonstration of momentum cooling to enhance the potential of cancer treatment with proton therapy". *Nature Physics* 19, 10 Oct. 2023, pp. 1437–1444. DOI: 10.1038/s41567-023-02115-2.

[140] Winklehner, D., Minervini, J. V., Bromberg, L., Forton, E., Mandrillon, J., Michael, P. C., and Radovinsky, A. "A compact, lightweight, variable-energy cyclotron for conventional and FLASH ion beam radiotherapy". *Frontiers in Oncology* 15, Oct. 2025. DOI: 10.3389/fonc.2025.1648237.

[141] Liu, X., Wang, W., Liang, Z., Zhao, R., Liu, K., and Qin, B. "Design of a light and fast energy degrader for a compact superconducting gantry with large momentum acceptance". *Physica Medica* 73, May 2020, pp. 43–47. DOI: 10.1016/j.ejmp.2020.04.008.

[142] Goethem, M. J. van, Meer, R van der, Reist, H. W., and Schippers, J. M. "Geant4 simulations of proton beam transport through a carbon or beryllium degrader and following a beam line". *Physics in Medicine and Biology* 54, 19 Oct. 2009, pp. 5831–5846. DOI: 10.1088/0031-9155/54/19/011.

[143] Rizzoglio, V., Adelmann, A., Baumgarten, C., Frey, M., Gerbershagen, A., Meer, D., and Schippers, J. "Evolution of a beam dynamics model for the transport

line in a proton therapy facility". *Physical Review Accelerators and Beams* 20, 12 Dec. 2017, p. 124702. DOI: 10.1103/PhysRevAccelBeams.20.124702.

[144] Chen, W., Yang, J., Qin, B., Liang, Z., Chen, Q., Liu, K., Li, D., and Fan, M. "Transmission calculation and intensity suppression for a proton therapy system". *Nuclear Instruments and Methods in Physics Research Section A: Accelerators, Spectrometers, Detectors and Associated Equipment* 881, Feb. 2018, pp. 82–87. DOI: 10.1016/j.nima.2017.10.047.

[145] Pedroni, E., Bearpark, R., Böhringer, T., Coray, A., Duppich, J., Forss, S., George, D., Grossmann, M., Goitein, G., Hilbes, C., Jermann, M., Lin, S., Lomax, A., Negrazus, M., Schippers, M., and Kotrle, G. "The PSI Gantry 2: a second generation proton scanning gantry". *Zeitschrift für Medizinische Physik* 14, 1 2004, pp. 25–34. DOI: 10.1078/0939-3889-00194.

[146] Maradia, V., Giovannelli, A. C., Meer, D., Weber, D. C., Lomax, A. J., Schippers, J. M., and Psoroulas, S. "Increase of the transmission and emittance acceptance through a cyclotron-based proton therapy gantry". *Medical Physics* 49, 4 Apr. 2022, pp. 2183–2192. DOI: 10.1002/mp.15505.

[147] Richardson, J. R., Blackmore, E. W., Dutto, G., Kost, C. J., Mackenzie, G. H., and Craddock, M. K. "Production of Simultaneous, Variable Energy Beams from the Triumf Cyclotron". *IEEE Transactions on Nuclear Science* 22, 3 June 1975, pp. 1402–1407. DOI: 10.1109/TNS.1975.4327895.

[148] Baumgarten, C. "Cyclotrons with fast variable and/or multiple energy extraction". *Physical Review Special Topics - Accelerators and Beams* 16, 10 Oct. 2013, p. 100101. DOI: 10.1103/PhysRevSTAB.16.100101.

[149] Finlan, M., Kruip, M., and Wilson, M. "A light, superconducting H- cyclotron for medical diagnostics and neutron radiography". *Proceedings of the Eleventh International Conference on Cyclotrons and their Applications, Tokyo, Japan.* IONICS Publishing Co., 1986.

[150] Shirai, K., Fukata, K., Adachi, A., Saitoh, J. ichi, Musha, A., Abe, T., Kanai, T., Kobayashi, D., Shigeta, Y., Yokoo, S., Chikamatsu, K., Ohno, T., and Nakano, T. "Dose–volume histogram analysis of brainstem necrosis in head and neck tumors treated using carbon-ion radiotherapy". *Radiotherapy and Oncology* 125, 1 Oct. 2017, pp. 36–40. DOI: 10.1016/j.radonc.2017.08.014.

[151] Chen, D., Motlagh, S. A. O., Stappen, F. V., Labarbe, R., Bell, B., Kim, M., Teo, B. K., Dong, L., Zou, W., and Diffenderfer, E. S. "Secondary neutron dosimetry for conformal FLASH proton therapy". *Medical Physics* 51, 7 July 2024, pp. 5081–5093. DOI: 10.1002/mp.17050.

[152] Zou, W., Dong, L., Pin, A., Nilsson, R., Kim, M., Apinorasethkul, O., Pakela, J., Friberg, A., Koger, B., Labarbe, R., Fuentes, C. L., Cengel, K., Traneus, E., Girdhani, S., Koumenis, C., Stappen, F. V., Diffenderfer, E., Bradley, J., Teo, B.-K. K., and Lin, A. "Deliverable proton conformal FLASH radiotherapy treatment planning for head and neck re-irradiation patients". *Radiotherapy and Oncology* 216, Mar. 2026, p. 111349. DOI: 10.1016/j.radonc.2025.111349.

[153] Schaefer, R, Psoroulas, S, and Weber, D. C. "In situ correction of recombination effects in ultra-high dose rate irradiations with protons". *Physics in Medicine & Biology* 68, 10 May 2023, p. 105013. DOI: 10.1088/1361-6560/accf5c.

[154] Setianegara, J., Wang, A., Gerard, N., Nys, J., Szczepanski, M., Gao, H., and Lin, Y. "Feasibility of prototype diamond detectors for pulsed UHDR PBS small-field proton dosimetry for proton FLASH experiments". *Physics in Medicine & Biology* 70, 19 Oct. 2025, p. 195001. DOI: 10.1088/1361-6560/ae023b.

[155] Romano, F., Bailat, C., Jorge, P. G., Lerch, M. L. F., and Darafsheh, A. "Ultra-high dose rate dosimetry: Challenges and opportunities for FLASH radiation therapy". *Medical Physics* 49, 7 July 2022, pp. 4912–4932. DOI: 10.1002/mp.15649.

[156] Valdetaro, L. B., Høye, E. M., Skyt, P. S., Petersen, J. B. B., Balling, P., and Muren, L. P. "Empirical quenching correction in radiochromic silicone-

based three-dimensional dosimetry of spot-scanning proton therapy". *Physics and Imaging in Radiation Oncology* 18, Apr. 2021, pp. 11–18. DOI: 10.1016/j.phro.2021.03.006.

[157] Villoing, D., Koumeir, C., Bongrand, A., Guertin, A., Haddad, F., Métivier, V., Poirier, F., Potiron, V., Servagent, N., Supiot, S., Delpon, G., and Chiavassa, S. "Technical note: Proton beam dosimetry at ultra-high dose rates (FLASH): Evaluation of GAFchromic™ (EBT3, EBT-XD) and OrthoChromic (OC-1) film performances". *Medical Physics* 49, 4 Apr. 2022, pp. 2732–2745. DOI: 10.1002/mp.15526.

[158] Darafsheh, A. and Ghaznavi, H. "A review on radiochromic film dosimetry in radiation therapy". *Journal of Applied Clinical Medical Physics* 26, 12 Dec. 2025. DOI: 10.1002/acm2.70365.

[159] Wei, S., Qi, H., Xu, L., Selvaraj, B., Zhao, X., Zheng, A., Vermeulen, M., Lee, N. Y., Bakst, R., Guha, C., Tsai, P., Kang, M., Wu, X., Yacoub, I., Choi, J. I., Chhabra, A., Simone, C. B., and Lin, H. "Proton pencil beam scanning ultra-high dose rate 3D lattice radiotherapy: A proof-of-concept FLASH SFRT study". *Medical Physics* 52, 12 Dec. 2025. DOI: 10.1002/mp.70187.

Appendix A

Treatment Plan Information and Data for MIROpt and RayStation Plans

The data presented in Appendix A is related to the work in Chapters 3 and 4.

```
1
2
3  ############################################################
4
5  # Example MIROpt Configuration File Objectives and Constraints
       for a Brain Case
6  # More information can be found on:
7  # https://github.com/openFLASH/conformalFLASH/ (accessed
       04/09/2025)
8
9  ############################################################
10
11 TargetROI:   ct_target        # name for target ROI
```

```
ExternalROI: ct_BODY          # name for external ROI - the
   body contour

optFunction:
- name: maxDVH                # Objective type: min, max,
   max_mean, min_mean,
# minDVH, maxDVH, minDR, minDRm, minDADRm
ROIname:   ct_target         # ROI to which the objective
   function is applied
intersect: ''                # Intersection ROI (blank if none)
remainder: ''                # Remainder ROI (blank if none)
Dref:      10.5              # Reference dose [Gy]
DRref:     0                 # Not used
Vref:      0.02              # Reference volume [%] (DVH
   objectives only)
impw:      0.5               # Importance weight (impw > 0)


- name: minDVH                # Objective type: min, max,
   max_mean, min_mean,
# minDVH, maxDVH, minDR, minDRm, minDADRm
ROIname:   ct_target         # ROI to which the objective
   function is applied
intersect: ''                # Intersection ROI (blank if none)
remainder: ''                # Remainder ROI (blank if none)
Dref:      10                # Reference dose [Gy]
DRref:     0                 # Not used
Vref:      0.95              # Reference volume [%]
impw:      0.5               # Importance weight (impw > 0)


```

```
- name: minDVH                  # Objective type: min, max,
   max_mean, min_mean,
# minDVH, maxDVH, minDR, minDRm, minDADRm
ROIname:   ct_target          # ROI to which the objective
   function is applied
intersect: ''                 # Intersection ROI (blank if none)
remainder: ''                 # Remainder ROI (blank if none)
Dref:      9.5                # Reference dose [Gy]
DRref:     0                  # Not used
Vref:      1.0                # Reference volume [%]
impw:      0.85               # Importance weight (impw > 0)


- name: max                    # Objective type: min, max,
   max_mean, min_mean,
# minDVH, maxDVH, minDR, minDRm, minDADRm
ROIname:   ct_BODY            # ROI to which the objective
   function is applied
intersect: ''                 # Intersection ROI (blank if none)
remainder: ''                 # Remainder ROI (blank if none)
Dref:      12                 # Reference dose [Gy]
DRref:     0                  # Not used
Vref:      0.95               # Reference volume [%]
impw:      0.5                # Importance weight (impw > 0)


- name: minDR                  # Objective type: min, max,
   max_mean, min_mean,
# minDVH, maxDVH, minDR, minDRm, minDADRm
ROIname:   ct_BODY            # ROI to which the objective
   function is applied
```

```
intersect: ''               # Intersection ROI (blank if none)
remainder: ''               # Remainder ROI (blank if none)
Dref:      2                # Dose per fraction threshold [Gy]
DRref:     40               # Reference dose rate [Gy/s]
Vref:      0.98             # Not used
impw:      0.00000001       # Importance weight (impw > 0)


- name: max                   # Objective type: min, max,
   max_mean, min_mean,
# minDVH, maxDVH, minDR, minDRm, minDADRm
ROIname:   ct_Brain         # ROI to which the objective
   function is applied
intersect: ''               # Intersection ROI (blank if none)
remainder: ''               # Remainder ROI (blank if none)
Dref:      12               # Reference dose [Gy]
DRref:     0                # Not used
Vref:      0.95             # Reference volume [%]
impw:      0.5              # Importance weight (impw > 0)


- name: minDR                 # Objective type: min, max,
   max_mean, min_mean,
# minDVH, maxDVH, minDR, minDRm, minDADRm
ROIname:   ct_Brain         # ROI to which the objective
   function is applied
intersect: ''               # Intersection ROI (blank if none)
remainder: ''               # Remainder ROI (blank if none)
Dref:      2                # Dose per fraction threshold [Gy]
DRref:     40               # Reference dose rate [Gy/s]
Vref:      0.98             # Not used
```

```
89 impw:       0.00000001        # Importance weight (impw > 0)
```

Listing A.1: Example MIROpt YAML configuration file outlining the objective functions for both dose and dose rate constraints across different structures. Comments have been simplified from the original file to improve clarity for demonstration purposes.

Table A.1: Beam angles (°) used for the intensity modulated proton therapy and spread-out Bragg peak FLASH proton therapy (FLASH-PT) plans in Chapters 3 and 4. The same beam angles were used for the two techniques unless explicitly stated. Due to a physical space constraint in the treatment head for the FLASH-PT plans in MIROpt, certain angles led to collisions between the conformal energy modulator (CEM) and the range shifter (RS), and a different beam angle was used, as shown for Lung 1 (5 fraction), Lung 3 (3 fraction), and Lung 3 (5 fraction). MIROpt did not allow for use of the Couch angle, and so all beam angles in the table have an associated couch angle of 0°.

Patient	**Beam 1 (°)**	**Beam 2 (°)**	**Beam 3 (°)**	**Beam 4 (°)**	**Beam 5 (°)**
Brain 2	50	90	130	-	-
Brain 3	230	270	310	-	-
Brain 4	170	280	-	-	-
Lung 1 (3 fraction)	0	60	120	-	-
Lung 1 (4 fraction)	40	90	140	350	
Lung 1 (5 fraction)	330	20	70	120	170 (180 for FLASH due to CEM RS error)
Lung 2 (3 fraction)	60	120	180	-	-
Lung 2 (4 fraction)	30	80	130	180	
Lung 2 (5 fraction)	40	80	120	160	200
Lung 3 (3 fraction)	10	250 (260 for FLASH due to CEM RS error)	310	-	-
Lung 3 (4 fraction)	0	230	270	310	
Lung 3 (5 fraction)	10	210 (240 for FLASH to CEM RS error)	250 (260 for FLASH to CEM RS error)	290	330

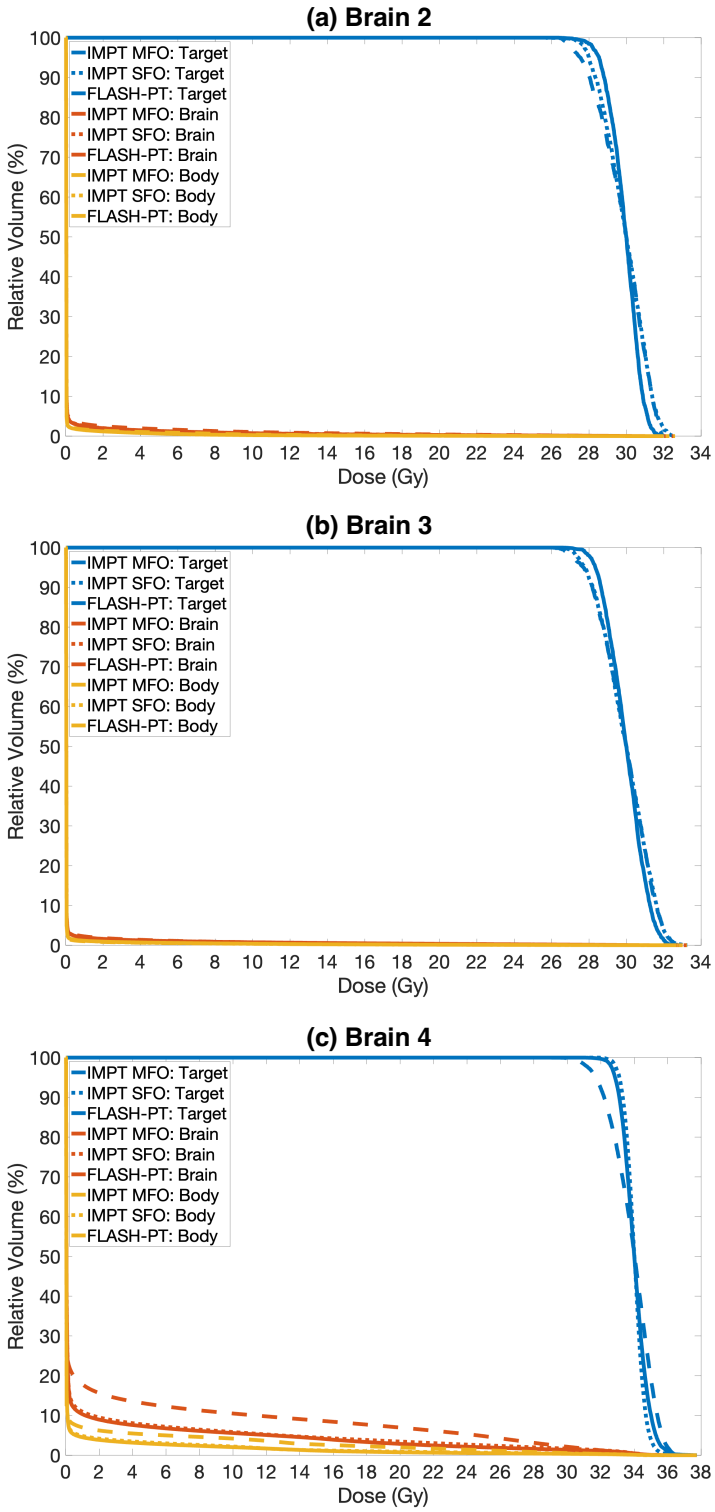


Figure A.1: Dose volume histograms for (a) Brain 2, (b) Brain 3, and (c) Brain 4. In each case, doses to the target and organ at risk structures are shown for each treatment technique: multi-field optimised intensity modulated proton therapy (IMPT MFO), single-field optimised intensity modulated proton therapy (IMPT SFO), and spread-out Bragg peak FLASH proton therapy (FLASH-PT).

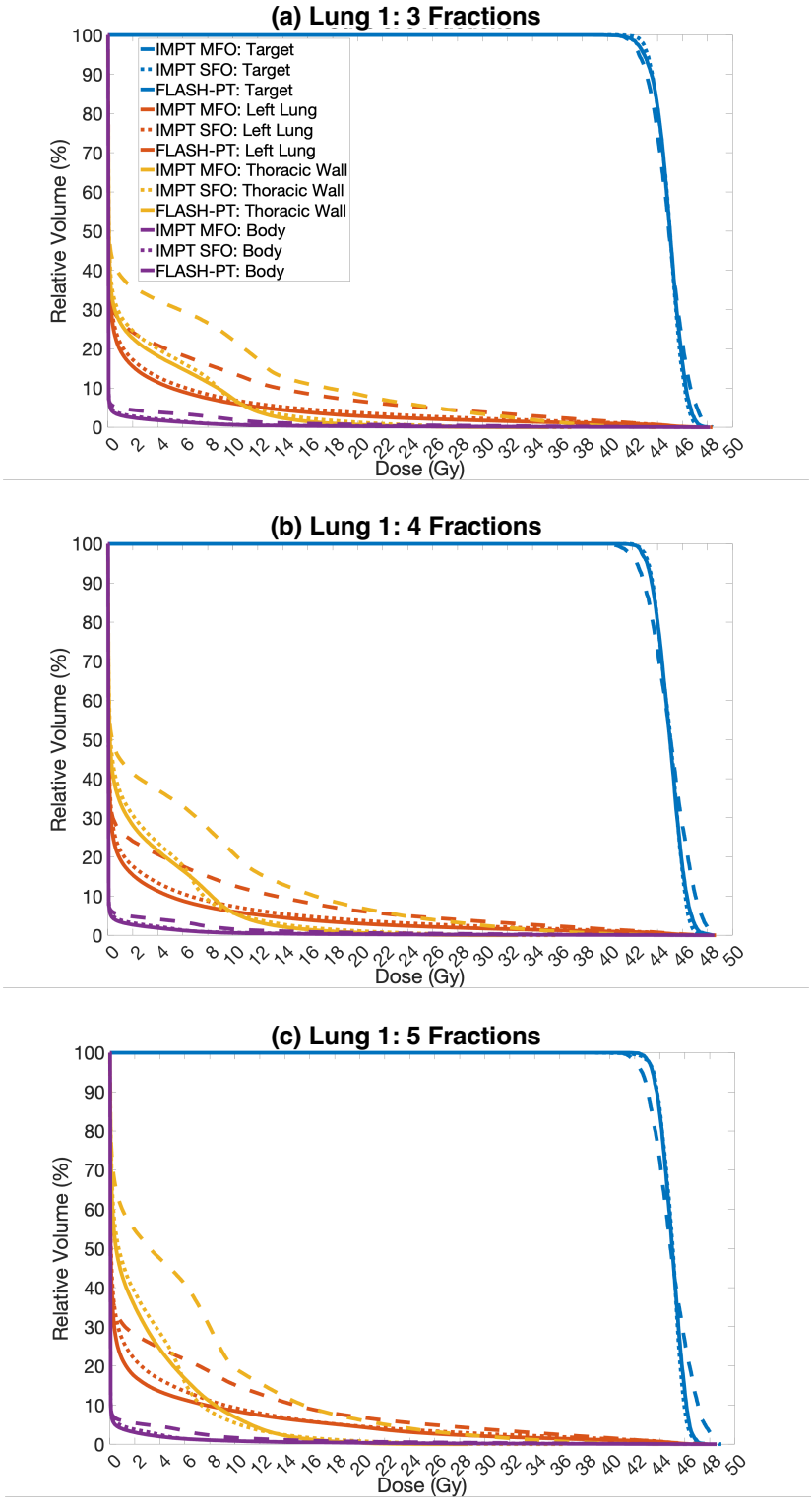


Figure A.2: Dose volume histograms for Lung 1 for the (a) 3, (b) 4, and (c) 5 fraction treatment plans. In each case, doses to the target and organ at risk structures are shown for each treatment technique: multi-field optimised intensity modulated proton therapy (IMPT MFO), single-field optimised intensity modulated proton therapy (IMPT SFO), and spread-out Bragg peak FLASH proton therapy (FLASH-PT).

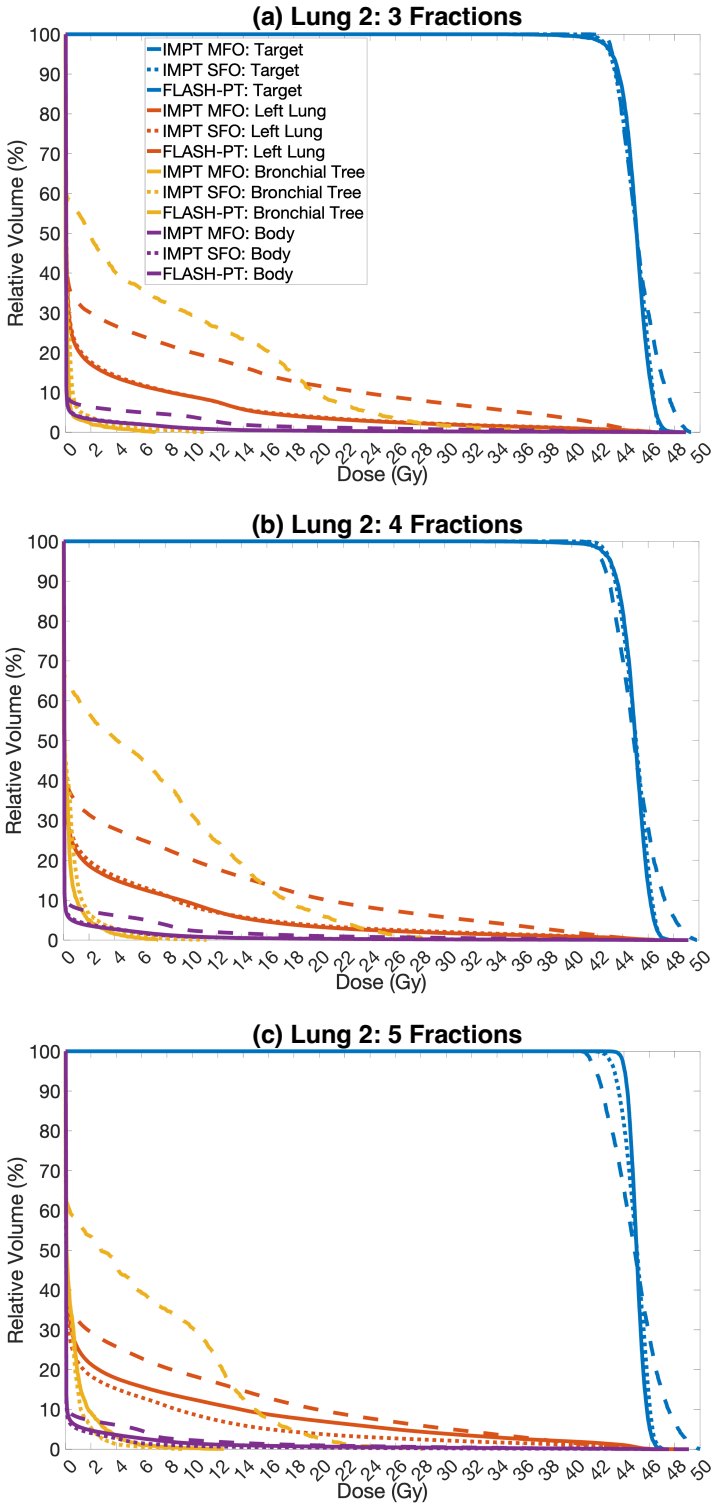


Figure A.3: Dose volume histograms for Lung 2 for the (a) 3, (b) 4, and (c) 5 fraction treatment plans. In each case, doses to the target and organ at risk structures are shown for each treatment technique: multi-field optimised intensity modulated proton therapy (IMPT MFO), single-field optimised intensity modulated proton therapy (IMPT SFO), and spread-out Bragg peak FLASH proton therapy (FLASH-PT).

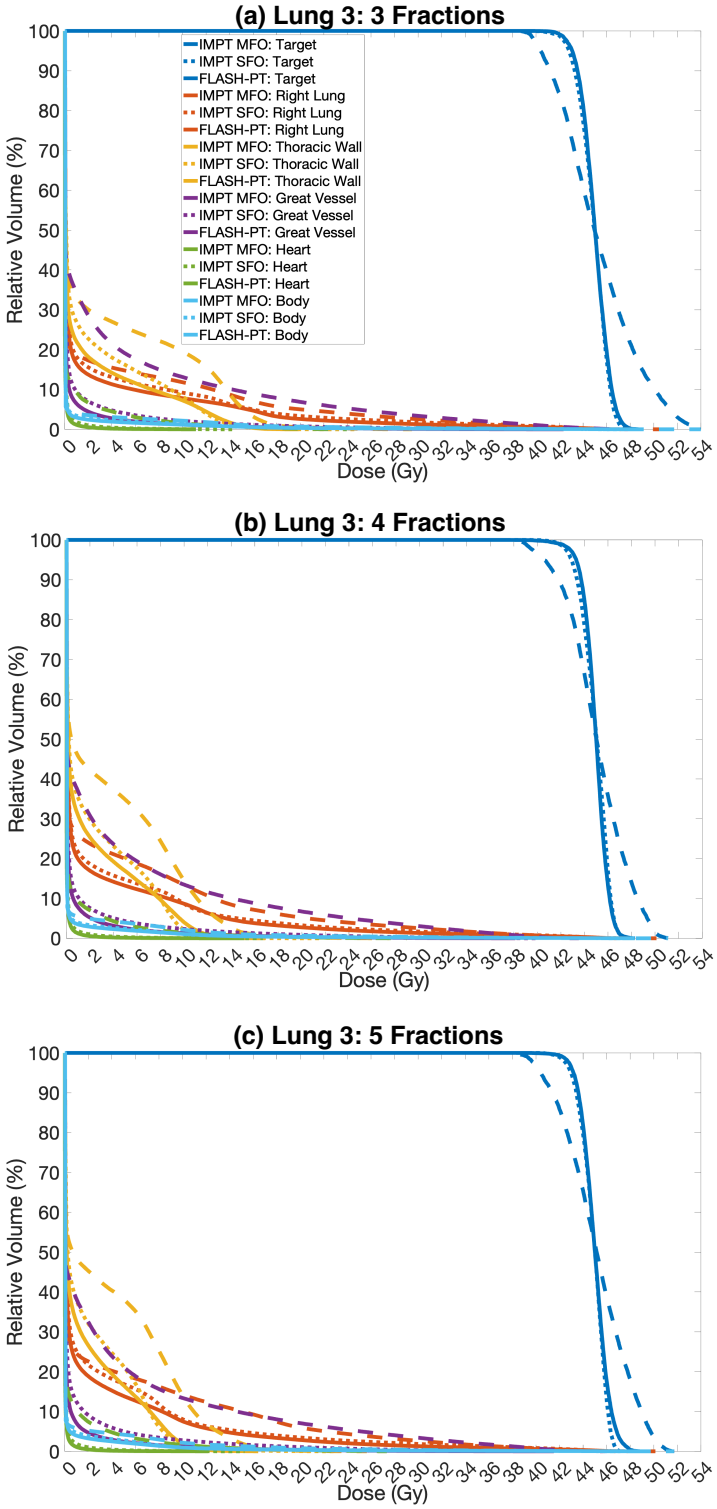


Figure A.4: Dose volume histograms for Lung 3 for the (a) 3, (b) 4, and (c) 5 fraction treatment plans. In each case, doses to the target and organ at risk structures are shown for each treatment technique: multi-field optimised intensity modulated proton therapy (IMPT MFO), single-field optimised intensity modulated proton therapy (IMPT SFO), and spread-out Bragg peak FLASH proton therapy (FLASH-PT).

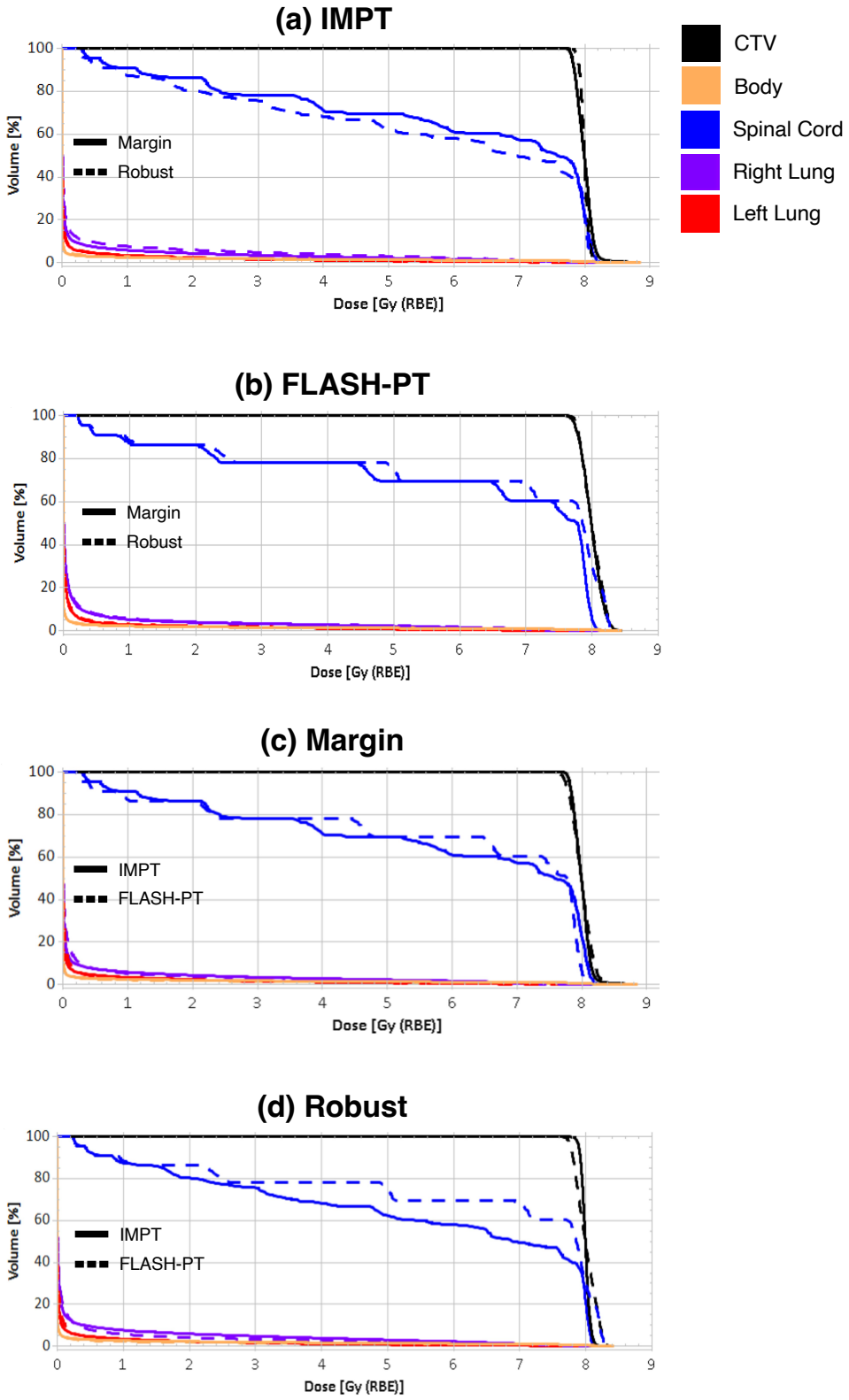


Figure A.5: Dose volume histograms (DVHs) for RayStation plans simulated for an example bone case (Bone 1). Treatment techniques (margin vs. robust) are compared for both (a) intensity modulated proton therapy (IMPT) and (b) spread-out Bragg peak FLASH proton therapy (FLASH-PT) plans. Comparisons of IMPT and FLASH-PT plans are made for (c) margin-based and (d) robust plans. Treatment planning system comparisons could not be made for any bone case as MIROpt plans could not be generated due to target size constraints.

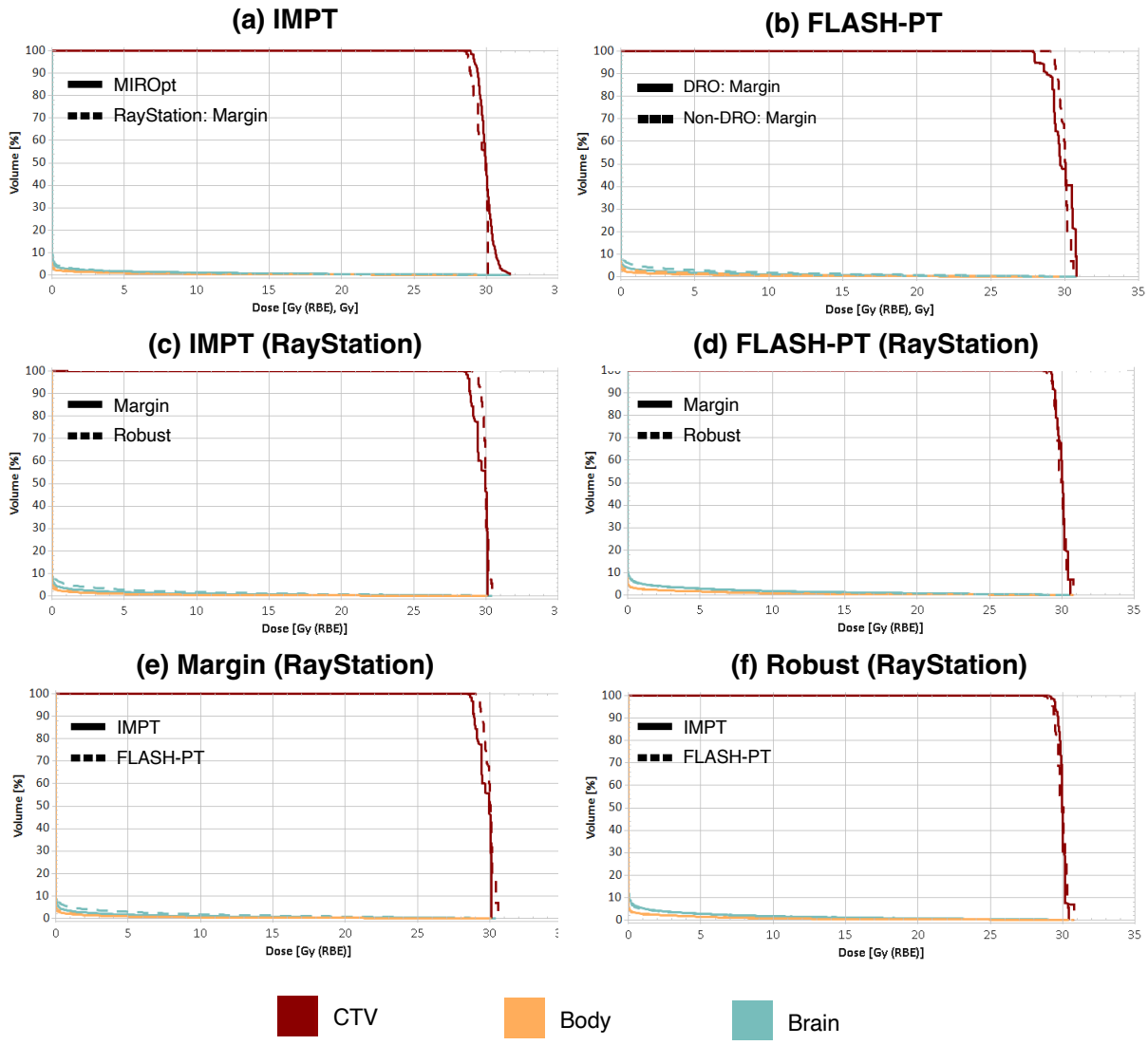


Figure A.6: Dose volume histograms (DVHs) for an example brain case (Brain 2). Treatment planning system comparison (MIROpt vs. RayStation) is made for (a) intensity modulated proton therapy (IMPT) plans, with (b) comparisons between dose rate optimised (DRO) and non-dose rate optimised (non-DRO) spread-out Bragg peak FLASH proton therapy (FLASH-PT), treatment techniques (margin vs. robust) are then compared for both (c) IMPT and (d) FLASH-PT plans simulated using RayStation. Comparisons between IMPT and FLASH-PT plans are then shown for both (e) margin-based and (f) robust IMPT and FLASH-PT plans.

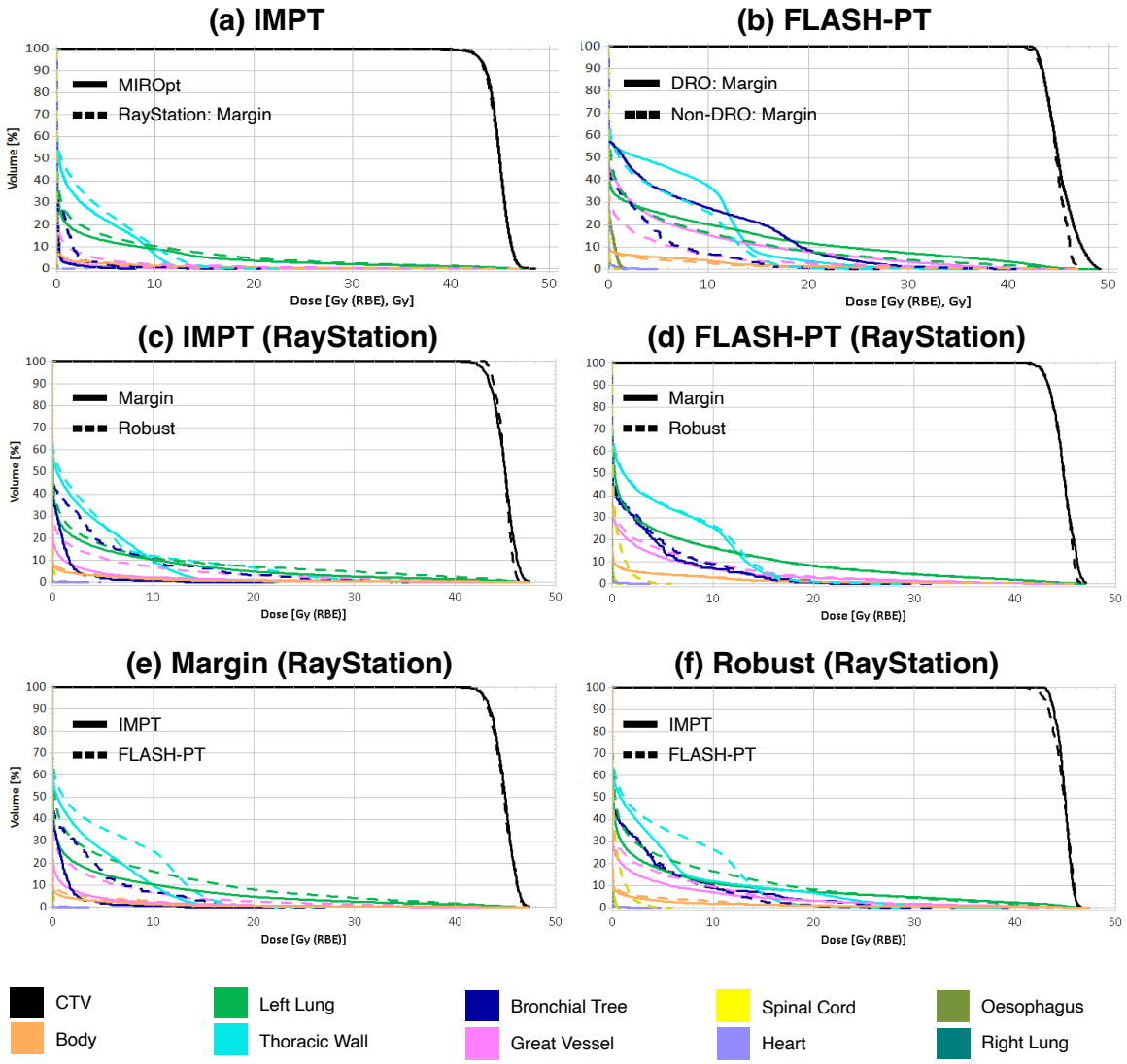


Figure A.7: Dose volume histograms (DVHs) for an example lung case (Lung 2). Treatment planning system comparison (MIROpt vs. RayStation) is made for (a) intensity modulated proton therapy (IMPT) plans, with (b) comparisons between dose rate optimised (DRO) and non-dose rate optimised (non-DRO) spread-out Bragg peak FLASH proton therapy (FLASH-PT), treatment techniques (margin vs. robust) are then compared for both (c) IMPT and (d) FLASH-PT plans simulated using RayStation. Comparisons between IMPT and FLASH-PT plans are then shown for both (e) margin-based and (f) robust IMPT and FLASH-PT plans.

Table A.2: Intensity modulated proton therapy doses to organs at risk (OAR) for the different brain cases (Brain 1, Brain 2, Brain 3, Brain 4), treatment planning systems (MIROpt and RayStation) and treatment planning techniques (margin-based and robust optimisation). Protocols used are for three fraction stereotactic body radiotherapy treatments from CORSAIR [121]. OAR dose constraints are given for each OAR, protocol, patient case, and treatment planning system/technique. Dashes (-) indicate that the specific OAR/constraint did not apply to that specific patient case. Brain 1 and Brain 4 were palliative and so the target volumes both exceeded 20 cm^3; the first constraint could therefore not be applied to these cases. The Brain Stem was not contoured for Brain 4 due to complete overlap with the CTV; for Brain 2 and Brain 3 the target was not located near the Brain Stem and so it was not applicable as an OAR.

Patient			**Brain 1**			**Brain 2**			**Brain 3**			**Brain 4**		
Technique			**MIROpt: Margin**	**RayStation: Margin**	**RayStation: Robust**	**MIROpt: Margin**	**RayStation: Margin**	**RayStation: Robust**	**MIROpt: Margin**	**RayStation: Margin**	**RayStation: Robust**	**MIROpt: Margin**	**RayStation: Margin**	**RayStation: Robust**
Protocol	**OAR**	**Constraint**												
CORSAIR	Brain + target volume	D20 cm^3 $>$ 20 Gy (Gy) (optimal)	Target volume $>$ 20 cm^3	Target volume $>$ 20 cm^3	Target volume $>$ 20 cm^3	8.45	7.52	7.84	4.96	5.97	7.85	Target volume $>$ 20 cm^3	Target volume $>$ 20 cm^3	Target volume $>$ 20 cm^3
CORSAIR	Brain + target volume	D_{max}(0.035cm^3) $<$ 18 Gy (Gy) (optimal)	-	-	-	-	-	-	-	-	-	0.00	0.00	0.00

Table A.3: Spread-out Bragg peak FLASH proton therapy doses to organs at risk (OAR) for the different brain cases (Brain 1, Brain 2, Brain 3, Brain 4), dose rate optimisations (dose rate optimised (DRO) (MIROpt) and non-dose rate optimised (non-DRO)), and treatment planning techniques (margin-based and robust optimisation). Protocols used are for three fraction stereotactic body radiotherapy treatments from CORSAIR [121]. OAR dose constraints are given for each OAR, protocol, patient case, and treatment planning system/technique. Dashes (-) indicate that the specific OAR/constraint did not apply to that specific patient case. Brain 1 and Brain 4 were palliative and so the target volumes both exceeded 20 cm^3; the first constraint could therefore not be applied to these cases. The Brain Stem was not contoured for Brain 4 due to complete overlap with the CTV; for Brain 2 and Brain 3 the target was not located near the Brain Stem and so it was not applicable as an OAR.

Patient			**Brain 1**			**Brain 2**			**Brain 3**			**Brain 4**		
Technique			**DRO: Margin**	**Non-DRO: Margin**	**Non-DRO: Robust**	**DRO: Margin**	**Non-DRO: Margin**	**Non-DRO: Robust**	**DRO: Margin**	**Non- DRO: Margin**	**Non-DRO: Robust**	**DRO: Margin**	**Non-DRO: Margin**	**Non-DRO: Robust**
Protocol	**OAR**	**Constraint**												
CORSAIR	Brain + target volume	D20 cm^3 < 20 Gy (Gy) (optimal)	Target volume > 20 cm^3	Target volume > 20 cm^3	Target volume > 20 cm^3	8.77	14.81	14.08	5.12	6.79	12.26	Target volume > 20 cm^3	Target volume > 20 cm^3	Target volume > 20 cm^3
CORSAIR	Brain + target volume	D_{max}(0.035cm^3) < 18 Gy (Gy) (optimal)	-	-	-	-	-	-	-	-	-	0.00	0.00	0.00

Table A.4: Intensity modulated proton therapy doses to organs at risk (OAR) for the different lung cases (Lung 1, Lung 2, Lung 3), treatment planning systems (MIROpt and RayStation), and treatment planning techniques (margin-based and robust optimisation). Protocols used are the 3 fraction UK Consensus on Normal Tissue Dose Constraints for Stereotactic Radiotherapy and data for 3 fraction stereotactic body radiotherapy treatments from CORSAIR [121, 123]. OAR dose constraints are given for each OAR, protocol, patient case, and treatment planning system/technique. Dashes (-) indicate that the specific OAR/constraint did not apply to that specific patient case. For Lung 1, the target was not located near the Great Vessel or the Bronchial Tree and so these were not applicable as OARs.

Patient			**Lung 1**			**Lung 2**			**Lung 3**		
Technique			**MIROpt: Margin**	**RayStation: Margin**	**RayStation: Robust**	**MIROpt: Margin**	**RayStation: Margin**	**RayStation: Robust**	**MIROpt: Margin**	**RayStation: Margin**	**RayStation: Robust**
Protocol	**OAR**	**Constraint**									
UK Consensus (Stereotactic)	Heart	Dmax (0.5 cm^3) <24 Gy (Gy) (optimal)	0.08	0.12	0.29	0.06	0.11	0.99	4.99	8.04	11.78
UK Consensus (Stereotactic)	Great Vessel	D_{max}(0.5cm^3) <45 Gy (Gy) (mandatory)	-	-	-	6.69	22.97	39,16	25.2	36.91	43.51
CORSAIR	Great Vessel	D10cm^3 <39 Gy (Gy) (optimal)	-	-	-	0.09	0.66	4.1	2.74	5.8	12.38
CORSAIR	Lung	D_{mean} <8 Gy (Gy) (optimal)	2.03	2.69	4.06	2.44	2.99	3.82	2.02	2.48	3.09
CORSAIR	Lung	V20 Gy <15% (%) (mandatory)	2.88	4.05	6.76	3.58	4.74	7.05	5.8	4.03	5.01
CORSAIR	Lung	V20 Gy < 10% (%) (optimal)	2.88	4.05	6.76	3.58	4.74	7.05	5.8	4.03	5.01
CORSAIR	Spinal Cord	D_{max}(0.1 cm^3) <18 Gy (Gy) (optimal)	0	0	0	0.09	0.05	0.47	0	0	0
UK Consensus (Stereotactic)	Bronchial Tree	D_{max}(0.5 cm^3) <30 Gy (Gy) (optimal)	-	-	-	0.26	1.69	1.42	0.21	0.79	0.59

Table A.5: Spread-out Bragg peak FLASH proton therapy doses to organs at risk (OAR) for the different lung cases (Lung 1, Lung 2, Lung 3), dose rate optimisations (dose rate optimised (DRO) (MIROpt) and non-dose rate optimised (non-DRO)), and treatment planning techniques (margin-based and robust optimisation). Protocols used are the 3 fraction UK Consensus on Normal Tissue Dose Constraints for Stereotactic Radiotherapy and data for 3 fraction stereotactic body radiotherapy treatments from CORSAIR [121, 123]. OAR dose constraints are given for each OAR, protocol, patient case, and treatment planning system/technique. Dashes (-) indicate that the specific OAR/constraint did not apply to that specific patient case. For Lung 1, the target was not located near the Great Vessel or the Bronchial Tree and so these were not applicable as OARs. Bold values indicate that they exceeded the optimal dose constraint, whereas bold and underlined values indicate that they exceeded the mandatory dose constraints.

Patient			**Lung 1**			**Lung 2**			**Lung 3**		
Technique			**DRO: Margin**	**Non-DRO: Margin**	**Non-DRO: Robust**	**DRO: Margin**	**Non-DRO: Margin**	**Non-DRO: Robust**	**DRO: Margin**	**Non- DRO: Margin**	**Non-DRO: Robust**
Protocol	**OAR**	**Constraint**									
UK Consensus (Stereotactic)	Heart	Dmax (0.5 cm^3) $<$ 24 Gy (Gy) (optimal)	0.01	0.34	0.38	2.66	1.31	1.71	20.29	17.79	17.19
UK Consensus (Stereotactic)	Great Vessel	D_{max}(0.5cm^3) $<$ 45 Gy (Gy) (mandatory)	-	-	-	38.98	35.33	34.46	**<u>45.29</u>**	40.02	40.83
CORSAIR	Great Vessel	D10cm^3 $<$ 39 Gy (Gy) (optimal)	-	-	-	13.03	4.81	7.43	29.05	22.71	27.57
CORSAIR	Lung	D_{mean} $<$ 8 Gy (Gy) (optimal)	3.82	3.93	4.52	5.73	4.67	4.73	2.88	3.54	3.59
CORSAIR	Lung	V20 Gy $<$ 15% (%) (mandatory)	6.72	5.81	6.58	<u>11.66</u>	7.98	8.22	5.01	5.95	5.51
CORSAIR	Lung	V20 Gy $<$ 10% (%) (optimal)	6.72	5.81	6.58	<u>11.66</u>	7.98	8.22	5.01	5.95	5.51
CORSAIR	Spinal Cord	D_{max}(0.1 cm^3) $<$ 18 Gy (Gy) (optimal)	0	0	0	0	0.41	3.86	0	0	0
UK Consensus (Stereotactic)	Bronchial Tree	D_{max}(0.5 cm^3) $<$ 30 Gy (Gy) (optimal)	-	-	-	18.94	6.51	8.23	0.01	3.84	3.72

Table A.6: Intensity modulated proton therapy doses to the spinal cord for the different bone cases (Bone 1, Bone 2, Bone 3) and treatment planning techniques (margin-based and robust optimisation), generated using RayStation. The dose protocol used for these cases is RTOG 0631 [121].

Protocol	**OAR**	**Constraint**	**Patient Case**					
			Bone 1		**Bone 2**		**Bone 3**	
			Margin	**Robust**	**Margin**	**Robust**	**Margin**	**Robust**
RTOG 0631	Spinal Cord	10 Gy $<$ 10% volume (%)	0	0	0	0	0	0
RTOG 0631	Spinal Cord	Max 10 Gy ($D_{1\%}$) (Gy)	8.20	8.11	8.20	8.28	8.06	8.09

Table A.7: Spread-out Bragg peak FLASH proton therapy doses to the spinal cord for the different bone cases (Bone 1, Bone 2, Bone 3) and treatment planning techniques (margin-based and robust optimisation), generated using RayStation. The dose protocol used for these cases is RTOG 0631 [121].

Protocol	**OAR**	**Constraint**	**Patient Case**					
			Bone 1		**Bone 2**		**Bone 3**	
			Margin	**Robust**	**Margin**	**Robust**	**Margin**	**Robust**
RTOG 0631	Spinal Cord	10 Gy $<$ 10% volume (%)	0	0	0	0	0	0
RTOG 0631	Spinal Cord	Max 10 Gy ($D_{1\%}$) (Gy)	8.07	8.28	8.52	8.77	8.47	8.27

Table A.8: Table of spot spacings (mm), layer spacings (mm), and target margins for spot placements (mm) for each patient case considered in Chapters 3 and 4 for intensity modulated proton therapy plans (with multi field optimisation) using the MIROpt treatment planning system.

Patient	**Spot Spacing (mm)**	**Layer Spacing (mm)**	**Target Margin (mm)**
Brain 2	2	2	[2, 2, 2]
Brain 3	3	3	[2, 2, 2]
Brain 4	2	2	[4, 4, 4]
Lung 1 (3 fractions)	3	3	[5, 5, 5]
Lung 1 (4 fractions)	3	3	[5, 5, 5]
Lung 1 (5 fractions)	3	3	[5, 5, 5]
Lung 2 (3 fractions)	3	3	[5, 5, 5]
Lung 2 (4 fractions)	4	4	[5, 5, 5]
Lung 2 (5 fractions)	3	3	[5, 5, 5]
Lung 3 (3 fractions)	3	3	[5, 5, 5]
Lung 3 (4 fractions)	3	3	[5, 5, 5]
Lung 3 (5 fractions)	3	3	[5, 5, 5]

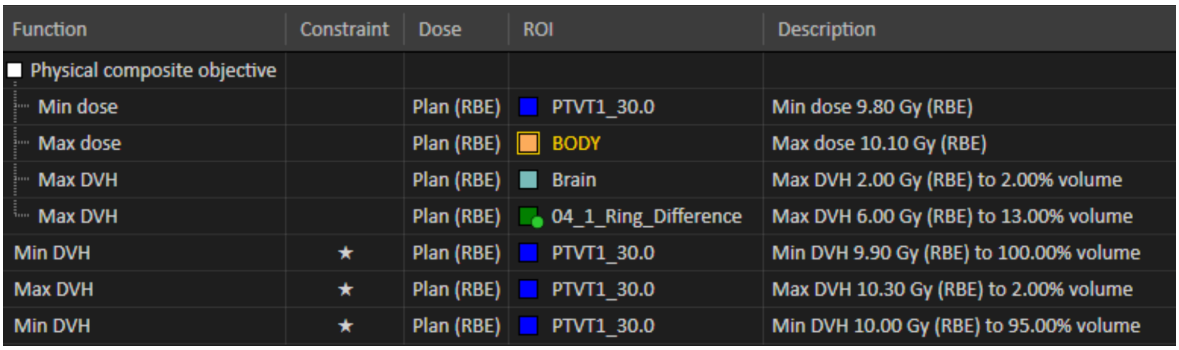


Figure A.8: Example dose objectives and constraints for a margin-based spread-out Bragg peak FLASH proton therapy plan generated for a brain case using RayStation

Patient	**Fraction**	**Spot Spacing (mm)**	**Layer Spacing (mm)**	**Target Margin (mm)**
Brain 2	1	1	1	[2, 2, 2]
Brain 2	2	1	1	[2, 2, 2]
Brain 2	3	1	1	[2, 2, 2]
Brain 3	1	1	1	[2, 2, 2]
Brain 3	2	1	1	[3, 3, 3]
Brain 3	3	1	1	[3, 3, 3]
Brain 4	1	2	2	[5, 5, 5]
Brain 4	2	2	2	[5, 5, 5]
Lung 1 (3 fractions)	1	2	2	[5, 5, 5]
Lung 1 (3 fractions)	2	5	5	[5, 5, 5]
Lung 1 (3 fractions)	3	5	5	[5, 5, 5]
Lung 1 (4 fractions)	1	5	5	[5, 5, 5]
Lung 1 (4 fractions)	2	5	5	[5, 5, 5]
Lung 1 (4 fractions)	3	5	5	[5, 5, 5]
Lung 1 (4 fractions)	4	5	5	[5, 5, 5]
Lung 1 (5 fractions)	1	5	5	[5, 5, 5]
Lung 1 (5 fractions)	2	5	5	[5, 5, 5]
Lung 1 (5 fractions)	3	5	5	[5, 5, 5]
Lung 1 (5 fractions)	4	5	5	[5, 5, 5]
Lung 1 (5 fractions)	5	5	5	[5, 5, 5]
Lung 2 (3 fractions)	1	2	2	[5, 5, 5]
Lung 2 (3 fractions)	2	2	2	[5, 5, 5]
Lung 2 (3 fractions)	3	2	2	[5, 5, 5]
Lung 2 (4 fractions)	1	2	2	[5, 5, 5]
Lung 2 (4 fractions)	2	2	2	[5, 5, 5]
Lung 2 (4 fractions)	3	2	2	[5, 5, 5]
Lung 2 (4 fractions)	4	2	2	[5, 5, 5]
Lung 2 (5 fractions)	1	2	2	[5, 5, 5]
Lung 2 (5 fractions)	2	2	2	[5, 5, 5]
Lung 2 (5 fractions)	3	2	2	[5, 5, 5]
Lung 2 (5 fractions)	4	2	2	[5, 5, 5]
Lung 2 (5 fractions)	5	2	2	[5, 5, 5]
Lung 3 (3 fractions)	1	3	3	[5, 5, 5]
Lung 3 (3 fractions)	2	5	5	[5, 5, 5]
Lung 3 (3 fractions)	3	3	3	[5, 5, 5]
Lung 3 (4 fractions)	1	3	3	[5, 5, 5]
Lung 3 (4 fractions)	2	5	5	[5, 5, 5]
Lung 3 (4 fractions)	3	5	5	[5, 5, 5]
Lung 3 (4 fractions)	4	2	2	[5, 5, 5]
Lung 3 (5 fractions)	1	3	3	[5, 5, 5]
Lung 3 (5 fractions)	2	5	5	[5, 5, 5]
Lung 3 (5 fractions)	3	5	5	[5, 5, 5]
Lung 3 (5 fractions)	4	3	3	[5, 5, 5]
Lung 3 (5 fractions)	5	3	3	[5, 5, 5]

Table A.9: Table of spot spacings (mm), layer spacings (mm), and target margins for spot placements (mm) for each patient case considered in Chapters 3 and 4 for one-beam-per-fraction intensity modulated proton therapy plans (with single field optimisation) using the MIROpt treatment planning system.

Patient	Fraction	Spot Spacing (mm)	Layer Spacing (mm)	Target Margin (mm)	Aperture Margin (mm)
Brain 2	1	8	13	[4, 4, 4]	[4, 4, 4]
Brain 2	2	9	16	[12, 12, 12]	[5, 5, 5]
Brain 2	3	9	19	[12, 12, 12]	[5, 5, 5]
Brain 3	1	7	14	[5, 5, 5]	[4, 4, 4]
Brain 3	2	7	18	[5, 5, 5]	[4, 4, 4]
Brain 3	3	7	18	[8, 8, 8]	[3, 3, 3]
Brain 4	1	10	18	[12, 12, 12]	[12, 12, 12]
Brain 4	2	12	18	[14, 14, 14]	[14, 14, 14]
Lung 1 (3 fractions)	1	10	10	[18, 18, 18]	[15, 15, 15]
Lung 1 (3 fractions)	2	10	25	[12, 12, 12]	[12, 12, 12]
Lung 1 (3 fractions)	3	18	18	[15, 15, 15]	[15, 15, 15]
Lung 1 (4 fractions)	1	15	20	[12, 10, 12]	[12, 12, 12]
Lung 1 (4 fractions)	2	15	15	[12, 12, 12]	[12, 12, 12]
Lung 1 (4 fractions)	3	18	15	[15, 15, 15]	[15, 15, 15]
Lung 1 (4 fractions)	4	18	15	[12, 12, 12]	[12, 12, 12]
Lung 1 (5 fractions)	1	10	25	[12, 10, 12]	[12, 12, 12]
Lung 1 (5 fractions)	2	10	25	[12, 10, 12]	[12, 12, 12]
Lung 1 (5 fractions)	3	18	20	[15, 15, 15]	[15, 15, 15]
Lung 1 (5 fractions)	4	10	14	[12, 10, 12]	[12, 12, 12]
Lung 1 (5 fractions)	5	9	18	[12, 10, 12]	[12, 12, 12]
Lung 2 (3 fractions)	1	14	20	[18, 18, 18]	[15, 15, 15]
Lung 2 (3 fractions)	2	10	20	[18, 18, 18]	[15, 15, 15]
Lung 2 (3 fractions)	3	10	20	[18, 18, 18]	[18, 18, 18]
Lung 2 (4 fractions)	1	10	20	[15, 15, 15]	[15, 15, 15]
Lung 2 (4 fractions)	2	14	18	[18, 18, 18]	[15, 15, 15]
Lung 2 (4 fractions)	3	14	18	[18, 18, 18]	[15, 15, 15]
Lung 2 (4 fractions)	4	10	20	[18, 18, 18]	[15, 15, 15]
Lung 2 (5 fractions)	1	8	18	[12, 10, 12]	[12, 12, 12]
Lung 2 (5 fractions)	2	18	20	[18, 18, 18]	[15, 15, 15]
Lung 2 (5 fractions)	3	12	18	[18, 18, 18]	[18, 18, 18]
Lung 2 (5 fractions)	4	15	18	[18, 18, 18]	[15, 15, 15]
Lung 2 (5 fractions)	5	12	18	[12, 10, 12]	[12, 12, 12]
Lung 3 (3 fractions)	1	12	25	[15, 15, 15]	[12, 12, 12]
Lung 3 (3 fractions)	2	10	20	[15, 15, 15]	[15, 15, 15]
Lung 3 (3 fractions)	3	12	25	[18, 18, 18]	[15, 15, 15]
Lung 3 (4 fractions)	1	15	18	[18, 18, 18]	[18, 18, 18]
Lung 3 (4 fractions)	2	15	12	[16, 16, 16]	[16, 16, 16]
Lung 3 (4 fractions)	3	13	10	[18, 18, 18]	[18, 18, 18]
Lung 3 (4 fractions)	4	13	20	[18, 18, 18]	[15, 15, 15]
Lung 3 (5 fractions)	1	12	20	[18, 18, 18]	[18, 18, 18]
Lung 3 (5 fractions)	2	13	15	[15, 15, 15]	[15, 15, 15]
Lung 3 (5 fractions)	3	13	15	[18, 18, 18]	[18, 18, 18]
Lung 3 (5 fractions)	4	13	15	[18, 18, 18]	[18, 18, 18]
Lung 3 (5 fractions)	5	13	20	[18, 18, 18]	[14, 14, 14]

Table A.10: Table of spot spacings (mm), layer spacings (mm), and target margins for spot placements (mm) for each patient case considered in Chapters 3 and 4 for one-beam-per-fraction spread-out Bragg peak FLASH proton therapy plans (with single field optimisation) using the MIROpt treatment planning system.

Function	Constraint	Dose	ROI	Description	Robust
Physical composite objective					
Max DVH		Plan (RBE)	GTVT1_30.0	Max DVH 10.50 Gy (RBE) to 2.00% volume	★
Min DVH		Plan (RBE)	GTVT1_30.0	Min DVH 9.50 Gy (RBE) to 95.00% volume	★
Min DVH		Plan (RBE)	GTVT1_30.0	Min DVH 10.00 Gy (RBE) to 95.00% volume	★
Max dose		Plan (RBE)	Brain	Max dose 10.60 Gy (RBE)	
Max dose		Plan (RBE)	BODY	Max dose 10.50 Gy (RBE)	
Max DVH		Plan (RBE)	04_1_Ring_Difference	Max DVH 8.00 Gy (RBE) to 3.00% volume	

Figure A.9: Example dose objectives and constraints for a robust spread-out Bragg peak FLASH proton therapy plan generated for a brain case using RayStation

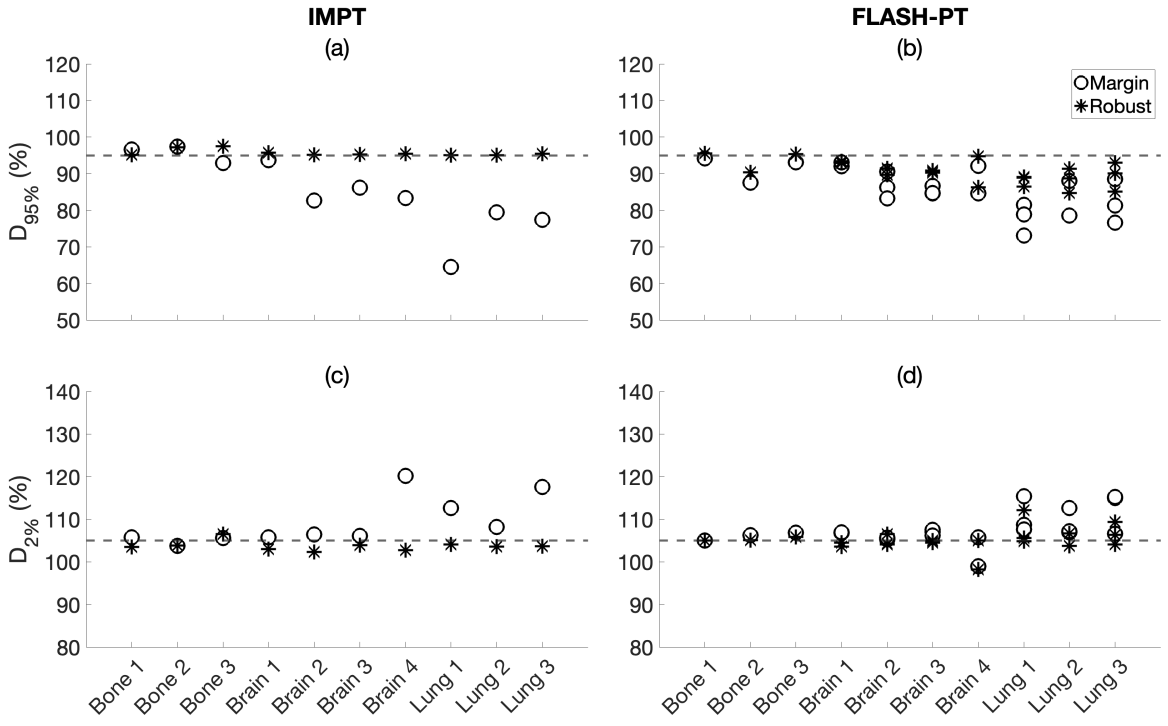


Figure A.10: Worst-case scenario comparisons between margin (o) and robust (*) optimisation techniques for intensity modulated proton therapy (IMPT) and Bragg peak FLASH proton therapy (FLASH-PT) treatment plans generated using RayStation. The worst-case scenarios were evaluated for $D_{95\%}$ and $D_{2\%}$ of the target volumes and are shown for each individual patient case for both IMPT and FLASH-PT, and for each individual fraction for FLASH-PT . Grey dashed lines indicate target dose limits of $D_{95\%} = 95\%$ for (a) and (b), and $D_{2\%} = 105\%$ for (c) and (d).

Appendix B

Treatment Plan Data for Non-Maximal Energy SOBP FLASH Proton Therapy

The data presented in Appendix B is related to the work in Chapter 5.

Table B.1: Beam and couch angles (°) used for the intensity modulated proton therapy and spread-out Bragg peak FLASH proton therapy treatment plans in Chapter 5.

Patient	**Beam 1 (º)**	**Beam 2 (º)**	**Beam 3 (º)**
1	(288, 0)	(242, 0)	(275, 90)
2	(90, 340)	(75, 0)	(105, 0)
3	(80, 350)	(280, 10)	(290, 90)
4	(285, 15)	(75, 345)	(330, 90)
5	(250,0)	(270, 15)	(280, 10)
6	(310, 90)	(80, 350)	(280, 10)
7	(80, 350)	(280, 10)	(310, 90)
8	(185, 0)	(255, 0)	(285, 0)
9	(45, 0)	(255, 0)	(285, 0)
10	(90, 0)	(270, 0)	(315, 90)

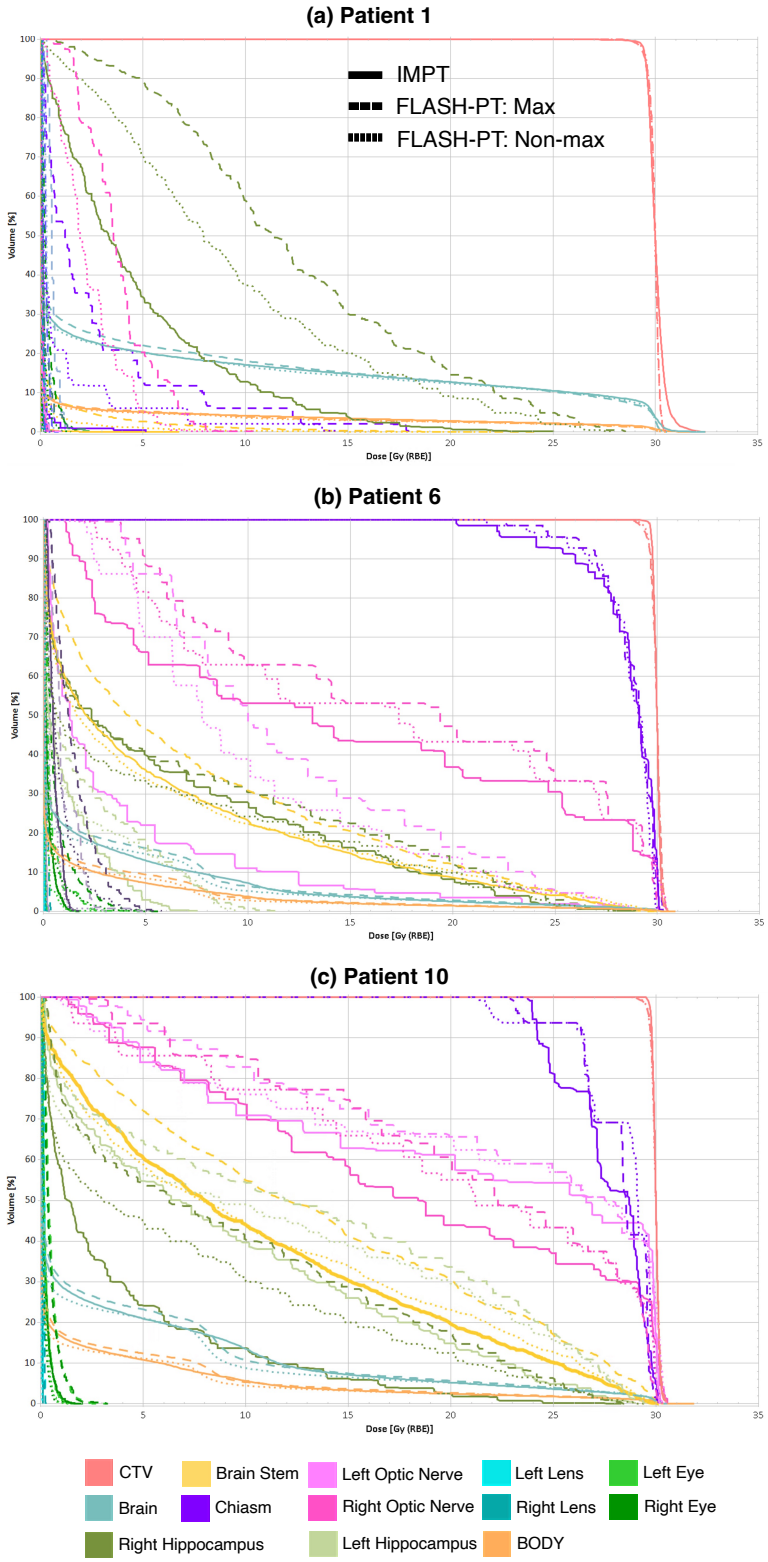


Figure B.1: Dose volume histograms (DVHs) for treatment plans for Patients (a) 1, (b) 6, and (c) 10 in Chapter 5. Comparisons are made between intensity modulated proton therapy (IMPT), spread-out Bragg peak FLASH proton therapy (FLASH-PT) delivered with the maximum beam energy (Max), and FLASH-PT delivered with non-maximal beam energies (Non-max).

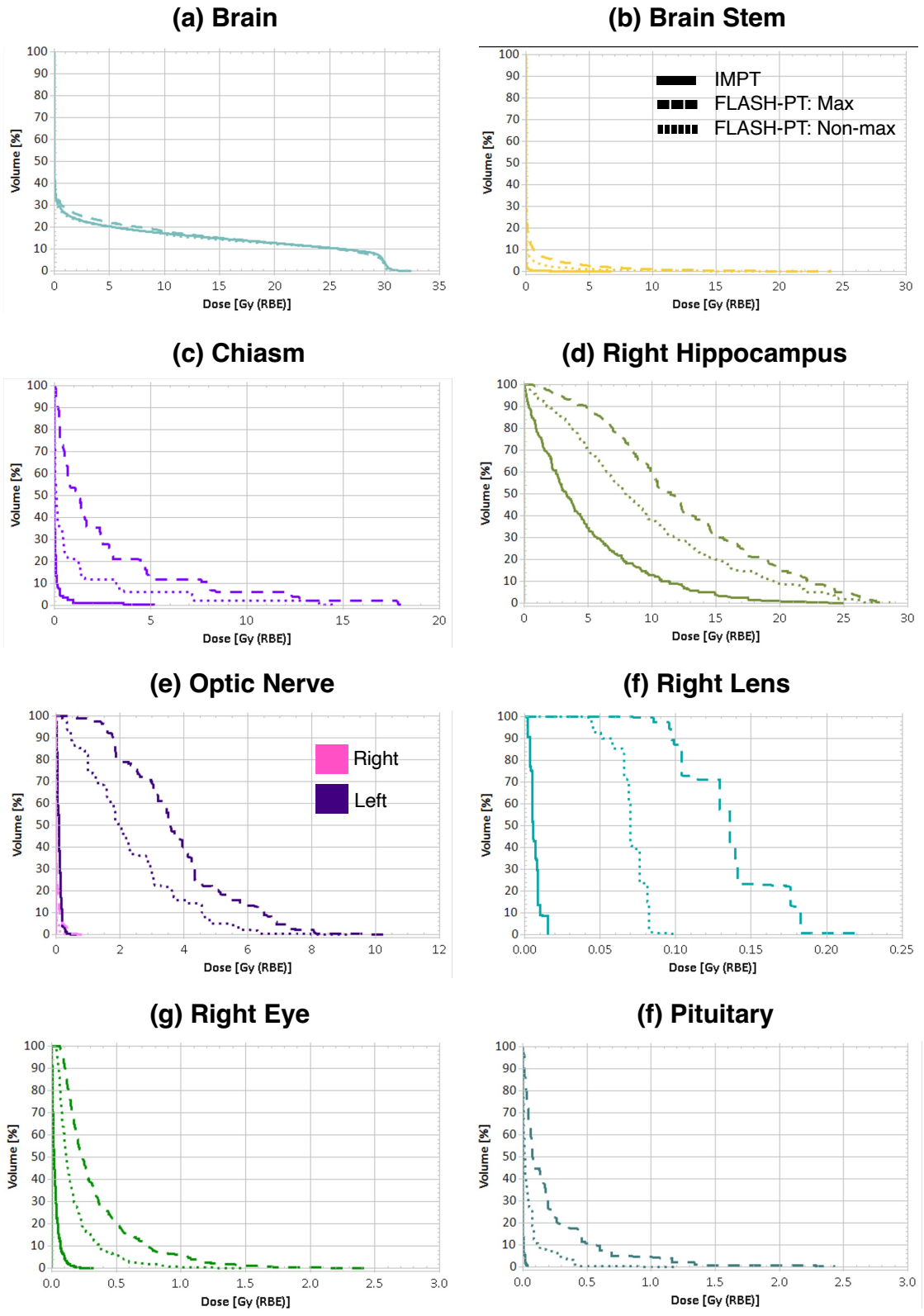


Figure B.2: Dose volume histograms (DVHs) for organs at risk for Patient 1 in Chapter 5. Comparisons are made between intensity modulated proton therapy (IMPT), spread-out Bragg peak FLASH proton therapy (FLASH-PT) delivered with the maximum beam energy (Max), and FLASH-PT delivered with non-maximal beam energies (Non-max).

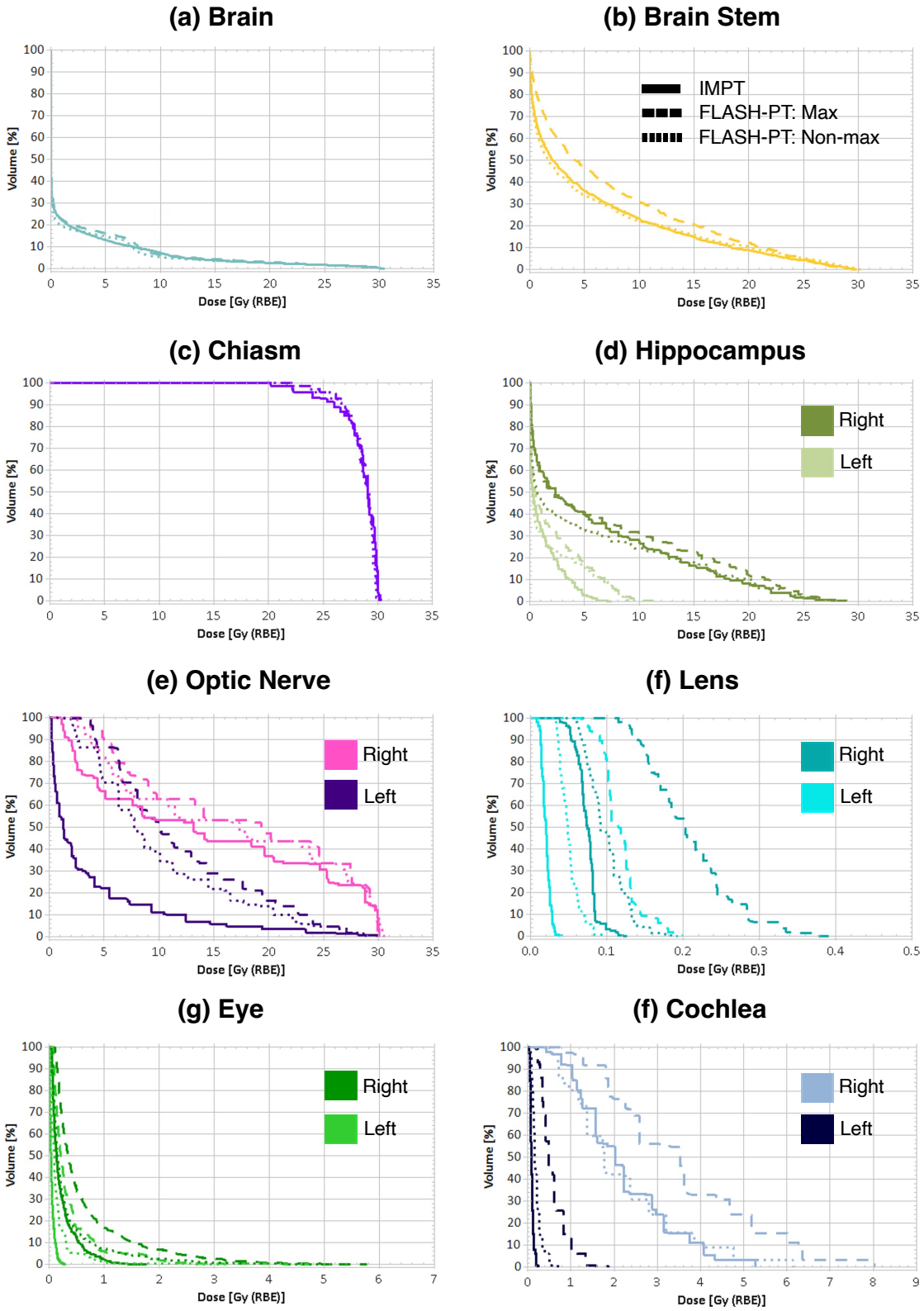


Figure B.3: Dose volume histograms (DVHs) for organs at risk for Patient 6 in Chapter 5. Comparisons are made between intensity modulated proton therapy (IMPT), spread-out Bragg peak FLASH proton therapy (FLASH-PT) delivered with the maximum beam energy (Max), and FLASH-PT delivered with non-maximal beam energies (Non-max).

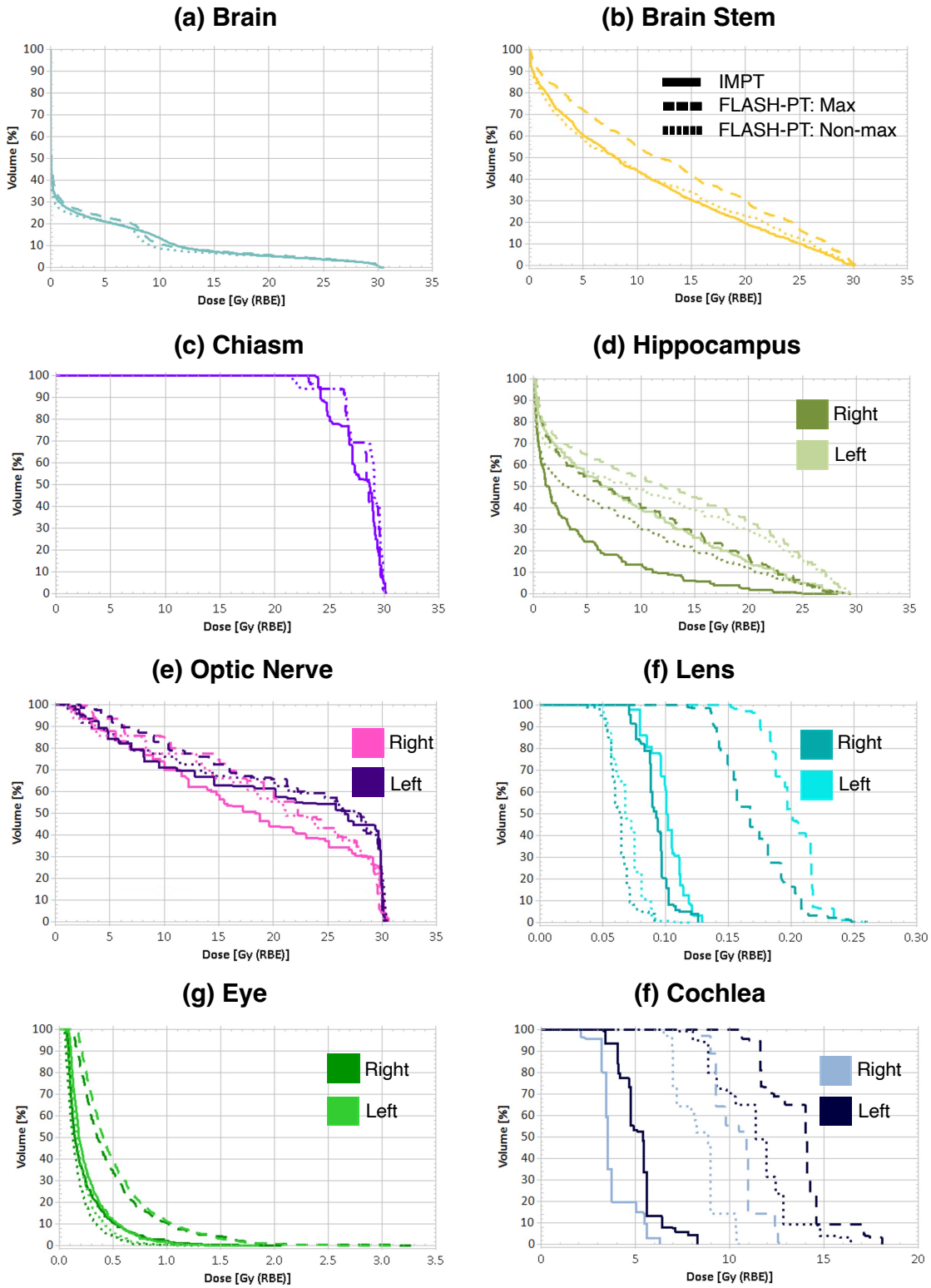


Figure B.4: Dose volume histograms (DVHs) for organs at risk for Patient 10 in Chapter 5. Comparisons are made between intensity modulated proton therapy (IMPT), spread-out Bragg peak FLASH proton therapy (FLASH-PT) delivered with the maximum beam energy (Max), and FLASH-PT delivered with non-maximal beam energies (Non-max).

Table B.2: Comparisons of $D_{20cm^3} < 20$ Gy to the Brain using the 3 fraction CORSAIR protocol [122]. Target volumes for patients 1-5, 7-8, and 10 all exceeded 20 cm^3 and the constraint could therefore not be applied to these cases. As no established treatment protocols currently exist for FLASH proton therapy, stereotactic body radiotherapy (SBRT) protocols were considered for reference. However, it should be noted that SBRT targets are typically much smaller than those considered in this work. OAR dose constraints are given for each patient case, and treatment planning system/technique. Dose comparisons were therefore made between intensity modulated proton therapy (IMPT) plans simulated for the work in Chapter 5, spread-out Bragg peak FLASH proton therapy (FLASH-PT) plans simulated using the maximum beam energy, and FLASH-PT plans using non-maximal beam energies. Bold values indicate cases which exceeded the optimal dose constraint.

Brain: $D_{20cm^3} < 20$ Gy (optimal)

Patient	**Simulated IMPT (30 Gy/3 fx)**	**FLASH-PT Max (30 Gy/3fx)**	**FLASH-PT Non-max (30 Gy/3fx)**
1	Target Volume > 20cm^3	Target Volume > 20cm^3	Target Volume > 20cm^3
2	Target Volume > 20cm^3	Target Volume > 20cm^3	Target Volume > 20cm^3
3	Target Volume > 20cm^3	Target Volume > 20cm^3	Target Volume > 20cm^3
4	Target Volume > 20cm^3	Target Volume > 20cm^3	Target Volume > 20cm^3
5	Target Volume > 20cm^3	Target Volume > 20cm^3	Target Volume > 20cm^3
6	**24.74**	**25.35**	**25.12**
7	Target Volume > 20cm^3	Target Volume > 20cm^3	Target Volume > 20cm^3
8	Target Volume > 20cm^3	Target Volume > 20cm^3	Target Volume > 20cm^3
9	8.62	19.57	17.02
10	Target Volume > 20cm^3	Target Volume > 20cm^3	Target Volume > 20cm^3

Table B.3: Comparisons of $D_{max}(0.035\ cm^3) < 18$ Gy to the Brain Stem using the 3 fraction CORSAIR protocol [122]. As no established treatment protocols currently exist for FLASH proton therapy, stereotactic body radiotherapy (SBRT) protocols were considered for reference. However, it should be noted that SBRT targets are typically much smaller than those considered in this work. OAR dose constraints are given for each patient case, and treatment planning system/technique. Dose comparisons were therefore made between intensity modulated proton therapy (IMPT) plans simulated for the work in Chapter 5, spread-out Bragg peak FLASH proton therapy (FLASH-PT) plans simulated using the maximum beam energy, and FLASH-PT plans using non-maximal beam energies. Bold values indicate cases which exceeded the optimal dose constraint.

Brain Stem: $D_{max}(0.035\ cm^3) < 18$ Gy (optimal)

Patient	**Simulated IMPT (30 Gy/3 fx)**	**FLASH-PT Max (30 Gy/3fx)**	**FLASH-PT Non-max (30 Gy/3fx)**
1	1.92	**18.13**	13.99
2	**30.08**	**30.25**	**29.99**
3	**28.44**	**29.84**	**29.98**
4	**30.57**	**30.30**	**30.28**
5	0.00	0.40	0.01
6	**29.50**	29.16	**29.87**
7	**26.77**	**28.69**	**28.22**
8	**30.30**	**30.11**	**30.17**
9	0.00	0.04	0.01
10	**29.93**	**30.24**	**29.94**

Table B.4: Comparisons of Mean Dose < 17.1 Gy to the Left Cochlea using the 3 fraction UK Consensus on Normal Tissue Dose Constraints for Stereotactic Radiotherapy [123]. As no established treatment protocols currently exist for FLASH proton therapy, stereotactic body radiotherapy (SBRT) protocols were considered for reference. However, it should be noted that SBRT targets are typically much smaller than those considered in this work. OAR dose constraints are given for each patient case, and treatment planning system/technique. Dose comparisons were therefore made between intensity modulated proton therapy (IMPT) plans simulated for the work in Chapter 5, spread-out Bragg peak FLASH proton therapy (FLASH-PT) plans simulated using the maximum beam energy, and FLASH-PT plans using non-maximal beam energies. Bold values indicate cases which exceeded the optimal dose constraint.

Left Cochlea : Mean Dose < 17.1 Gy (mandatory)

Patient	**Simulated IMPT (30 Gy/3 fx)**	**FLASH-PT Max (30 Gy/3 fx)**	**FLASH-PT Non-max (30 Gy/3 fx)**
1	0.00	0.00	0.00
2	**27.18**	**29.05**	**29.74**
3	0.62	6.60	5.04
4	0.09	0.45	0.16
5	0.00	0.00	0.00
6	0.11	0.59	0.21
7	0.33	0.84	0.31
8	0.22	0.44	0.17
9	0.10	0.46	0.20
10	5.21	13.65	11.35

Table B.5: Comparisons of Mean Dose < 17.1 Gy to the Right Cochlea using the 3 fraction UK Consensus on Normal Tissue Dose Constraints for Stereotactic Radiotherapy [123]. As no established treatment protocols currently exist for FLASH proton therapy, stereotactic body radiotherapy (SBRT) protocols were considered for reference. However, it should be noted that SBRT targets are typically much smaller than those considered in this work; therefore, clinically delivered treatment plans (although with conventional fractionation schemes) were also used as comparative references. OAR dose constraints are given for each patient case, and treatment planning system/technique. Dose comparisons were therefore made between intensity modulated proton therapy (IMPT) plans, IMPT plans simulated for the work in Chapter 5, spread-out Bragg peak FLASH proton therapy (FLASH-PT) plans simulated using the maximum beam energy, and FLASH-PT plans using non-maximal beam energies. Bold values indicate cases which exceeded the optimal dose constraint.

Right Cochlea : Mean Dose < 17.1 Gy (mandatory)

Patient	**Simulated IMPT (30 Gy/3 fx)**	**FLASH-PT Max (30 Gy/3 fx)**	**FLASH-PT Non-max (30 Gy/3 fx)**
1	0.16	0.62	0.34
2	0.06	0.25	0.24
3	0.14	1.44	0.91
4	0.06	0.17	0.08
5	1.48	5.02	2.26
6	2.22	3.58	2.19
7	3.55	10.87	8.07
8	**28.62**	**29.96**	**29.93**
9	0	0	0
10	3.85	10.41	8.36

Table B.6: Comparisons of $D_{2\%} \leq 18$ Gy to the Chiasm using protocol information from Skåne University Hospital (Lund, Sweden) courtesy of Ingrid Fagerström Kristensen. As no established treatment protocols currently exist for FLASH proton therapy, stereotactic body radiotherapy (SBRT) protocols were considered for reference. However, it should be noted that SBRT targets are typically much smaller than those considered in this work. OAR dose constraints are given for each patient case, and treatment planning system/technique. Dose comparisons were therefore made between intensity modulated proton therapy (IMPT) plans simulated for the work in Chapter 5, spread-out Bragg peak FLASH proton therapy (FLASH-PT) plans simulated using the maximum beam energy, and FLASH-PT plans using non-maximal beam energies. Bold values indicate cases which exceeded the optimal dose constraint.

Chiasm : $D_{2\%} \leq 18$ Gy

Patient	**Simulated IMPT (30 Gy/3 fx)**	**FLASH-PT Max (30 Gy/3 fx)**	**FLASH-PT Non-max (30 Gy/3 fx)**
1	0	17.22	12.65
2	**30.24**	**30.25**	**29.99**
3	**29.65**	**29.99**	**29.88**
4	**23.04**	**24.22**	**24.85**
5	0	0.08	0.01
6	**30.08**	**30.27**	**29.9**
7	**30.16**	**30.23**	**30.06**
8	**30.22**	**30.13**	**30.09**
9	0	0.03	0
10	**30.09**	**29.92**	**30.04**

Table B.7: Comparisons of $D_{2\%} \leq 18$ Gy to the Left Optic Nerve using protocol information from Skåne University Hospital (Lund, Sweden) courtesy of Ingrid Fagerström Kristensen. As no established treatment protocols currently exist for FLASH proton therapy, stereotactic body radiotherapy (SBRT) protocols were considered for reference. However, it should be noted that SBRT targets are typically much smaller than those considered in this work. OAR dose constraints are given for each patient case, and treatment planning system/technique. Dose comparisons were therefore made between intensity modulated proton therapy (IMPT) plans simulated for the work in Chapter 5, spread-out Bragg peak FLASH proton therapy (FLASH-PT) plans simulated using the maximum beam energy, and FLASH-PT plans using non-maximal beam energies. Bold values indicate cases which exceeded the optimal dose constraint.

Left Optic Nerve : $D_{2\%} \leq 18$ Gy

Patient	**Simulated IMPT (30 Gy/3 fx)**	**FLASH-PT Max (30 Gy/3 fx)**	**FLASH-PT Non-max (30 Gy/3 fx)**
1	0.01	0.36	0.1
2	**30.51**	**30.3**	**30.16**
3	**29.83**	**30.18**	**30.29**
4	3.85	8.42	5.13
5	0	0.1	0
6	**23.4**	**27.11**	**27.27**
7	**30.35**	**30.11**	**29.8**
8	**28.02**	**28.63**	**28.64**
9	9.24	**21.98**	**20.99**
10	**30.21**	**30.12**	**30.41**

Table B.8: Comparisons of $D_{2\%} \leq 18$ Gy to the Right Optic Nerve using protocol information from Skåne University Hospital (Lund, Sweden) courtesy of Ingrid Fagerström Kristensen. As no established treatment protocols currently exist for FLASH proton therapy, stereotactic body radiotherapy (SBRT) protocols were considered for reference. However, it should be noted that SBRT targets are typically much smaller than those considered in this work. OAR dose constraints are given for each patient case, and treatment planning system/technique. Dose comparisons were therefore made between intensity modulated proton therapy (IMPT) plans simulated for the work in Chapter 5, spread-out Bragg peak FLASH proton therapy (FLASH-PT) plans simulated using the maximum beam energy, and FLASH-PT plans using non-maximal beam energies. Bold values indicate cases which exceeded the optimal dose constraint.

Right Optic Nerve : $D_{2\%} \leq 18$ Gy

Patient	**Simulated IMPT (30 Gy/3 fx)**	**FLASH-PT Max (30 Gy/3 fx)**	**FLASH-PT Non-max (30 Gy/3 fx)**
1	0.31	7.5	5.78
2	**29.82**	**29.56**	**29.81**
3	**24.97**	**29.81**	**29.76**
4	8.48	10.27	6.58
5	16.7	**21.1**	18.03
6	**30.08**	**30.04**	**30.42**
7	**30.18**	**30.40**	**30.26**
8	**30.18**	**29.97**	**29.98**
9	0.02	0.34	0.03
10	**30.45**	**30.05**	**30.19**

Table B.9: Comparisons of $D_{2\%} \leq 4$ Gy to the Right Lens using protocol information from Skåne University Hospital (Lund, Sweden) courtesy of Ingrid Fagerström Kristensen. As no established treatment protocols currently exist for FLASH proton therapy, stereotactic body radiotherapy (SBRT) protocols were considered for reference. However, it should be noted that SBRT targets are typically much smaller than those considered in this work. OAR dose constraints are given for each patient case, and treatment planning system/technique. Dose comparisons were therefore made between intensity modulated proton therapy (IMPT) plans simulated for the work in Chapter 5, spread-out Bragg peak FLASH proton therapy (FLASH-PT) plans simulated using the maximum beam energy, and FLASH-PT plans using non-maximal beam energies.

Right Lens : $D_{2\%} \leq 4$ Gy

Patient	**Simulated IMPT (30 Gy/3 fx)**	**FLASH-PT Max (30 Gy/3 fx)**	**FLASH-PT Non-max (30 Gy/3 fx)**
1	0	0	0
2	0.61	0.82	0.53
3	0.04	0.11	0.1
4	0.05	0.05	0.03
5	0	0	0
6	0.03	0.18	0.08
7	0.19	0.39	0.14
8	0	0.01	0
9	0.21	0.59	0.3
10	0.13	0.23	0.09

Table B.10: Comparisons of $D_{2\%} \leq 4$ Gy to the Left Lens using protocol information from Skåne University Hospital (Lund, Sweden) courtesy of Ingrid Fagerström Kristensen. As no established treatment protocols currently exist for FLASH proton therapy, stereotactic body radiotherapy (SBRT) protocols were considered for reference. However, it should be noted that SBRT targets are typically much smaller than those considered in this work. OAR dose constraints are given for each patient case, and treatment planning system/technique. Dose comparisons were therefore made between intensity modulated proton therapy (IMPT) plans simulated for the work in Chapter 5, spread-out Bragg peak FLASH proton therapy (FLASH-PT) plans simulated using the maximum beam energy, and FLASH-PT plans using non-maximal beam energies.

Left Lens : $D_{2\%} \leq 4$ Gy

Patient	**Simulated IMPT (30 Gy/3 fx)**	**FLASH-PT Max (30 Gy/3 fx)**	**FLASH-PT Non-max (30 Gy/3 fx)**
1	0.02	0.18	0.08
2	0.15	1.45	0.83
3	0.05	0.16	0.11
4	0.04	0.03	0.02
5	0.28	0.24	0.11
6	0.11	0.34	0.16
7	0.15	0.46	0.21
8	0.06	0.06	0.03
9	0	0	0
10	0.13	0.23	0.09